AN INVESTIGATION OF THE FIELD ELECTRON EMISSION PROCESSES RESPONSIBLE FOR THE FLASHOVER OF HIGH VOLTAGE VACUUM DEVICES

Trevor Joseph Fielding B.Sc.

A Thesis Submitted for the Degree of
Doctor of Philosophy

The University of Aston in Birmingham

July, 1986.

THE UNIVERSITY OF ASTON IN BIRMINGHAM

AN INVESTIGATION OF THE FIELD ELECTRON EMISSION PROCESSES RESPONSIBLE FOR THE FLASHOVER OF HIGH VOLTAGE VACUUM DEVICES

Trevor Joseph Fielding B.Sc.

Submitted for the Degree of Doctor of Philosophy, 1986

SUMMARY

This thesis is concerned with the field electron emission processes that are associated with vacuum insulated broad-area high voltage electrodes in the field range 5-40MV/m, and also includes a discussion of the various theories that have been proposed to account for such field emission. More specifically, it describes an extensive investigation that has been made into the factors that limit the high voltage capacity of a vacuum gap, with particular regard to the conditioning of electrodes to increase this capacity. Also included are details of the design and construction of an experimental system suitable for such investigations.

The work on conditioning adopted the novel approach of a localised treatment of the actual emitting area, rather than the conventional approach of treating the whole electrode surface. Various techniques of "local" conditioning were evaluated, and were generally found to produce a significant reduction in the emission current at a given applied field; in particular, the use of an ion-beam to locally etch away the individual emission sites was found to be especially effective. The ion-beam technique also allowed the marking of an emission site, thus enabling its subsequent re-location under an electron microscope, or in an Auger/X-ray analysis system. Such analyses provided information as to both the physical and chemical composition of the micro-regime giving rise to emission. The work on electrode conditioning also provided a demonstration of the multiple "switch-on" of emission sites at applied fields in the range 35 - 45MV/m. The potential application of the various conditioning techniques to commercial high-voltage devices is also discussed. Lastly, the phenomenon of optical electroluminesence has been investigated, and found to be apparently not a general effect associated with electron emission, as had previously been thought.

KEY WORDS: Field electron emission, high voltage breakdown, electrode conditioning, localised conditioning

CONTENTS

CHAPTER PAGE

1. INTRODUCTION 14

1.1 Electrical Breakdown in Vacuum 14

1.2 Field Induced Electron Emission Processes 15

1.3 Aims 17

1.4 Experimental Programme 19

1.5 Physical and Technological Implications of Conditioning 20

2. FIELD EMISSION PHENOMENA OCCURRING BETWEEN VACUUM INSULATED HIGH-VOLTAGE ELECTRODES 22

2.1 Introduction 22

2.2 Early Work on Field Electron Emission 23

2.3 Metallic Micro-protrusion Hypothesis 27

2.3.1 Localised Field Enhancement 27

2.3.2 Evidence for the Metallic Micro-protrusion Hypothesis 28

2.3.3 Evidence against the Metallic Micro-protrusion Hypothesis 32

2.4 Evidence in Favour of a Non-Metallic Emission Regime 40

2.5 Energy Distributions of Field Emitted Electrons 47

2.5.1 Field Emission from Metals 47

2.5.2 Field Emission from Semiconductors 49

2.5.3 Field Emission through Adsorbates 52

2.5.4 Field Emission from Broad-Area Electrodes 54

CHAPTER PAGE

2. Cont.

2.6 Non-Metallic Field Electron Emission Models 56

2.6.1 General Assumptions 56

2.6.2 Band Theory Interpretation 57

2.6.3 The Filamentary Model 59

2.6.4 The Insulator Switching Model 63

2.6.5 Critical Observations 67

2.7 The Hot-Electron Model 67

2.7.1 Assumptions of the Model 67

2.7.2 The Switch-On Mechanism 70

2.7.3 The Energy Distribution of Emitted Electrons 77

2.7.4 Successes of the Hot-Electron Model 78

2.8 The Physical Basis of General Electrode Conditioning Techniques 78

2.8.1 Electrode Conditioning 78

2.8.2 Electrode Preparation 79

2.8.3 Current Conditioning 80

2.8.4 "Spark" Conditioning 84

2.8.5 Gas Conditioning 85

2.8.6 Glow Discharge Conditioning 87

2.9 Localised Conditioning Techniques 89

2.9.1 The Concept of Localised Conditioning 89

2.9.2 Ion-Beam Conditioning 89

2.9.3 Electron-Beam Conditioning 90

CHAPTER PAGE

3. DEVELOPMENT OF EXPERIMENTAL SYSTEMS AND THE OPERATION OF CONDITIONING PROCEDURES 91

3.1 General Considerations 91

3.2 Construction of Vacuum System and Experimental Chamber 91

3.3 Development of Electrode Assemblies 93

3.3.1 Electrode Design Considerations 93

3.3.2 The Specimen Mount Assembly 96

3.3.3 The Anode Assembly 102

3.4 Design of Anode Modules 103

3.4.1 Ion Source Module 103

3.4.2 Gas Sputtering Module 106

3.4.3 Electron Beam Module 106

3.4.4 Glow Discharge Module 110

3.5 Ion Source Characteristics 110

3.6 General Experimental Procedures 116

3.6.1 Specimen Preparation 116

3.6.2 Initial Location and Characterisation of Emission Sites 119

3.7 Conditioning Techniques 121

3.7.1 Localised Ion-Beam Conditioning 121

3.7.2 Localised Gas Sputtering Conditioning 124

3.7.3 Localised Electron-Beam Conditioning 126

3.7.4 Localised "Spark" Conditioning 130

3.7.5 Glow Discharge Conditioning 131

CHAPTER PAGE

4. EVALUATION OF CONDITIONING TECHNIQUES 134
4.1 General Considerations 134
4.1.1 Effect of the Anode Aperture 134
4.1.2 Effectiveness of Conditioning Techniques 136
4.1.3 Analysis of Data 137
4.2 Evaluation of Localised Conditioning Techniques 138
4.2.1 Ion-Beam Conditioning 138
4.2.2 Electron-Beam Conditioning 146
4.2.3 "Spark" Conditioning 154
4.2.4 Gas Sputtering Conditioning 154
4.3 Generalised Glow Discharge Conditioning 159
5. FUNDAMENTAL STUDIES OF ELECTRON EMISSION PROCESSES 167
5.1 Introduction 167
5.2 Investigation into Electroluminescence 168
5.2.1 Background 168
5.2.2 Experimental Technique 172
5.2.3 Experimental Observations of Optical Phenomena 177
5.2.4 Physical Significance of Optical Emission Phenomena 187
5.3 Differential Ion-Etching of Emission Sites 188
5.3.1 Calibration of Etching Rate 188
5.3.2 Etching of Emission Sites 192

CHAPTER PAGE

5. Cont.

5.3.3 Effects of Partial Etching on Emission Characteristics 192

5.3.4 Observations of Surface Features in the Emission Site Area 194

5.4 Electron Spectrometry Studies 205

5.5 Physical Implications of Subsidiary Experimental Investigations 210

6. TECHNOLOGICAL IMPLICATIONS OF LOCALISED ELECTRODE CONDITIONING 214

6.1 Evaluation of Conditioning Techniques 214

6.2 Problems of Localised Conditioning 220

6.3 Conditioning of Commercial Devices 222

6.3.1 Electrode Preparation 222

6.3.2 Feasibility of Conditioning 224

7. CONCLUSION 228

7.1 General Considerations 228

7.2 Experimental Findings 229

7.2.1 Conditioning Experiments 229

7.2.2 Analytical Investigations 230

7.3 Future Work 231

7.3.1 Conditioning 231

7.3.2 Nature of Emission Sites 232

REFERENCES 234

ACKNOWLEDGEMENTS 241

APPENDIX A.1 242

LIST OF TABLES

Table		Page
T3.1	Impurity Specifications For O.F.H.C. Copper (courtesy of EEV Ltd.)	117
T4.1	Representative Results From Localised Ion-Etching Experiments	139
T4.2	Results From Localised Electron-Beam Heating Experiments	150
T4.3	Representative Results From Gas Sputtering Experiments	156
T4.4	Results From Ar/O_2 Glow-Discharge Experiments (Specimens 1 & 2)	162
T4.5	Results From Ar Glow-Discharge Control Experiment (Specimen 3)	163
T4.6	Effectiveness Of Glow-Discharge Conditioning	163
T5.1	Calibration Of Ion-Beam Etching Rates	191
T5.2	The Changes In F-N Characteristics Produced By Partial Etching Of Sites	196
T6.1-T6.3	Tables Summarising Results From: (1) Localised Ion-Beam Conditioning (2) Gas Sputtering Conditioning (3) Glow-Discharge Conditioning	215

LIST OF FIGURES

Figure No.		Page
2.1	Schematic Representation of Metallic Field Electron Emission	25
2.2	Rectangular Pulse Conduction (from Powell & Chatterton)(24)	34
2.3	(i) The Ignition-Hysteresis Region (ii) F-N Plot Of The Ignition-Hysteresis Region (from Powell & Chatterton)(24)	34
2.4	An Irreversible "Hysteresis-Like" I-V Plot (from Cox)(26)	39
2.5	"Negative-Resistance" I-V Characteristics (from Hurley)(45)	39
2.6	(i) S.E.M. Micrograph Showing Emission Site At Grain Boundary (ii) A Map Of The Emission Current In The Anode Plane (from Cox)(34)	42
2.7	(i) Spectrum Of Light From A Cathode Spot (ii) Optical Activity In An HV Gap (from Hurley & Dooley)(46)	45
2.8	(a) Theoretical Total And Normal Energy Distributions (b) Theoretical And Experimental Total Energy Distributions (from Young)(54)	48
2.9	(a)-(d) Four Stages In The F.E.E.D. From An Idealised Semiconductor	50
2.10	Surface States Of Ge According To Handler(68)	53
2.11	Energy Distributions From Intrinsic Germanium (from Modinos)(67)	53
2.12	F.E.E.D.´s Produced By Adsorbates On Tungsten (from Swanson & Crouser)(74)	55
2.13	F.E.E.D.´s From: (i) A Tungsten Emitter (ii) A Broad-Area Site On Copper (from Allen & Latham)(78)	55
2.14	Micro-Regime Responsible For Emission From Broad-Area Electrodes (from Allen et al)(75)	58
2.15	Energy Band Structure For Surface Impurity Inclusion (from Allen & Latham)(78)	58

Figure No.		Page
2.16	(a)-(c) Phenomena Expected As A Result Of The Electroformed Filament Model (from Hurley)(45)	61
2.17	(a) Switched Energy Band Diagram (b) Various Potentials Acting On Energy Bands (from Athwal & Latham)(47)	61
2.18	(i)-(v) Stages In Emission From The Hot-Electron Model (from Bayliss & Latham)(96)	72
2.19	Field Distribution Around Conducting Channel (from Bayliss & Latham)(96)	75
2.20	Detailed Energy Levels In Channel On-State (from Bayliss & Latham)(96)	75
2.21	Schematic Illustration Of Current Conditioning(from Latham)(2)	82
2.22	(i)-(ii) Electrode Surface Before And After "Spark" Polishing (from Juttner)(110)	82
2.23	Selective Ion-Bombardment Of Micro-Protrusion (from Alpert)(112)	88
2.24	The "Pressure Effect" Associated With Gas Sputtering (from Hackam & Altcheh)(114)	88
3.1	Electrical Control Circuit For Vacuum System	94
3.2	Photograph Of Cathode Assembly	97
3.3	Diagram Of Scanning System	98
3.4	Photograph Of Cathode Assembly (front)	99
3.5	Stepped-Arc Scan	101
3.6	Specimen Alignment	101
3.7	(a) Photograph Of Anode Assembly (b) Anode Assembly Installed	104
3.8	(a) Ion-Beam Module (b) Gas Sputtering Module	105
3.9	Electron Gun Module	105
3.10	Electron Gun Control Circuit	108
3.11	Electron Trajectories - (a) No Bias Potential (b) With Bias Potential (c) Filament Nearer	108
3.12	Gas Mixing Apparatus	111
3.13	Potential Distribution Of Saddle-Field Ion-source (from McIlraith)(118)	111

Figure No. Page

3.14 Operating Modes Of Ion-Source (from Fitch et al.)(119) 114

3.15 Diagram Of Saddle-Field Ion-Source (from Ali & Fitch)(127) 114

3.16 Energy Spectra Of: (a) Ar^+ And Ar^{++} Ions (b) Ar^o Neutrals (from Ali & Fitch)(127) 115

3.17 Standard Specimen Dimensions 117

3.18 Specimen Profile: (a) Before Polishing (b) After Polishing 120

3.19 Illustration Of General Experimental System 120

3.20 Experimental System For Ion-Beam Conditioning 122

3.21 Experimental System For Gas Sputtering 125

3.22 Experimental System For Electron Beam Heating 128

3.23 Diagram Of Experimental System For Glow-Discharge Conditioning 132

3.24 Photograph Of A Glow-Discharge 133

4.1 (i)-(iii) Field Plots Showing Anode Aperture Effects With Different Electrode Gaps 135

4.2 (i)-(iii) F-N Plots For Ion-Beam Conditioning 142

4.3 (i)-(iii) Changing Locations Of Dominant Emission Sites In Fig.4.2(i)-(iii) 143

4.4 F-N Plots Investigating A Possible Relaxation Effect 144

4.5 (i)-(ii) F-N Plots From "Artificial" Sites 145

4.6 (i)-(iii) Profiles Of Electron Beam At Increasing Beam Powers 147

4.7 F-N Plots Showing Effect Of Electron-Beam Bombardment Of Copper 151

4.8 F-N Plots Showing Effect Of Electron-Beam Bombardment Of Titanium 151

4.9 Site Locations Of Copper & Titanium Specimens 152

4.10 F-N Plots For Spot-Knocking Technique 152

4.11 (i)-(ii) Surface Damage After Spot-Knocking 153

4.12 F-N Plots For Gas Sputtering Technique 157

4.13 (i)-(iii) Changing Locations Of Dominant Emission Sites In Fig.4.12 158

Figure No. Page

4.14 Schematic Illustration Of Glow-Discharge Complex Switching Processes 161

4.15 (i)-(iii) F-N Plots For Glow-Discharge Conditioning 164

4.16 (i)-(iii) Changing Locations Of Dominant Emission Sites In Fig.4.15 165

4.17 S.E.M. Micrographs Showing: 166
(a) Glow-Discharge Surface Effect
(b) Surface "Snow" From C.E.R.N. Specimen

5.1 Experimental Arrangement Used By Hurley (from Hurley)(42) 169

5.2 Spectra Of: (a) Cathode Electroluminescence 170
(b) Anode Transition Radiation
(from Hurley)(45)

5.3 Experimental System For Optical Investigation 173

5.4 Photograph Of Optical Module 173

5.5 (i) Photograph Of Probe Opposite Specimen 176
(ii) Line Diagram Of Features In Fig.5.5(i)

5.6 (i) Image Of Anode Aperture Area 178
(ii) Line Diagram Of Features In Fig.5.6(i)

5.7 Profusion Of Light Spots Around Aperture 179

5.8 Probe With Anode Spots: (i) Low Current 179
(ii) High Current

5.9 Definite Anode Spot On Edge Of Aperture 182

5.10 Possible Cathode Spot Opposite Probe 182

5.11 For Anode Spot Of Fig.5.9: 183
(i) Plot Of $\mathrm{Ln}(I_P-I_D)$ Versus V
(ii) Plot Of $\mathrm{Ln}(I_P-I_D)$ Versus $V^{-1/2}$

5.12 For Possible Cathode Spot Of Fig.5.10: 184
(i) Plot Of $\mathrm{Ln}(I_P-I_D)$ Versus V
(ii) Plot Of $\mathrm{Ln}(I_P-I_D)$ Versus $V^{-1/2}$

5.13 Spectrum Of Light Spot Shown In Fig.5.10 185

5.14 (i)-(iii) Plots Of $\mathrm{Ln}(I_P-I_D)$ Versus Various f(V) (from Hurley)(27) 185

5.15 (i)-(iii) 'Tallysurf' Traces Showing Depth Of Surface Etching 190

Figure No.		Page
5.16	S.E.M. Micrographs Showing: (i) Etched Area (ii) Unetched Area	193
5.17	(i)-(ii) F-N Plots Showing Changes Produced By Partial Etching Of Emission Sites	195
5.18	(a)-(b) S.E.M. Micrographs Of Marked Emission Site Areas	198
5.19	(a)-(b) S.E.M. Micrographs Of Anomalous Surface Microstructures	199
5.20	Marked Emission Site With Heavy Surface Damage Nearby	200
5.21	Microstructure Used For ´Kevex´ Analysis	200
5.22	´Kevex´ Spectra From: (a) Bulk Copper (b) Surface Microstructure	201
5.23	S.E.M. Micrograph Of: (a) Marked Emission Site (b) Elemental Map	203
5.24	Auger Traces Showing Concentrations Of: (i) Cu/C In Bulk (ii) C/Cu In Site Area	204
5.25	More Auger Traces Showing Concentrations Of: (i) C/Cu In Site Area (ii) C/Cu In Bulk	204
5.26	Auger Traces From: (i) C/Cu Concentration From Microstructure (ii)Cu/C Concentration From Bulk	204
5.27	Schematic Diagram Of Electron Spectrometer System (from Allen & Latham)(79)	207
5.28	F-N Plots Showing Changing Characteristics During Transfer And Conditioning	207
5.29	´Site´ Map produced By Spectrometer	208
5.30	Changes In F.E.E.D. With Applied Field	208
5.31	(i) Distribution Of Etch Scars On Specimen (ii) Line Drawing Labelling Etch Scars	209
5.32	Differential Etching Of Surface And Insulating Inclusion	212
6.1	Localised ´Spot-Knocking´ Module	219
6.2	Surface Of A ´Spot-Knocked´ HV Capacitor	225
6.3	Suggested Probe Method For Localised Conditioning Of HV Capacitor	225

CHAPTER 1

INTRODUCTION

1.1 Electrical Breakdown in Vacuum

From a dielectric viewpoint, ultra high vacuum (U.H.V.) should possess the property of providing perfect electrical insulation. However, it can be readily shown that a considerable current may flow between vacuum-insulated high voltage electrodes; such currents have been found to be strongly dependent upon the electric field applied to the electrode gap, and are known as pre-breakdown currents. The term ′electrical breakdown′ is used to describe the catastrophic, irreversible process which occurs if the electric field is increased to a certain critical point where an arc is struck between the two electrodes; thus resulting in the effective gap resistance falling to zero. The technological problem of such electrical breakdown is both a serious and a very common one in industry, due to the prevalence of using vacuum for the insulation of high-voltage in such diverse commercial equipment as power capacitors, high-energy particle accelerator cavities, transmitting valves, klystrons etc. In the case of, for example, a transmitting valve, where the output power may be of several mega-watts and its cost many thousands of pounds, such a failiure would not only be disastrous from an operational point of view, but would be financially very expensive. Traditionally, the problem has been tackled, in an industrial setting, by such empirical methods as maximising the dimensions of vacuum gaps, the use of special materials and surface finishes for the electrodes, and the incorporation of sophisticated electronic protection circuitry. Hence, there is a great deal of industrial interest not only in discovering the fundamental physical processes giving rise to the phenomenon of electrical breakdown, but in ways of treating the devices so as to reduce the likelihood of breakdown.

For applied electric fields in the range 20 - 50MVm^{-1}and inter-electrode spacings of <5mm, there is strong evidence to suggest that the pre-breakdown electron currents are responsible for initiating electrical breakdown. However, for larger electrode gaps, it is generally assumed that breakdown is initiated by loosely adhering micro-particles that are electrostatically pulled off the electrode surfaces and, because of their charge, accelerated by the gap field to gain sufficient energy to trigger a breakdown: a process that occurs at significantly lower fields (<10MV.m^{-1}) than those required for the flow of continuous pre-breakdown currents. Although this micro-particle initiated breakdown mechanism is possibly an important consideration in the performance of a commercial device, the scope of the present investigation was restricted to small-gap regimes where breakdown is normally initiated by field electron emission.

1.2 Field-Induced Electron Emission Processes

As discussed more fully in the following chapter, pre-breakdown conduction has traditionally been explained in terms of a Fowler-Nordheim type of tunnelling mechanism; where surface features, such as metal protrusions (or ´whiskers´), geometrically enhance the macroscopic gap field to the required threshold magnitude (>10^{9}V.m^{-1}) for this mechanism to operate. This model was supported by three major observations:

(i) Electron emission had been observed to arise from a small number of microscopically localised sites.

(ii) The current-voltage characteristics of conditioned electrode gaps appeared to follow the predictions of ´metallic´, Fowler-Nordheim field emission theory.

(iii) Microscopic protrusions were observed on electrodes previously exposed to high electric fields.

However, this interpretation has now been largely superseded by models of an emission mechanism based upon electrical conduction through insulating or semi-conducting surface inclusions. The development of these various ´hot-electron´ models, culminating in the most recent version that has been able to give a quantitative explanation of the field emission process, is described in some detail in the next chapter; however, a brief introduction will be given here.

Recent experiments have indicated that unrealistically high geometrical field enhancement factors are required in the metallic whisker model, and that no direct observation of these whiskers could be made in the areas from which electrons were emitted. Optical experiments and measurements of the energy distributions of the emitted electrons have provided further direct evidence against the metallic field emission theory, and yielded results more consistent with an interpretation based on insulating surface layers or inclusions, which are invariably present on nominally clean metal surfaces. Early models, based on an emission micro-regime consisting of an insulating inclusion embedded in a metal surface, were only of a qualitative nature and unable to explain many subsequent experimental findings. Further theoretical developments suggested that emission occurs as a result of an electron ´heating mechanism´ acting at the ends of thin conducting channels penetrating through the insulating layer to the metal surface. The final stage in the development of this model defines the conditions required for emission to occur, i.e. the presence, within the insulating surface inclusions, of sufficient numbers of donor and electron trapping centres. It also explains a number of previously anomalous experimental results, allowing a semi-quantitative development of several of these features.

1.3 Aims

Much of the work undertaken in this laboratory has concentrated on more fundamental studies of pre-breakdown electron emission processes using a sophisticated U.H.V. electron spectrometer facility. Indeed, many of these studies are discussed in the following chapter, together with a full review of the development of a model which attempts to provide an explanation of the mechanism behind field-electron emission.

To complement these studies, this project was designed to exploit the technological implications of the fundamental insights into the nature of field electron emission sites gathered by previous, and parallel, spectroscopic studies. Hence, the main aim of this investigation was to develop improved techniques for the conditioning of electrodes; whereby an increased voltage may be applied between the test electrodes without breakdown occuring. Most conventional conditioning techniques attempt to treat the whole electrode surface, normally by some means of generalised low-energy gas sputtering technique; making no attempt to isolate the localised emission sites and monitor the effect of the conditioning process on these individual areas. In fact, quite often these conventional ′total-electrode′ conditioning methods result in the creation of as many new sites as there are old ones destroyed; this is particularly true with the ′spot-knocking′ technique, which is used extensively in the commissioning of commercial high-voltage equipment. The approach to conditioning adopted in this study is based on the concept that conditioning should be restricted to the localised "active" region of an electrode surface; with improved voltage hold-off being produced by the repeated, localised destruction of the dominant emission sites. To achieve such a local conditioning action, individual emission sites must first be located and then treated without affecting the remainder of the electrode surface. The localised conditioning techniques investigated consist of ion-beam etching (using a saddle-field ion source), gas sputtering, localised heating using an electron gun, and spot-knocking. In addition, a generalised glow-discharge technique was also investigated; although it should be noted that, with the gas sputtering technique, no localisation of action was observed. The theoretical concepts behind all these techniques are discussed in the latter part of the next chapter.

In an effort to further the knowledge of the micro-regime giving rise to such emission, studies were also made into various phenomena associated with the emission process. One such area of investigation was the phenomenon of cathode-generated electroluminescence, where, initially, the objectives were to duplicate and further refine the observations of earlier researchers. However, as the investigation proceeded, the observation of any electroluminescent emission proved very difficult, and the experimental aim became to determine whether or not the observed optical emission could be attributed to electroluminescence or anode-generated transition radiation. Another series of experiments was designed to provide knowledge as to the physical properties of the emission regime: one set of experiments consisted of an investigation into how sensitive the emission characteristics of sites are to localised changes in the surface conditions; while a second set attempted to observe any surface anomalies typically present in the immediate area of an emission site. Further experimental work consisted of electron spectroscopy studies of specimens (using the U.H.V. electron spectrometer facility available within the laboratory), followed by transfer to the usual experimental system for conditioning.

1.4 Experimental Programme

Before the investigative aspects of this project could be pursued, various systems had to be developed. Firstly, a vacuum system which provided the necessary experimental flexibility had to be designed and constructed; as did the various conditioning modules. The use of such "localised" conditioning treatments also required the development of a specimen scanning system which allows the examination of the surface of a specimen, and some means of detecting the presence of an emission site. These systems are all described in detail in Chapter 3, as is a full description of the experimental procedures used in specimen preparation and the operation of all the conditioning techniques.

In Chapter 4, various parameters allowing the assessment of the relative effectiveness of each conditioning technique are defined, and an evaluation of the various conditioning techniques presented. This evaluation includes various representative graphical and tabloid summations of the experimental data.

In principle, Chapter 5 is concerned with fundamental studies of the physical properties of emission sites. The problems and results of the investigation into the phenomena of electroluminescent emission are also described. This chapter also includes details of the investigations into how the emission characteristics of an individual site changes during the localised removal of surface material (by means of the ion-beam technique), and into whether any surface anomalies were characteristic of emission site locations; the ion-beam technique was again of use here, in order to lightly mark the location of the emitting area for subsequent examination under S.E.M., Auger and X-ray analysis systems. Again, the significance of these results, relative to the knowledge of the composition of the emission micro-regime, is discussed. Also included in this chapter is a description of the electron spectroscopy studies, the experimental objectives behind them, and an examination of the information provided by them.

1.5 Physical and Technological Implications of Conditioning Processes

Chapter 6 considers the technological implications of localised conditioning. It includes an evaluation of the various techniques, together with a discussion of the physical implications of these findings, with reference to the nature and distribution of emission sites, and the problems and limitations of localised conditioning. Further, the conditioning of commercial devices is considered, with particular reference to the feasibility of applying localised conditioning to such devices.

To conclude the thesis, Chapter 7 contains a review of the experimental findings, and suggestions as to the most profitable direction of possible future work on both electrode conditioning and on the nature of emission sites.

CHAPTER 2

Field Emission Phenomena Occurring Between Vacuum Insulated High Voltage Electrodes

2.1 Introduction

The first part of this chapter, seeks to present a summary of over eighty years of research into the origin of pre-breakdown conduction between vacuum-insulated high-voltage electrodes, and will trace the development of various models for explaining the physical origin of the underlying field-induced electron emission process. The survey will start with the development of the original Fowler-Nordheim theory, progress through the modifications required for the metallic microprotrusion hypothesis, to the non-metallic ´insulator-switching model´, and culminate in a description of the ´hot-electron´ model. Reviews of much of the work leading to the development of an initial non-metallic emission model may be obtained from several sources; for example, Noer(1) and, along with an exhaustive description of other electrode processes, Latham(2). In the second part of the chapter, a discussion will be given of the physical basis, and limitations, of the various ´standard´ conditioning techniques; i.e. the procedures used to raise the voltage hold-off of a pair of HV electrodes. In this context, the practical advantages of the localised approach to conditioning will be outlined.

2.2 Early Work on Field Electron Emission

In 1918, Millikan and co-workers(3,4) published some important observations concerning pre-breakdown conduction from extended area parallel electrodes. They found that field emission from tungsten electrodes was ordinarily observed with fields in the range $1\text{-}5\times10^{7}\mathrm{Vm}^{-1}$. However, after annealing of the elctrodes at 2700K, the cooled tungsten withstood a field of $4\times10^{8}\mathrm{Vm}^{-1}$ before emission.In addition, discrete spots of light were observed on the anode, and the emission current at a given field was found to be independent of temperature, up to 1000K; with a plot of the logarithm of the current versus the inverse of the field, always producing a straight line. From these findings, Millikan et al. concluded that emission took place either from localised cathode regions of low work function, resulting from chemical impurities, or from regions with a high local field produced by surface roughness. It should, however, be noted that these results were obtained with a comparatively poor vacuum, usually around 10^{-6}mbar.

Subsequently, in 1923 Schottky(5) made the first attempt to quantify the origin of ´cold´ field electron emission from metals. He postulated a complete reduction of the potential barrier at the metal surface, due to a combination of the external electric field and the electron image-force potential; an extension of the mechanism that had been verified for thermionic emission under low-field conditions. However, a quantitative application of this model to cold high-field electron emission processes, led to wrong predictions in terms of the emitted current not rising as rapidly with the applied field as demanded by the thermionic equation.

The first theory to satisfactorily describe the ´cold emission´ of electrons from metals was formulated by Fowler and Nordheim in 1928$^{(6)}$; they considered the quantum mechanical tunnelling of electrons through the modified potential barrier that results from the presence of a high external electric field acting on an atomically clean surface, a situation illustrated in Fig.2.1. The Fowler-Nordheim (F-N) model of field electron emission assumes: (i) that Fermi-Dirac statistics may be used to describe the rate of arrival of the electrons at the metal surface; (ii) the probability of an electron penetrating the surface potential barrier can be found from a solution of the Schrödinger wave equation. Thus, the theory requires the following parameters to be defined:

a) $N(W)\,dW$ = The supply function, giving the number of electrons, with the z-axis energy component within the range W to $W+dW$, incident on the surface per second per unit area.

b) $D(W)$ = The probability that an electron with energy W will penetrate the barrier.

c) $P(W)\,dW = N(W).D(W)\,dW$ = The number of electrons in the range W to $W+dW$, penetrating the barrier (the normal-energy distribution)

d) $J = e\int_W P(W)\,dW$ = The current emitted per unit area.

However, the detailed evaluation of $N(W).D(W)$ and the analytical integration of $P(W)\,dW$, are extended and involved mathematical exercises, with comprehensive treatments being given by Good & Müller$^{(7)}$ and Van Oostrom.$^{(8)}$.

For low temperatures (T<300K), when few electron states above the Fermi level are occupied, the emitted current density is

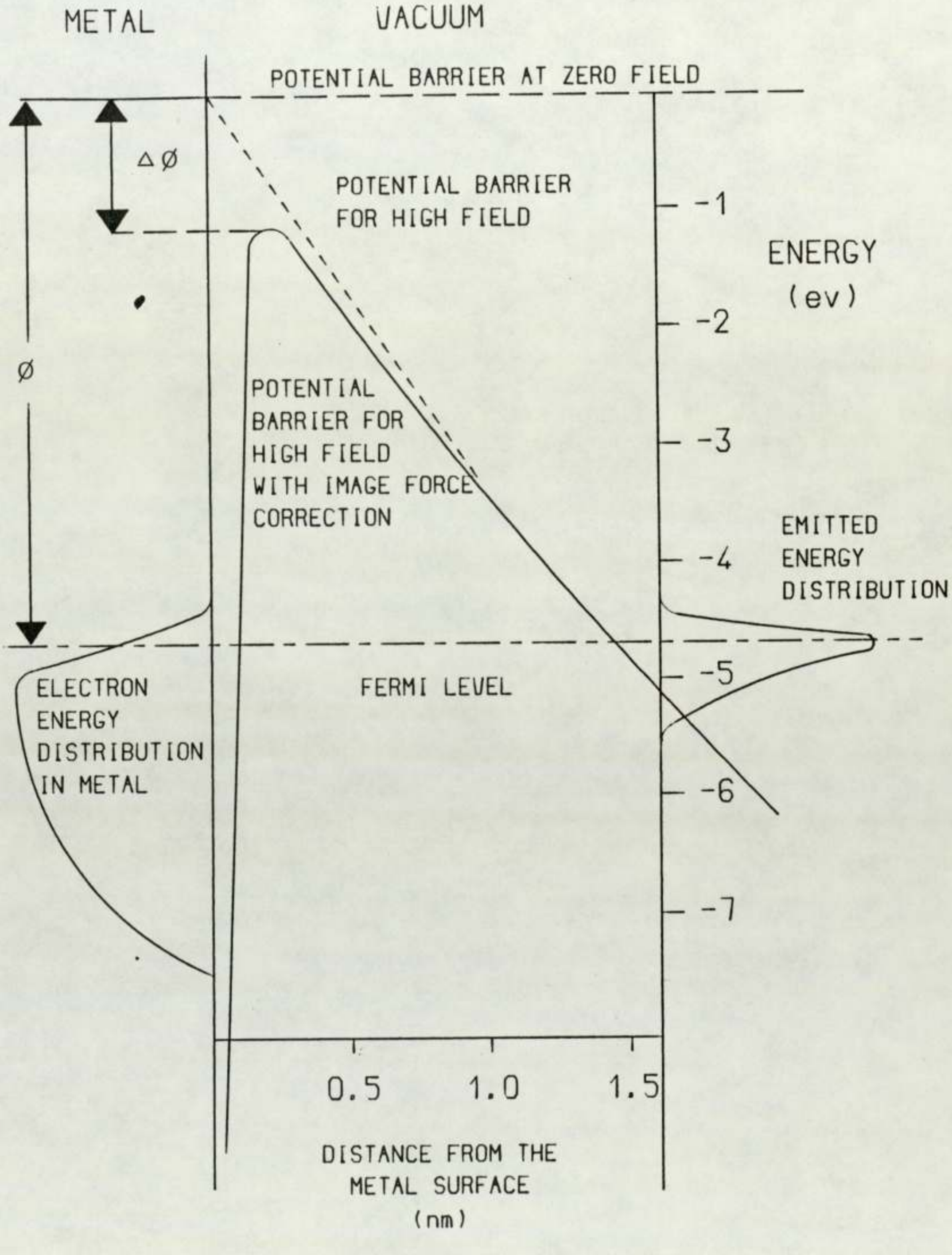

Fig.2.1 SCHEMATIC REPRESENTATION OF METALLIC FIELD ELECTRON EMISSION

usually expressed in the form:

$$J = \frac{1.54\times10^{-6}.E^2}{\phi.t(y)^2}\exp[\frac{-6.83\times10^{9}.\phi^{3/2}.v(y)}{E}] \qquad E.2.1$$

This is known as the Fowler-Nordheim equation, where

$\mathbf{J}$ is the current-density (Am^{-2})

$\mathbf{E}$ is the surface electric field (Vm^{-1})

ϕ is the metal work-function (eV)

$\mathbf{t(y)}$, $\mathbf{v(y)}$ are tabulated dimensionless elliptic functions of the parameter $\mathbf{y}$(7,9); where

$$y = 3.79\times10^{-5}.\ \frac{E^{1/2}}{\phi}$$

For the field range of stable emission current ($1\times10^9 < \mathbf{E} < 6\times10^9 Vm^{-1}$), $\mathbf{t(y)}$ approximates to unity and $v(y) = 0.956 - 1.062y^2$. Substituting these approximations into equation E2.1 and re-arranging, gives:

$$J = 1.54\times10^{-6}.\ \frac{10^{4.54\phi^{-1/2}}.\ E^2}{\phi}\exp[\frac{-6.53\times10^{9}.\ \phi^{3/2}}{E}] \qquad E2.2$$

F.N. theory was first tested by Haefer in 1940(10), using a point cathode with a planar anode, and subsequently by Dyke et al.(11,12) in 1953, using micro point emitters having an accurately known geometry, and hence surface field (about $10^9 Vm^{-1}$); good agreement was obtained with theory over several orders of current. However, departures from F-N theory did occur at high current-densities, and these were accounted for by space-charge considerations.

2.3 Metallic Microprotrusion Hypothesis

2.3.1 Localised Field Enhancement

For broad-area parallel plate geometries, Dyke et al.(11,12) obtained emission current at fields of one or two orders of magnitude lower than theory would predict. This finding can be explained if it is assumed that some surface feature causes the applied field to be locally enhanced by a factor β over the uniform gap value; also, if the emission occurs from an emitting area **A**. Hence, the resulting emission current will be given by I = J.A and, assuming uniform field over the emitting region, the field-enhancement factor can be defined as:

$$E_{microscopic} = \beta \, x E_{macroscopic} \qquad E2.3$$

Since, for a plane-parallel electrode gap, $E_{mac} = V/d$, where **V** is the applied potential difference and **d** is the electrode gap spacing,

$$E_{mic} = \beta . V/d \qquad E2.4$$

Hence, substituting this expression into equation E2.2, gives the F.N. equation in terms of the applied potential difference and the measured emission current:

$$I = 1.54x10^{-6} . \frac{10^{4.54\phi^{-1/2}} . A\, \beta^2 V^2}{\phi d^2} \exp\left[\frac{-6.53x10^9 . \phi^{3/2} d}{V}\right] \qquad E2.5$$

It follows that, if the current-voltage characteristic of a gap having a single emitter is plotted in the form $\log_e(I/V^2)$ versus $1/V$, i.e. an F-N plot, the result will be a straight line of gradient M:

$$M = \frac{6.53 \times 10^9 . \, \phi^{3/2} . d}{\beta}$$

and intercept C:

$$C = \log_e[1.54 \times 10^{-6} . \, \frac{10^{4.54\phi^{-1/2}} \beta^2}{\phi d^2}]$$

Thus, since d is known, and the work-function ϕ of the emitter is assumed to have the same value as for the bulk electrode material, the slope of the F.N. plot will give a measure of the emitter β -value; furthermore, the value of the intercept may be used to determine the emitting area.

Although there will normally be a number of emitters distributed over the cathode surface, computer simulation studies by Tomasche & Alpert(13) have shown that the pre-breakdown current will usually be dominated by the emitter with the highest field-enhancement factor. The associated F.N. plot gives, as might be expected, a straight line, with the overall β-factor reflecting that of the dominant site; while the emission area is approximately the sum of the individual emission areas.

2.3.2 Evidence for the Metallic Microprotusion Hypothesis

Experiments employing an extended area parallel plate geometry have a long history, which can be conveniently separated into two eras, viz. before and after the introduction of ultra-high vacuum techniques. In the earlier period, as already mentioned, Millikan et al.(3,4) produced a detailed analysis of emission phenomena; finding that emission current was: a) reduced by annealing; b) was independent of temperature (<1000K); c) occured from localised cathode regions - all of these findings being consistent with the metallic microprotrusion hypothesis.

The introduction of ultra-high vacuum (U.H.V.) techniques made it possible to carry out experiments in which contamination from the vacuum system,or by residual gases, could be eliminated or controlled, and the nature of the cathode surface better defined. In particular, Boyle, Kisliuk & Germer(14) in 1955, carried out an investigation to discover if the earlier results of Dyke et al.(11,12), for point-plane geometries, could be repeated for a broad-area geometry under U.H.V conditions. Pulsed fields were used to prevent undue heating of the electrodes, which were in the shape of crossed tungsten wires of small (0.75mm) diameter; nevertheless, these were considered broad area in the sense that the gap spacings used were smaller than ,or comparable to, the dimensions of the electrodes. Their results gave good straight-line F-N plots, but they observed a variation of the β-factor with the electrode gap spacing, which they explained as being due to the enhancement of the electric field at very small ($<10^{-15}m^2$) projections on the surface of the cathode. Values of β ranged from unity, at gap spacings of a few angstroms, up to values as high as 30 for 10 micron gaps, and this was shown to be consistent with an explanation based on the presence of small projections on the cathode surface.

The work of Boyle et al.(14) was extended to more practical regimes by Alpert et al(15), using 35mm. diameter disc electrodes, cut from single crystal tungsten, and gap spacings of 5 microns to 4mm. Again, good F-N fits were found with gap-dependent β-values of 50-200. The authors considered two contributions to β : a microscopic one, caused by protusions on the cathode, and a macroscopic effect, due to changes in the electric field caused by electrode end-effects when the gap was large.

Little & Smith(16) and Tomasche & Alpert(17), obtained further evidence for the metallic microprotrusion model from electron microscopy studies. The latter workers, using shadow electron-micrographs, observed that, following electrical breakdown, projections of micron-dimensions were formed on previously smooth areas of the blunt-end of a 70 micron tungsten wire. Moreover, very small gaps showed large current fluctuations which, if allowed to proceed for several minutes, produced a large proliferation of whisker-like projections ($\approx 0.1\,\mu$m in height) on previously smooth cathodes. An annealing procedure, at 2000K, removed the current fluctuations and the emission current followed an F.N. relationship right up to breakdown of the gap.

Similar results were reported by Little & co-workers(16,18) using 13 mm diameter buttons of aluminium, stainless steel, Kovar, nickel, silver and copper. They also used a fluorescent anode, with a gap of 0.1mm, and observed that, as current flowed, one or more fluorescent spots (<0.2mm diameter) appeared on the anode; furthermore, it was usually noted that the spots appeared suddenly, i.e. with a rise-time less than a millisecond. The cathode could be repositioned in the same vacuum system for shadow-electron microscope investigation, where it was found that every cathode surface included one, or more, protrusions which could have given rise to sufficient field enhancement for F-N type emission, and which were not present before the application of the electric field. Another important observation made for stainless steel and tungsten cathodes, was that the emission current was independent of temperature (within 30%) until 1000 K, after which the current began to rise exponentially, indicating the onset of thermionic emission. This verified that pre-breakdown emission does not originate from areas of extremely low work-function, as was further confirmed by their subsequent observation that illumination of the cathode with visible light had no effect on the pre-breakdown emission.

An investigation into the properties of electron emitting sites associated with a 0.125mm diameter nickel wire cathode, in conjunction with a 76mm cylindrical phosphorescent anode, was made by Brodie(19,20). When current was drawn, elliptical spots, a few millimetres across, were observed on the anode. Calculations by the author, assuming a prolate spheroid geometry for the microprotrusion, from the measured β-factors and geometry of the system, gave whisker dimensions from 7nm to $1\,\mu m$ high. However, the structure within the larger ellipses could not be related to the field-emission images obtained from single-crystal nickel surfaces by Gomer(21). At high fields ($>5\times10^7 Vm^{-1}$) new, extremely intense, emission centres, capable of delivering several milliamps without blowing up, suddenly appeared; the elliptical images of these spots being posessed of very large major axes - up to 60mm.

Davies & Biondi(22,23) reported measurements of the pre-breakdown current flowing between copper electrodes under

U.H.V. conditions. The O.F.H.C copper electrodes were metallographically polished and then electrolytically polished, prior to assembly in the vacuum system. The electrodes were maintained at a temperature of 1100K, by means of in situ tungsten filaments, for a period of ≈ 20 hours before their I-V characteristics were recorded. This resulted in linear F-N plots having β-values in the range 140 - 240, with no correlation to the electrode gap settings, at least over the range 0.3 - 2mm. They further reported that the I-V characteristics were independent of cathode temperature over the investigated range of 313K to 913K.

2.3.3 Evidence Against the Metallic Microprotrusion Hypothesis

From the preceeding section, it is clear that a considerable body of experimental work was accumulated favouring the cathode microprotusion hypothesis for the source of electron emission on broad-area cathodes. However, from the reports of Powell & Chatterton(24), Hackam & Salman(25), Cox(26) and Hurley(27), a variety of effects were found to be at odds with this model: such as curved and variable F.N. plots, current noise, temporal variation of emission current, ignition-hysteresis phenomena, high-current and negative resistance sites. Although these effects are most common in poor vacuum conditions ($>10^{-6}$mbar), as indicated in the review by Hawley & Zaky(28), many of the phenomena still manifest themselves, even if less frequently, in U.H.V. baked systems.

In particular, the work of Powell and Chatterton(24) serves well to illustrate that the frequently reported straight line F-N plots, are not necessarily typical of the conduction between unconditioned electrodes. These authors carried out an investigation into the pre-breakdown conduction between stainless steel, copper, aluminium and tungsten electrodes - consisting of a hemisphere in conjunction with a rounded, planar disc - at small gaps (<10mm), and in both U.H.V. and poor vacuum. They found great similarity in behaviour for the different materials, but the variability with time and general non-reproducibility of the emission current, made the measurement of I-V characteristics very difficult. This necessitated the use of a fast-response current measuring system, enabling a plot of the I-V relationship,using a storage oscilloscope, to be made in five steps over the current range 10^{-9} to 10^{-3}A, with each step taking about a half-second. Application of this fast measuring system revealed the presence of irregular bursts of charge, termed microdischarges (previously observed by Pivovar and Gordienko(29,30)). These occurred in bursts rather than singly, and were variable in magnitude, from less than a micro-amp to approximately 10 mA, and in duration, from 10^{-5}s. to 10^{-2}s. Current conditioning did not reduce the steady current component; rather, at least in the early stages, the current tended to increase, for a given voltage, after the passage of a microdischarge. Fig.2.2(i)-(ii) shows typical traces of current against time for a fixed voltage.

Powell & Chatterton(24) also observed an ignition-hysteresis phenomena for currents in the region of 10^{-6}A, as shown in Fig.2.3(i)-(ii). Initially, for a steadily increasing voltage, the current would also steadily increase, but for very little further rise in voltage, the current would then rise very rapidly; thus

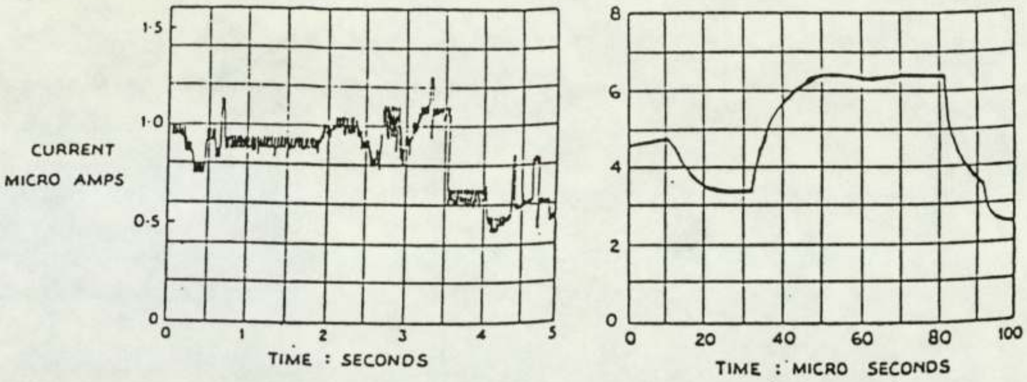

Fig.2.2 Rectangular Pulse Conduction

(from Powell & Chatterton)(24)

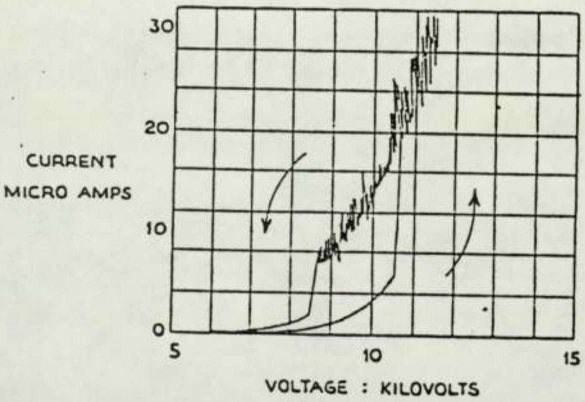

(i) The Ignition-Hysteresis Region

Fig.2.3

(from Powell & Chatterton)(24)

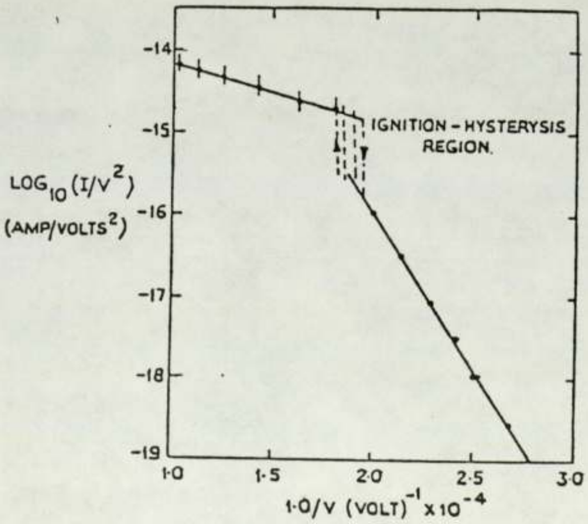

(ii) F-N Plot Of The Ignition-Hysteresis Region giving the "ignition" effect. Upon reducing the voltage, the current then remained at a high level until a lower "extinction" voltage was reached. Both of these effects were suppressed at current levels over $>10^{-4}$A, while, at $\simeq 10^{-3}$A, the ignition-hysteresis could be removed altogether; this was known as "ageing", and was entirely a current effect, occurring at the same current value for all gaps. At a constant applied voltage, the emission current would fall with time; a process known as ´de-ageing´. Subsequently, if the current was kept below 10^{-6}A, a return to rectangular pulse conduction would result, after about 20 min. in a rather poor vacuum (10^{-7} mbar). The ignition phenomena only resumed after several days of de-ageing, or after contamination of the vacuum system, such as resulted from not filling the liquid nitrogen traps. Notably, de-ageing in a clean baked system having a pressure of 3×10^{-9}mbar took several hours, but, if air was admitted to a pressure of 2×10^{-6}mbar for a few minutes, the electrodes completely de-aged.

The authors explained the various temporal instabilities in terms of variable gas coverage of a microprotrusion as the emission current increased, but similar conclusions may be drawn for gas coverage of almost any emitting surface. Thus, for the microprotrusion case at low currents, molecules would arrive at the tip, due to field-assisted surface migration, and the gas coverage would increase. At intermediate currents, the tip temperature would tend to rise, increasing the positive ion sputtering of the tip, which, in turn, tends to reduce the gas coverage. For high values of current, the tip may become very hot and gas coverage be reduced drastically. A further assumption made, was that gas coverage suppresses electron emission; so, under these circumstances, an F-N plot could be expected to be non-linear as the gas coverage varied with the current.

A plausible explanation for the ignition-hysteresis effect was given by a comparison with the molecular images seen in field-emission microscopes by Good & Muller(31), where ignition would occur when, as the field was increased, empty electron energy levels in the adsorbate dipped below the Fermi level of the metal protrusion, causing sudden enhanced emission. Ageing was thus explained as the near complete removal of adsorbed gas from the emitting protrusion, while de-ageing resulted from its gradual recontamination; the rectangular pulse conduction was attributed to the migration of small groups of atoms across the emission region.

Hackam & Salman(25), studying conditioned, aluminium electrodes under U.H.V. conditions, reported two distinct types of F.N. plot: small gaps, <0.76mm, produced straight line F.N. plots showing no ignition effects; while larger gaps, >0.89 mm, produced an ignition-hysteresis phenomena in the current range 2.4 - $6.6\mathrm{x}10^{-9}$A. During ignition, the current increased in two stages, rising slowly to 6 - $10\mathrm{x}10^{-9}$A, followed by a sudden jump to the range 0.26 - $6.5\mathrm{x}10^{-7}$A, all without an increase in voltage; subsequent voltage increases gave a distinctly curved F-N plot. Hackam & Salman(25) also studied ageing and de-ageing effects: a fast current monitoring technique revealed that, after 5 minutes with zero field, ignition was not observed; after 6 minutes, a much diminished ignition re-appeared; while after 10 minutes, ignition returned to its maximum value.

Other types of non-linear F-N current relationships were revealed by Cox(26) and by Hurley(27). Cox made a large number of tests on 14mm diameter copper-chromium alloy vacuum switch contacts, with a 6mm plane parallel gap and under a vacuum of $2x10^{-10}$mbar (reached after a 520K bake-out). De-conditioning, to simulate in-service conditions, was achieved with a 14kHz ringing discharge having a 16kA first peak. The majority of results then gave F-N plots with β-values in the range 300 - 500; however, some tests produced unstable emission with the irreversible hysteresis-like I-V characteristic, shown in Fig.2.4. A third type of emission site "switched-on", going from a current of less than 10^{-7}A to more than 10^{-5}A, with virtually no change in applied voltage; this type of result occurred in about 1% of tests, and are distinct from the ignition sites reported by Powell & Chatterton(24) because the switch-on only occurred once, even if the maximum current was limited. A further type of site was also reported, similarly rare, which could pass the maximum available current of 0.5 mA without causing a breakdown, and which had β-factors in the region of 1000.

Hurley(27), using a pointed anode probe to locate and measure the emission from individual sites on O.F.H.C. copper, showed the existance of both "a" and "b" sites. The "a"-sites were typically characterised by β-values in the range 150 - 300, with calculated emitting-areas of about 10^{-16} - $10^{-14}m^2$, and producing breakdown and site destruction for currents of about $5x10^{-5}$A. However, the "b"-sites possessed β-factors in the range 10 - 150, and emitting areas ranging from $10^{-13}m^2$ to the "impossible" value of $10m^2$. For currents in the region of 10^{-5}A, a current controlled negative resistance was observed, with the current adjusting itself to an equilibrium value that was partly determined by a 23 MΩ series safety resistor. If this resistor was removed, breakdowns occurred randomly in the current range 10^{-5} - 10^{-3}A, with the total current being limited only by the power supply, without destruction of the emitting site. Fig.2.5 illustrates this 'negative resistance' behaviour.

All of these reports indicate that the assumption of metallic microprotrusions being solely responsible for the pre-breakdown emission from broad-area electrodes is apparently incorrect. This assumption rests, essentially, on just two facts: namely, the linearity of F-N plots, and the observation that metallic field-enhancing features usually exist on electrode surfaces after a breakdown or micro-discharge event. It has been seen that the first condition has many exceptions, whilst, for the second, there is no direct evidence, for unconditioned electrodes, correlating electron emission from broad-area electrodes with metallic surface protrusions of dimensions sufficient (Latham & Braun(32)) to produce a high enough β-factor. In fact, even with the experimental regime described earlier by Brodie(19,20), the large (60mm) ellipses suggested whiskers up to 20 microns high should be present; these could not be observed on the cathode surface.

Pre-breakdown conduction is thus seen to be much more complicated than can be explained by a simple application of Fowler-Nordheim theory. A number of recent experimental results, summarised in the following section, have given rise to an alternative hypothesis; viz. that of conduction through embedded insulating impurity particles and contaminated oxide layers.

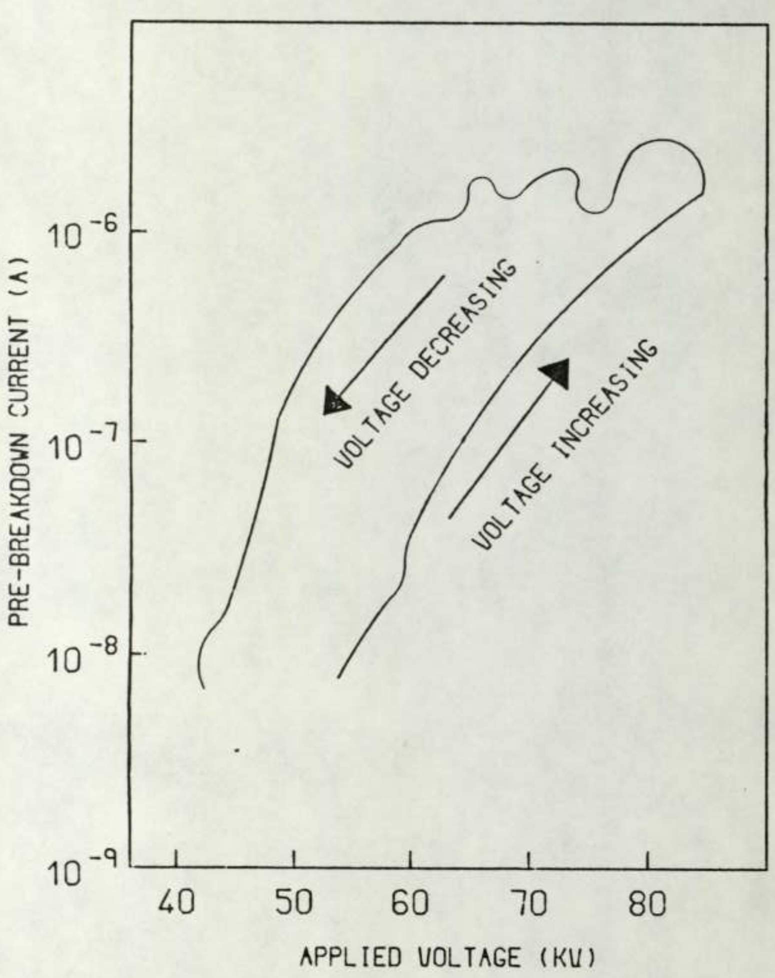

IRREVERSIBLE "HYSTERESIS" EFFECT
(FROM COX)$^{(26)}$

Fig.2.4

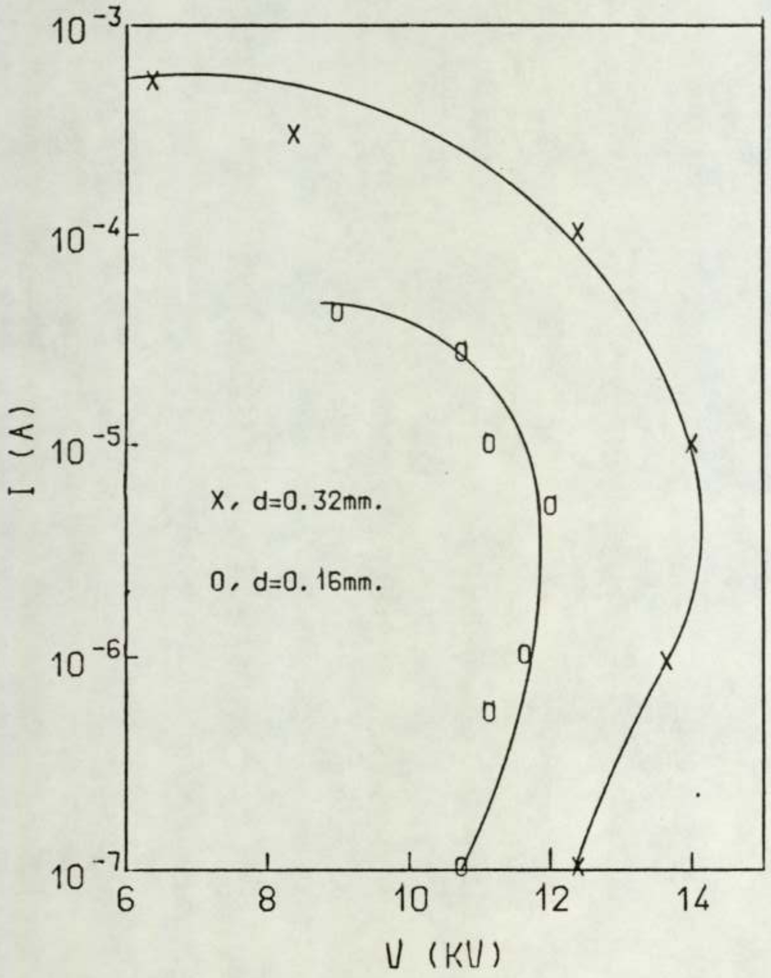

"NEGATIVE-RESISTANCE" CHARACTERISTICS
(FROM HURLEY)$^{(45)}$

Fig.2.5

2.4 Evidence in Favour of a Non-Metallic Emission Regime

A number of recent experiments have provided a diverse body of evidence which cannot be explained by simple metallic emission processes, but instead suggests a non-metallic emission regime involving surface oxide layers or insulating inclusions.

In 1972, Cox & Wort(33) developed a refined method for locating and mapping the constant-current contours of emission sites on broad-area electrodes, using two 0.5 mm diameter anode probe holes, one behind the other; thus allowing each site position to be determined, to an accuracy of 0.1mm, by moving the anode assembly relative to the specimen surface. An interesting early result was obtained by using this equipment to plot the emission from a simulated site - consisting of a tungsten tip inserted into a planar copper surface. Emission was recorded from a position close to, but definitely separate from, the artificial protrusion; thus showing that the most likely source of emission, from a field enhancement point-of-view, is not necessarily the actual emitter.

Later, Cox(34) improved the probe-hole facility and incorporated it into a U.H.V. scanning electron microscope (S.E.M.). Using this system, emission sites were first located by scanning the specimen in a raster pattern beneath a large anode aperture; a smaller probe aperture was then selected, and the specimen positioned such that the current collected by the movable probe was maximised. Repeating this procedure for smaller and smaller specimen - anode gaps, allowed the electron trajectories from the beam centre to be plotted and, thus, the site co-ordinates determined to within 20 microns. With the probe hole moved out of the way, this area was examined using the S.E.M. Results showed that, even though the F.N. plots for individual sites gave β-factors of >100, no surface features could be identified which would give such high field-enhancement. Dust particles were found to be the cause of many emission centres; these were largely prevented by preparing, and installing, the specimen under ´clean-room´ conditions. Subsequent sites were found at cracks or grain boundaries, as in Fig.2.6(i) (with the associated ´contour´ map of the emission site shown in Fig.2.6(ii)), or, despite attempts at reducing field intensification near the specimen sides by profiling the electrodes, at the specimen edge. The same technique was used by Cox & Williams(35) to examine emission sites on unpolished stainless-steel, which was found to give an exceedingly strong emission, with a β-factor of 735, from a 5 micron diameter insulating particle.

An extensive amount of data has been gathered on the breakdown initiating effects of microparticles. In particular, Donaldson & Robinowitz(36) found that the thermal decomposition of glass generates particles having diameters between 10^{-8}m and 0.5×10^{-6}m, and containing a variety of elements including sodium, potassium and boron. These particles were not removed during a system bakeout at 725K, and were found to reduce breakdown voltage by up to 50% if present on an electrode surface. Pakrovaskaya-Soboleva et al.(37) have demonstrated that insulating inclusions (FeS, Al_2O_3, SiO_2 and alumina-silicate glass) added to pure iron cathodes produce 20 - 30% degradation in breakdown voltage; with

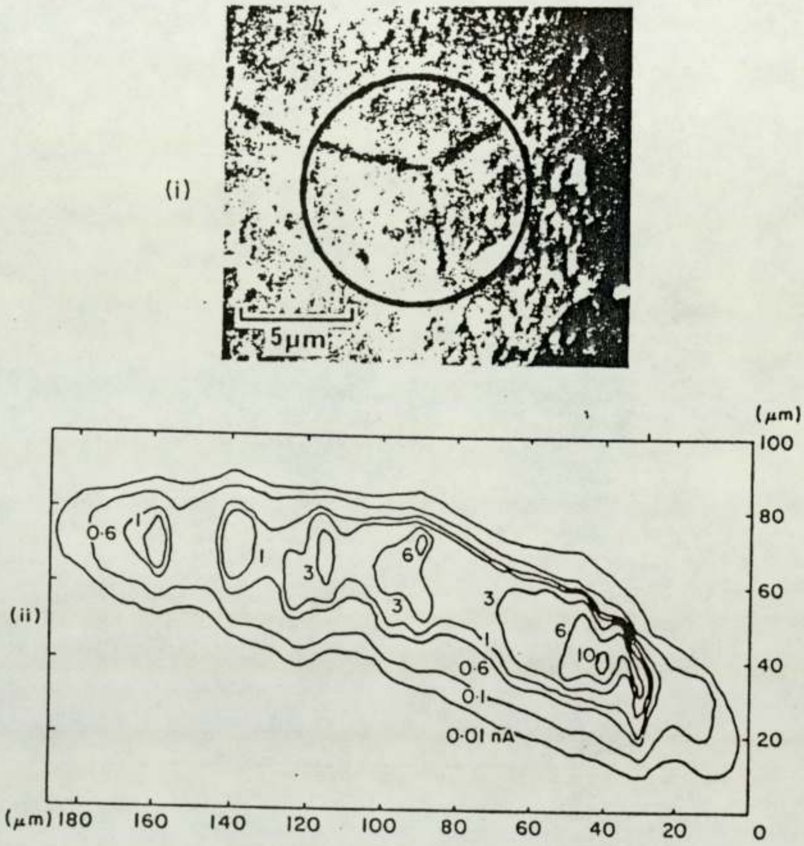

Fig.2.6 (i) A scanning electron micrograph showing the region of an electrode surface (circled) that has been identified as containing an emission site, and (ii) the complementary distribution map of the field emission current associated with this site. (from Cox)(34)

large particles, 50 - 500 μm in diameter, giving the greatest and longest-lasting reduction. Confirming the earlier work of Maskrey & Dugdale(38), they then suggested that breakdown events were localised to regions containing the inclusions. In the case of refractory SiO_2 particles, breakdown events fused the iron near the inclusion; whereas, for cathodes having the more easily melted FeS particles, it was the inclusion material which melted.

In 1972, Farrall et al.(39,40) performed experiments using a phosphor screen as an anode in order to locate the emission sites. After location, the screen was replaced by an anode coated with lead, some of which would then vapourise under the bombardment of the emitted electron beams. They theorised that, close to the cathode emitter, some of the lead vapour would be ionised and, hence, be drawn close to the emitting region; effectively "tagging" the emitter. Later location of these leaded areas showed them to be concentrated on isolated insulating particles. More recently, Farrall et al.(41) have investigated the effect on voltage hold-off of deliberatly contaminating copper electrodes with alumina powder. When 50 μm diameter particles were present, prior to the occurrence of any breakdown events, emission currents of 10^{-5}A were obtained at voltages 30% lower than those required for uncontaminated surfaces. Pulsed breakdowns at high current led to the eventual convergence of the emission properties for all surface treatments. Later examination showed that metal-insulator boundaries were associated with the breakdown events, since, when observed in the S.E.M., all the particles showed signs of melting at the edges; also observed were cavities, which appeared to be places from where particles had been ejected.

A different type of observation was due to Hurley & Dooley(42), they carried out an investigation into the spots of light which seem to appear on cathode surfaces when pre-breakdown current flows, the same phenomena as briefly noted by Klyarfell & Pokrovskya-Soboleva(43). Using broad-area copper electrodes, their experimental technique involved observing the spots of cathode light (K-spots) through an image intensifier, and then measuring a simplified optical spectrum using a photo-multiplier in conjunction with a series of filters. The type of spectrum that was typically obtained is shown in Fig.2.7(i), and corresponds neither to black body radiation nor to any obvious discharge spectra. It was, however, suggestive of electroluminescence, normally a ´non-metallic´ phenomenon. A measurement of the applied voltage-light intensity relationship over a reasonable range of field, confirmed that the optical intensity of these K-spots seemed to obey the Alfrey-Taylor(44) expression, characteristic of electroluminescent cells. Hurley(45), in a later experiment using a pointed anode probe, demonstrated that electron emitting sites on copper electrodes are also the source of the observed elctroluminescence. Hurley & Dooley(46) then examined electrodes of O.F.H.C. and high-purity copper, molybdenum, stainless steel and duralumin. All of these gave similar results, with the authors finding that discharges were sometimes seen to occur from within the light emitting areas, and could be correlated with the onset of discharge flares and gap breakdown events. In the case of copper, straight tracks were sometimes seen originating from the K-spots which were believed to be caused by uncharged particles being ejected from the electrode surface; this optical activity of

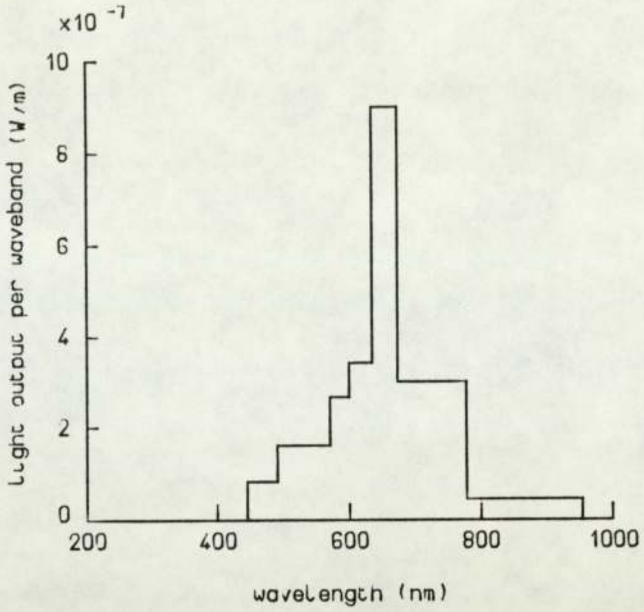

(i) SPECTRUM OF OPTICAL EMISSION FROM CATHODE SPOT

Fig.2.7 (from Hurley & Dooley)(46)

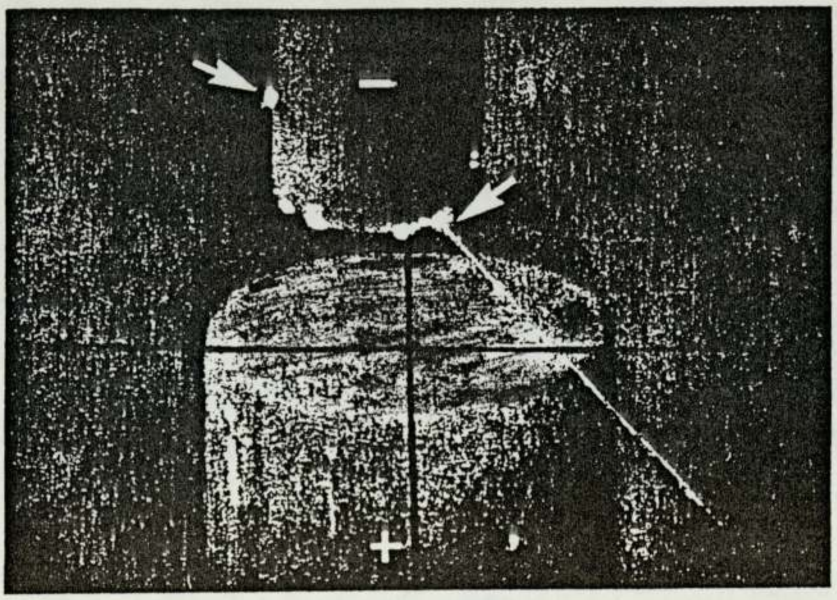

(ii) An open-shutter photograph of an electrically stressed planar high voltage gap showing both anode and cathode spots. Also shown arrowed are flares and discharge tracks emanating from cathode-spots.

a HV gap is shown in Fig.2.7(ii).

Subsequently, experiments by Athwal & Latham(47) using an improved anode-probe technique, similar to that of Cox(34) in making use of an in situ S.E.M., also found indications that electron emission takes place from sub-micron to micron-sized impurity particles adhering to the electrode surfaces; rather than from the numerous field-enhancing features, such as polishing marks, which were also present on the electrode surface. Here again, no projections were found capable of yielding the high β-factors required by the associated F-N plots. The technique was developed for studies in a conventional S.E.M., and used three progressively sharper anode probes to home-in onto the emitting area, giving an estimated resolution of 3 - 4μm. Subsequent X-ray analysis of the emission zone, using an associated facility coupled directly to the S.E.M., showed the presence of compounds (probably oxides) of the electrode metal and some foreign elements, particularly silver.

Early work on the electron energy distributions associated with broad area emission was published by Allen & Latham(48), at about the same time as Hurley´s work on electroluminescence. This has shown that the electron energy spectrum for each emission site, is indeed incompatible with emission from a metallic microprotrusion. In fact, as will be shown, it is more characteristic of a semi-conducting emitter.

2.5 Energy Distributions of Field Emitted Electrons

2.5.1 Field Emission from Metals

Early work using metallic micro-point emitters by, for example, Henderson & co-workers(49,50) and Müller(51,52), seemed to obtain good experimental agreement with the theoretical energy distribution used in the derivation of the F-N equation. However, in 1959 Young & Müller(53), using an improved retarding potential analyser, obtained a much narrower energy distribution from emitted electrons than that assumed in the F-N model.

In the previous derivation of the F-N equation, the tunnelling probability was determined by the normal component of energy, i.e. that directed towards the surface. However, for anything other than a perfectly plane emitter-collector geometry, the transverse component of energy, conserved in the tunnelling process, is transferred to the normal direction once the electron has left the emitter. Accordingly, Young(54) re-formulated the F-N equation, using free-electron theory, in terms of the total-energy distribution. By re-defining the parameters N(W)dW, P(W)dW etc., in terms of the number of electrons having a total energy in a particular range, he obtained theoretical expressions characterising the total-energy distibution, including the full-width-at-half-maximum (F.W.H.M.) of the distribution at zero temperature. Fig.2.8(a) shows both the normal and total theoretical energy distributions for a metallic emitter, while Fig.2.8(b) shows the theoretical and experimental total energy distributions.

The effects on the energy distributions of non-free-electron behaviour in metals, have been explained by various authors - such

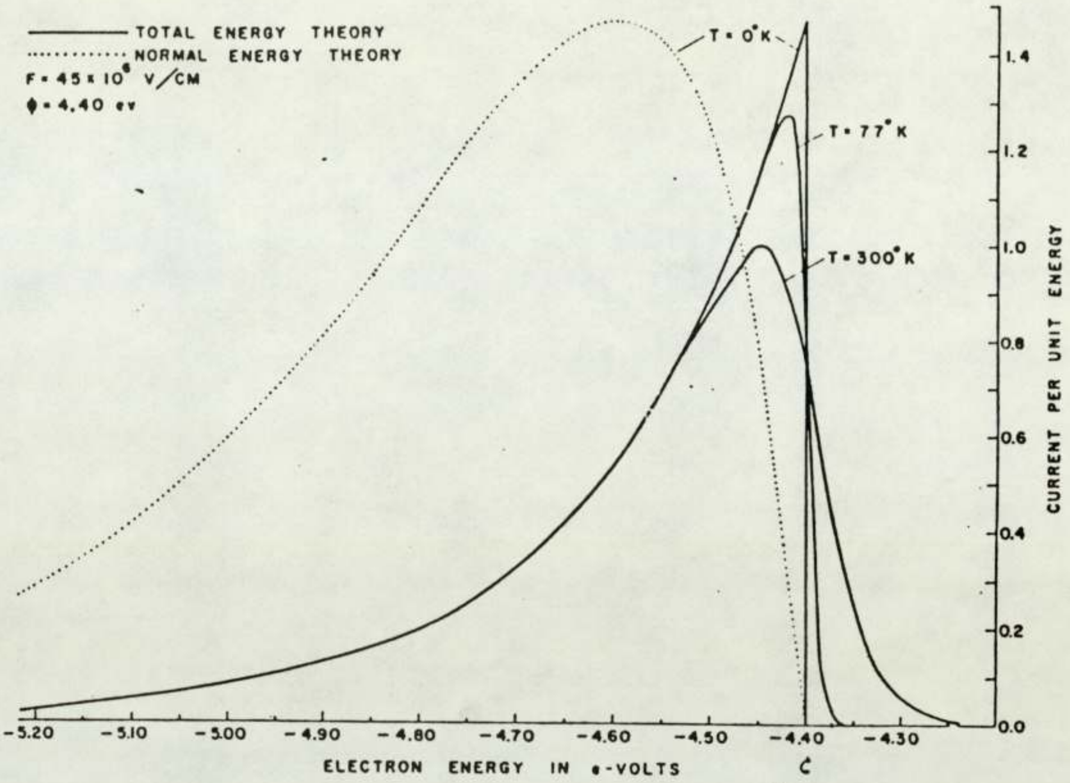

a) Total- and normal-energy distributions for field emitted electrons. The 300°K curve is arbitrarily normalized.

Fig.2.8 (from Young)(54)

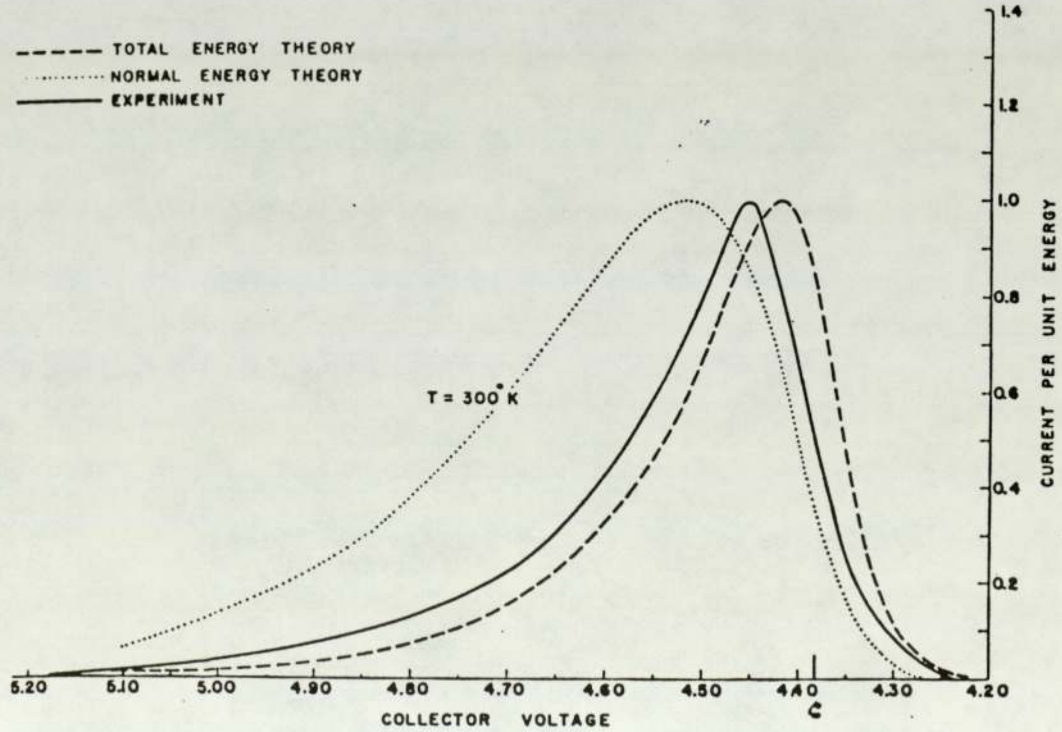

b) Theoretical and experimental total-energy distributions of field-emitted electrons at room temperature. The theoretical normal-energy distribution is shown for comparison. All three curves are arbitrarily normalized.

as Swanson & Crouser(55), Nicolou & Modinos(56) and Dionne & Rhodin(57)- as being due to a combination of band-structure effects, local variations in the density of states at the metal-vacuum interface, relaxation processes involving bulk scattered electrons(58), and energy broadening due to tunnelling life-times. However, these phenomena give only small perturbations in the resulting F.E.E.D., and no observable effect on the F-N plot.

2.5.2 Field Emission from Semiconductors

A number of additional factors have to be taken into account when considering the emission process from semiconductors:

a) the greater complexity of the band stuctures
b) the presence of inter-band surface states
c) the penetration of the external field into the semiconductor surface layer
d) the ohmic potential dropped within the emitter, due to its higher electrical resistance.

In a theoretical treatment of field emission from semiconductors, Stratton(59,60,61) assumed an F-N type surface barrier, with a modified image-force correction to account for the dielectric constant of the material, and surface state effects on field penetration; although not emission from these states. Briefly, he concluded that the excess charge which may be stored in these surface states would produce a field giving rise to energy-band bending, and that the application of an increasing external field would produce a number of distinct phases in the behaviour of the F.E.E.D. These stages may be seen in Fig.2.9(a)-(d), with the

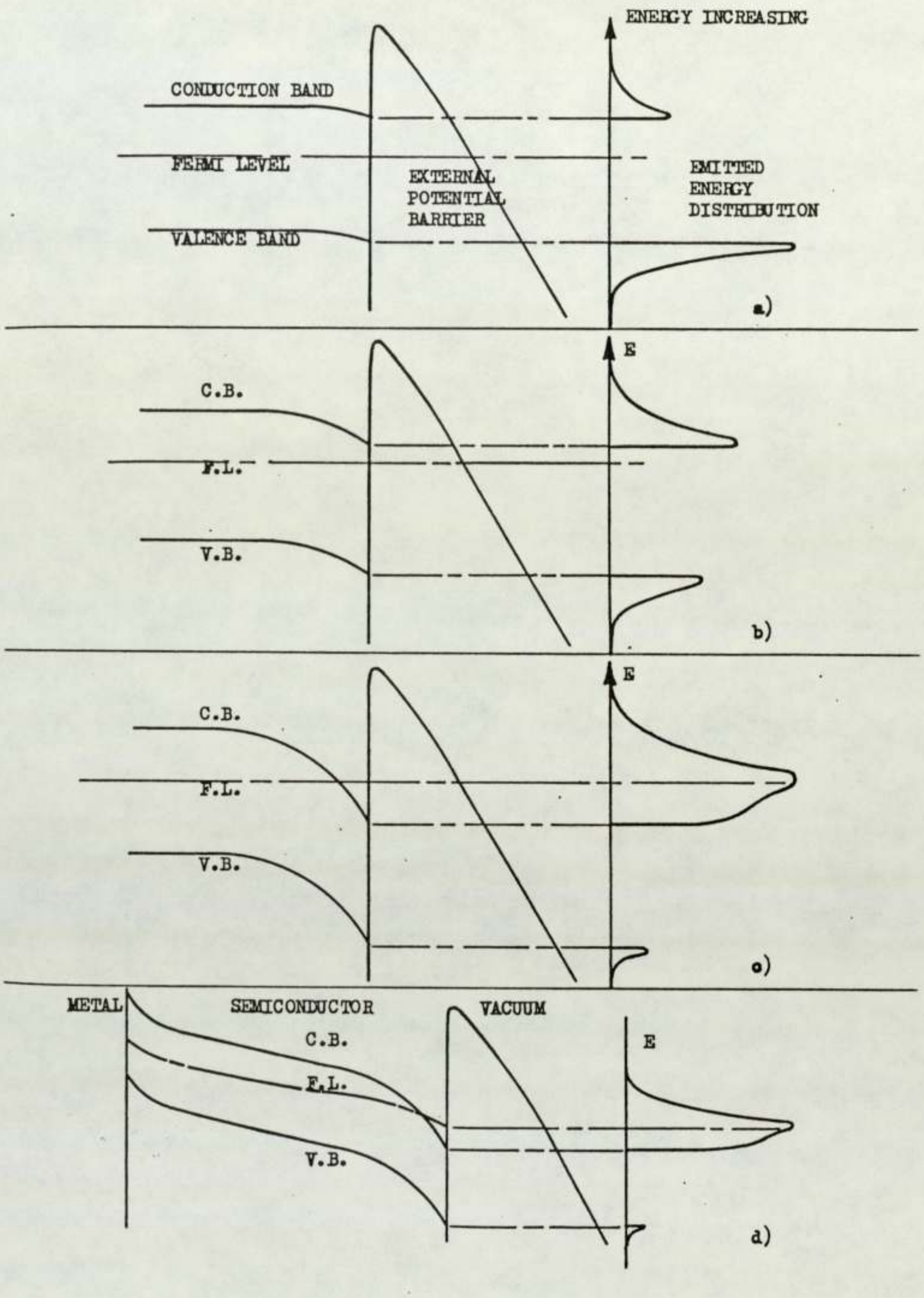

Fig.2.9 Stages In The F.E.E.D. From An Idealised Semiconductor With Increasing Field

effect of any particular field value depending on the semiconductor properties: viz, the width of the band gap, position of the Fermi level, density of states in the valence band etc. Initially, field emission is possible from the valence band or the Boltzmann tail of electrons in the conduction band, this situation would produce a two peaked F.E.E.D. and is shown in Fig.2.9(a). As the remaining surface states fill, field penetration causes band bending and the movement of both peaks to lower energies (Fig.2.9(b)). At higher fields, the conduction band will become degenerate, due to the conduction band being pulled below the Fermi level (Fig.2.9(c)), resulting in an enhanced emission current; with the major contribution being from the conduction band peak, which should then remain fixed for additional increased field. Fig.2.9(d) allows for the ohmic voltage drop occuring within the semiconductor, and the subsequent variation in Fermi level, together with additional band bending caused by work function differences.

Stratton also deduced the current-voltage characteristic to be expected from his assumptions: at low fields, emission occurs from the valence band; while, at high fields, emission is predominantly from the conduction band - both of these cases giving essentially linear F-N plots. For the case of intermediate fields, theory predicted that the current should increase more rapidly as the conduction band population increases. However, agreement between Stratton´s theory and experimental current-voltage measurements was rather poor for this field range, a factor which led Baskin et al.(62) to consider the effect of carrier conduction on the emission current, giving qualitative agreement with experiment, but with smaller saturation currents than expected. Further experimental work on F.E.E.D.´s from several semiconductors, by authors such as Arthur(63), Hughs & White(64), Salmon & Braun(65) and Lewis & Fischer(66), demonstrated that the observed distributions were wider and of a different shape to those predicted in Strattons theory.

Modinos(67), in 1973, included emission from surface states by extending a model of the semiconductor surface proposed by Handler(68), and shown in Fig.2.10; here it was assumed that a uniformly dense band of surface states extended right across the band gap and into the valence and conduction bands. The application of an F-N type barrier on the resulting density of states function allows the derivation of expressions for the emission current density and energy distribution; thus, Fig.2.11 shows the theoretical F.E.E.D.´s for intrinsic germanium at different field values. This theory has given reasonable agreement when tested against the experimental work of Arthur(63) and Shepherd & Peria(69) on germanium, Sykes & Braun(70) on lead telluride, and Richon(71) using zinc oxide. However, significant shifts from the Fermi level in the F.E.E.D.´s with increasing field were not noted, possibly due to the fairly low current densities used.

2.5.3 Field Emission through Adsorbates

Any surface not specifically cleaned will be covered by adsorbed gas molecules. Duke & Alferieff(72) have shown, theoretically, that such coverage of a field-emitting region will considerably modify its electron energy distribution. The major

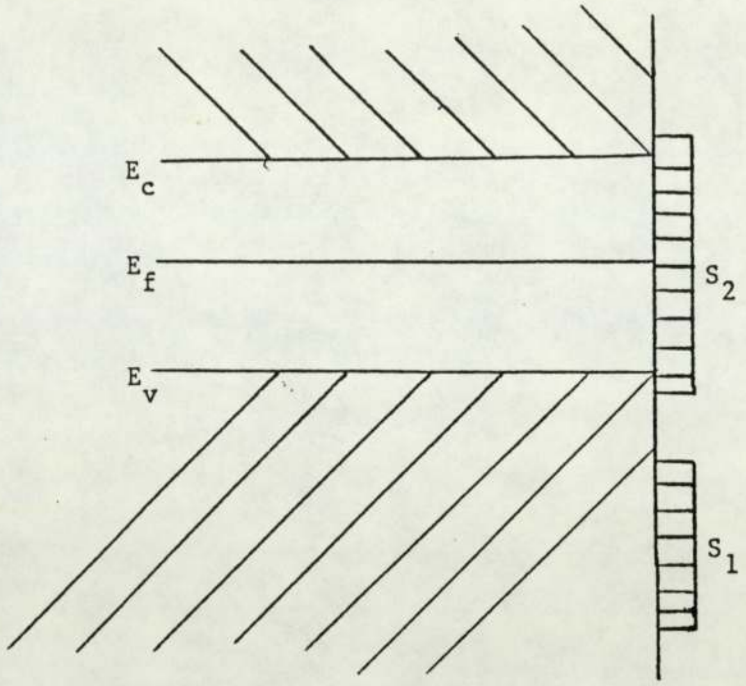

Fig.2.10 Surface States Of Ge (according to Handler)(68)

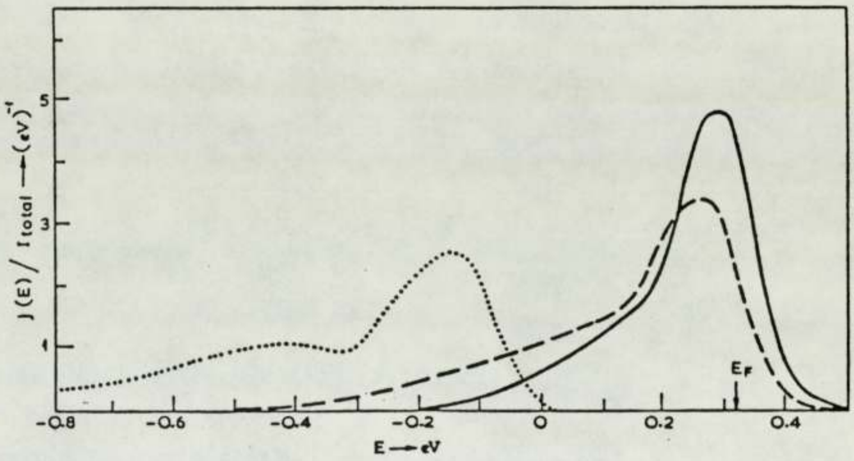

Total energy distributions for $u_b = 0$.

Solid line: $F = 0.2$ V/Å, $V_s = -10\,kT$, $E_F - F_t < kT$, $I_c = 1.9 \times 10^{-12}$ A cm^{-2}, $I_s \simeq 1.75 \times 10^{-3}$ A cm^{-2}, $I_v = 9.98 \times 10^{-4}$ A cm^{-2}, $\log I_{total} = -2.56$.

Broken line: $F = 0.3$ V/Å, $V_s = -7.5\,kT$, $E_F - F_t < kT$, $I_c = 1.36 \times 10^{-8}$ A cm^{-2}, $I_s = 9.14$ A cm^{-2}, $I_v = 7.04$ A cm^{-2}. $\log I_{total} = 1.21$.

Dotted line: $F = 0.4$ V/Å, $V_s = 10\,kT$, $E_F - F_t = 16.25\,kT$, $I_c = 13.15$ A cm^{-2}, $I_s = 6.98 \times 10^{2}$ A cm^{-2}, $I_v = 6.98 \times 10^{2}$ A cm^{-2}, $\log I_{total} = 3.15$.

Fig.2.11 Energy Distributions From Intrinsic Ge (from Modinos)(67) effects of adsorbed gas are the change in real work function, caused by the alteration of the surface barrier height, and the change in the effective barrier thickness, due to the attractive potential well of the adatom; these changes could drastically alter the electron tunnelling probabilities, and thus affect both F-N plots and energy spectra.

Application of quantum mechanical double-barrier potential theory by Merzebacher(73), allows some predictions to be made about the various ad-atom effects. Various adsorbates, such as hydrogen, oxygen, germanium and alkaline earth metals, on tungsten tips have been used to check this theory(58). Swanson & Crouser(74) observed the F.E.E.D.´s produced by the adsorbtion of large molecules onto various faces of tungsten or molybdenum; the important result from this work was that the peak shifts caused by the adsorbates were a linear function of applied field, as shown in Fig.2.12. Also, changes in the adsorbate-substrate configuration could be brought about by thermal or field induced phenomena, thus affecting the energy distributions.

2.5.4 Field Emission from Broad-Area Electrodes

Measurements of F.E.E.D.´s from broad-area electrodes were first obtained by Allen & Latham(48), using a high-resolution, hemispherical differential spectrometer under U.H.V. conditions. Compared to a reference tungsten microtip, typical spectra from sites on copper electrodes showed three important differences. Referring to Fig.2.13(i)-(ii): firstly, all electrons being emitted from states well below the bulk-metal Fermi level; secondly, a considerably greater half-width (F.W.H.M.) than for

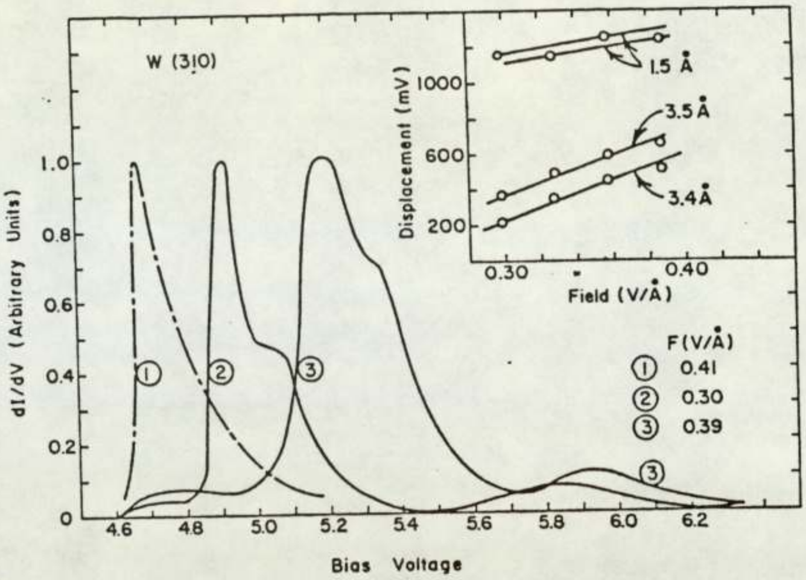

TED spectra pentacene on W (310); curve 1 is clean, $\Delta\phi = -1.7$ eV, $B = 2.0$; $I_a/I_c = 680$.

Fig.2.12 F.E.E.D.'s Produced By Adsorbates On Tungsten (from Swanson & Crouser)(74)

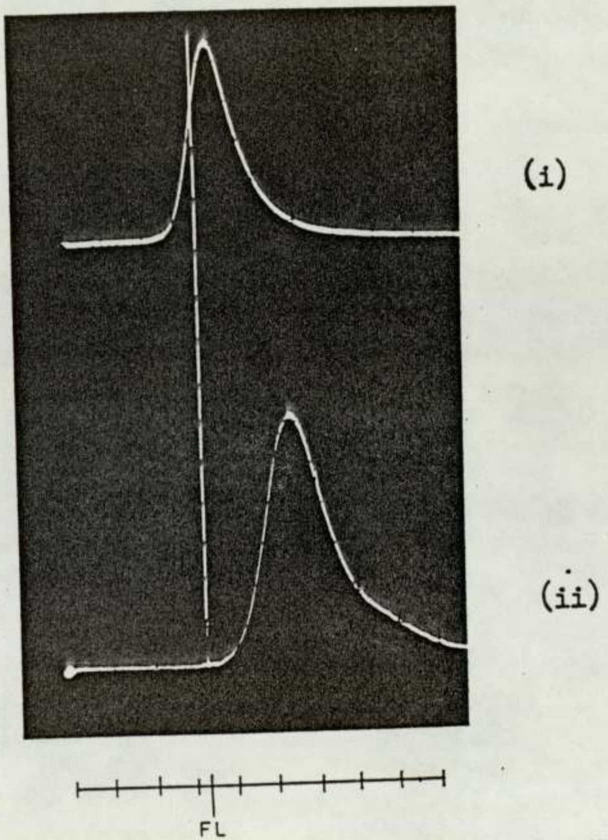

Fig.2.13 Electron energy spectrum obtained from (i) a reference tungsten emitter and (ii) a site on a broad-area copper cathode. The position of the Fermi level (FL) of each emitter is also shown. Electron energy in eV, 0·2 eV/div, is x axis (going from high energy to low energy left to right). Electron current per unit energy is y axis.

(from Allen & Latham)(78)

metallic emission processes; and thirdly, a more symmetrical spectrum lacking the sharp high-energy edge characteristic of metallic F.E.E.D.´s.

The resemblance of broad-area energy distributions to those of semiconducting tips, led to an early model by the authors explaining these results in terms of very localised semiconductor impurities embedded in the electrode surface. Further work by Latham and his co-workers(75,48), and particularly Athwal(76), reported a considerable variety of emission effects: such as multi-peaked and variable distributions, switching phenomena, non-linear F-N plots and F.E.E.D. shifts with applied fields. In the next section, the development of a model to explain these effects is outlined; culminating in the hot-electron emission model of Bayliss & Latham(77), described in Section 2.7.

2.6 Non-Metallic Field Electron Emission Models

2.6.1 General Assumptions

This section presents the various models which have been proposed to describe conduction through "insulating" inclusions. Except for Hurley´s filament model, they all consider the emission of hot electrons over the potential barrier at the insulator-vacuum boundary; a proposition which is necessary because the fields required to obtain a measurable pre-breakdown current are normally too low, by a factor of at least 100, for barrier tunnelling to occur. A further similarity between the models lies in the energy band diagrams used to describe the electron conduction processes, although the underlying mechanisms may be quite different.

2.6.2 Band Theory Interpretation.

A band theory model was first developed by Latham and co-workers$^{(75,78)}$ in 1978, where early electron spectrometry results were interpreted in terms of a semiconducting or insulating impurity embedded in the surface of a metal electrode, i.e. the regime shown in Fig.2.14. Electron microscopy studies$^{(35,79)}$ suggest that these micro-inclusions tend to be oxides of the substrate metal, or oxides of elements which may be associated with the smelting of the substrate metal, or possibly carbon which is known to accumulate at grain boundaries during the metal preparation; equally, it could result from electrode polishing operations when diamond paste is used.

In the absence of any applied field, the idealised energy band representation of the regime would appear as in Fig.2.15(i), where the band bending at the metal-insulator and insulator-vacuum interfaces was assumed to arise from work function differences and the presence of surface states. With a high applied field, there would be field penetration of the micro-inclusion to the metal substrate, resulting in the band structure and surface potential shown in Fig.2.15(ii). Electrons were then envisaged as tunnelling from the metal into the bottom of the insulator conduction band, and being "heated" by 2 - 3eV in the insulator bulk as a result of the penetrating field. Hence, emission was considered as being due to enhanced tunnelling through the top of the surface potential barrier by the hot electrons. A second low energy peak sometimes appeared in an electron energy spectrum, the authors explained this as variable surface ad-atom resonance tunnelling, as was

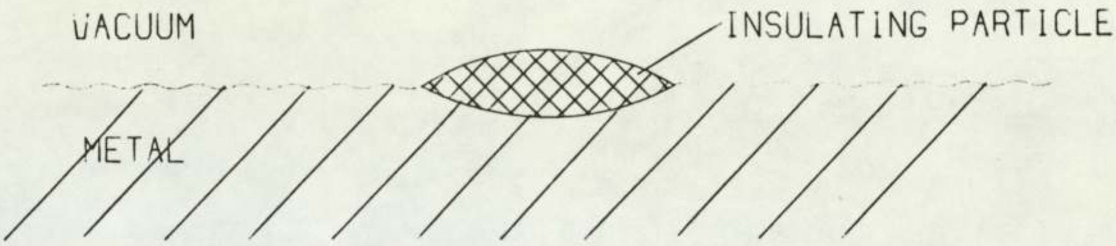

Fig.2.14 SURFACE IMPURITY EMBEDDED IN METAL SUBSTRATE

(from Allen & Latham)(78)

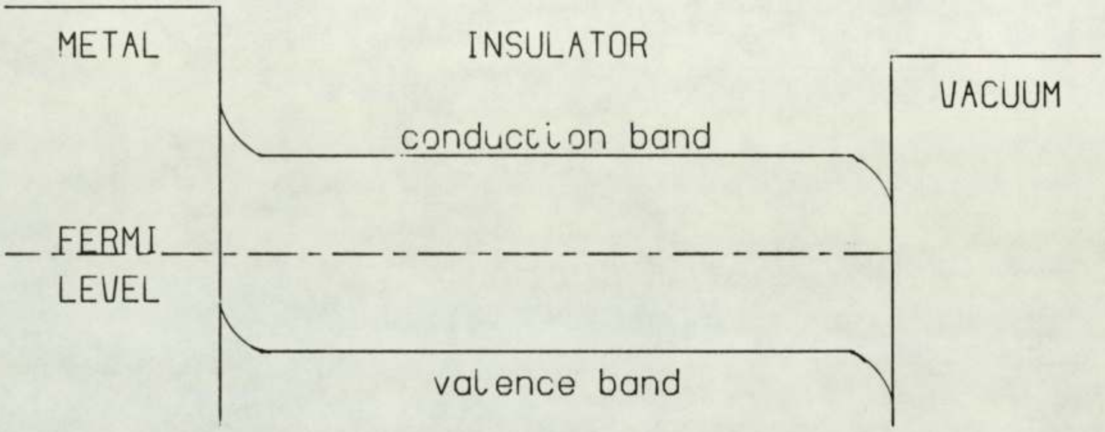

(i) ZERO APPLIED FIELD

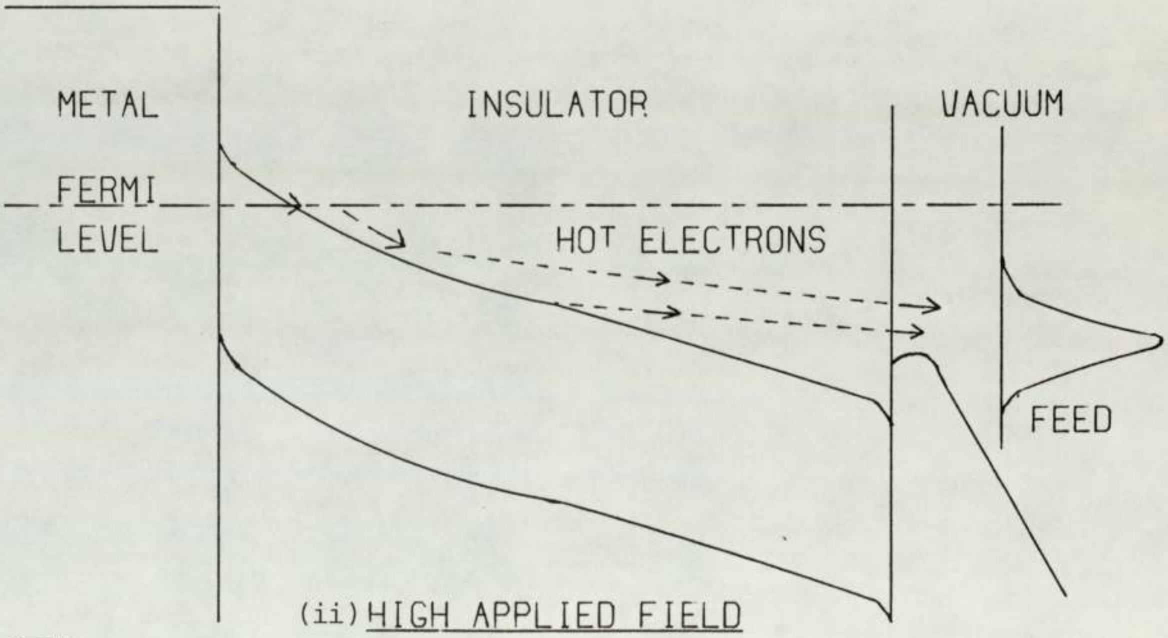

(ii) HIGH APPLIED FIELD

Fig.2.15

ENERGY BAND STRUCTURE FOR IMPURITY INCLUSION

(according to Allen & Latham)(78)

described by Duke & Alferieff(72). The model also included a level of interband impurity states near the bottom of the conduction band, tunnelling electrons could then either penetrate the barrier directly or go via the impurity energy level.

Consideration of this model shows that an F-N type I-V characteristic will be produced without having to postulate field enhancement, since the hot electrons will experience a much reduced surface barrier. Also, as experimentally observed, the electron spectra will clearly be shifted below the substrate Fermi level. Further support for this model was provided by Allen et al(75), who noted that the 2 - 3eV acquired in the penetrating field by hot electrons was appproximately that required to produce the electroluminescence observed by Hurley & Dooley(43).

2.6.3 The Filamentary Model.

Using the same impurity micro-regime as the above model, Hurley(45) based his work on the idea of electroformed conducting filaments, developed by Dearnaley(80) for explaining the behaviour of some dielectric devices. Certain semiconducting and insulating materials, particularly metallic oxides, nitrides and fluorides and amorphous semiconducting glasses, of nanometre to micron thickess show a "switching" phenonema when a high field (10-100 $MV.m^{-1}$) is applied via surface electrodes. The measured resistance may change by a factor of as much as 10^{-8} when the device changes from the non-conducting "off", to the conducting "on" state. Such a switching event is also accompanied by various external phenomena, viz. microscopically localised electroluminescent and electron emission processes. If the field was applied for sufficient lengths of time, the conducting filament became "electroformed" through the dielectric, in the same way as Dearnaley et al(80) described, the atoms or molecules becoming permanently, or semi-permanently, rearranged. Electroforming times were typically in the 1 - 10ms range, whereas switching times were usually $<1\times10^{-6}$s. The filament diameter was shown to vary with the length of the filaments, such that 40nm to 500 μm thick films gave filament diameters of 1nm to 50 μm(80,81).

Hurley´s emission model assumes a random distribution of surface impurity inclusions, some occurring at regions where the field is locally enhanced by a factor β, such as at cracks or grain boundaries. An impurity inclusion with dielectric constant ε will then have an internal electric field given by $\beta.E/\varepsilon$ which will allow electroforming of filaments when the average field E is about $100MV.m^{-1}$ and, if β and ε are both about 5 - 10. Fig.2.16(a)-(c) show various phenomena which may be observed as a result of the electroformed filament model: it can be seen that the essentially metallic filament behaves as a whisker embedded in a dielectric, which may produce sufficient field enhancement at its vacuum interface for field electron emission to occur. Extending the analogy with the Dearnaley filamentery model, Hurley assumed that high resistance

spots in the formed filament would give rise to "hot" carriers which could then be scattered into the surrounding oxide and produce electroluminescence through impact ionisation or recombination processes, as discussed by Hickmott(82). The injection of electrons from the metal substrate into the filament, was assumed to arise from a number of semiconductor-metal junction

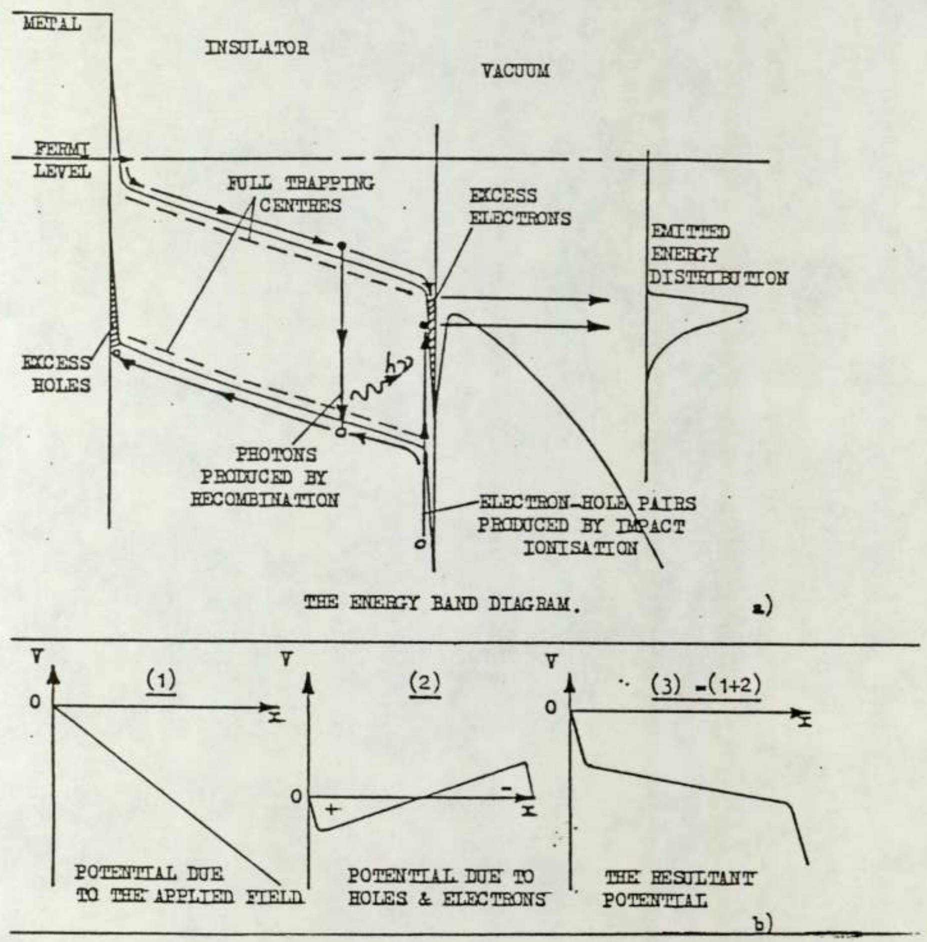

Fig.2.17 (from Athwal & Latham)(47)

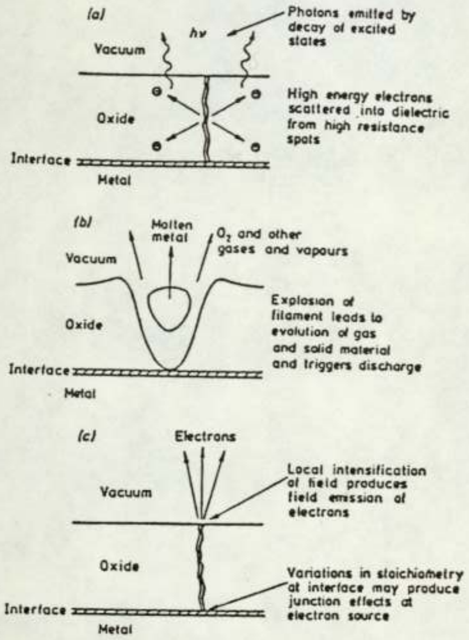

Production of electroluminescence, vacuum breakdown and electron emission from electroformed conducting filaments in oxide impurities. (*a*) Electroluminescence. (*b*) Vacuum breakdown. (*c*) Electron emission.

Fig.2.16 Phenomena Expected As A Result Of The Filament Model (from Hurley)(45) effects; these were also held responsible for some of the non-linear F-N plots and the shifts in the electron energy spectra which have been experimentally observed.

Several experimental observations could be explained on the basis of this model: Jüttner et al$^{(83,84)}$ demonstrated that electron emission is suppressed by "active" gases such as oxygen, carbon monoxide and nitrogen, while Hurley noted that the associated electroluminescence was also suppressed by raising the ambient pressure. Thus, these effects could be attributed to the "poisoning" mechanism proposed by Dearnaley$^{(85)}$, in which absorbed gases fill the oxygen vacancies that are thought to exist in a conducting filament. Discontinuities in the I-V characteristics and marked deviations from F-N theory, could be attributed to additional filaments forming as the field was raised, or to thermal rupturing and reforming of filaments already present. The thermal rupture of filaments provides a mechanism whereby eventual breakdown would occur based on the thermal instability model of Cook$^{(81)}$, where, at a certain current level, the filament temperature would rise high enough to cause a molten impurity particle to be ejected into the electrode gap. Evidence for this process was reported by Hurley & Dooley$^{(46)}$. The current controlled "b"-sites were held to be the result of filaments which either terminated short of the insulator-vacuum boundary, or short of the metal-insulator junction. In both cases, the emission was believed to be dependent on the formation of a reversed biassed rectifying contact at the metal-insulator junction, which might exhibit negative resistance as the voltage was increased.

2.6.4 The Insulator Switching Model

Although each of the previous models provides a reasonable explanation for many of the recorded observations, they both have evident limitations. In particular, the energy band model of Fig.2.15(ii) does not readily explain how hot electrons are able to pass through a micron-sized impurity without losing most of their energy in phonon scattering processes; neither is it clear that a sufficient field exists for tunnelling at the metal-insulator contact. Equally, the filament model offers no detailed explanation of the electron spectrometry data, and it is also improbable that any filament would be thin enough to give adequate field-intensification at its end without melting, since a β-factor in the range 200-400 is still required for F-N type electron emission.

Athwal & Latham(47) then developed a new model to incorporate the best features of both previous models, and also the new observation that emission sites usually required a lower field to maintain conduction than to initiate them. This model was based on the phenomena of 'Ovshinsky switching'(86,87), where an amorphous insulator switches from low conductivity ($<10^{-7}\,\Omega^{-1}\mathrm{cm}^{-1}$) to a high conductivity ($>10\,\Omega^{-1}\mathrm{cm}^{-1}$) state in about 1ns. Film thicknesses of 0.1 - 10 μm sandwiched between metal electrodes, requiring a potential difference of 1 - 10V across the electrodes to initiate switching, were studied. Chalcogenide glasses have been found to be the most useful materials commercially, but a large number of amorphous insulators have been investigated by Coelho & Debeau(88).

Although the surface insulating impurity was assumed to be essentially amorphous, so that energy band theory should not strictly be applicable, Adler(89) suggests that the band structures shown in Fig.2.15 are nevertheless justified if additional localised energy states are included in the energy gap. Athwal & Latham(47) applied the concepts of switching, as discussed by Adler et al(90), to modify the energy band diagram of Fig.2.15(ii) to that of Fig.2.17(a), the highly distorted shape resulting from the super-position of the potentials due to space charges and the penetrating field shown in Fig.2.17(b). The space charges were seen as arising in the insulator from an excess of electrons near the vacuum boundary and from an excess of holes close to the metal-insulator junction, similar to the manner envisaged in the double injection dynamic conduction model due to Mott(91). The barrier at the metal-insulator contact would then be thin enough to allow electron tunnelling into the insulator; where rapid thermalisation, by impact with the insulator structure, enables these electrons to cross the low field region of the insulator bulk in the bottom of the conduction band, where their lifetimes may be $<10^{-8}$s(92). Near the vacuum boundary, the second high field region re-accelerates (heats) the electrons so that they pass over the top of the insulator electron affinity barrier and so into the vacuum space. Hence, the two primary objections to the original energy band model were overcome, and the poisoning phenomena described by Jüttner could still be accounted for in terms of electron traps or oxygen vacancies.

Conduction was believed to be started by the tunnelling of a few electrons into the insulator when the local field was above a critical value, impact ionisation processes then induced an avalanche effect. The electrons and holes so created would drift in opposite directions, the holes to the metal interface and the electrons to the vacuum boundary, where they would be caught in the large number of localised interband trapping levels. Thus, the two internal boundary fields would be enhanced and the electron tunnelling probability increased.

The large population of holes moving towards the metal contact required by this model, were assumed to be generated in the high-field region near the vacuum boundary from impact ionisation of the insulator lattice by hot electrons arriving from the metal. This process was believed to lead to electroluminescence, when some of the holes and electrons may recombine in trapping states(92). Other suggested light producing processes were the impact, or field, ionisation of luminescent centres at the insulator surface.

In order to satisfy the current density requirements for electro-forming found by Peterson & Adler(93), Athwall & Latham(47) had to further postulate that, once switched on, the conducting filament underwent a forming process similar to that assumed by Hurley(44), in which the filament became more crystaline. However, calculations show that in order to obtain observed currents as low as 10^{-14}A, the film thickness would have to be of the order of 3×10^{-12}m, which is clearly impossible. Also, it may not be possible for the necessary quantity of holes to be produced or, due to various recombination processes, be possible for them to reach the metal-insulator contact. The latter fact was recognised by the authors, and the model as presented did explain, in a general way, a great many of the observations. In particular, the emission site switch-on and electroluminescence were features incorporated into its development, although it should be noted that emission sites do not always exhibit elecroluminescence, as will be discussed in Chapter 5. In subsequent studies by Latham & co-workers(94), concerning emission from artificially produced carbon sites, the authors explained their results using a variation on this model but assuming a modified metal-insulator-metal emission regime. High current "a"-sites and current controlled "b"-sites clearly fit the model in a general sort of way, while some of the non-linear F-N plots may be explained by assuming changes in the structure of the conducting channel. For example, the crystallinity may change, or the channel width may be restricted by the size of the insulating surface inclusion. The shift observed in the electron energy spectrum arises from the same effects as in the simple band model, i.e. from the sum of the potentials dropped at the metal-insulator contact, at the insulator-vacuum boundary and in the insulator bulk. Although it is not so clear that the correct functional relationships result from this model, the I-V functions describing only the injection of electrons have been found to fit the experimental data quite well.

Some of the anomalous phenomena, for example F-N plots with sharp discontinuities, and the hysteresis effects observed by Chatterton(24) etc., may be attributed to either changes in the surface barrier height brought about by gas desorption, or to the scattering of electrons out of the conducting channel into the surrounding higher resistivity material. In relation to some of these phenomena, it should be emphasised that it is unlikely that emission from single sites has been investigated in the past; since, as shown by Bayliss & Latham(94,95,96), what was previously considered to be a single emission site, usually consists of several sources of emission current (sub-sites) and that each of these may switch on and off at random, especially for currents $>10^{-7}$A.

2.6.5 Critical Observations.

All of the preceding models tend to be predominantly qualitative, and are particularly speculative about the nature of the potentials dropped across the metal-insulator contact, and across the bulk of the insulator. In fact, none of the models give any real idea of the functional form such potential differences might take as the current varies, although for the switching model Athwal & Latham(47) and Latham(97) indicated that if the current was dependent upon the potential barrier at the contact, then an approximate F-N relationship should follow; this property was also supposed to account for the F-N character of the emission current. However, Latham & Bayliss showed(95,77) that a detailed model based on the emission of hot electrons over the vacuum surface potential barrier is sufficient to account for the observed phenomena without additional complications, such as high current densities in the conducting channels.

2.7 The Hot Electron Model

2.7.1 Assumptions of the Model

The basic hot-electron model, described by Latham et al(97), proposed a qualitative interpretation of how field penetration internally heated electrons by several eV, in order that they could be emitted over the surface potential barrier. It also attempted to provide a quantitative explanation of linear F-N plots and the field-dependence of F.W.H.M.´s. This new model is described in detail by Bayliss(94) and by Bayliss & Latham(77); so, only a brief outline will be given here.

The central contribution of this model is that it provides a very much more detailed picture of how the electronic parameters of the emission regime alter the basic hot-electron model described by Latham(97). It also circumvents the need to always assume high current densities ($>10^8 Am^{-2}$) in the bulk of the conducting channels, as had been necessary in the earlier model based on the properties of MIM devices(47,96). In addition, the widths of the conducting channels do not have to be approximately equal to the thickness of the insulting layer, as had previously been assumed; this is confirmed by the experimental emission images, whose average size indicates that the widths of the channels are in fact much smaller than the insulater thickness; this conclusion is also reinforced by the authors theoretical analysis. Finally, it proposes an alternative switch-on mechanism which more closely fits the known experimental and theoretical properties of the system. This model provides an explanation for the non-linearities that occur in F-N plots, together with quantitative relationships for the field dependence of the shift and F.W.H.M. of the electron spectra.

The assumed structure of an emission site remains unchanged from earlier models, i.e. a metal-insulator-vacuum (MIV) structure as shown in Fig.2.14. It is also assumed that such inclusions are only partially crystalline and almost certainly impure, so that there will be a distribution of both trapping states and donor centres within the inclusion. As in the previous models, the independent sub-sites are assumed to be the external manifestations of the formation of conducting channels in the dielectric that bridges the metal substrate and vacuum.

This suggested regime implies that, firstly, the electron emission characteristics will be influenced by the electronic properties of both the metal-insulator contact junction, and the bulk material of the insulator. Secondly, there is a strong likelihood of additional field intensification being associated with the conducting channels, since there will be an enhanced electron density relative to the non-conducting surrounding region, i.e. in a similar manner to that proposed by Hurley(45) but without necessarily assuming a metal-like electron density throughout the whole filament. It is thus proposed that the electrons are essentially emitted over the barrier. For such a classical type of emission mechanism to occur, the electrons need to gain an energy of 2 - 3eV, which is approximately equal to the electron affinity of the insulator. With the present MIV emission regime, @this energy can be acquired by electron heating due to penetration of the enhanced field into the tip of the channel, with the electrons being emitted in a quasi-thermionic manner as suggested in the earlier model of Latham(97). In the development of this model, greater attention was paid to the nature of the insulator-metal contact and to the insulator bulk parameters than in the previous models.

2.7.2 The Switch-On Mechanism

Earlier versions of the model by Latham & co-workers assumed that channel formation resulted from an avalanche process, similar to that assumed to occur in MIM switching devices(90). However, the work of Simmons(98,99) indicated that an electron would have to acquire an energy of at least 5eV ($\simeq 3/2.E_g$) within the bulk of an insulator having a normal band gap, to initiate such a process; a situationn which seems unlikely from considerations of the potential distribution across a sub-micron dielectric inclusion at gap fields of 10 - 20MVm^{-1}. Furthermore, it is not evident how an avalanche model can explain the important experimental finding referred to by Bayliss(95): namely, that the field at which switch-on occurs is influenced by the way in which the field is initially increased across a virgin gap, a result typically found during this present experimental work. Bayliss reported that by applying the field in increasingly small increments, with an increasing delay between increments, the threshold field for switch-on was significantly raised. Hence, to initiate switch-on, a voltage "surge" is required to be superimposed on some threshold gap field. The hot-electron model provides a qualitative explanation of this phenomena.

Bayliss & Latham(77) assume that the metal-insulator interface forms a blocking contact (i.e $\text{Ø}_M > \text{Ø}_I$), otherwise electrons would be able to flow relatively freely from the metal even at low fields, thereby charging the insulator and so screening the metal from the applied field. In addition, it may be assumed that there will be one or more microscopic locations on this interface where the local electronic conditions present a favourable tunnelling contact, i.e. such as would be created by local concentrations of impurity atoms in the insulator that could provide the necessary donor centres to produce marked band bending. Thus, as the external field is slowly increased, it will be at these locations that electrons will first start tunnelling from the metal into the insulator. Under zero-field conditions, the energy band diagram of such a localised region will appear as in Fig.2.18(a), i.e. with a high internal field at the metal-insulator interface, and a depletion region just within the insulator.

When an external field is first applied, it will penetrate through the whole insulating layer and reinforce the internal contact field. In fact, the majority of the potential drop across the insulator will occur at the contact, since the depletion region has a lower electron density than the bulk. As the external field is progressively increased, the conduction band edge is lowered to the metal Fermi level and the metal-insulator barrier becomes thin enough for electrons to tunnel into the conduction band of the insulator, as shown in Fig.2.18(b). With increasing field, these electrons will eventually fill any empty traps existing just below the conduction-band edge, throughout the thickness of the insulator. A further increment of field will result in more electrons tunnelling from the metal, but since all the traps in the insulator are now full, these electrons will eventually accumulate close to the metal-vacuum interface; so filling the surface states and creating a degenerate pool of cold electrons in the insulator conduction band. Furthermore, these electrons will effectively screen the bulk of the insulator from the external field so that the conduction band edge will rise and

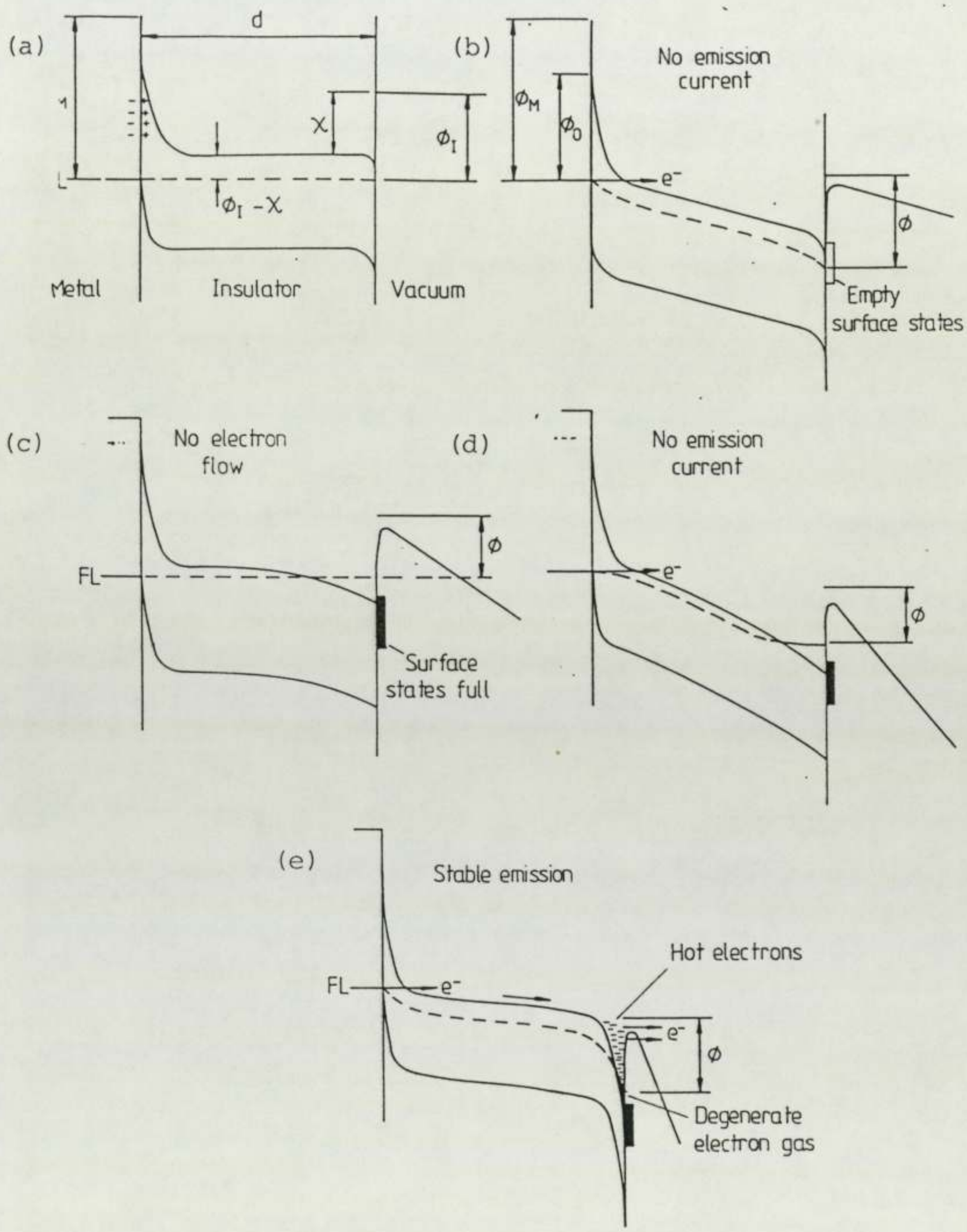

Fig.2.18 Stages In Emission From The Hot-Electron Model (from Bayliss & Latham)$^{(96)}$

cut off the continued supply of electrons, as shown in Fig.2.18(c). Because of this screening effect, it now requires several increments in the external field before the band structure approaches the situation shown in Fig.2.18(d), when electrons can again tunnel from the metal. A subsequent increment of field will thus generate a surge of high energy electrons that will experience a relatively high field and be swept towards the insulator-vacuum region where, through scattering processes, they will raise the effective temperature T_e of the electrons stored near the insulator surface. Hence, at some point sufficient energy will be available to raise T_e to the critical point for initiating the thermionic emission of electrons over the reduced Schottky barrier. Under such circumstances, a situation is created where several phenomena reinforce each other to produce a continuous emission current. Thus, as hot electrons are generated near the vacuum surface, and the barrier height decreases, a large proportion of the surface charge and any charge stored within the conduction band of the insulator, will be emitted in a burst of current. As a result, the external field will more effectively penetrate to the metal-insulator contact, and so give rise to an increased tunnelling current. At the same time, the surface-field will greatly increase relative to the bulk-field, since it is the electrons at the vacuum surface which are preferentially emitted. This will lead to a further lowering of the potential barrier and an additional increase in the electron temperature, i.e. both effects will tend to push the system towards a highly conducting state; a trend which may be further reinforced by the migration of any holes, formed during the scattering processes near the vacuum interface, back to the metal-insulator contact region. Dynamic equilibium will then be rapidly established by a mechanism similar to that discussed by Mott(91). The dynamic charge distribution will then adjust itself to give the highest density a short distance into the insulator, thus stabilizing the vacuum surface field at a high value, as illustrated in the energy band diagram of Fig.2.18(e), which represents the equilibrium on-state. The field distribution associated with a conducting channel, may be estimated from the slope of the conduction band edge in Fig.2.18(e), and from the fact that the field in the dielectric is uniform well away from the channel; this field distribution is shown schematically in Fig.2.19, and indicates that the field lines must converge at the channel tip in order to provide the very high surface field associated with the local electron concentration gradient near the vacuum interface.

The authors of the model then consider two field intensifcation factors for a stable conduction channel: the first β_1 refers to the ratio of the vacuum field immediately above the channel tip, to the electrode gap field. The second β_2, relates the average field within the channel, to the insulator field well away from the channel.

Since β_2 represents a ratio of average fields, and β_1 determines the highest field at a particular point, it follows that $\beta_1 \geqslant \beta_2$.

It follows directly from the model, that it would be possible to reduce the applied field to well below its switch-on value before the emission current falls to zero, due to the actual field in the channel region being enhanced to well above that initially required for switch-on. Also, if the applied field is reduced to

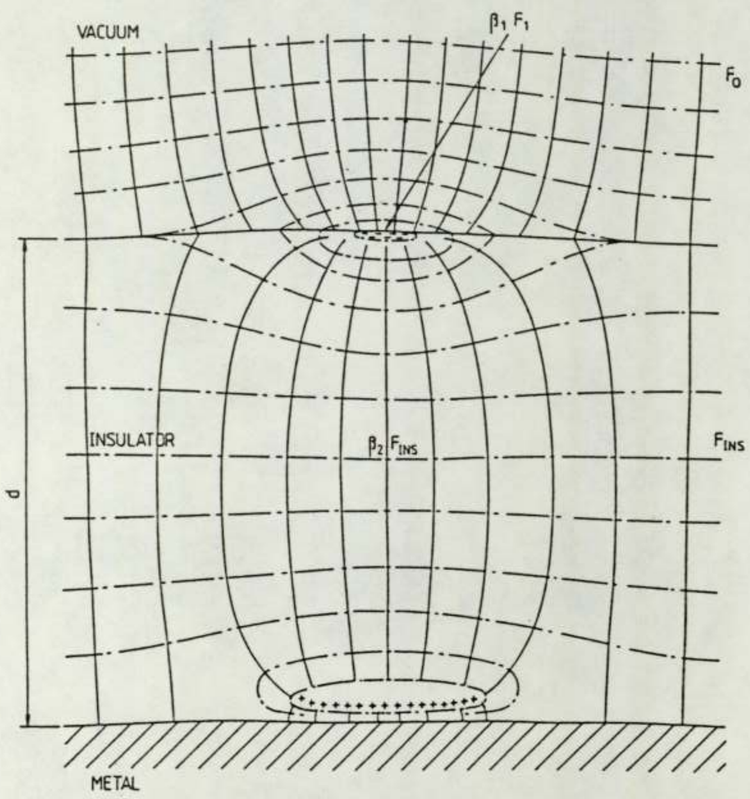

Fig.2.19 Field Distribution Around Conducting Channel (from Bayliss & Latham)$^{(96)}$

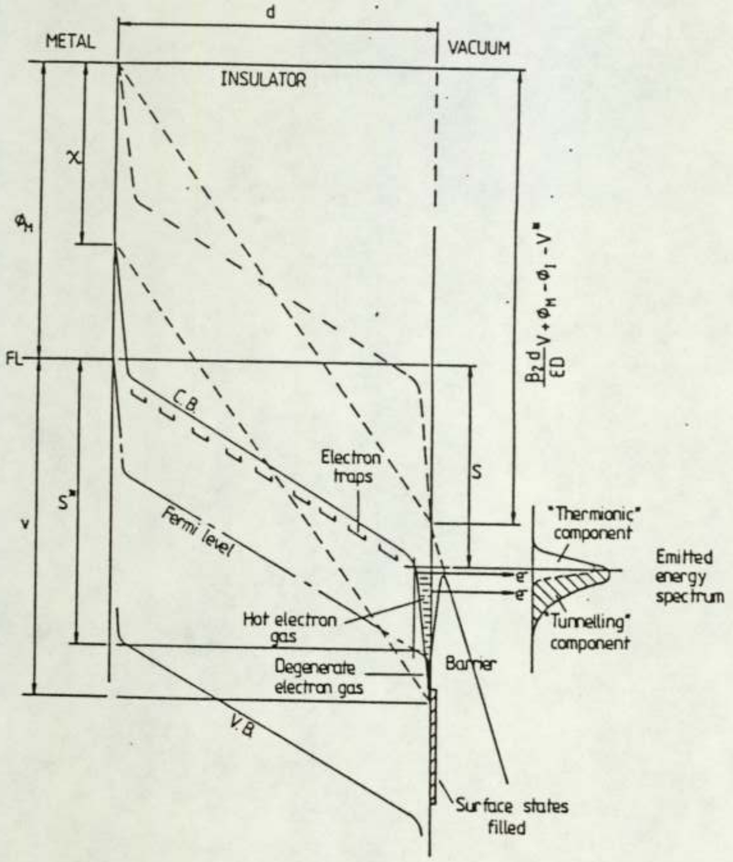

Fig.2.20 Detailed Energy Levels In Channel On -State (from Bayliss & Latham)$^{(96)}$

zero for a short time and then reapplied, it is unlikely that a similar switch-on behaviour will be observed. This is because the electron trapş and surface states will not have had sufficient time to relax back to their preconduction empty state, i.e. the channel path is essentially memorized by the system and the surface charges remain so that an emergy band configuration similar to that of Fig.2.18(d) probably results immediately the field is reapplied. It is also probable that the thermal effects produced by the high current density which immediately follows switch-on, results in permanent structural changes, analogous to the forming process discussed by Dearnaley(85) in the context of MIM devices.

With a switched-on channel, the current density tunnelling through the metal-insulator contact junction will have a similar form to that described by Simmons(98,99) for a blocking contact (Schottky barrier) situation. Hence, a sharply rising current dependence with applied voltage, and, consequently, an essentially temperature independent, rapidly falling contact resistance. For the high-field case, the authors show that the conductivity of the bulk insulator is field dependent and that a contaminated insulator is required to ensure a thin enough depletion region for electron tunnelling at the metal contact, and to give the bulk insulator a finite conductivity. If the insulator contains a high donor density ($>10^{24}m^{-3}$) and a high trap density ($>10^{25}m^{-3}$), the depletion region will be very thin and its bulk conductivity low. At low voltages, electrons tunnel into the insulator conduction band and the current rises sharply with voltage, with most of the voltage appearing across the contact, giving a virtually thickness-independent J-V characteristic. As bulk resistance falls less rapidly with voltage than the contact resistance, after some point subsequent voltage increases will appear mainly across the bulk, and so will rise less sharply than in the initial phase as it will now be controlled by thickness-dependent bulk processes.

2.7.3 Energy Distribution of Emitted Electrons

Fig.2.20 shows a detailed version of the channel on-state shown in Fig.2.18(e). Bayliss & Latham(76) show that by using the measured spectral shift S, and assuming reasonable values for the work function of the insulator and electron affinity, the equations describing the conduction processes may be checked. It can also be seen from Fig.2.20 that the measured spectrum will not only represent hot-electrons being emitted over the barrier, but also a significant component resulting from electrons tunnelling through the top of the barrier.

The theory also provides an explanation of various other spectal parameters. The authors show that consideration of the F.W.H.M. of the energy spectra can give important information about the factor β_1, and the temperature of the hot-electron population. If typical values for the various spectral characteristics are used, values obtained for the field intensification factors are: $\beta_1= 80$, $\beta_2= 15$. The magnitude of the switching field may also be estimated, this turns out to be about $18MV.m^{-1}$, a typical experimental value for copper electrodes.

2.7.4 Successes of the Hot Electron Model

The quantitative predictions of this model have been shown to closely fit the experimental data obtained from typical emission sites: the spectral shape, the field-dependence of both the F.W.H.M. and spectral shift from the metal Fermi level. A particularly important contribution of this model is the recognition that, at low fields, the emission process is controlled by the metal-insulator contact junction, while at high fields it is controlled by the bulk properties of the insulator material.

2.8 The Physical Basis of General Electrode Conditioning Techniques

2.8.1 Electrode Conditioning

The aim of all these conditioning techniques is to raise the voltage hold-off before breakdown; the basic concept being to quench as many sources of pre-breakdown current and primary micro-particle events as possible. For small electrode gaps (<2mm), where current instabilities stem predominantly from field electron emission processes, breakdown is field dependent. However, for large gaps (>5mm) micro-particle processes are thought to be the dominant causes of breakdown, i.e. gap breakdown becomes voltage dependent, as reported by Maitland(100). For a high voltage device, the choice of electrode conditioning treatment depends on its design and function: where the principle aim is to avoid arcing between electrodes, a pre-breakdown current conditioning procedure is generally the most useful; while, for devices where arcing is an operational feature, "spark" conditioning is more appropriate. Much of the experimental data on conditioning techniques, detailed later in this section, was interpreted by the various authors in terms of the effects on a metallic microprotrusion type of emitter, although the same concepts may be applied to the embedded insulating particle regime described in the previous section. In laboratory systems it is largely possible to eliminate micro-particle processes, and so the conditioning techniques investigated in this work, and the majority of conditioning work reviewed in this section concentrates on procedures for the general elimination of electron emission sites wherever they occur on the surface.

2.8.2 Electrode preparation

Whichever model of electron emission is assumed, a thorough specimen preparation procedure is essential to enable electrodes to be conditioned to as high a voltage hold-off as possible. For a laboratory-type electrode set, a standard preparation procedure would consist of:

a) Machine radiussing of the specimen edges to the appropriate choice of specimen profile, in order to reduce, as much as possible, field-enhancement at the edges of the flat face. Details of several different profiles are given by Rogowski(101), Bruce(102), and Harrison(103); the particular choice of profile depending on the gap characteristics, particularly the electrode separation.

b) Mechanical polishing down to 1 μm surface finish is typical, thus reducing field-enhancement caused by gross surface features and removing thick oxide layers.

c) Various cleaning processes, electrolytic or ultra-sonic, immediately before installation in the vacuum system; thus removing contaminents and loosly adhering dust from the electrode surface. That this process is important, both for micro-particle initiated breakdown and electron emission processes, is evidenced by the work on artificial carbon sites of Latham and co-workers(94).

For industrial devices, such as vacuum capacitors, travelling-wave tubes etc., careful design is important in eliminating unnecessary sharp edges; although in some cases they are unavoidable, for example at the end of capacitor fins. It is also obviously impractical to mechanically polish the entire surface of the device, so great care must be taken in the impurity specifications of raw materials and cleanliness of assembly. A standard preparatory routine is to use various chemical treatments, such as "bright" cleaning in acid solution, to remove the majority of any surface contamination; followed by ultra-sonic cleaning, in a solvent such as methanol, after several stages in assembly.

2.8.3 Current Conditioning

In 1918, Millikan & Sawyer(3) reported on the use of current conditioning as a means of electrode treatment. This is both the simplest and probably the most widely used technique, and is particularly suitable for the initial treatment of ´virgin´ electrodes(2). The applied voltage is increased in small discrete steps, such that the prebreakdown current is allowed to stabilise at each stage before progressing. Fig.2.21 illustrates this process, and highlights the general reduction in both the noise level of the continuous prebreakdown current and the frequency of random current spikes caused by microdischarges; with the time constant of the stabilisation process being typically around 30 mins. Another common feature of current conditioning is the sudden and irreversible fall in the mean level of the prebreakdown current, such as that which follows a microdischarge in the V_3 conditioning stage. A current-limiting series resistor is important for this technique. If there is a random surge in the pre-breakdown current, the voltage across the resistor will correspondingly increase and result in a lowering of the gap voltage, thus reducing the emission current. If the conditioning process is halted at the voltage V_4, where the stable pre-breakdown current is I_4, the gap will have a stable and reversible current-voltage characteristic up to the limiting values (I_4, V_4). In practical applications, this conditioning procedure would be continued until the intended operating voltage has been reached, or more frequently exceeded by a safety margin of about 25%. Clearly, there is a limit to the effectiveness of this treatment, since current drawn from the residual stable emitting sites will eventually reach the critical level for the onset of thermal instability and the consequent gap breakdown. However, with an optimum electrode design, coupled with the correct choice of electrode material and surface preparation, it can be reasonably anticipated that a voltage hold-off of at least $20MV.m^{-1}$. This is a significant improvement in performance, but the micro-discharges that occur can cause considerable surface contamination.

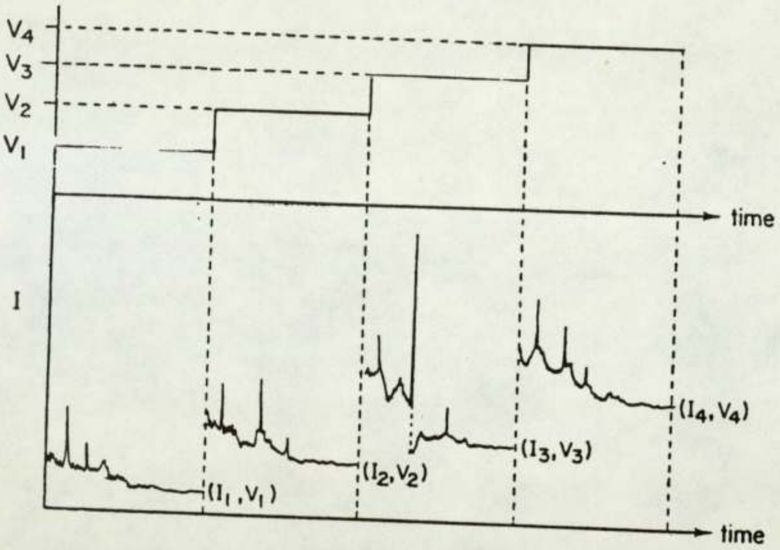

Fig.2.21 Schematic Illustration Of Current Conditioning (from Latham)(2)

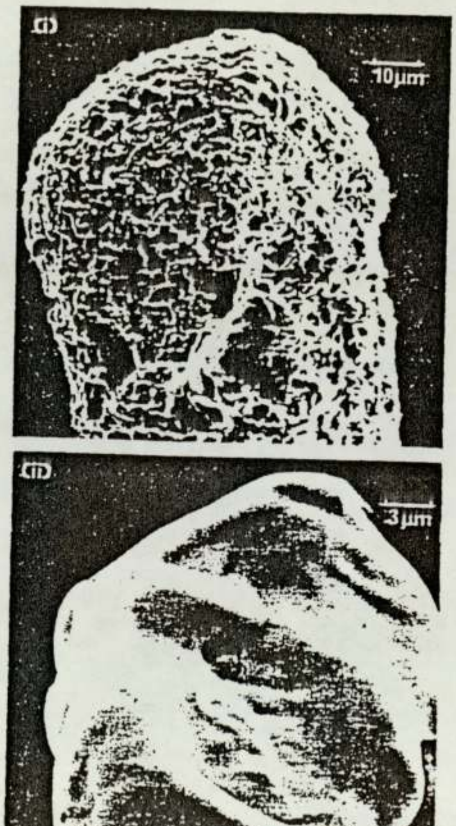

Fig.2.22 Electrode Surfaces (i) Before (ii) After Spark Polishing (from Juttner)(110)

Traditionally, speculation as to the physical processes giving rise to the stabilising effects of current conditioning, has been mainly(100) confined to the influence of high fields on electrode microprotrusions, loosely adhering microparticles and micro-reservoirs of occluded gas. Thus, the sharpest field emitting microprotrusions were assumed to be either thermally blunted following excessive electron emission or, if mechanically unstable, removed altogether from the electrode surface by the strong electro-magnetic forces associated with the applied field. In the case of loosely adhering microparticles, it has been demonstrated experimentally by Beukema(104) that, with a slowly increasing conditioning voltage, these will be detached at the lowest possible field and hence acquire only a minimum charge; as a result, their single-transit kinetic energies will be too low for a breakdown initiating explosive impact. Similarly, the field-desorption of residual gas trapped in grain boundaries etc., will be more controlled under a slowly increasing field, so that the risk of a large gas burst sufficient to initiate a breakdown is minimised. The existence of such a gradual desorption process has been directly confirmed by the mass spectrometer measurements of, for example, Cornish, Latham & Braun(105), and Panitz(106). The involvement of gas in the conditioning process is further supported by the observation that the time constant associated with the relaxation is pressure dependent, even down to 10^{-10} mbar.

2.8.4 "Spark" Conditioning

This technique is also known as "spot-knocking", as the basic concept behind the technique is to remove high-β cathode emission sites, or spots, by arc erosion, as reported by Miller & Farrall(107); however, it has also been found efficient in eliminating micro-discharges and diminishing the incidence of micro-particle processes. The required circuitry need consist of no more than a power supply and current-limiting resistor, typically about 100kΩ , in order to increase the rate of dissipation of energy in the "spark". Alternatively, the effect can be achieved by a over-voltage pulse technique, such as described by Miller & Farrall(107). It has been found that the number of sparkings required to achieve the maximum regeneration of a gap is unpredictable, but is usually in the range 5 - 10 for common electrode materials such as copper, stainless steel and molybdenum; however, this number can be much larger for severely arced electrodes. With copper, for example, Cox(108) showed that the breakdown field increased with the number (up to 5) of low-current (<1A) conditioning arcs, and interpreted his findings in terms of a local hardening of the surface in the vicinity of the emitting regions. In order to apply this conditioning technique effectively, Hackam(109) reported that it is necessary for the external capacitance associated with the gap to be minimised, so that only a limited amount of energy (<10J) is dissipated in the gap during sparking.

Using a more sophisticated form of "spark" conditioning, Jüttner(110) has shown that it was possible to achieve an electrode polishing effect using nano-second discharges under

U.H.V. conditions, and that this procedure can lead to a dramatic improvement in the voltage hold-off capability of a gap. Fig.2.22(a)-(b) shows the change in the micro-topography of an electrode surface brought about by this polishing action.

This procedure is extensively used in industrial devices. In high-voltage vacuum capacitors, for example, ´spot-knocking´ is used to bring the device upto the specified operating voltage without subsequent breakdown events. Using automatic circuitry, the voltage is progressively raised to a point about 20 - 30% over operating voltage; every time a "spark" occurs, the voltage is reduced slightly. A course of conditioning often consists of several hundred arcing events, and it should be noted that the arcing process can produce significant metallic surface features, as well as contamination of the surface.

On the basis of the ´insulating particle´ model, the effectiveness of this technique can be explained as the destruction of the particular qualities of the particle/oxide configuration that caused emission.

2.8.5 Gas Conditioning

Extensive investigations have been made into the gas conditioning technique, which aims at a sputtering action by low-energy ions, selectively localised to emitting sites on the cathode electrode. The experimental procedure, was originally reported by Lyman, Alpert and co-workers(111,112,113) and later used by Beukema(104); it involved introducing an inert gas, such as argon, into the system at a pressure of 10^{-3} mbar, and then running a low pre-breakdown current at a high voltage. Under such conditions, Alpert et al.(112) proposed that positive ions would be formed by electron impact in the higher field region in the immediate vicinity of a field emitting microprotrusion, which would then be accelerated back to the emitter to blunt its tip by their sputtering action; this process being illustrated in Fig.2.23. The effectiveness of this treatment was monitored by noting the fall-off in current at constant voltage, with the authors quantifying this improvement by comparing the β-values of the gap before and after conditioning.

There have been contradictory reports as to the influence of this conditioning procedure on the voltage hold-off of a gap. For example, Ettinger & Lyman(113) found a 3 to 5 times improvement in breakdown voltage with tungsten and copper electrodes, they assumed the improvement to be limited by the condition that the rate of blunting of existing protrusions was balanced by the rate of formation of new ones; while Hackam & Altcheh(114) also reported a significant improvement in performance, the improvement depending on pressure and electrode separation as shown in Fig.2.24. However, Beukema(104) observed no significant improvement with stainless steel and titanium electrodes. Although, such inconclusive findings are not surprising if no precautions were taken against micro-particle initiated breakdown events.

A similar sputtering process can be used to explain the observed conditioning effects using the ´insulating particle´ regime, with the gas atoms being locally ionised by the emitted electrons. Alternatively, a ´poisoning´ of the conducting channels after physi-sorption. It should be noted that when this conditioning technique was used during the course of this work, it was not possible to monitor the increasing voltage required to maintain a particular emission current, the technique used by several workers(111-114), due to the great instability of the emission current under ´gassy´ conditions.

2.8.6 Glow Discharge Conditioning

In this technique, the primary aim is to use the sputtering action of low-energy gas ions to remove contaminants from electrode surfaces; a secondary improvement could also result from an increase of emitter work function due to its coverage by inert gas atoms. The experimental procedure, as reported by Danloy & Simon(115), Steib & Moll(116), and Hackam & Raju(117), involves raising the presure in the vacuum chamber to 10^{-3}- 10^{-2} mbar, via a suitable gas handling system, so that a low voltage a-c glow discharge can be struck between the electrodes. This low current discharge can be conveniently derived from a 50 Hz source and, for optimum results, is typically run at 30 mA for up to 1 hr., longer periods of ion sputtering can often lead to a rapid degradation of the performance of a pair of electrodes. The effectiveness of this technique has been shown to be markedly dependent upon the residual gas species used to promote the glow discarge. Thus, from among the gases studied (H_2, D_2, He, Ar, N_2, SF_6 and dry air), helium, followed by nitrogen, consistently give the best results; as measured by the improvement in the hold-off voltage of the gap and the reduction in β-factor of the associated F-N plot. Considerable advantages have been claimed for this treatment over current conditioning, and it is now common practice to subject

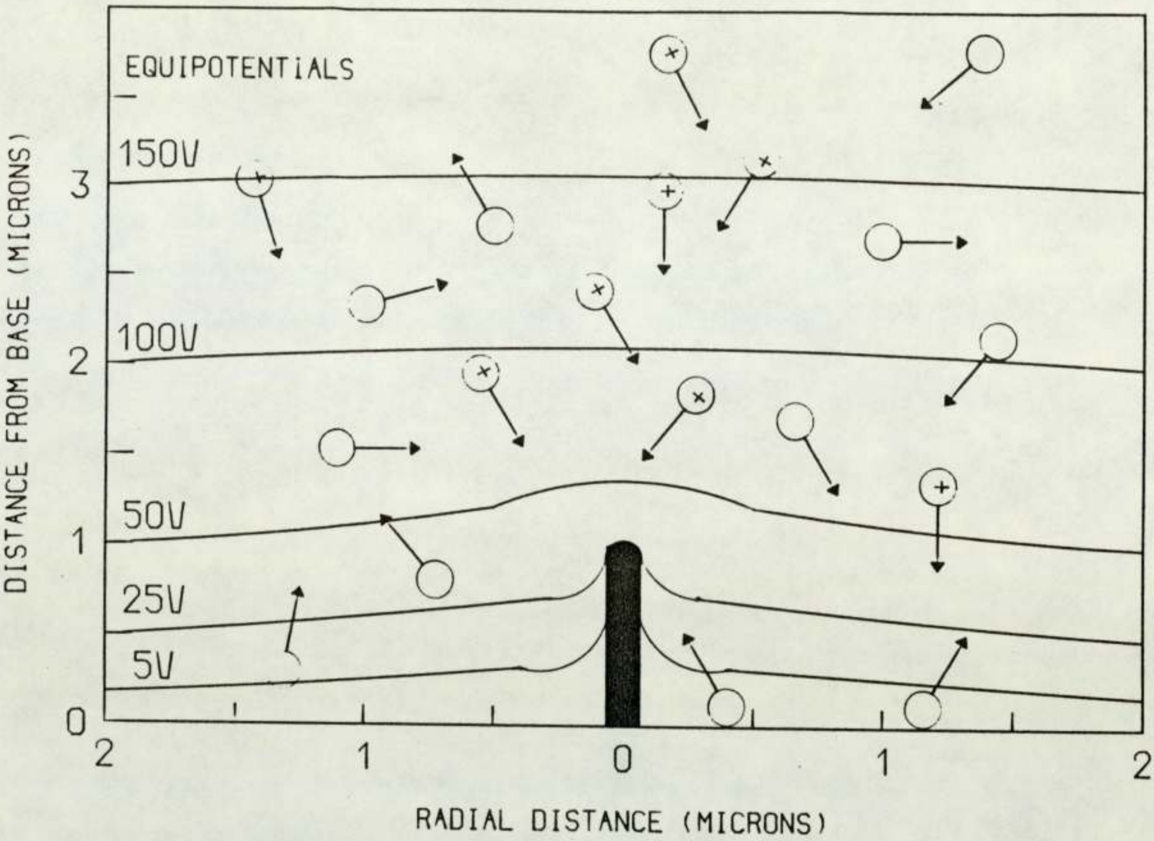

Fig.2.23 SELECTIVE ION-BOMBARDMENT OF A SURFACE PROJECTION (FROM ALPERT et al)(112)

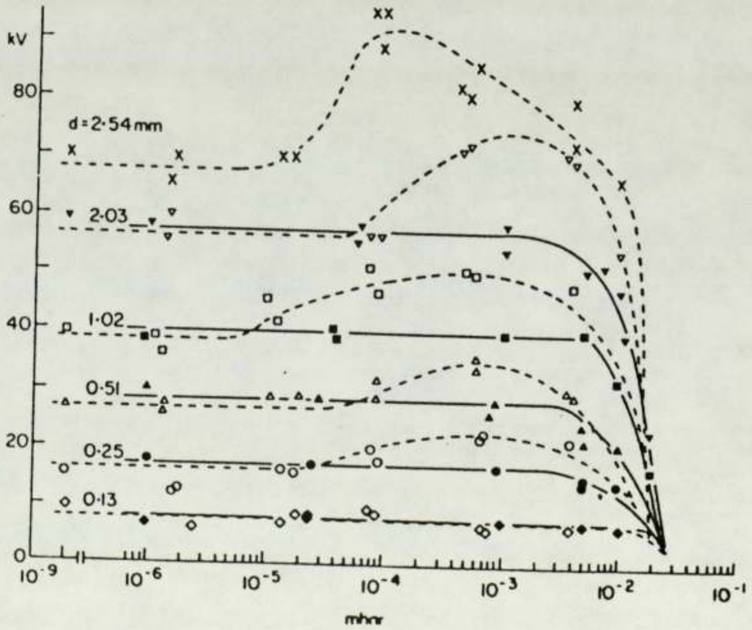

Fig.2.24

The "pressure effect", illustrated by a family of plots showing how the d-c (dotted lines and open symbols) and a-c (solid lines and closed symbols) breakdown voltages of a pair of plane-parallel Cu-electrodes depend on the pressure and gap separation.

(from Hackam & Altcheh)(114)

such high voltage devices as particle-beam separators to an initial glow-conditoning treatment with helium, at a pressure of 10^{-3}mbar. A glow-discharge technique is also used by C.E.R.N. for conditioning their RF cavities with an argon/oxygen mixture

2.9 Localised Conditioning Techniques

2.9.1 The Concept of Localised Conditioning

As mentioned in the previous chapter, one of the major contributions of this work lies in the experimental application of localised conditioning, i.e. the restriction of the conditioning activity to a specifically chosen region, usually the dominant emission site. All of the conditioning techniques discussed previously have been general treatments, allowing no spatial selectivity in their application. As shall be shown in later chapters, this spatial selectivity has advantages from both a technological viewpoint, allowing a greater improvement in voltage hold-off than ´general´ treatments, and for obtaining more fundamental insights into the properties of electron emission sites.

In addition to the principles of the two obviously localised techniques described below, electron- and ion-beam bombardment, attempts were also made to localise the action of the gas sputtering and spot-knocking techniques, and these will be dicussed in the next chapter.

2.9.2 Ion Beam Conditioning

This technique, which was both the most successful and the most extensively evaluated, relied on conditioning by means of localised ion-bombardment of emission sites. The ions, which were produced using energetic argon ions from a cold-cathode saddle-field ion source, producing a sputtering action at the target surface. Some 25% of the beam produced by this type of ion-source consists of energetic neutral particles, so making this type of source particularly useful when considering the erosion of particles of insulating material. Some of the theory behind the saddle-field ion source(118), and characteristics of the beam produced(119), are described in the following chapter.

2.9.3 Electron Bombardment

This method relies on electron beam bombardment producing localised heating in the target, and so cause the destruction of the emission site.

Assuming a steady-state axial and surface temperature distribution, Vine & Einstein(120) gave the temperature reached at the centre of the bombarded area as:

$$T_r = 0.414a.W/\pi^{1/2}K.R_g \qquad \text{E.2.6}$$

Where W is the beam power (assuming the voltage to be <25kV for negligible electron penetration); a is a correction factor for power losses through radiation and backscattered electrons; K is the mean thermal conductivity of the target material (in $W.m^{-1}K^{-1}$); R_g approximates to the beam radius.

Obviously, the beam power density required to cause localised surface melting, varies with the target material. For copper, the range 10^2-$10^4 A.m^{-2}$ at 1-10kV was thought to be sufficient to destroy an emission site.

CHAPTER 3

Development of Experimental Systems and the Operation of Conditioning Procedures

3.1 General Considerations

Some of the major experimental problems that had to be considered at the outset of this work were: (a) the design and construction of a vacuum system able to achieve ultra-high vacuum, i.e. pressures $<10^{-8}$mbar, and be able to cope with the large volumes of gas required by many of the conditioning techniques; (b) the development of a specimen mount and manipulating assembly, allowing controlled X-Y movement of the specimen to be achieved by a single, rotational type, exterior manipulator; (c) the design of various localised conditioning techniques for the elimination of localised emission sites.

3.2 Construction of Vacuum System and Experimental Chamber

The original experimental chamber, supplied by GEC Co. Ltd., was that used by Hurley et al(42,45,46) for their work on electro-luminescence effects associated with pre-breakdown electron emission. Its vacuum system consisted of a liquid-nitrogen sorption pump for initial system pumpdown, followed by a getter-ion pump combined with a titanium sublimation pump to achieve, after baking, an ultimate system pressure of $<10^{-9}$mbar. This pumping combination was thought to be ideal for an investigation into such a surface-sensitive phenomenon as field electron emission; since, unlike a rotary/diffusion pump system, it provided a "clean" vacuum; one inherently free from residual pump oil contamination. The sorption pump, containing a zeolite cooled to liquid-nitrogen temperatures, was used to "rough-out" the system to a pressure of 10^{-2}mbar. Final operating pressure was then achieved by baking the system to $\approx 300^{o}C$, by means of the getter-ion pump.

There were two major shortcomings of this type of pumping system: firstly, the relatively long time required to achieve the operating pressure, resulting in a slower "turn-around" time between specimens; secondly, its inability to cope with the large gas loadings generated during many of the conditioning procedures. This second problem was particularly important if a gas such as argon was used, since the pumping action of a getter-ion pump is relatively ineffective for an inert gas.

For the reaons outlined above, it was decided to replace the sorption/getter-ion pump system with a rotary pump backed, oil diffusion pump system; with a liquid nitrogen "cold-trap" being used to minimise hydro-carbon contamination from the pump oil, and so improve the ultimate pressure achievable by the system. The performance of the diffusion pump was enhanced by the use of a polyphenyl ether pump fluid, thus reducing the possibility of the deposition of insulating films on the specimen surface. The rotary pump, an Edwards EDM5 with a pump speed of $5\ l.s^{-1}$, was used to initially evacuate the experimental chamber to a pressure of $4 x10^{-2}$mbar. At this point, the diffusion pump, an Edwards E150 with a pump speed of $150\ l.s^{-1}$, was switched-on and, when a pressure of 10^{-4}mbar was reached, the liquid-nitrogen cold-trap was filled; lowering the chamber pressure to $< 10^{-6}$mbar.

Subsequently, the chamber was "baked-out" at a temperature of 180°C overnight; primarily, in order to improve the chamber pressure due to desorption of water vapour and other volatile materials from the chamber walls and contents. After the chamber had cooled, and the cold-trap been re-filled, a chamber pressure of $<3\times10^{-9}$mbar could be obtained.

The purpose-designed electrical control system for the pumps is shown in Fig.3.1, and includes several devices to insure the safe continuous operation of the experimental system. Thus, the water pressure switch monitored the pressure of the water used to cool the diffusion pump, a pressure-sensitive switch monitored the pressure in the ´backing-line´ to the diffusion pump, and a thermal cut-out switch regulated the temperature in the heater unit. As can be seen from the diagram, the devices were wired in series; so, if any of the monitored variables moved out of the desired range, power to the diffusion pump heater unit was cut-off, and a visible indication given on the control panel. As a further precaution, the power supply was wired through a relay; so, if the power supply was interrupted, the pumps would remain off until re-set.

3.3 Development of Electrode Assemblies

3.3.1 Electrode Design Considerations

The initial objectives behind the design of the experimental systems were: firstly, to obtain and measure the pre-breakdown field-electron emission current from a series of specimen electrodes; secondly, to develop a technique such that the position of the localised emission sites giving rise to this

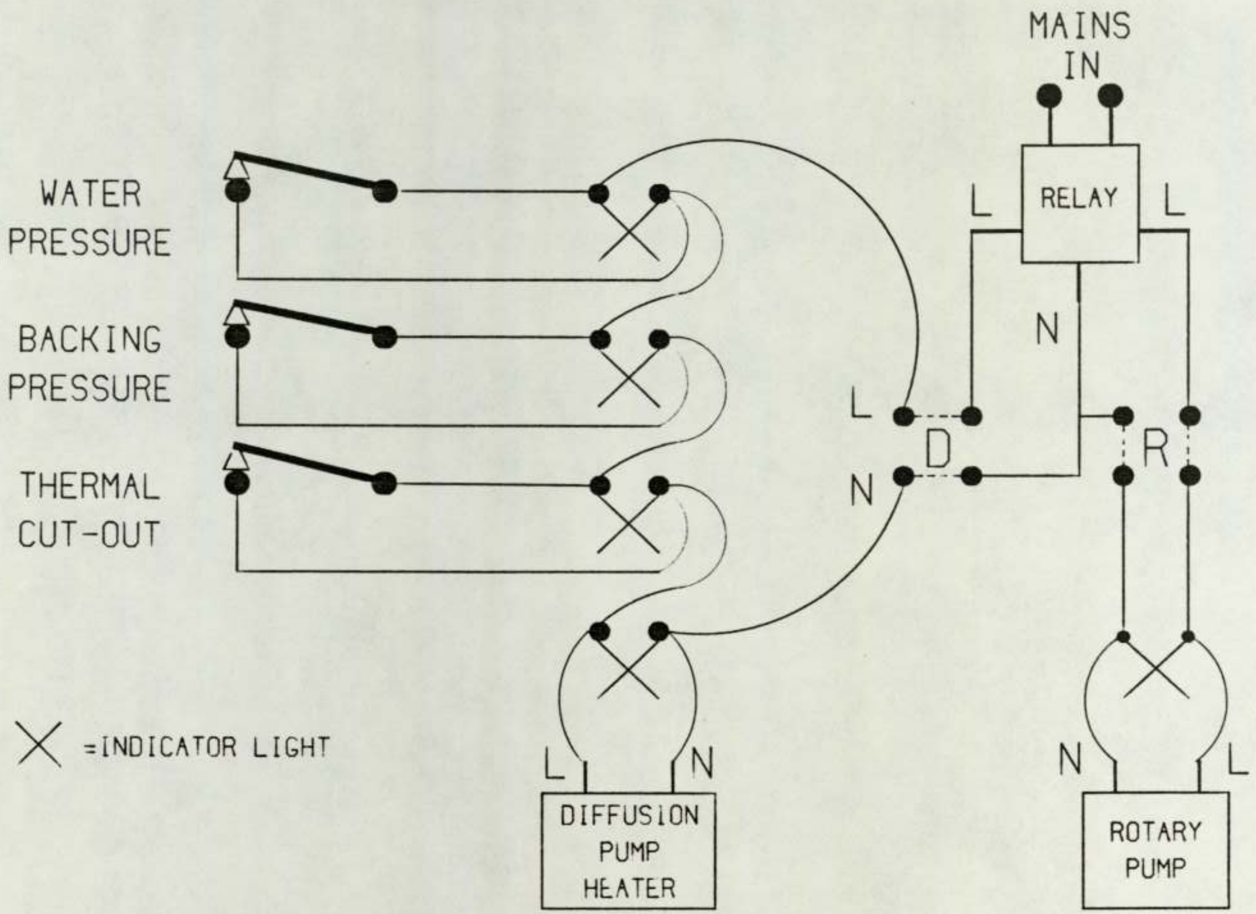

Fig.3.1 ELECTRICAL CONTROL CIRCUIT FOR VACUUM SYSTEM

current could be located and studied.

The problem of locating a field-electron emission site on a broad area electrode has, in the past, been solved using a variety of techniques, as reviewed by Latham(2). As mentioned in the previous chapter, Cox(33-35) scanned a series of successively smaller apertures over the test electrode, until an emission current was detected passing through the aperture; thus locating the emission site. The method adopted for this study, as for the majority of systems within this laboratory, was similar, in principle, to this technique. It consisted of a static anode, with a 0.75mm axial probe aperture, and a movable test electrode (cathode) which was systematically scanned across the probe hole. In addition, some form of Faraday cage was located behind the aperture to collect electrons from any emission sites passing in front of it.

A static anode assembly has a number of advantages for the present investigation. Principally, a variety of systems may be installed behind the anode to act locally on that part of the cathode surface located opposite the probe hole; for example, an emission site. In addition, having the anode aperture as a fixed reference point, enables the location of an emission site to be easily recorded.

The experimental system could, in principle, have been designed with either cathode or anode as the H.V. electrode. However, for practical reasons, such as the necessity to install various conditioning modules in close proximity to the anode, it was easier to make the static anode the low voltage electrode; with the movable cathode the H.V. electrode.

3.3.2 The Specimen Mount Assembly

For the reasons described above, the specimen cathode was not only required to be operated at H.V., but be able to be mechanically scanned fully over the anode aperture. Furthermore, the geometry of the experimental chamber required that the scanning action be generated from a single, rotary motion. Other design constraints were that the electrode spacing be not only adjustable whilst the system was under vacuum, but that it could be accurately measured for the precise determination of the applied field. It was also essential that the scanning action should maintain, as far as possible, a constant electrode spacing during a scan, with the whole assembly being stable against vibration. Lastly, the specimen should be easily accessible, in order to facilitate changing the specimen.

A photograph of the complete cathode assembly is shown in Fig.3.2. It was capable of being moved in and out using the chain drive, shown on the right of the figure; a facility that enabled the electrode spacing to be accurately measured to better than 0.05mm. This was achieved by setting the inter-electrode gap to approximately zero, using a capacitance bridge in conjunction with optical examination.

A diagrammatic representation of the scanning mechanism is shown in Fig.3.3, and shows how a rotary movement, applied via a U.H.V. manipulator to the drive shaft, is transferred to the drive pinion assembly via a pin linkage. This type of linkage removed the need for the drive shaft and pinion to be absolutely on-axis to each other, and also made the assembly and disassembly of the

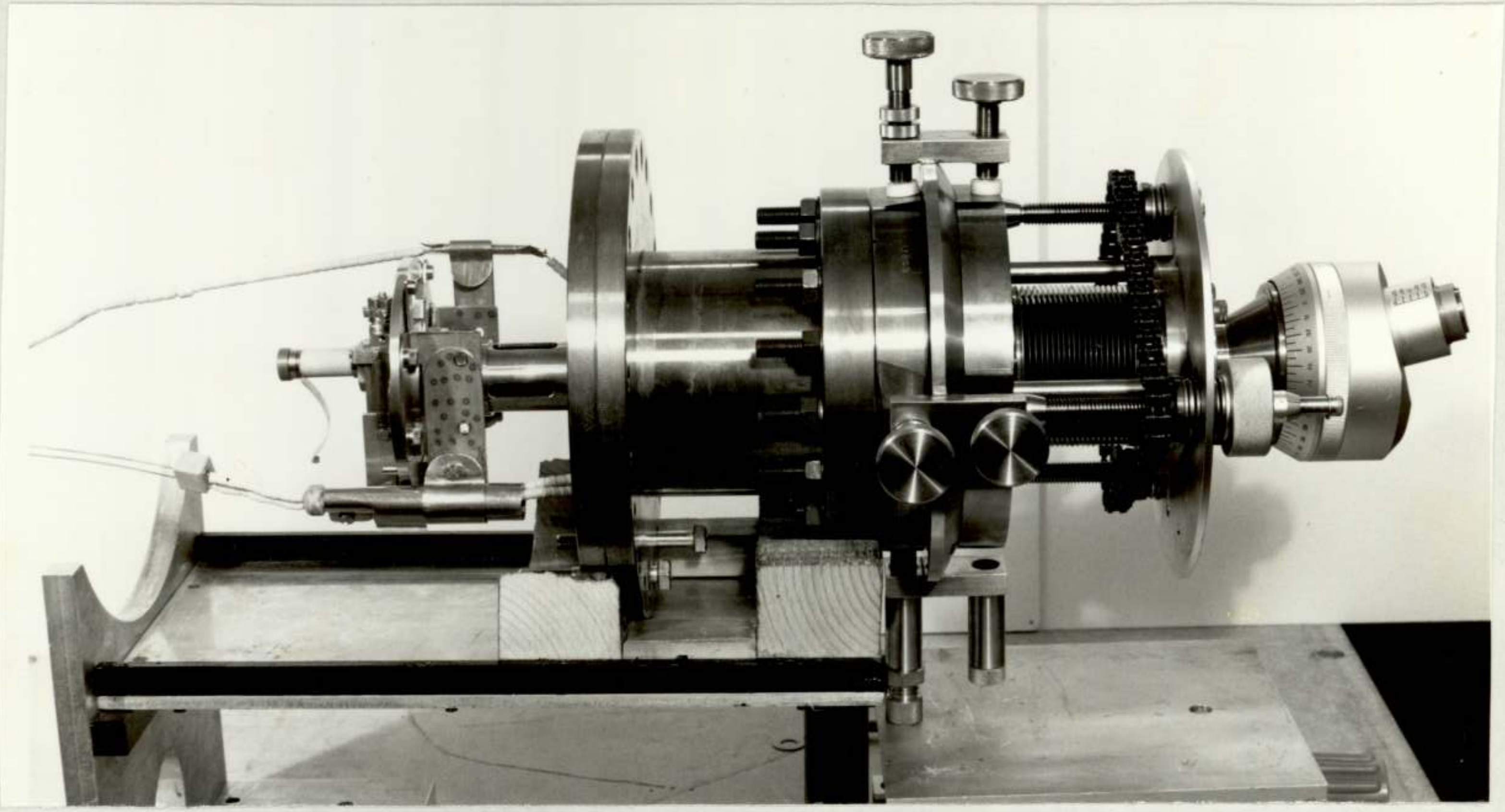

Fig.3.2 Photograph Of Complete Cathode Assembly - The Chain-Drive Mechanism On The Right Allowing The Electrode Gap To Be Varied

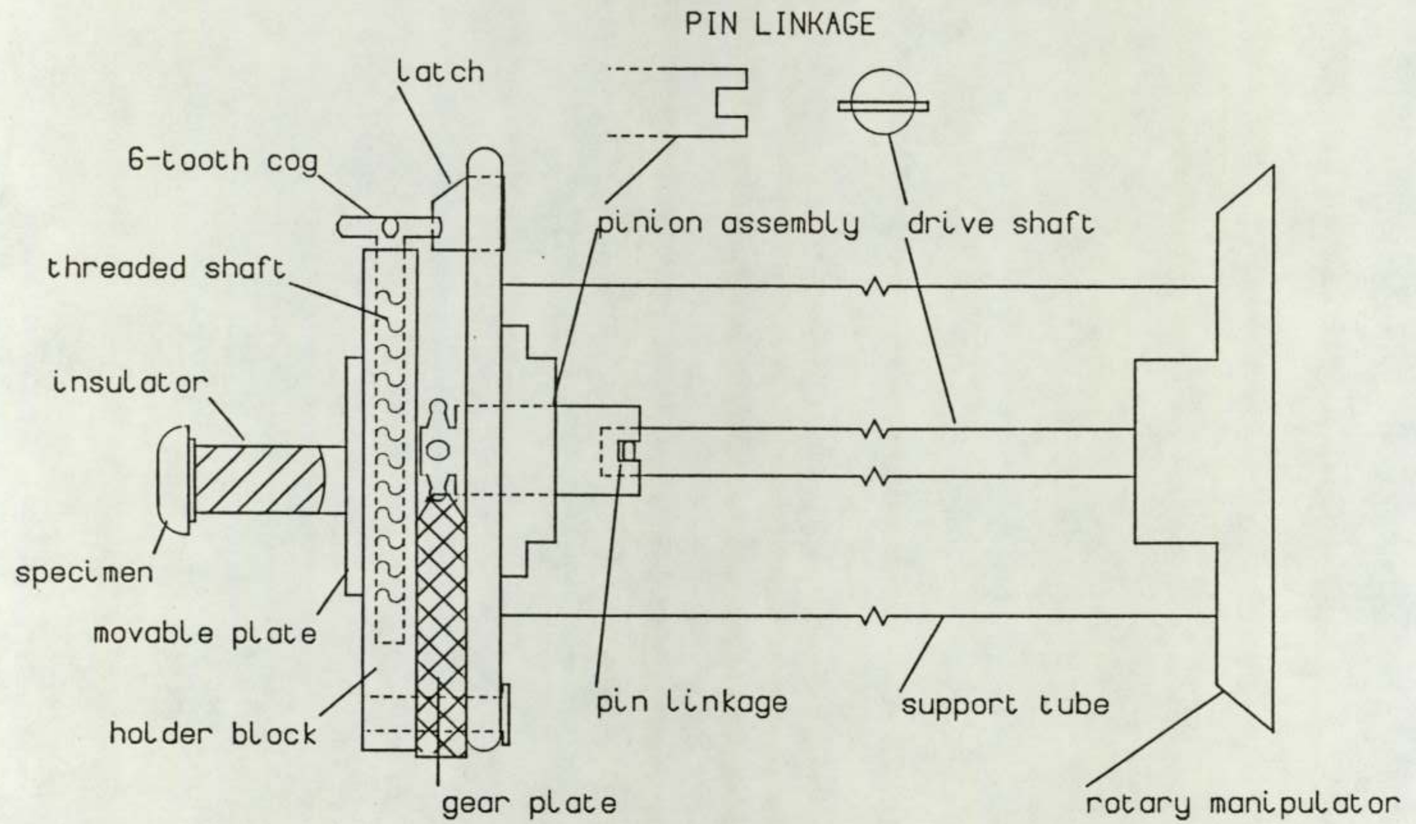

Fig.3.3 DIAGRAMMATIC REPRESENTATION OF SCANNING MECHANISM

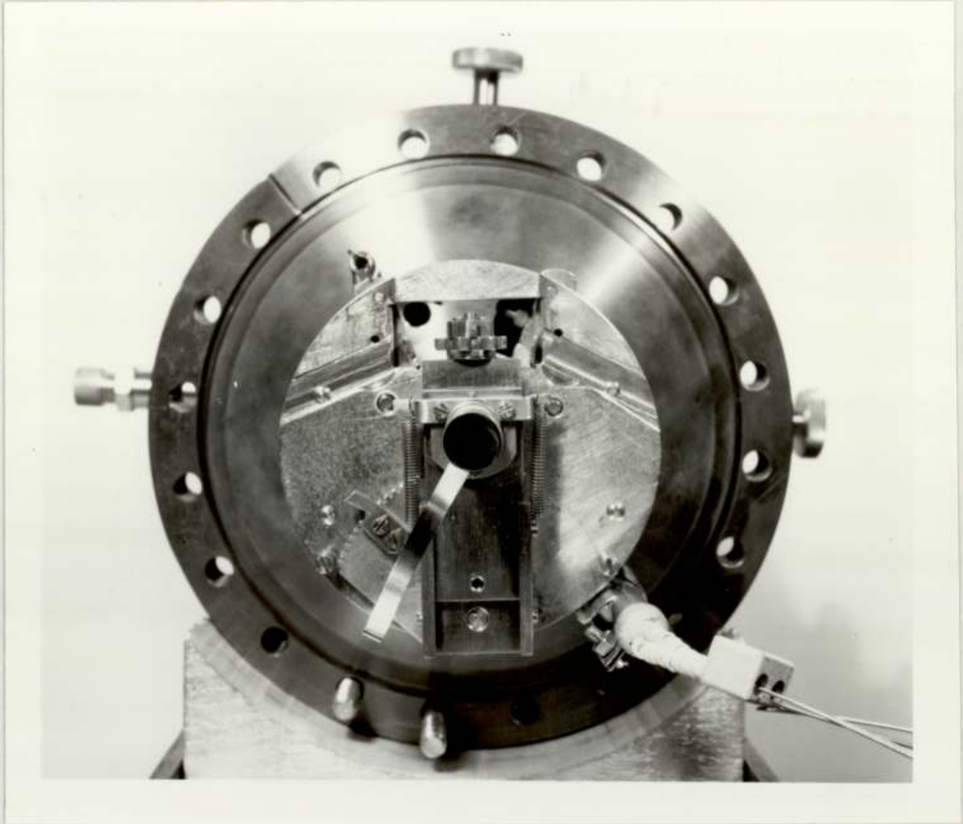

Fig.3.4 Photograph Of Cathode Assembly (front)

system easier. The pinion engages the gear plate, forming a 13:1 speed-reducing system, thus scanning the specimen holder block in an arc. Fig.3.4 shows this block in greater detail, with the gear plate clearly visible. As the holder block is scanned to the left, the 6-tooth cog is rotated by the latch; thus turning the threaded shaft and causing the plate, with the specimen attached to it, to move up. As the holder block moves back to the right, the latch pivots away instead of turning the cog. In order to scan in the reverse direction, the holder block is scanned to the right; so the cog is turned by the right-hand latch, moving the specimen down. Since the shaft has a thread pitch of 20 threads-per-inch, each turn of the cog causes a vertical movement of:

$$(1/20) \times (1/6) \times 25.4 = 0.21\text{mm}$$

Hence, the scanning mechanism produces a series of stepped arcs, with each step being $\simeq$ 0.2mm, as shown in Fig.3.5.

As with any mechanical system, there is some error, due mostly to backlash, in both vertical and horizontal movement. In order to minimise the backlash in the vertical plane, the springs, which can be seen in Fig.3.4, were used to exert a force pulling the movable plate downwards; whilst backlash in the pinion and gear system was minimised, as far as possible, by using involute curves etc. in the design of the gear teeth.

The high voltage contact is made to the specimen by means of the stainless steel strip also visible in Fig.3.4. When the system is assembled, this strip is pushed against a plate mounted onto an H.V. feedthrough; the plate being sufficiently large so that contact is maintained even though the specimen moves both laterally and vertically. Originally, a 15kV feedthrough was

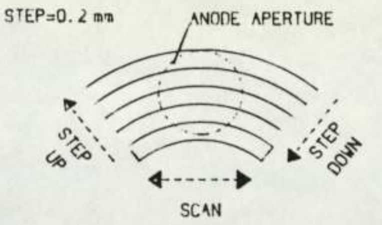

Fig.3.5 DIAGRAMMATIC REPRESENTATION OF STEPPED ARC SCAN

Fig.3.6

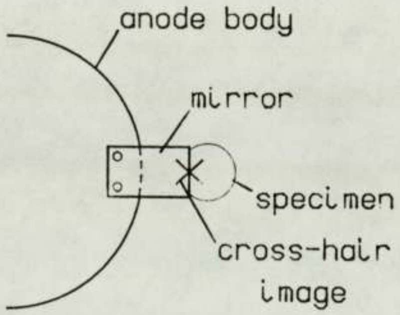

SPECIMEN ALIGNMENT

used, which gave a maximum applied field capability of 35 - 40MV.m^{-1}. However, as errors in the linearity of the scanning become important for gaps less than ≈ 0.35mm, a 25kV feedthrough was installed in order that as large an electrode spacing as possible be maintained.

3.3.3 The Anode Assembly

The choice of a static anode with an aperture for the detection of emitted electrons, fascilitated the design of the various systems for locally treating the individual emission sites. Obviously, this required that the conditioning system be able to act as an electron collector, in order to determine the location of an emission site, and that it act, primarily, along the central axis of the system in line with the anode aperture.

A modular design was adopted for the conditioning systems, as this enabled the various modules to be inter-changed easily and quickly while still maintaining relatively constant experimental conditions for all the techniques; so their relative effectivenesses could be easily compared.

The basic anode assembly consists of a stainless steel apertured anode mounted on a cylindrical body, into which the various modules could be inserted. This body was attached to a base plate by means of three adjustable sprung screws; thus allowing the angle of the anode to be altered until it was parallel with the face of the specimen. The parallelicity of the two electrodes was checked in two ways: firstly, a rough check was made by sighting along the axis of the inter-electrode gap. Secondly, a more accurate alignment was achieved by positioning the specimen opposite a small mirror mounted on the anode body, with Fig.3.6 showing a representation of the view from behind the anode, and using an eyepiece with a cross hair. As the surface of the specimen was polished to a 1micron mirror-finish, the anode was adjusted until the image was continuous across both mirror and specimen, i.e. they were parallel. The base plate of the anode assembly was attached, but electrically isolated from, an expansion ring which anchored the whole assembly firmly in position. Fig.3.7(a) shows the anode assembly, while Fig.3.7(b) shows the installed assembly containing the ion-source module; also shown, in the background, is the scanner assembly and, in the lower-left of the picture, the H.V. contact plate.

3.4 Design of Anode Modules

3.4.1 Ion-Source Module

A brief summary of the theory behind the saddle-field ion-source has been given in the following section, together with some of the general characteristics of the ion-beam produced by it. For this investigation, some modifications had to be made to the ion-source for it to be able to function in its secondary role as a Faraday cage-type of electron collector. Fig.3.8(a) shows the form of the ion-source module as it was actually used: the insulating porophylite jacket was necessary to electrically isolate the ion-source body from the anode assembly, so that it could be used to collect emitted electrons as they pass through the anode aperture. Whilst being used as an electron collector, the ion-source body was connected to a pico-ammeter, this connection having to be earthed when an ion-beam was being

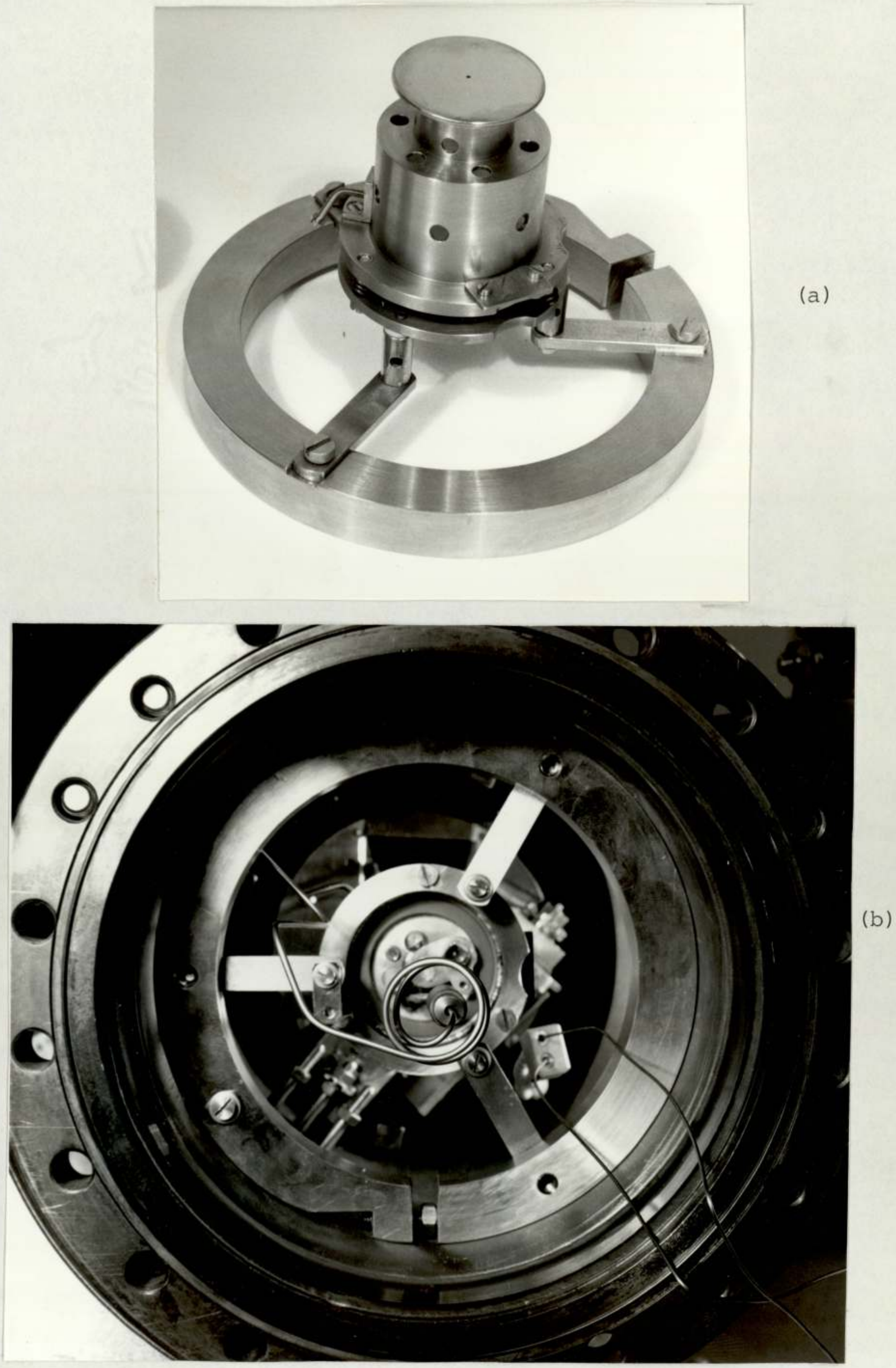

Fig.3.7 Photographs Of Anode Assembly

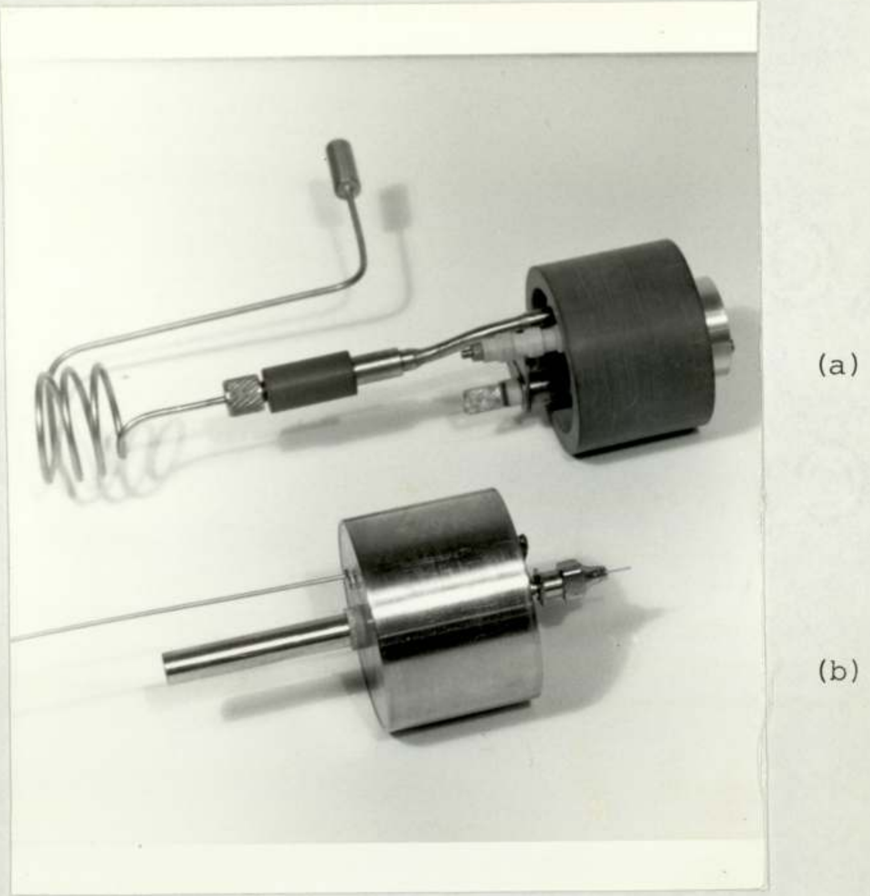

Fig.3.8 (a) Ion-Beam Module (b) Gas Sputtering Module

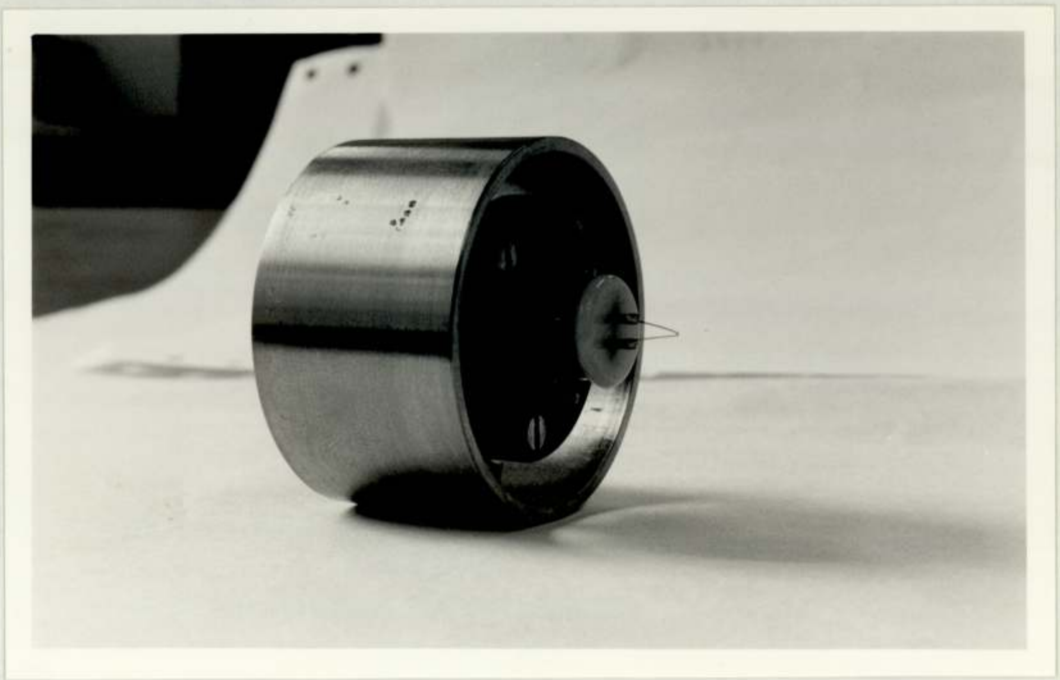

Fig.3.9 Electron Gun Module

produced. In order to produce as fine a beam of ions as possible, a 0.5mm diameter bore collimator was attached to the ion source, visible in the photograph at the right-hand end of the ion-source, whilst on the left, is the electrically isolated gas inlet pipe.

3.4.2 Gas Sputtering Module

Fig.3.8(b) shows a photograph of the gas sputtering module. It can be seen to consist of a section of stainless steel pipe terminating in a syringe-type end, which is mounted in, and insulated from, a stainless steel cylinder; the end of the pipe was attached, via an insulating connector, to the gas inlet. This whole assembly was inserted into the anode body so that the syringe-tip was in the approximate centre of the anode aperture. It was intended that the presence of a ′high′ pressure region in the vicinity of the syringe tip, would cause preferential sputtering of a localised region of the cathode surface. By making an external electrical connection to the syringe-end, it could be further used as a probe to detect any emitted electrons passing through the anode aperture.

3.4.3 Electron Beam Module

Fig.3.9 shows a photograph of the electron beam module. For various reasons, such as the space limitations imposed by the experimental chamber, the need to fit the module into the anode assembly and the restricted number of external electrical connections, the electron gun design could not be a particularly sophisticated one; it should be noted that the filament of the gun must also act as an electron collector while an emission site is being located. Thus, after consideration of various alternatives, a form of the cathode biassed electron gun described by Reigener(121) was constructed. The circuit required to operate the electron gun is shown in Fig.3.10; where R_c is in the range 0-10 Mega-ohms, and C_c is 0.5 micro-farads. Consideration of this diagram shows that the apertured electrode A, which acts as a cathode while the electron gun is in operation (with the specimen acting as the H.V anode), is negatively biassed with respect to the filament assembly F due to the collection of stray electrons, and will therefore act to restrict the beam spread. The variable resistor R_p is used to vary the power input to the filament. When using this type of gun, the electron beam current and diameter are controlled by varying R_c, thus altering the bias potential of the electrode. The height of the filament, i.e. the distance that the tip of the filament is recessed behind the top surface of the electrode A, is a very critical parameter in determining the characteristics of the gun; not only because this determines the quantity of electrons collected, and hence the magnitude of the bias potential, but also because of the effect on the field distribution. These effects are demonstrated in Figs.3.11(a)-(c), which consist of various computer-generated electron trajectory plots (produced, using a specialist program, by EEV Co. Ltd.) showing the effects different filament ′heights′ will have on the likely beam profiles produced by the idealised geometries of the filament and electrode structures. These indeed show that a lower filament height produces a much more compact beam and that, further, that the cross-over point, the point of maximum intensity, will be very near the surface of A; while further away,

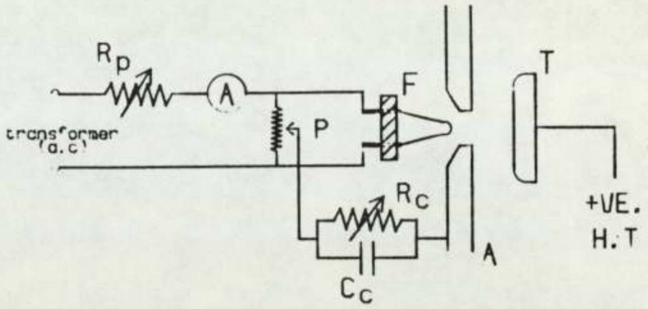

Fig.3.10 CONTROL CIRCUITRY FOR ELECTRON GUN

Fig.3.11 Electron Trajectories

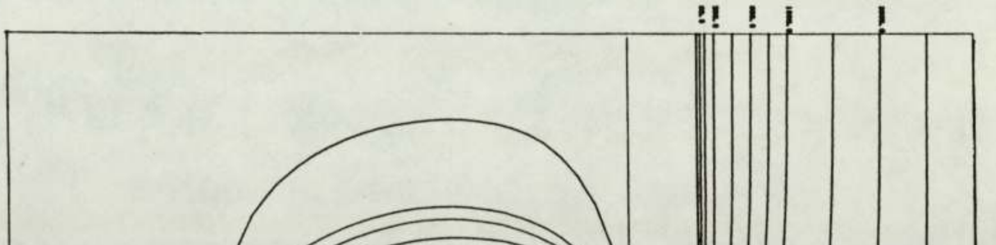

(a) No Bias Potential

(b) With Bias Potential

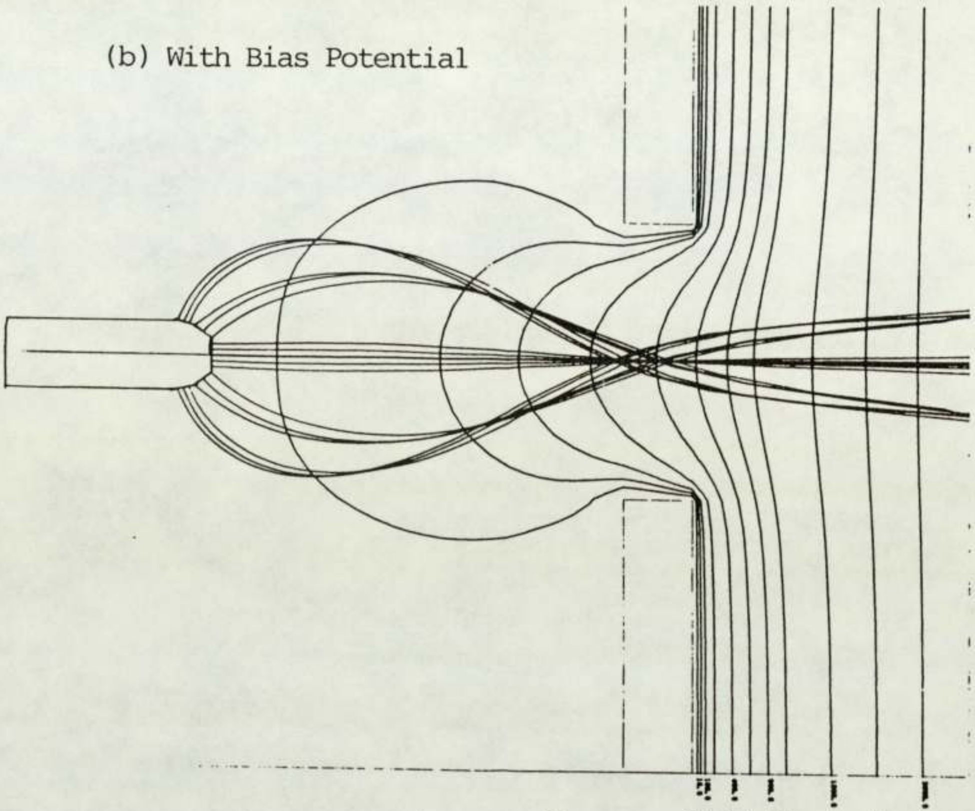

Fig.3.11 Electron Trajectories

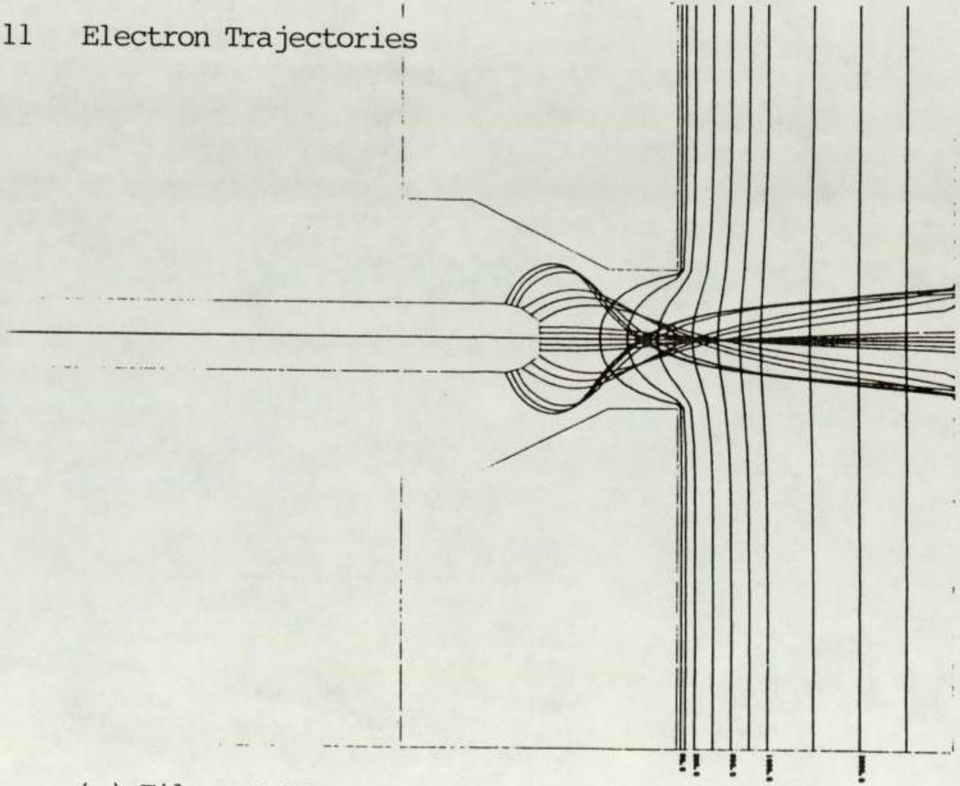

(c) Filament Nearer

the beam profile will be slightly annular in appearance.

3.4.14 Glow Discharge

This particular conditioning technique did not require the insertion of a special module into the anode body, since it was a "total" electrode treatment. However, in order to locate the emission sites, it was decided to use the ion-source module as the electron collector; this facility was also useful to mark the positions of the dominant sites found during the conditioning process.

To avoid contamination of the specimen by sputtered material from the stainless steel anode, it was necessary to install an ancillary anode: consisting of a copper electrode mounted on a stainless steel rod, attached to, but insulated from, the expansion ring. This technique also required a 90:10 argon/oxygen gas mixture, necessitating the development of a suitable gas-handling system; illustrated schematically in Fig.3.12 below. The mixing of the gases in the correct volumetric proportions was achieved using a modified oxy-acetylene mixing nozzle, where the flow rates of the individual gases were measured using a gas-flow meter.

3.5 Ion-Source Characteristics

Early work on cold-cathode saddle-field ion-sources was done by McIlraith(118) in 1966. He considered an electron, under high vacuum, starting from rest in a particular type of electric field, and showed that it would follow a long oscillating path between the anodes before being collected. Thus, there is a high

Fig.3.12

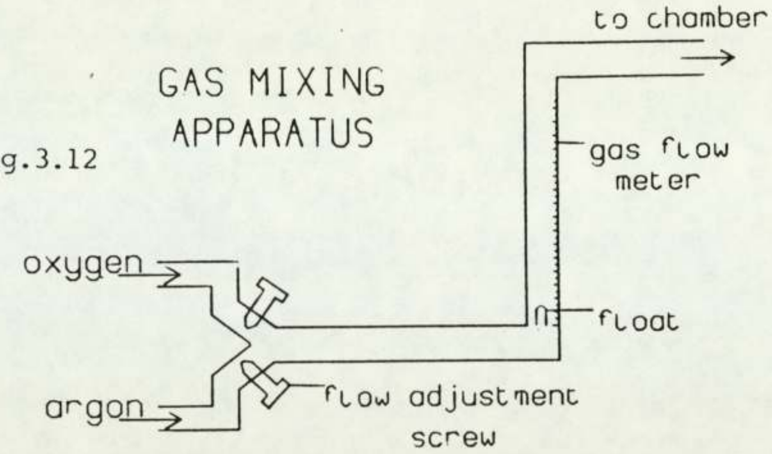

Fig.3.13 Potential Distribution Of Saddle-Field Ion-Source

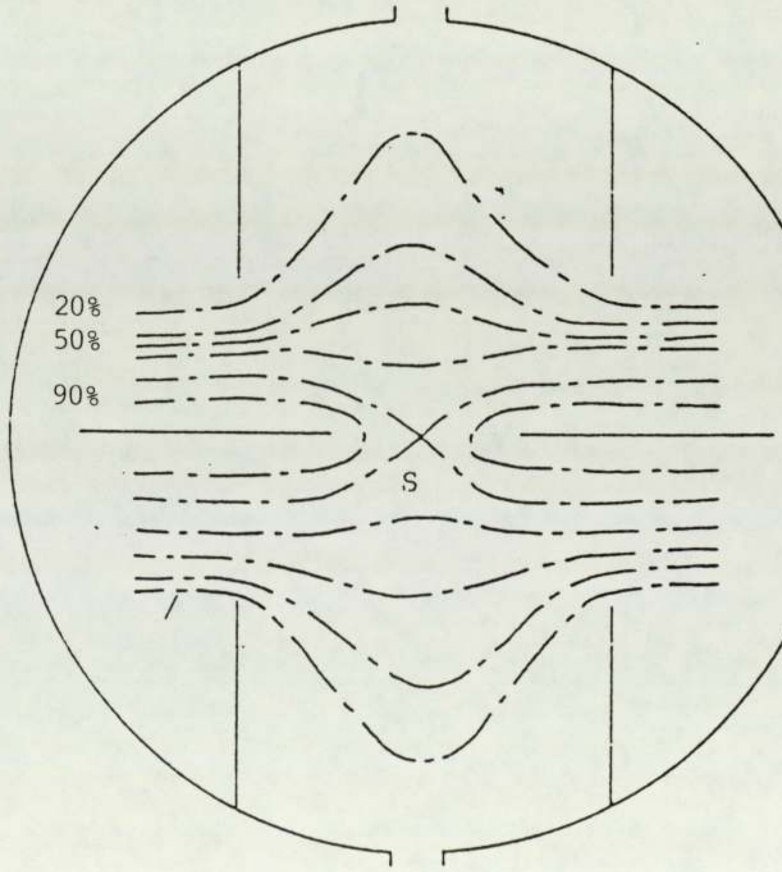

(from McIlraith)(118)

probability of an ionizing collision between the electrons and any gas molecules present, with the ions produced being accelerated towards the cathode by the field within the oscillator. The required potential distribution was calculated by McIlraith(118), and is shown in Fig.3.13. It can be seen that the electric field has a saddle-point midway between the two anodes, such that the accelerating force on the electron will always be towards this point. These ideas were verified experimentally by McIlraith and, subsequently, by Thatcher(122). Further work by McIlraith(123) on the required potential distribution, showed that both a stable and unstable type of electron orbit was possible, depending on the initial position of the electron.

Assuming a low pressure gas to be present, each electron will have many elastic collisions with the gas molecules before being collected by the anode. If the energy of the oscillating electron is higher than the ionization potential of the gas, a self-maintained discharge will eventually be produced; caused, not only of the primary ionization of the gas, but also from secondary electrons produced at the cathode surface by bombardment of the energetic ions. For this reason, the inserts containing the ion exit apertures are usually made from aluminium because of its high secondary electron yield.

The saddle-field ion source thus operates as a cold-cathode device, with the resulting ions being accelerated towards the cathode and a small proportion being allowed to escape through the cathode aperture. Work by Fitch et al(119)on a cylindrical source, showed that a beam of energetic ions of $1x10^{-4}A\ cm^{-2}$ at a pressure of $8x10^{-4}$mbar, could typically be produced. They found the source was characterized by three modes of operation: the oscillating mode, transition mode and glow mode. These modes are illustrated in Fig.3.14, with the variations of ion current with chamber pressure caused by changes in the mean-free-paths of the electrons. Normally, an ion source will be operated in the oscillating mode, characterized by a high ion beam current in the pressure range from $1x10^{-4}$ to $7x10^{-2}$mbar.

The ion source used in this present work was a modified version of the fine beam ion source developed by Ion Tech Ltd. This consisted of a short aluminium cylindrical body, two cylindrical stainless steel cathode sections and a stainless steel ring anode, and is illustrated in Fig.3.15. The operational characteristics of this source are very similar to those of the cylindrical source, but now the discharge is confined along the central axis with the ions again being self-extracted. Hence, the ion source produces an intense beam, with a divergence of about 4^{o}, symmetrical about the central anode plane. Two beams are produced on opposite sides of the anode: one of which is recorded on the monitor plate, and may thus be used to continuously monitor the performance of the source; while the other is used for etching.

The fine beam source produces a narrow beam of ions with a narrow energy spread, Khorassani & Fitch(124) finding that the average energies were about 75% of the anode voltage. However, some multi-charged ions are also produced; measurements by Fitch & Mahmoud(125) using argon, showed that about 1% of the beam is Ar^{3+}. The source also produces a significant number of energetic neutral particles, Fitch et al(126) showed that under typical operational conditions, the beam will contain about 25% neutrals;

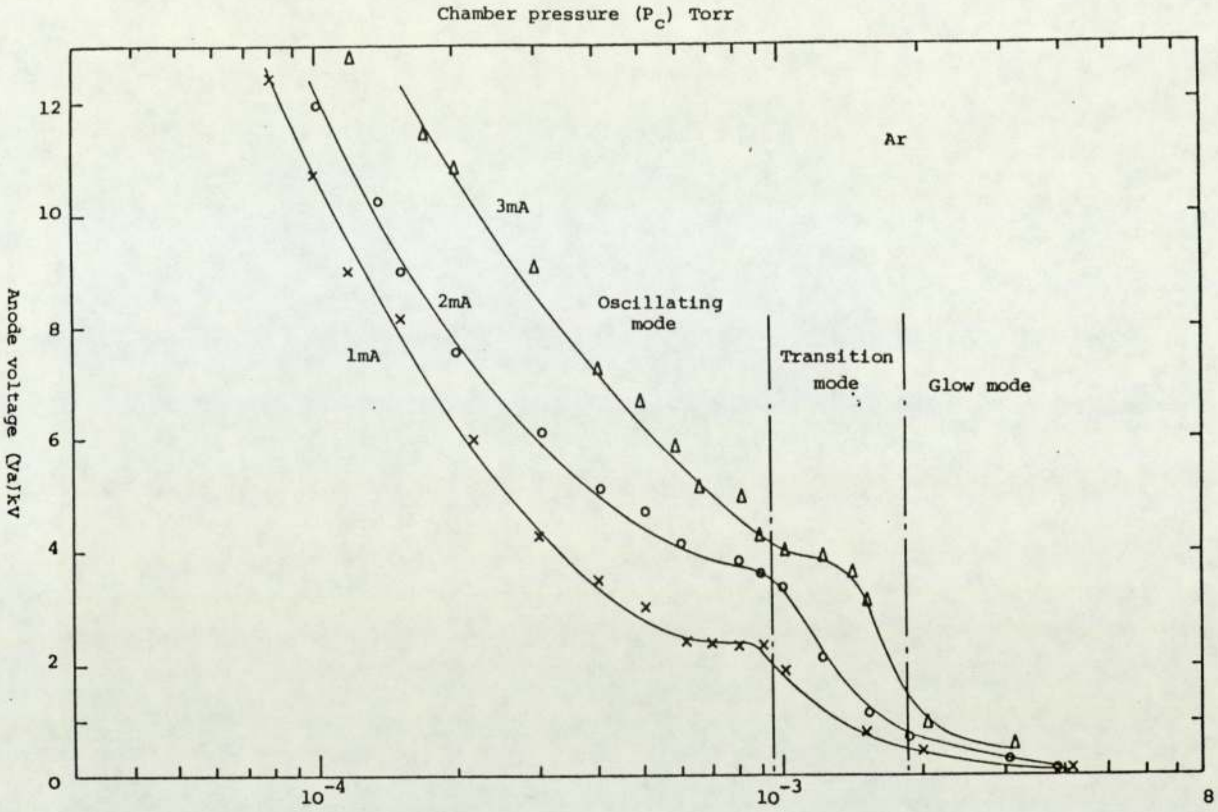

Fig.3.14 Operating Modes Of Ion-Source (from Fitch et al.)(119)

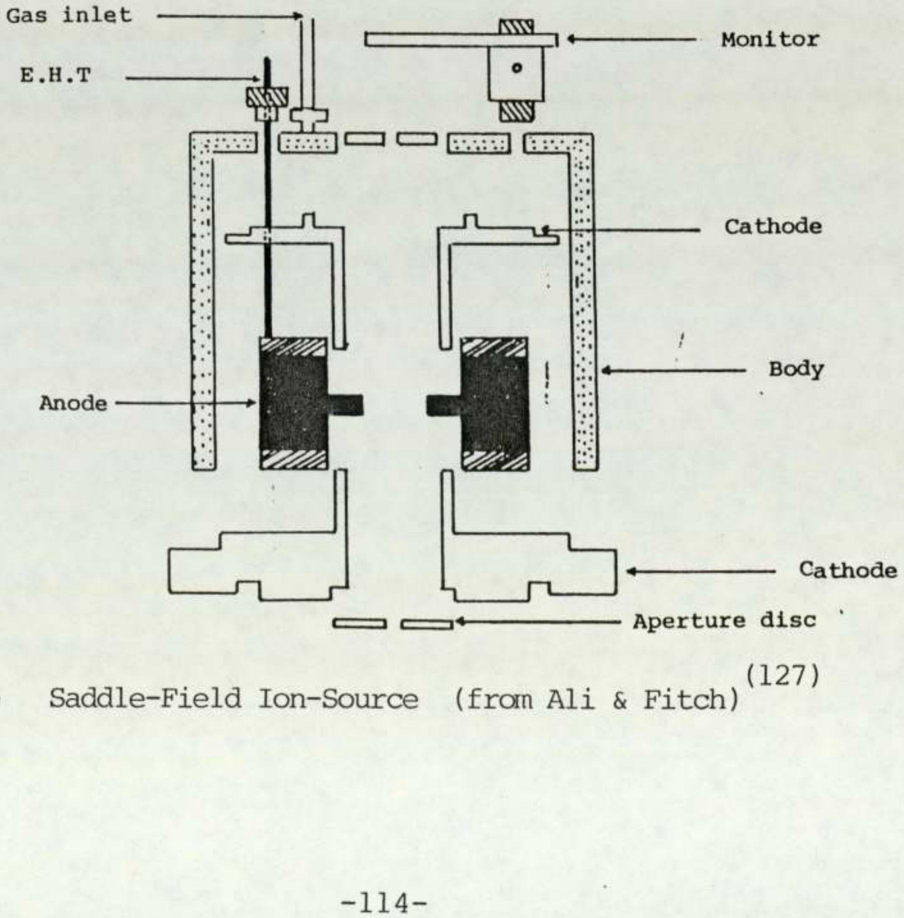

Fig.3.15 Saddle-Field Ion-Source (from Ali & Fitch)(127)

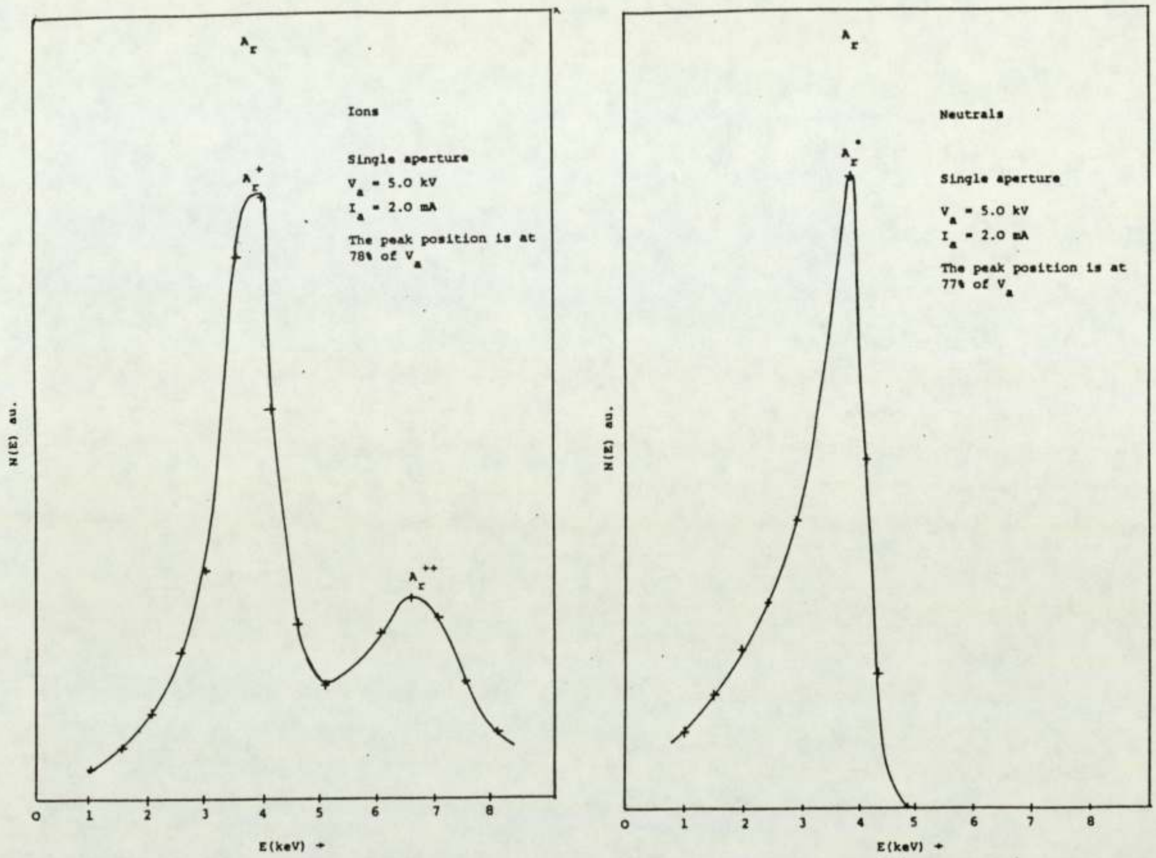

(a) Ar^+ And Ar^{++} Ions (b) Ar^0 Neutrals

Fig.3.16 Energy Spectra Of Various Ar Species this is obviously an important feature to consider when the etching of insulating particles at emission sites is to be performed. Measurements of the energy of these particles was obtained by Ali & Fitch(127), using a sophisticated time-of-flight spectrometer, and showed the same energy spread as for the singly charged ions. Figs.3.16(a)-(b) show the energy spectra for both charged and neutral particles.

3.6 General Experimental Procedures

3.6.1 Specimen Preparation

The majority of the experimental data was obtained from specimens of O.F.H.C. copper. Traditionally, this material is used as an industrial standard for high-voltage vacuum devices, e.g. vacuum capacitors, travelling-wave tubes etc. Also, past work in this laboratory has shown that this is a convenient material to study, since it tends to produce a stable pre-breakdown emission current at a relatively low applied field, i.e. often $<10\text{MVm}^{-1}$.

Much of the OFHC copper used in this work was supplied by EEV Co. Ltd., and as such complied with the impurity specifications given in Table T3.1. The disc-shaped copper specimens were dry-cut by lathe to standard 15mm diameter dimensions, as shown in Fig.3.17. This standardisation allowed specimens to be interchanged between all of the facilities available within the laboratory. In order to reduce the problems of field-intensification as much as possible, the edges of the specimen were radiused during machining. However, due to the relatively small sizes of the specimens electrode and the inter-electrode spacing (<1mm), traditional electrode profiles, As per B.S. 3839:1978 and B.S. 1954:1964.

Copper not less than	99.99%
Phosphorous	0.0003%
Sulphur	0.0020%
Lead	0.0010%
Total other volatile matter (arsenic + antimony + bismuth + cadmium + manganese + selenium + tellurium + zinc)	0.0050%
No single impurity to exceed	0.0025%

Table T3.1

Table Showing the Levels of Impurity Allowed in OFHC Copper

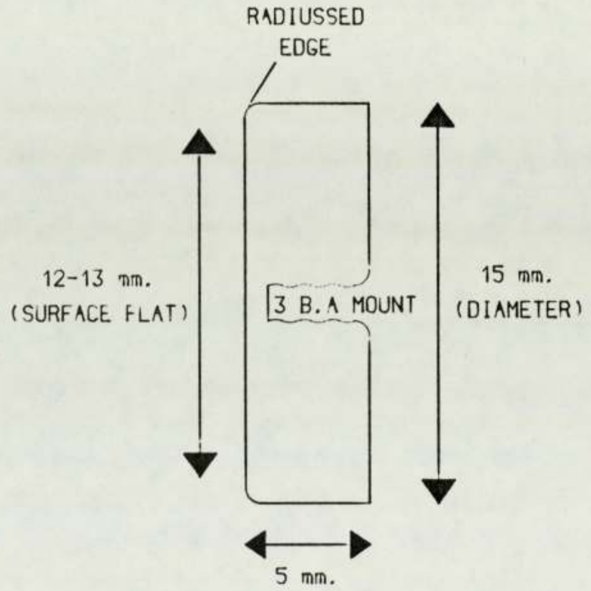

Fig.3.17 DIAGRAM SHOWING STANDARD SPECIMEN DIMENSIONS

such as those sugested by Rogowski(101) and Bruce(102) etc., were not used. Usually, these profiles attain their lower ´edge-fields´ at the expense of linearity of field across the flat face of the electrode(103) and, because of the high field-sensitivity of the electron emission process, it was important for this experimental work that a known constant field be maintained over as much of the face of the specimen as possible.

The main criterion for the final stages of specimen preparation was to achieve a reproducible surface finish, i.e. free from superficial debris, micro-protrusions and chemical contamination. Thus, after the machining process, the specimens were ground with progressively finer carborundum grits and, finally, polished to a surface finish of 1 micron, using alumina-diamond pastes. In fact, these grinding procedures were helpful in ´rounding-off´ the electrode profile, where Fig.3.18(a)-(b) shows typical electrode profiles before, and after, grinding. Immediately after polishing, the specimen electrodes were cleaned with acetone and then subjected to 5 - 10 minutes ultra-sonic cleaning in methanol. After cleaning, the specimens were quickly mounted in the experimental chamber and the system pumped down to a pressure of $<10^{-6}$mbar, followed by an overnight "bake-out", at a temperature of $>180^{o}$C. It should be noted that this baking process was not only necessary to produce U.H.V. conditions, but also tended to result in more stable electron emission due to the reduction in physi-sorbed gases etc.

An additional experimental process that was sometimes used was the artificial stimulation of electron emission. These ´artificial´ sites could be switched-on at unusually low fields, and so were often used in the initial testing of the various conditioning modules. They were produced by the contamination of the specimen with some form of carbon, usually graphite, after the final polishing stage. This technique was used on an empirical basis for some time; later work, at both CERN and this laboratory, provided an insight into the mechanism of this stimulation of electron emission(94).

3.6.2 Initial Location and Characterisation of Emission Sites

Fig.3.19 shows a schematic illustration of the important components in the experimental system, where R is a 19MΩ current-limiting resistor, placed in series with the power supply to limit damage to the electrodes in case of breakdown.

All of the specimen electrodes were initially characterised by recording how the total gap current I varied with the applied voltage and, hence, field E; from these quantities, its F-N characteristic, a plot of $\mathrm{Log}_e(I/E^2)$ versus $1/E$, was obtained. In order to measure the I-V characteristic of the gap, the specimen cathode was located opposite the anode at a known distance of between 0.5 - 0.75mm. A slowly increasing negative voltage was then applied to the specimen, until a continuous emission current was detected. The applied field was then increased until the emission current was in the $0.5 - 1\times10^{-6}$A range. This level of current was allowed to stabilise for about 5-10 minutes, in order to ensure that all potential emission sites in this field range were fully switched-on.

Following this stabilisation, the total F-N characteristic of the gap was obtained, with both increasing and decreasing fields.

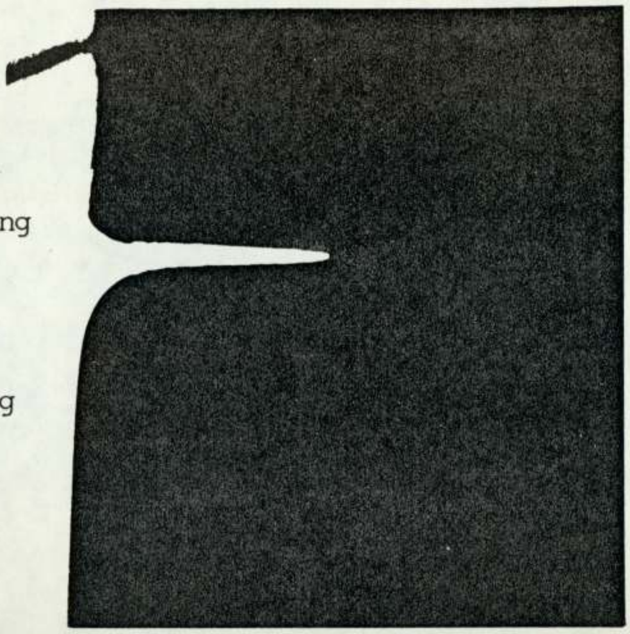

(a) Before Polishing

Fig.3.18 Specimen Profile:

(b) After Polishing

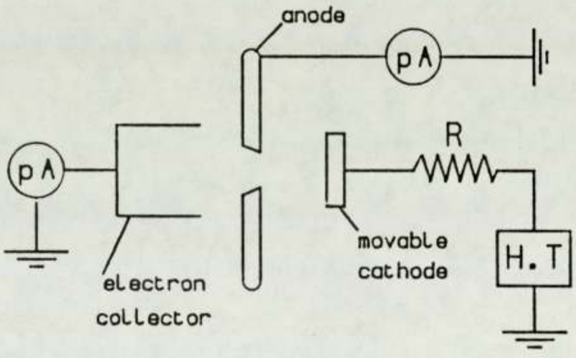

SCHEMATIC ILLUSTRATION OF EXPERIMENTAL SYSTEM

Fig.3.19

Subsequently, the specimen was systematically scanned over the anode aperture, in the stepped arc pattern described in Section 3.3.2, until electrons emitted from any emission sites were detected by the electron collector/pico-ammeter combination (the nature of the electron collector varied according to which anode module was installed). Once the dominant emission site, or sites, were located, their individual F-N characteristics were recorded before they were treated using one of the conditioning procedures.

3.7 Conditioning Techniques

3.7.1 Localised Ion-Beam Conditioning

Fig.3.20 shows a schematic illustration of the experimental system used in this phase of the work. However, before conditioning proceeded, the applied field required to give a total emission current of 1×10^{-8}A was recorded (represented by the value F_i in the tables of results given in the next chapter). The dominant emission site was then located opposite the anode aperture, and the electrode spacing increased to about 2 - 3mm to minimise contamination of the anode by copper sputtered from the specimen. The required changes were then made in the external electrical circuitry to allow the ion-source to function; these changes are denoted in Fig.3.20 by the dotted lines. The ion current incident on the specimen during conditioning was measured by connecting it to earth via a micro-ammeter.

Argon was introduced into the chamber to a pressure of 8×10^{-5}mbar, and the ion-source power supply (Ion-Tech IT5) set to a voltage of 5 - 8kV and 1 - 3mA, with the precise values used being determined by the requirement that an ion-beam current of

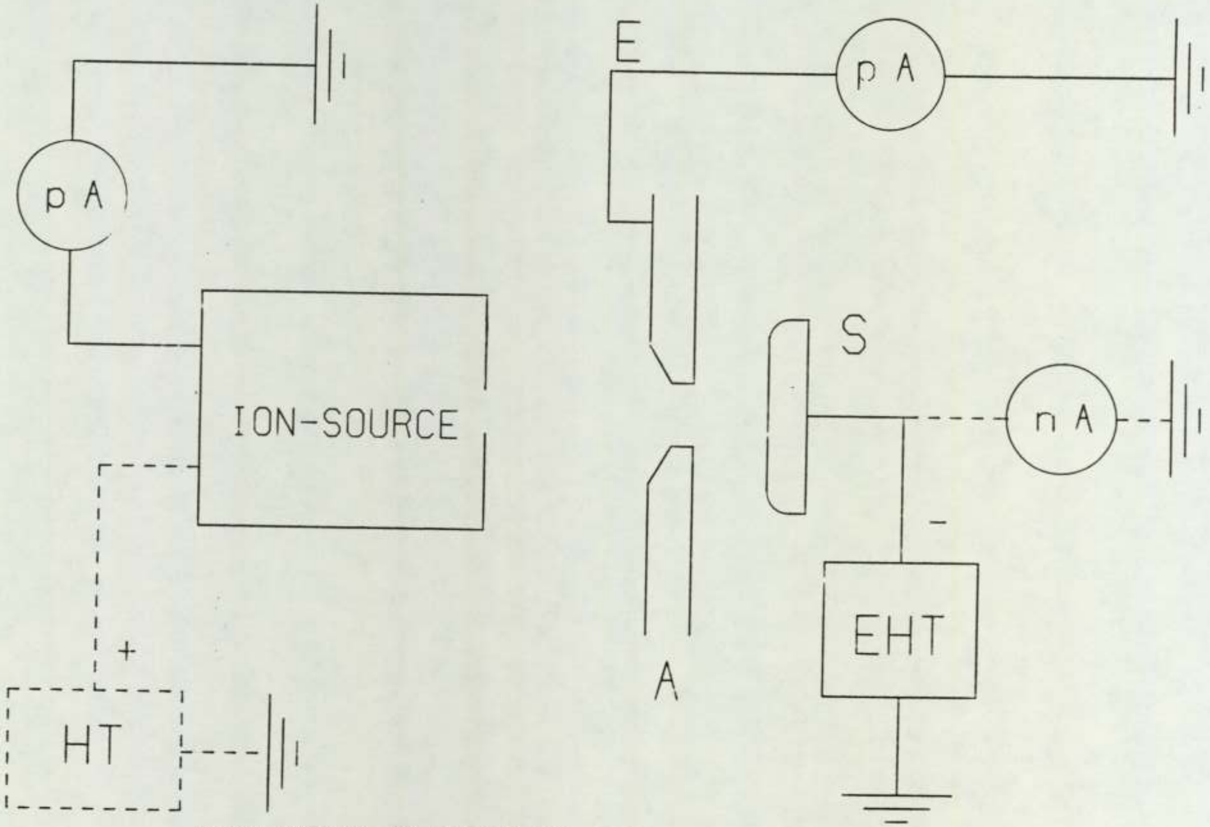

Fig.3.20 SCHEMATIC DIAGRAM OF EXPERIMENTAL EQUIPMENT FOR ION-SOURCE CONDITIONING

3×10^{-6}A be recorded on the specimen. To monitor the performance of the ion-source, the current from the rear of the source was also measured. This was usually 10-15 times larger than the specimen current due, primarily, to the production of secondary electrons caused by the impact of ions on the collimator assembly and anode aperture; thus resulting in a reduction of beam intensity. The beam was maintained for long enough, typically 15mins, to destroy the emission site; this usually corresponded to about 4 μ m being etched from the surface of the copper cathode. Details of the experiments to calibrate the etch-rate of the ion beam are described in Chapter 5, where an accurate knowledge of the rate of removal of the copper was essential for the ´partial-etching´ experiments. The emission site was assumed to be "destroyed" if no detectable emission current could be obtained upon the application of a field in the range previously needed.

After the ion-source was switched off, the chamber was re-evacuated to a pressure of $<3\times10^{-9}$mbar, the electrode spacing re-set to its previous value, and the external circuitry re-arranged for the ion-source to act in its electron-collector mode. Finally, a new emission site was located and characterised in the same way as the original one. The whole procedure, from obtaining, locating and measuring a stable emission current, to the destruction of the site by ion-beam etching, was repeated, as many times as possible, until the emission current could either no longer be localised, or the upper limit of applied field was reached. The field required to obtain a total emission current of 1×10^{-8}A was again found, and denoted in the tables of results as F_f. Hence, by the comparison of F_i and F_f, an idea may be gained as to the effectiveness of this technique as a means of electrode conditioning.

3.7.2 Localised Gas Sputtering Conditioning

Referring to Fig.3.21, which is a schematic diagram of the experimental system developed for the evaluation of this technique, the hyperdermic syringe S functioned as the electron-collector during the location and characterisation of the emission sites. Subsequently, during conditioning, it functioned as the final part of the gas handling system, which ensured that the pressure of argon was higher at the portion of the specimen located opposite the anode aperture; hence resulting in a higher sputtering rate. After following the steps detailed in Section 3.6.2, to obtain locate and characterise the dominant emission site, a value for F_I was obtained and the applied voltage reduced until the emission current was $<1x10^{-10}$A. Argon was then introduced into the chamber until a pressure of $1x10^{-6}$mbar was reached. The level of emission current was kept low during this critical entry of gas to minimise the possibility of a localised micro-discharge occuring. The applied voltage was then increased until an emission current of 1 - $5x10^{-7}$A was obtained; at this stage, the flow of argon was increased until the chamber pressure rose to $1x10^{-5}$mbar. According to the assumed mechanism for localised gas sputtering(112), discussed in the previous chapter, the sputtering rate will be faster for higher emission currents. However, because of the large instabilities that occur in the emission currents under these ´gassy´ conditions, it was necessary to limit the current to the above range if a discharge was to be

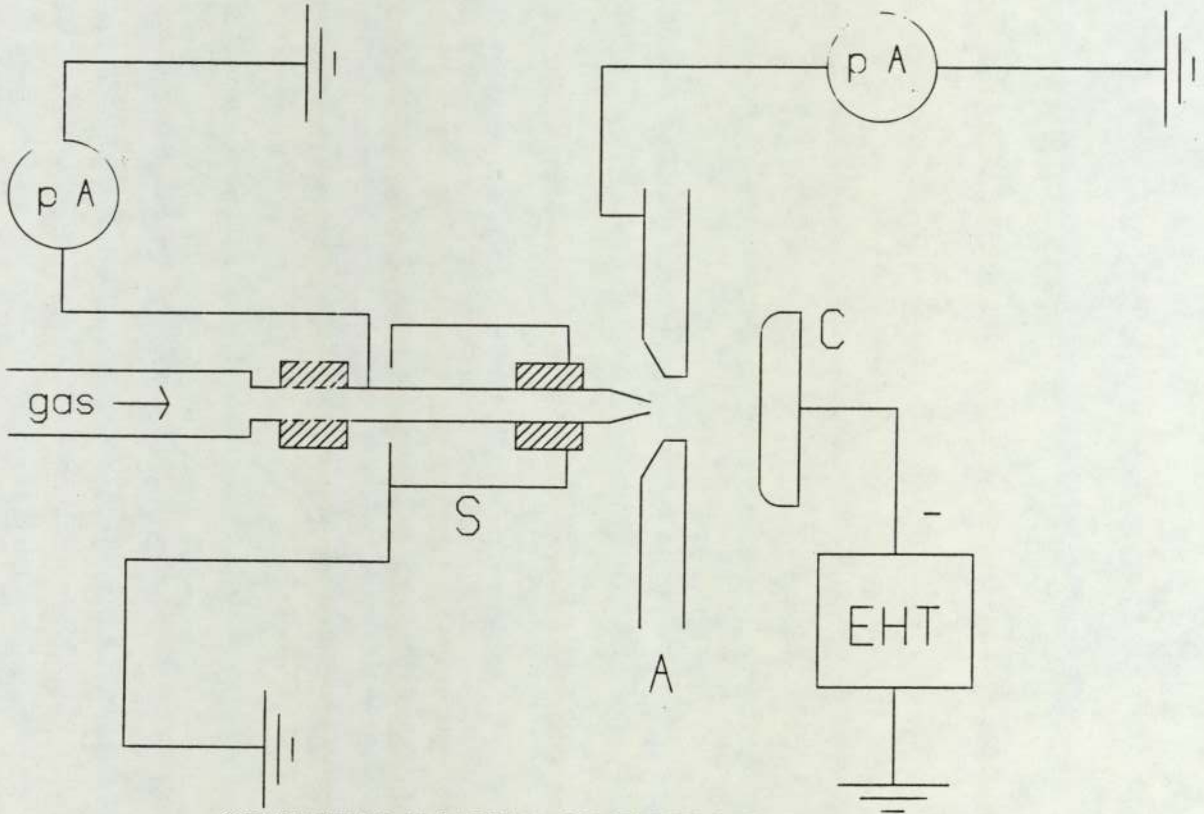

Fig.3.21 SCHEMATIC DIAGRAM OF EXPERIMENTAL SYSTEM
FOR GAS SPUTTERING

avoided. Accordingly, the applied voltage had to be continuously adjusted during conditioning to satisfy this requirement. The conditoning was usually continued until the emission current fell to a considerably lower level, typically $<10^{-10}$A; it was then assumed that the characteristics of the emission site had changed so significantly that the site was effectivly destroyed, even if, subsequently, a new site switched-on and was found to occupy a similar location. The conditioning was sometimes terminated if a significant, and continuing, de-conditioning was observed, as evidenced by a continually increasing emission current. This usually occurred if the instability in emission current resulted in a micro-discharge.

After each conditioning sequence, the chamber was re-evacuated to U.H.V. conditions, the specimen scanned and the location and F-N characteristic of the dominant site recorded. This whole cycle, of conditioning followed by the scanning and characterisation of emission sites, was repeated until, either, no further significant conditioning was observed, or the instability in emission current, even under U.H.V. conditions, made further measurement of the F-N characteristics impossible. As in the previous section, a value of F_f was obtained for each specimen; so, by comparing this with the corresponding values of F_i, the effectiveness of gas sputtering as a conditioning technique could be evaluated.

3.7.3 Localised Electron Beam Conditioning

As already noted, the ´height´ of the filament was a very critical factor governing the power density of the electron beam.

Consequently, a series of preliminary experiments were performed in order to optimise this, and other, experimental parameters, viz. the target distance, accelerating voltage on the target, and the variable resistance controlling the bias potential (R_c). In these preliminary experiments, the usual copper specimen was replaced by a 0.5 micron thick copper film deposited on a glass slide. For any particular filament height, the effect of a number of the other parameters could be evaluated by measuring both the beam current, using the milli-ammeter, and the diameter of the scar produced by the bombardment; these values enabling the current density of the beam to be roughly estimated.

Once these parameters had been optimised, the copper film was replaced with a standard copper specimen. Fig.3.22 shows the configuration of the experimental system developed for the evaluation of this technique. Then, following the same procedure used with the other tecniques, a steady emission current was obtained and the specimen scanned to locate the dominant emission site. After its F-N characteristic had been measured, with the filament of the electron gun being used as the electron collector, the relevant external connections were made and the target (specimen) moved some distance away; the filament current was then slowly increased to a value of 2.85A, usually giving rise to considerable out-gassing. The inter-electrode spacing was then set to about 2mm, and a high positive voltage (20 - 25kV) applied to it. R_c was then reduced until a beam current of 100 - 200mA was monitored on the milli-ammeter; this level of beam power was maintained for times varying from a few minutes to over 30 minutes. The gun was then turned-off and the specimen allowed to

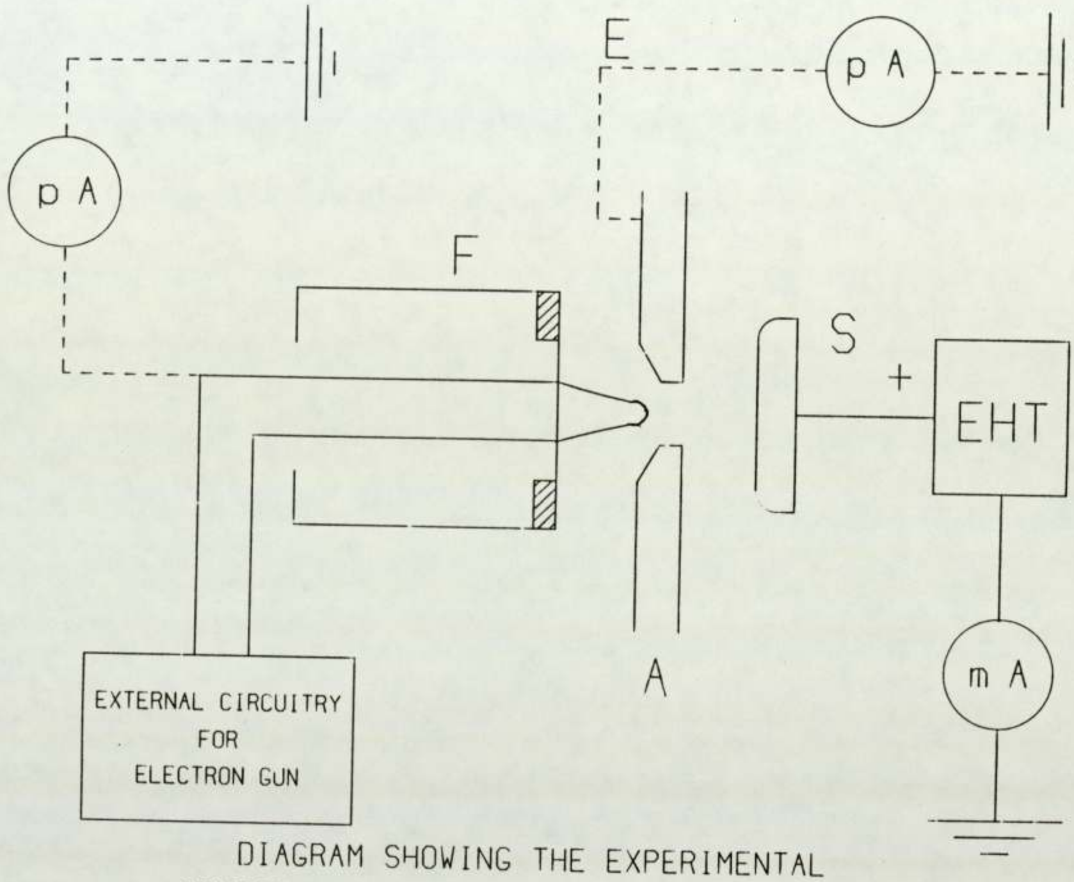

DIAGRAM SHOWING THE EXPERIMENTAL
CONFIGURATION FOR ELECTRON BOMBARDMENT

Fig.3.22

cool.

Following this treatment, both the location and F-N characteristic of the treated site were found to be unchanged; with a subsequent optical examination of the bombardment area failing to reveal any surface damage, other than a slight disclouration. As discussed more fully in the following chapter, the failure of this electron bombardment to cause localised surface damage was thought to be a consequence of the high thermal conductivity of copper which, in turn, prevented a large temperature rise at the impact zone. To conclusively demonstrate that the beam was not causing any significant surface damage to a bulk target, a copper specimen was coated with a 0.5 μm thick layer of aluminium. This gave a target with almost the same thermal conductivity as a pure copper one, but one where any surface damage would be easily visible due to the rupture of the aluminium coating. After electron beam bombardment, optical examination once again failed to show any evidence of surface disruption.

It was next decided to substitute a titanium specimen for the copper one, since calculation suggested that, due to its much lower heat conductivity, a much higher temperature would be produced on a titanium target than on a copper one for the same beam power density. The initial processing, described earlier in this section, was then repeated with the titanium specimen; this time, however, significant changes were found in the F-N characteristics of the treated sites. The physical significance of these results is discussed in the next chapter.

3.7.4 Localised "Spark" Conditioning

The anode module used for this technique was the same as that described in Section 3.7.2 for the gas sputtering method. However, for this application, instead of just providing the final stage of the gas delivery system, a voltage was applied to the syringe to produce a localised high-field. The experimental set-up was also similar to that shown in Fig.3.21, except that the syringe-tip was moved forward in order to protrude slightly through the anode aperture. This was so a slightly higher field would be produced when, for the conditioning process, it was connected to a high-voltage source.

The initial procedure for locating and characterising the dominant emission site was the same as for the other techniques. Following this characterisation, the field applied to the specimen was increased until the emission current was about $5\text{x}10^{-6}$A. A positive voltage was then applied to the syringe, in order that the higher field would cause a localised micro-discharge in the region of the emission site. The positive voltage was limited to about 1.5kV because of the possibility of breakdown occurring between the syringe and anode assembly; accordingly, the voltage was repeatedly cycled up to this limit until a micro-discharge occurred. The specimen was then re-scanned, its F-N characteristic measured, and the whole process repeated. These findings, together with the many problems associated with this technique, are discussed in the next chapter.

3.7.5 Glow Discharge Conditioning

This section of experimental work was designed to complement work done at C.E.R.N. on a similar method of conditioning used to treat R.F cavities. The experimental system required for this technique is illustrated in Fig.3.23. The preliminary steps required to locate and characterise any emission sites were carried out as usual. After this characterisation, the specimen was rotated into position opposite the ancillary anode A2 and the 90:10 mixture of argon/oxygen introduced into the chamber, to a pressure of 0.1 - 0.5mbar. A voltage of between 200-400V was then applied between the specimen and A2, in order to establish a glow discharge; a typical example of which is shown in Fig.3.24. The discharge current, and hence the number of ions incident on the specimen, was regulated by the variable resistance R in the high-voltage line, and monitored by the milli-ammeter; the ion-dosage was further controlled by varying the discharge time. Experiments were performed with both negative polarity voltage on the specimen, and a positive voltage on A2, i.e. the specimen was always the cathode.

After a particular ion-dosage, usually $\cong 1\text{x}10^{21}\text{ions.m}^{-2}$, the glow discharge was halted and the chamber re-evacuated to U.H.V. conditions. The specimen was then re-located opposite the apertured anode A, and the applied field increased until an emission current of $3\text{x}10^{-11}$A was detected; this field value is represented by E_c in the tabulated results of this technique. The field was then slowly increased until the complex switching-pattern of the emission current, characteristic of this conditioning process, was completed; this switching pattern is

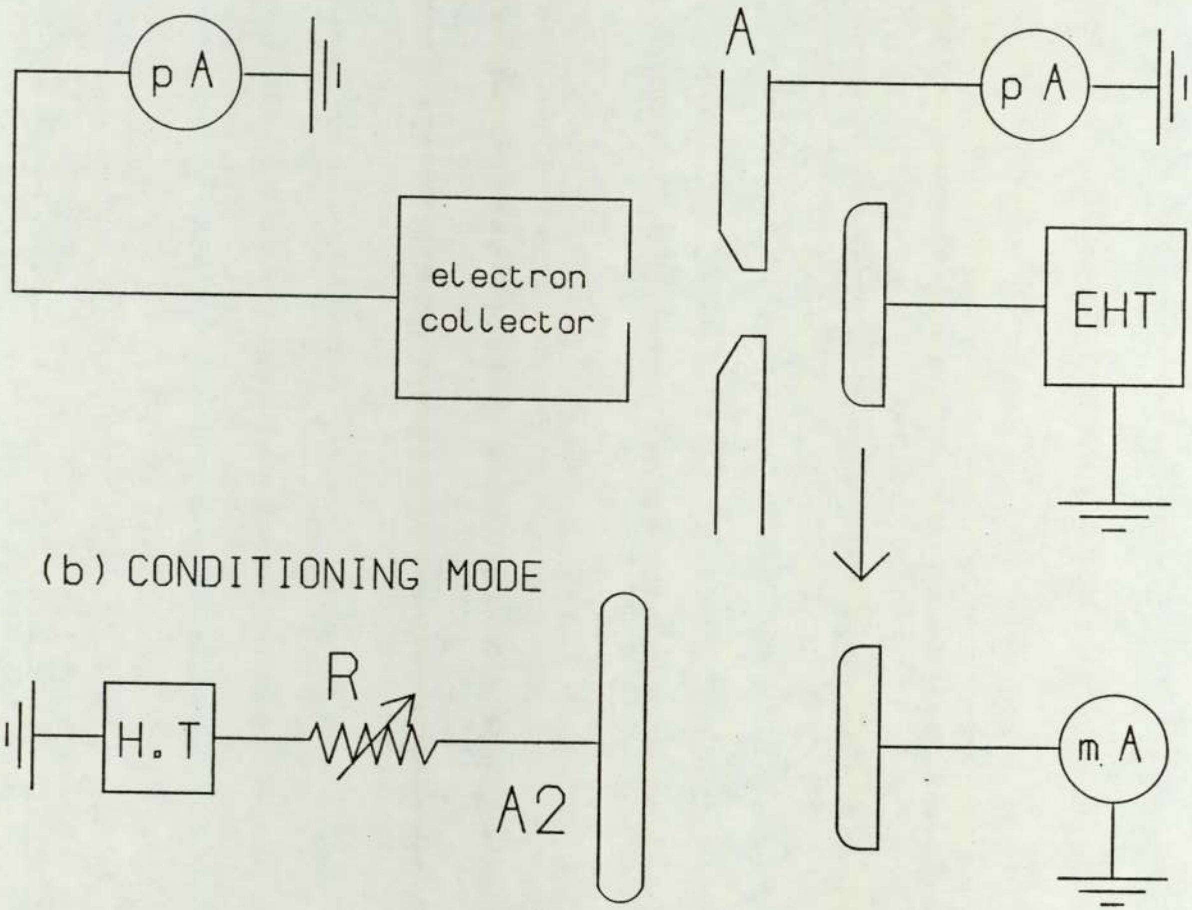
(a) CHARACTERISATION MODE

(b) CONDITIONING MODE

DIAGRAM OF EXPERIMENTAL SYSTEM REQUIRED FOR GLOW-DISCHARGE TECHNIQUE

Fig.3.23

described in the next chapter. After this, the field required to produce the same current of 3×10^{-11}A was again measured, and denoted by E_s. The dominant emission site was again located and characterised, and the whole process repreated until instabilities in the emission current prevented further measurements. As with the previous techniques, values of F_i and F_f were also obtained, so that the relative effectiveness of this method of conditioning could be gauged.

As a control experiment, to establish whether the oxygen had any significant effect on the observed conditioning, a specimen was processed in the same manner as described above, but using only argon rather than an argon/oxygen mixture.

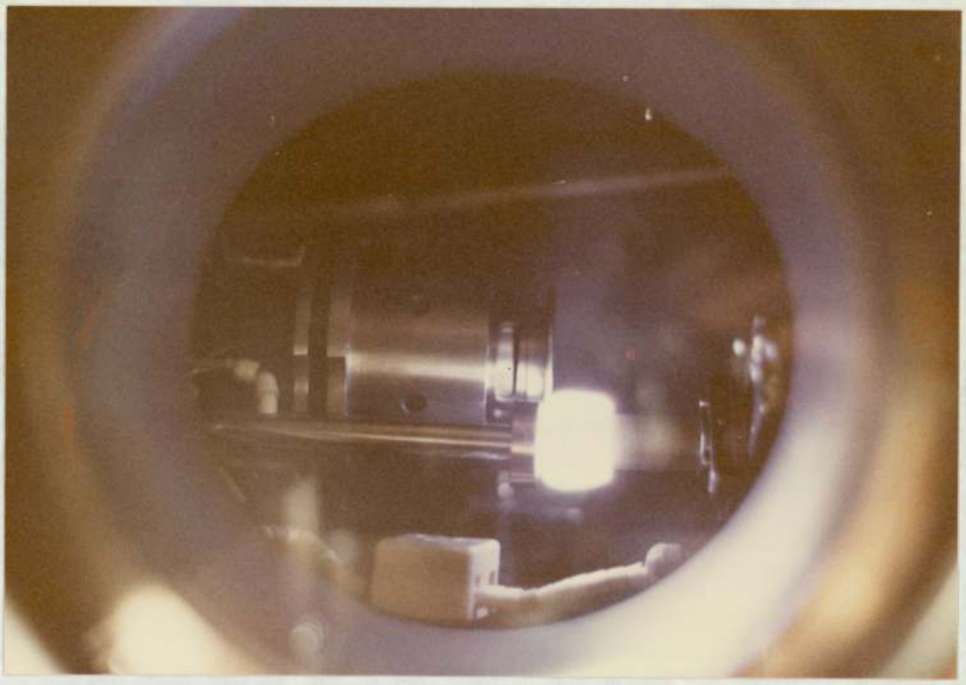

FIG.3.24 Photograph of a Glow-Discharge

CHAPTER 4

Evaluation of Conditioning Techniques

4.1 General Considerations

4.1.1 Effect of the Anode Aperture

For the plane-parallel electrode geometry used in this study, the macroscopic gap-field is essentially constant. However, the presence of the 1mm diameter anode aperture does lead to a significant local distortion of the field. In particular, there is a protrusion of the field into the anode space, and a consequent reduction of the cathode surface field directly opposite the aperture; it follows that the effect becomes more pronounced as the electrode separation is progressively reduced below 1mm. As a consequence of this effect, the F-N characteristic of the dominant emission site, (i.e. the one having the highest field-enhancement factor), when located opposite the aperture, could be expected to be shifted to a higher applied voltage range compared to that recorded when the site is located opposite the planar region of the anode. The magnitude of this effect is illustrated by Figs.4.1(i)-(iii), which present computer-generated (courtesy of A.P.Collis of EEV Ltd.) field plots for the cathode/anode-aperture system, at various electrode spacings. From these, it can be seen that for spacings of 1mm there is almost no field reduction, but that for spacings <0.33mm the reduction becomes very significant, due to the high field dependence of the emission current. Calculations from these plots enabled a semi-quantitative

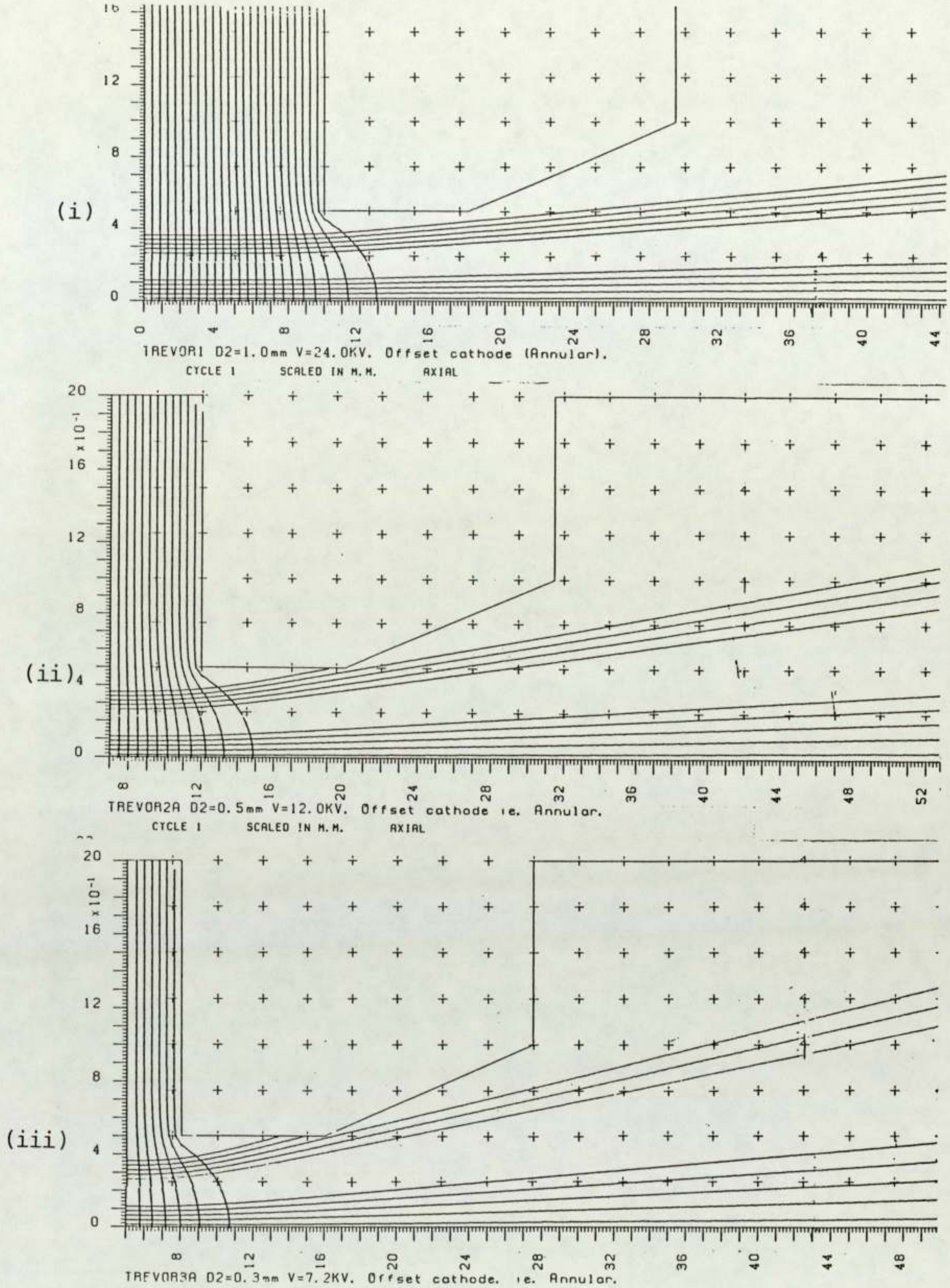

Fig.4.1 Field And Electron-Trajectory Plots Showing Field Reduction In Aperture Region For Different Electrode Spacings (D2)

correction factor to be applied to the planar gap field values if the F-N characteristic of an individual site was being recorded opposite the aperture.

The field plots in Fig.4.1 also include the associated electron trajectories. These show that for electrons emitted normally to the cathode surface, the field distortion around the aperture causes a significant deviation in their paths, with non-axial electrons impacting on the edges of the aperture. It can also be seen from Fig.4.1, that the magnitude of this effect increases with decreasing electrode spacing. As explained in Chapter 2, a particular emission site is normally made-up of a cluster of ´sub-centres´, which may be spread over a relatively large area ($\approx 0.1\text{mm}^2$). Hence, when an emission site is centralised opposite the aperture, some electrons are still likely to be collected on the edges of the anode aperture. This results in a lower current being collected by the Faraday cage, for a particular value of the applied field, than that recorded from the site in a planar electrode geometry. The problem of stray electrons impacting on the edges of the anode aperture is, for reasons detailed later, an effect of particular importance in the work on electroluminescence.

4.1.2 Effectiveness of Conditioning Techniques

In order to evaluate the effectiveness of a particular conditioning technique, it is necessary to characterise the emissivity of a specimen in terms of a set of well-defined quantities: (a) F_i and F_f, which, as explained in the previous chapter, represent,respectively, the magnitude of the applied field required to produce an emission current of $1\text{x}10^{-8}$A from an untreated specimen, and a specimen that had completed the conditioning procedure; (b) the β-factors and intercepts obtained from the plots of the F-N characteristics of individual emission sites; (c) an "improvement-factor" γ that can be calculated for each specimen following the completion of the conditioning treatment. This γ-factor was calculated by considering the change in applied field required to produce a current of $1\text{x}10^{-8}$A, before and after fully conditioning each specimen. Such that: $\gamma = F_f/F_i$. Also presented in the results is an indication of how effective each stage in conditioning has been;calculated by comparing the field value required for $1\text{x}10^{-8}$A emission current.

4.1.3 Analysis of Experimental Data

In order to simplify the task of data processing, the raw I-V data collected during the various experimental runs was processed by computer. The program, shown in Appendix A.1, calculates the F-N co-ordinates, correcting for the field-effect of the anode aperture if required. It then saves these co-ordinates to a floppy disc for subsequent plotting (using an additional graph-plotting program), produces a ´best-fit´ regression line, with statistical information regarding the standard deviation of the gradient and intercept, and calculates the field-enhancement factor and emission area associated with this ´best-fit´ line.

4.2 Evaluation of Localised Conditioning Techniques

4.2.1 Ion-beam Conditioning

Table T4.1 summarises a representative sample of ten results obtained using the ion-beam to locally condition the individual emission sites on a series of copper specimens; where the tabulated quantities have the significance described in Section 4.1 above. In addition, the results obtained from an artificially contaminated specimen is presented also. The effectiveness of the conditioning process is quantified in terms of, firstly, the changes in the F-N characteristics (the β-factors and intercepts) and, secondly, the increasing voltage hold-off of the electrodes, as represented by the values for F_i, F_f and the γ-factors. The final column of the table indicates which of the following four main reasons why further conditioning was abandoned:

a = an edge site that is not susceptible to further etching

b = the electrode gap is at the maximum limit of the applied field

c = the sudden switch-on of many sites distributed over the electrode surface

d = the occurrence of a large switching action, usually of a single site, often accompanied by general current instabilities, leading to a higher current for the same applied field.

To complement this data, the graphs of Fig.4.2(i)-(iii) show three typical examples of how the F-N characteristic of a specimen electrode changes during conditioning, as the dominant emission sites are progressively destroyed. Each plot represents the emission characteristic of the dominant emission site found between each stage of the conditioning. For completeness,

Table T4.1

Table Shows Representative Results From Localised Ion-Etching Experiments

F_i $(MV.m^{-1})$	F_f $(MV.m^{-1})$	γ	F_2/F_i;...etc.	β	Intercept (-)	Reason
* 3.3	13.0	3.9	2.9; 1.3; 1.1	840; 480; 382 308	25.5; 31.5; 35.5; 26.3	a
* 7.8	28.1	3.5	2.1; 1.4; 1.2	437; 245; 181 137	36.2; 35.3; 37.0; 26.5	a
13.2	35.0	2.7	1.5; 1.3; 1.5	250; 185; 166 97	31.3; 33.2; 42.1; 26.9	c
18.8	41.8	2.2	1.3; 1.7	170; 265; 130	31.8; 44.1; 43.7	b
12.9	31.3	2.4	1.9; 1.3	374; 230; 144	37.5; 40.5; 38.6	a
16.1	32.6	2.1	1.6; 1.0; 1.1 1.1; 1.8	258; 123; 281 96; 110; 50	38.1; 32.1; 45.5; 28.1; 37.1; 28.5	d
19.5	36.4	1.9	1.1; 1.4; 1.2 1.1	178; 180; 162 89; 97	33.3; 36.9; 38.8; 31.9; 34.9	c
11.2	31.7	2.4	1.6; 1.4; 1.2	450; 284; 130 218	38.5; 37.2; 32.3; 40.6	a
13.8	31.1	2.3	2.3	311; 180	36.1; 41.2	d
14.9	44.5	3.0	1.7; 1.4; 1.2	245; 97; 89 100	30.1; 27.8; 34.6; 44.0	c
15.1	35.0	2.3	1.5; 1.2; 1.2	232; 196; 148 91	28.6; 38.5; 38.2; 33.0	a

Fig.4.3(i)-(iii) refers respectively to Fig.4.2(i)-(iii), and shows how the spatial locations of these dominant emission sites varied during conditioning. As can be seen from this diagram, the position of the dominant emission site tends to ´migrate´ towards the edge of the specimen as conditioning proceeds. However, this simply reflects the fact that an edge-site is more difficult to accurately locate and destroy. It should also be noted that although a number of emission sites tended to occur in the same region, an emission site was rarely found to occupy exactly the same location (within the resolution of the scanning system).

During some of the early experiments, after a conditioning cycle the applied voltage limit of only 15kV was insufficient to produce a reasonable range of emission current (i.e. a maximum emission current in the 10^{-10}A range); this problem is descibed as reason b in Table T4.1. In fact, on several other occasions, this voltage limit required that a fairly small electrode spacing be used which, when combined with an unstable emission current, often gave rise to a large switching phenomenon (sometimes even a micro-discharge) leading to a de-conditioning; described as reason d in the table of results. In later experiments, this problem of limited field-capability was largely overcome by the installation of a 25kV electrical feedthrough. Inspection of Table T4.1 shows that a common reason for calling a halt to the conditioning process was the occurrence of an emission site located on the edge of the specimen. The field distortion present at the edges of the specimen was such that, due to the high spatial selectivity of the ion-beam conditioning, it was very difficult to locate the emission site opposite the aperture sufficiently accurately for it to be destroyed by the ion-beam. A very interesting phenomenon noted during the investigation of this technique was the large scale switch-on of emission sites under the application of high fields, usually in the 35 - 40MVm^{-1} range; once these sites were fully switched-on, a slight de-conditioning was commonly observed. Each of these high-field emission sites accounted for, typically, 1-10% of the total gap emission current; a fact making it very difficult to obtain a stable F-N characteristic for a single site over a reasonable current range. The physical significance of this phenomenon is discussed in a later chapter.

As can be seen from the values of the factors in Table T4.1 and the graphs of Fig.4.2, the magnitude of the field-shift of the F-N characteristics following ion-beam etching varied considerably. To investigate the possibility that the conditioning effects might be subject to a temporal relaxation process, the F-N characteristic of the gap was first recorded immediately after ion-bombardment of the previously dominant emission site, i.e. within 20 minutes, then again after the specimen had been subjected to an applied field for five hours, at a level sufficient to produce an emission current of 2x10^{-9}A, and finally after a further 19 hours, under zero applied field. These three characteristics are shown in Fig.4.4, together with the F-N characteristic of the gap after a further conditioning cycle to show the relative magnitude of the field-shifts associated with the two cases. From these, it can be seen that the improvement in voltage hold-off produced by the conditioning was permanent, and not subject to relaxation with time; for instance by re-growth of a surface oxide layer, or de-sorption of gas.

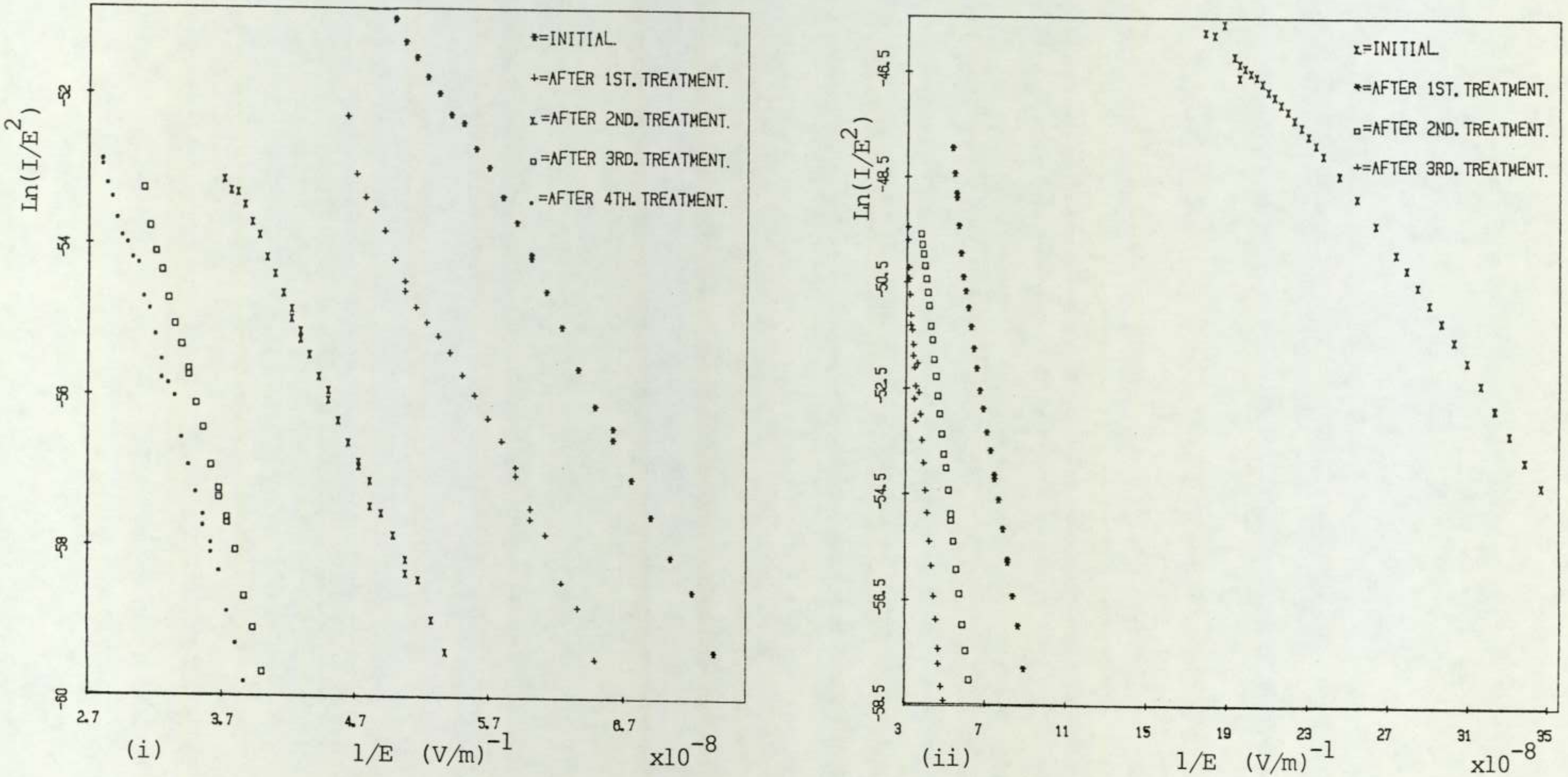

(i) (ii)

Fig.4.2 (i)-(iii) F-N Plots Showing The Successive Changes In Emission Characteristics

Produced By Ion-Beam Conditioning

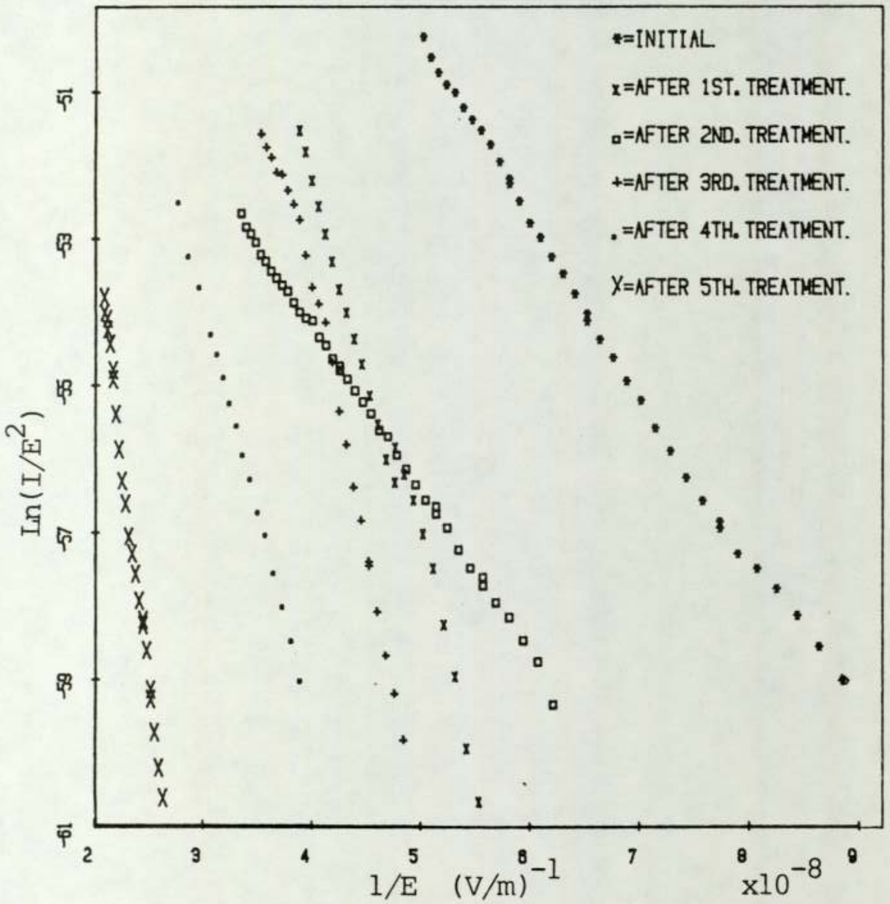

Fig.4.2 (iii)

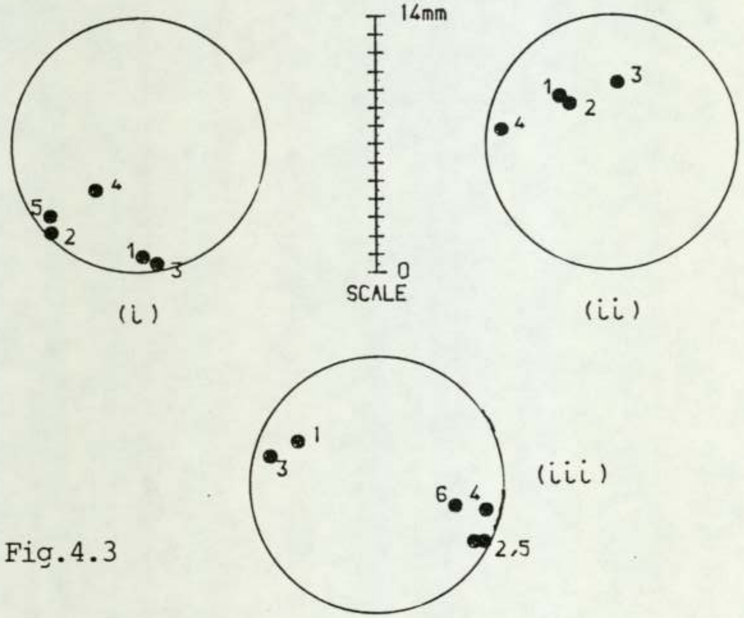

Fig.4.3

DIAGRAM SHOWING THE CHANGING LOCATION OF THE DOMINANT EMISSION SITE PRODUCED BY ION-BEAM ETCHING

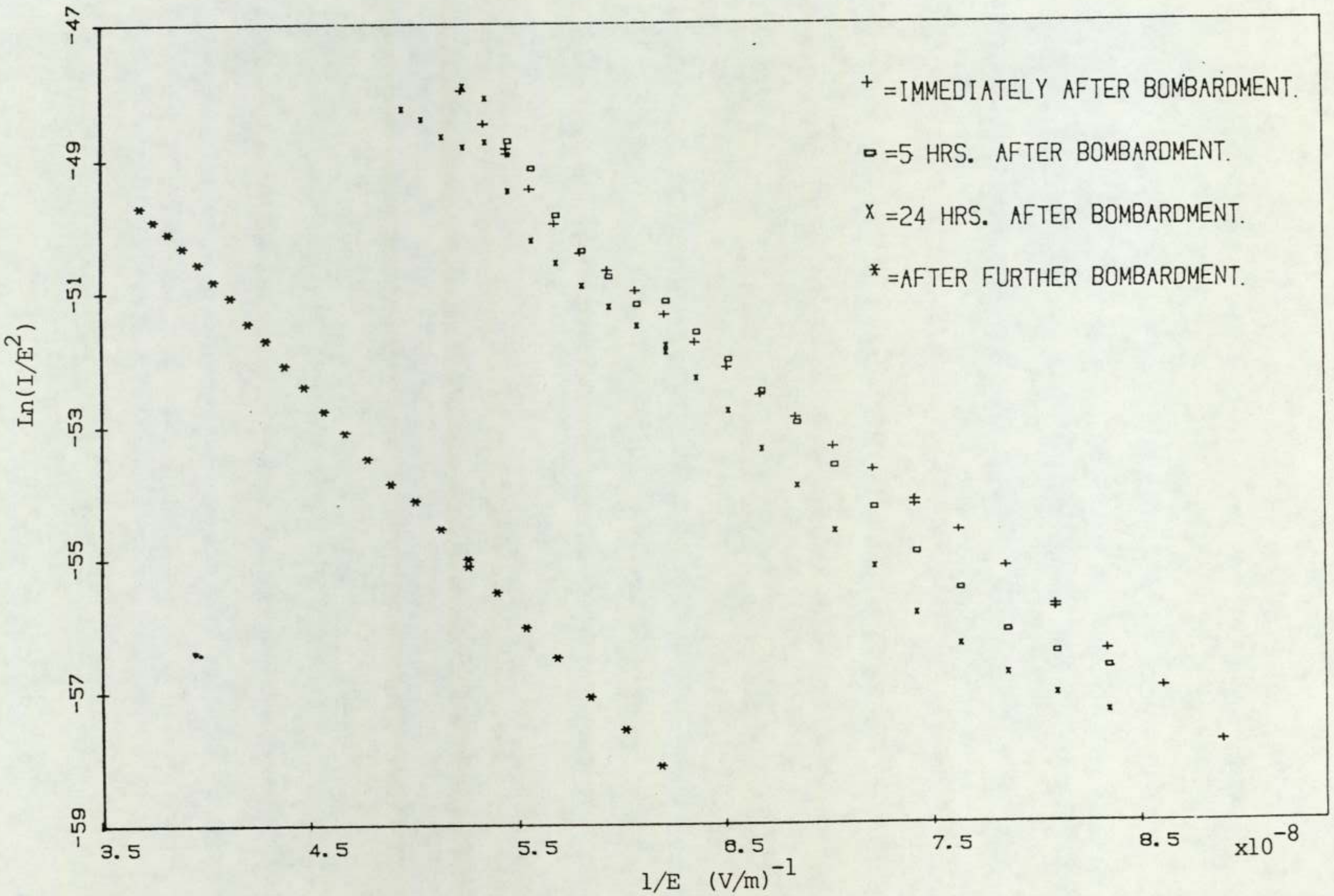

Fig.4.4 F-N Plots Investigating A Possible Temporal Relaxation Effect Associated With Ion-Beam Conditioning

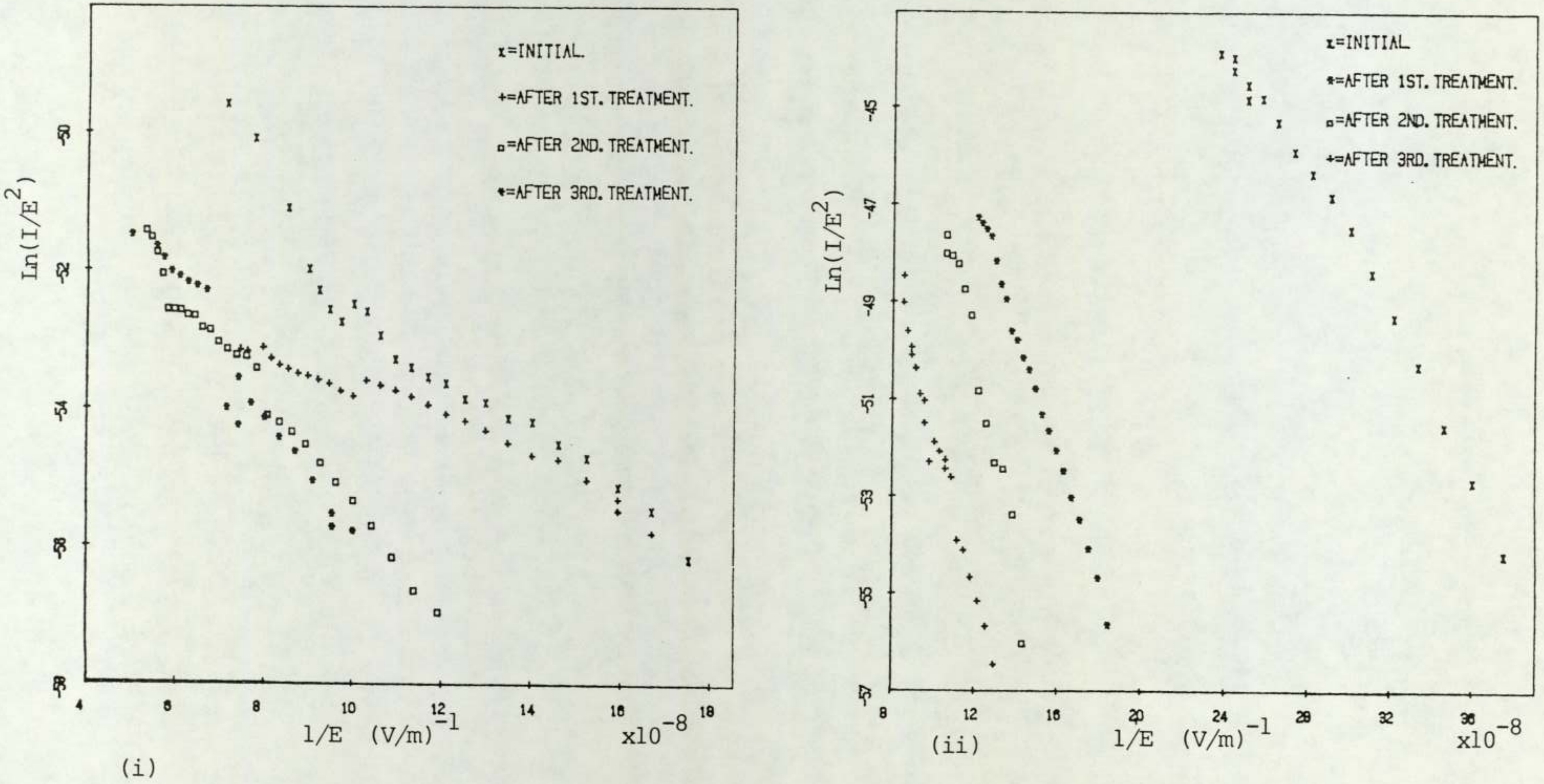

Fig.4.5 (i)-(ii) F-N Plots From "Artificial" Carbon Sites

Fig.4.5(i)-(ii) shows typical F-N plots produced by conditioning specimen cathodes contaminated with carbon in the form of graphite (marked with an asterisk in Table T4.1). As can be seen, these specimens tended to have very low initial switch-on fields (shown by the low values for F_I) and unusual F-N characteristics, reflected by the abnormally high field-enhancement factors and generally unstable emission currents. Associated with the high β-factors of these artificial sites, it was quite common to observe a distinct curvature to the F-N characteristic. Although, as an example of the diversity of the properties of emission sites, Fig.4.4(ii) shows the F-N characteristics of a ´normal´ specimen, where the initial curved characteristic (β_1=1220) is strongly reminiscent of an artificial site.

4.2.2 Electron Beam Conditioning

As discussed in Chapter 2, the critical beam power density for producing localised surface damage, by intense local heating, is in the region of 10^4 - 10^6A.m^{-2} at 1 - 10kV. The photographs shown in Fig.4.6(i)-(iii), show the effect increasing electron-beam power has on the beam profile produced on a glass-mounted copper film. From these it can be seen that the beam profile produced seems to be almost annular, with an intense, high-power, central portion having a diameter of 0.05 - 0.1mm (obtained by measurements from the copper films, and seeming to remain constant over a range of beam powers). This finding would seem to correlate with the electron trajectory plots shown in Fig.3.11. Hence, with a target voltage of 15 - 20kV and a beam current of, typically,

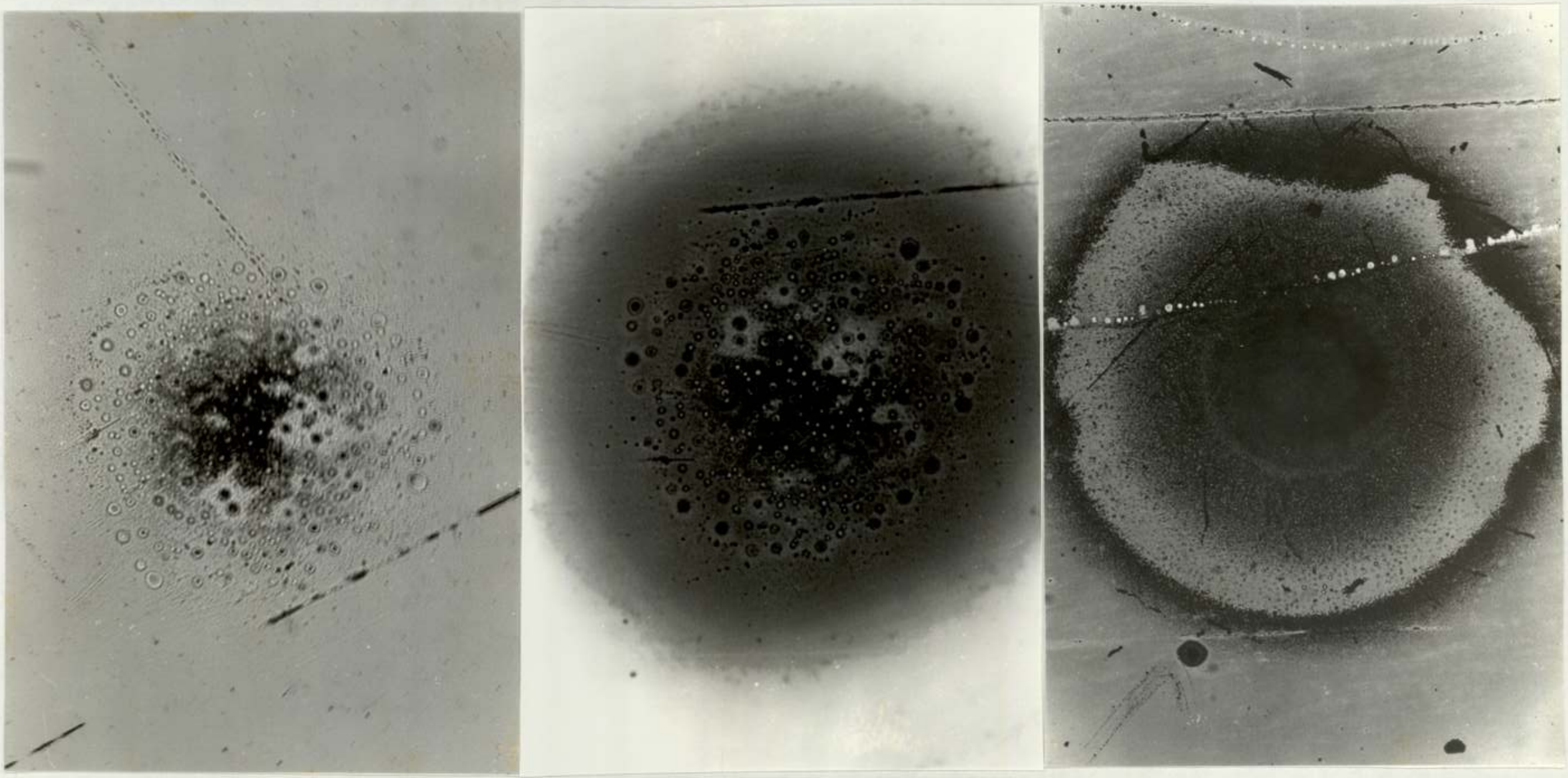
(i) (ii) (iii)

Fig.4.6 (i)-(iii) Profiles Of Electron Beam Bombardment Of A Copper Film (for increasing beam power)

0.2mA, a beam current density of $2\mathrm{x}10^{4}\mathrm{A.m}^{-2}$ could be produced, if it is assumed that the majority of current is contained within the central region of the beam; a value which is just over the minimum limit for producing surface damage. However, a consideration of Equation E.2.6 shows that the temperature rise T_r at the centre of a bulk target area could only be expected to be in the range 100 - 150deg K. Thus, for copper, where $K = 395\mathrm{W.m}^{-1}.\mathrm{K}^{-1}$, $V = 20\mathrm{kV}$, $I_B = 2\mathrm{x}10^{-4}\mathrm{A}$, and $R_B = 5\mathrm{x}10^{-5}\mathrm{m}$:

$$T_r = \frac{0.414V \,.\, I_B}{\pi^{1/2} .\, R_B .\, K} = 150 \text{ degK}$$

This temperature rise is so small that there is little likelihood of damaging or modifying the emission behaviour of a site. This conclusion was confirmed by the measurements reported in Section 3.7.3, where bombardment of the copper-coated aluminium specimen failed to produce any disruption of the 0.5 μm copper film. It therefore appears that the damage observed with the glass-mounted copper films was a consequence of the thermal conductivity of copper being lowered in a thin film form.

The above conclusion was further born out by the experimental findings illustrated in Fig.4.7, which show the effect electron-beam bombardment had upon the F-N characteristics of an emission site on a bulk copper specimen. As can be seen, this bombardment resulted in a somewhat higher, and more unstable, emission current for the same applied voltage; however, it produced no change in the position of the emission site. Also, a subsequent optical examination of the electrode surface failed to show any noticeable surface damage. Thus, it seems that the variation in emission characteristics could most plausibly be attributed to the electron-beam polymerisation of residual pump-oil contaminating the emitting site.

As described in the previous chapter, the same experiment was then performed with a titanium specimum which has a much lower thermal conductivity, $K = 21 W.m^{-1}.K^{-1}$. Thus, for the same beam parameters as before, a temperature rise of ≃ 2000deg K could be expected at the beam centre. Fig.4.8 shows how the F-N characteristics of a site on the titanium specimen changed after bombardment with the electron beam, and clearly reveals that this treatment did indeed produce a progressive conditioning effect following the two successive bombardments. However, after the third treatment, the emission current became unstable and suddenly switched. Subsequent optical examination of the specimen showed local discolouration on the surface, contiguous with the area of the emission site. Again, this was attributed to the polymerisation of residual pump oil: a conclusion which was subsequently confirmed by Auger analysis, which showed the localised area to be rich in hydro-carbons. It was therefore concluded that this surface carbon deposit had given rise to the type of "artificial" carbon site described previously.

Table T4.2. summarises the information relating to the changing F-N characteristics for the copper and titanium specimens. From this, it can be seen that a significant conditioning was produced on the titanium specimen by the first two bombardments, despite an overall ´deconditioning´.

	COPPER	TITANIUM
F_i ($MV.m^{-1}$)	18.1	17.8
F_f ($MV.m^{-1}$)	15.5	17.0
γ	0.85	0.95
F_2/F_i; etc.	0.97; 0.91; 0.97	1.1; 1.2; 1.2; 0.7
β	108; 158; 106; 124	138; 123; 87; 202
Intercepts	31.8; 38.4; 29.4; 29.3	29.2; 29.7; 26.6; 35.6
Bombardment Time (mins)	15; 40; 40	10; 10; 25

Table T4.2

Table Showing Results From Electron-Beam Heating Of

Cu And Ti Electrodes

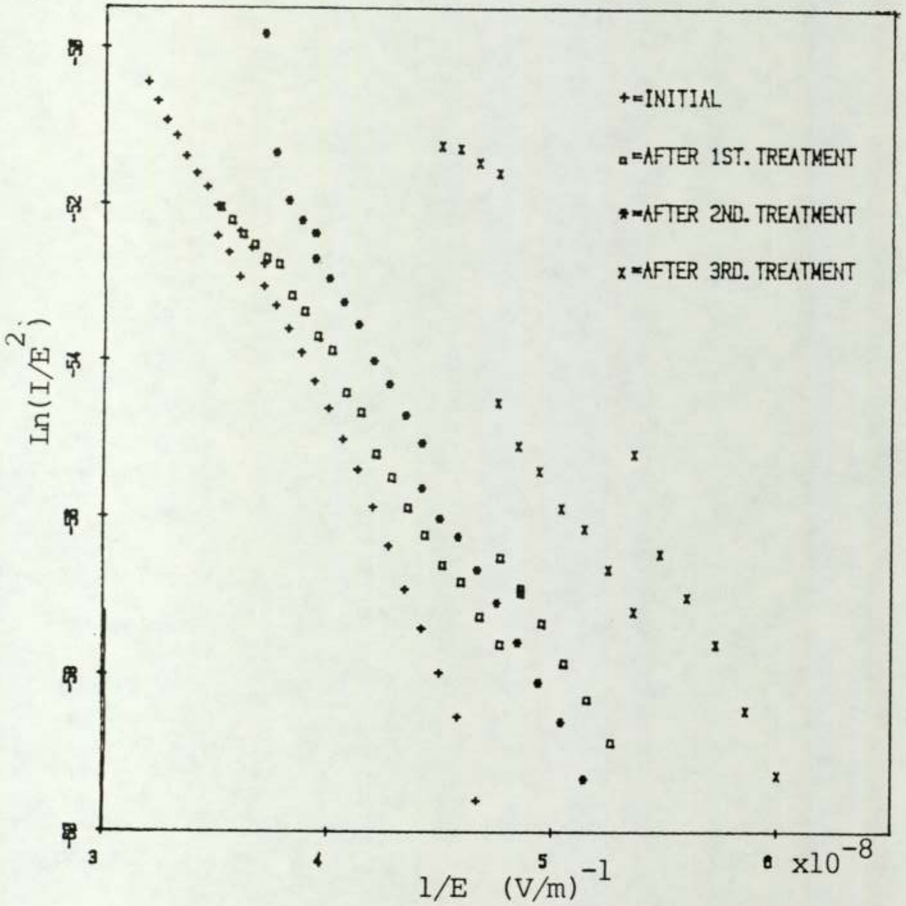

Fig.4.7 F-N Plots Showing Effects Of Electron Beam Bombardment On Copper

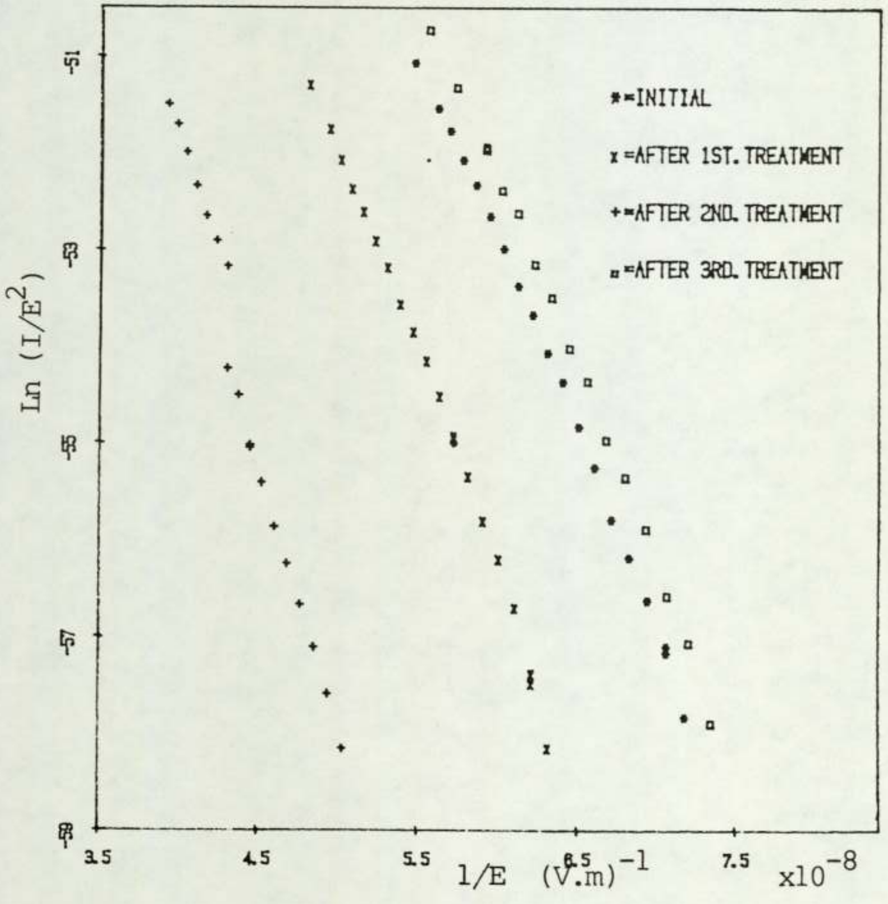

Fig.4.8 F-N Plots Showing Effects Of Electron Beam Bombardment On Titanium

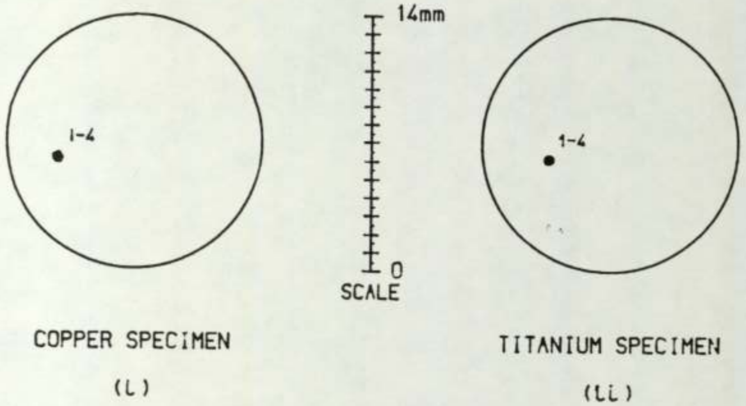

DIAGRAM SHOWING THE LOCATIONS OF THE
EMISSION SITES TREATED BY THE ELECTRON BEAM TECHNIQUE

Fig.4.9

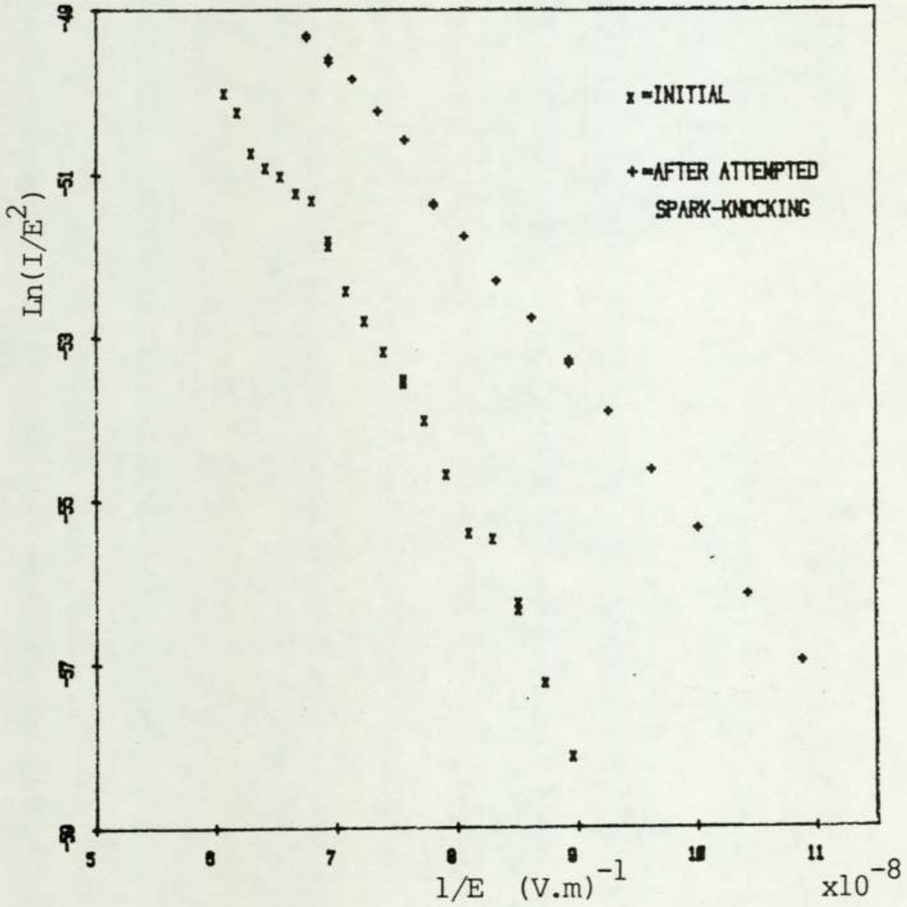

Fig.4.10 F-N Plots Showing Changes Produced By Attempted "Spark" Conditioning

(i)

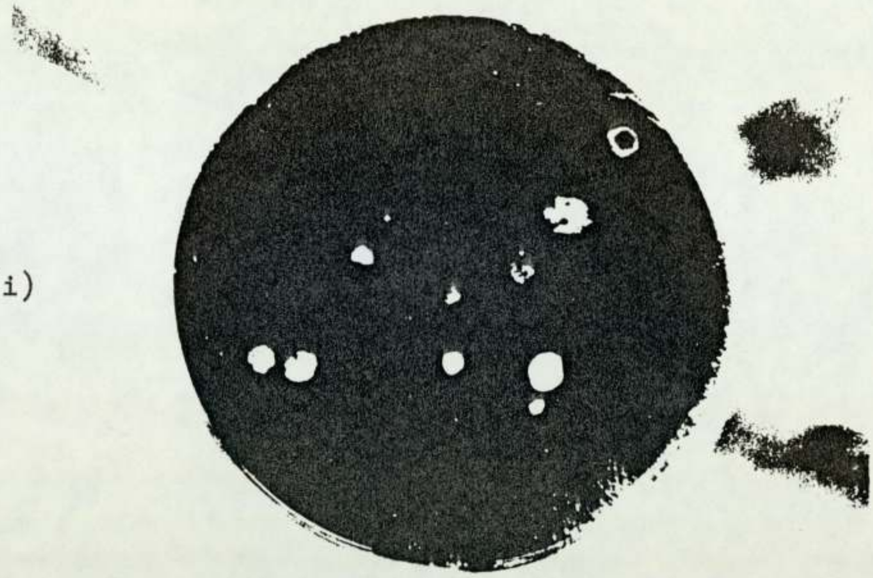

Fig.4.11 Electrode Surface Damage Produced By Attempted "Spark" Conditioning

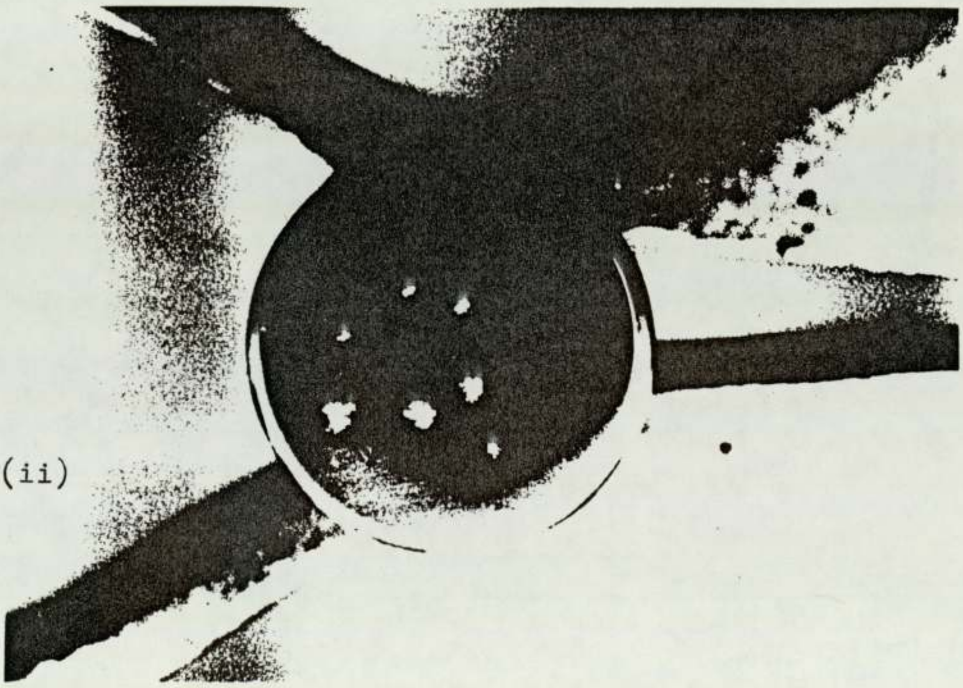

(ii)

4.2.3 "Spark" Conditioning

The process of achieving localised arcing was described in Section 3.7.4. In order to be able to generate an arc between the syringe tip and emission site, it was necessary to run the emission current at a high level, typically 10^{-6} - 10^{-5}A. Under these conditions, considerable surface damage was caused by micro-discharges, presumably initiated by the high current levels causing local gas desorption. Further damage was caused by the violence of the arc generated from the syringe tip. The effect of this "spark" conditioning technique on the F-N characteristic of the electrode gap is typically represented by the example shown in Fig.4.10, where it can be seen that there is frequently a deconditioning effect on the voltage hold-off of the electrode. The major problem with this technique was that micro-discharges occurred over the whole electrode rather than just the localised region opposite the aperture. Fig.4.11(i)-(ii) shows the surface of specimens after a single spot-knocking treatment, with the discharge marks visible over most of the electrode surfaces.

4.2.4 Gas Sputtering Conditioning

It should be noted that the syringe technique did not produce a particularly localised area of sputtering; in fact, it was found that no additional conditioning action resulted from the location of an emission site opposite the aperture. As described in Chapter 2, the speed of surface erosion was dependent on the level of emission current.

Table T4.3 presents representative results obtained using this technique. Apart from presenting the usual F-N variables, associated γ-factors, F_i and F_f values, the table also features the sputtering times required to produce each stage of the conditioning process. The graphs of Fig.4.12(i)-(iii), show typical sets of F-N characteristics for three specimens subjected to gas sputtering, with the diagrams of Fig.4.13(i)-(iii) showing the changes in position of the dominant emission site, as conditioning proceeded, for the same three specimens.

A typical feature of this technique was that after a few conditioning cycles the emission current became very unstable, often too unstable for further measurements. Furthermore, this instability sometimes led to the occurrence of a micro-discharge during the gassy conditioning phase, which usually produced a serious de-conditioning of the electrode, and led to the subsequent termination of the conditioning of that particular specimen. Two other significant features of this technique were: (i) that the location of the dominant emission site usually remained unchanged, even though the F-N characteristic was considerbly changed, and (ii) the emission current showed a greater tendency to become unstable, even in early phases of the conditioning cycle, than was found in the more localised ion-beam results.

The lack of spatial selectivity of this technique did have some advantages, in that, from a technological point-of-view, this method was very good for treating edge-sites, since the emission site did not have to be located over the central axis.

F_i $(MV.m^{-1})$	F_f $(MV.m^{-1})$	γ	F_2/F_i; F_3/F_2; ..etc.	β-Factor	Intercept (-)	Times (mins)
12.1	33.0	2.72	1.43; 1.90	270; 173; 121	31.4; 29.4 37.9	18; 8 (20)
21.0	41.1	1.95	1.08; 1.82	201; 130; 101	36.7; 30.2 38.2	25;15 (30)
12.7	33.9	2.67	1.14; 2.34	254; 283; 137	31.1: 36.1	25;35 (-)
15.2	22.8	1.50	0.95; 1.47; 1.07	269; 265; 190;193	36.1; 34.4 36.1; 37.3	6;12; 8(15)
16.9	32.1	1.90	1.41; 1.35;	204; 148; 110	33.0; 34.2 34.6	17;20 (40)
10.2	14.2	1.39	1.24; 1.06; 1.06	426; 372; 189;254	35.9; 37.6 25.6; 33.2	7;60 (20)
15.9	29.3	1.84	1.62; 1.14	200; 120; 99	31.3: 31.8 30.6	15;35 (-)
26.0	33.0	1.27	1.27	226; 121	41.3; 37.2	16; (-)
23.5	42.5	1.81	1.07; 1.69	181; 114; 85	36.9; 29.8 38.6	20;31 (27)

Table T4.3 Showing Representative Results From Gas Sputtering Experiments

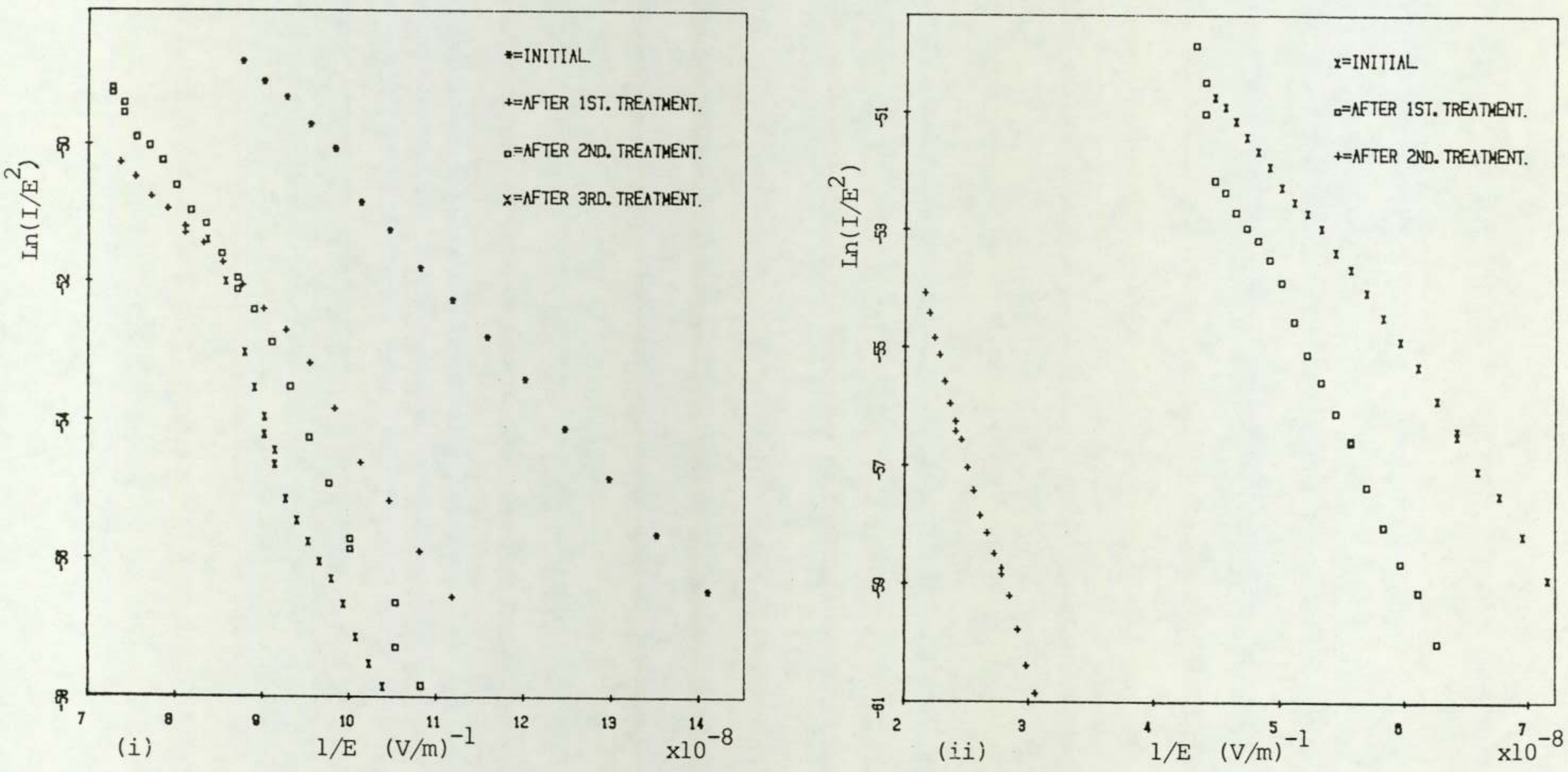

(i) (ii)

Fig.4.12 F-N Plots Showing The Changes In Emission Characteristics Produced By Gas Sputtering

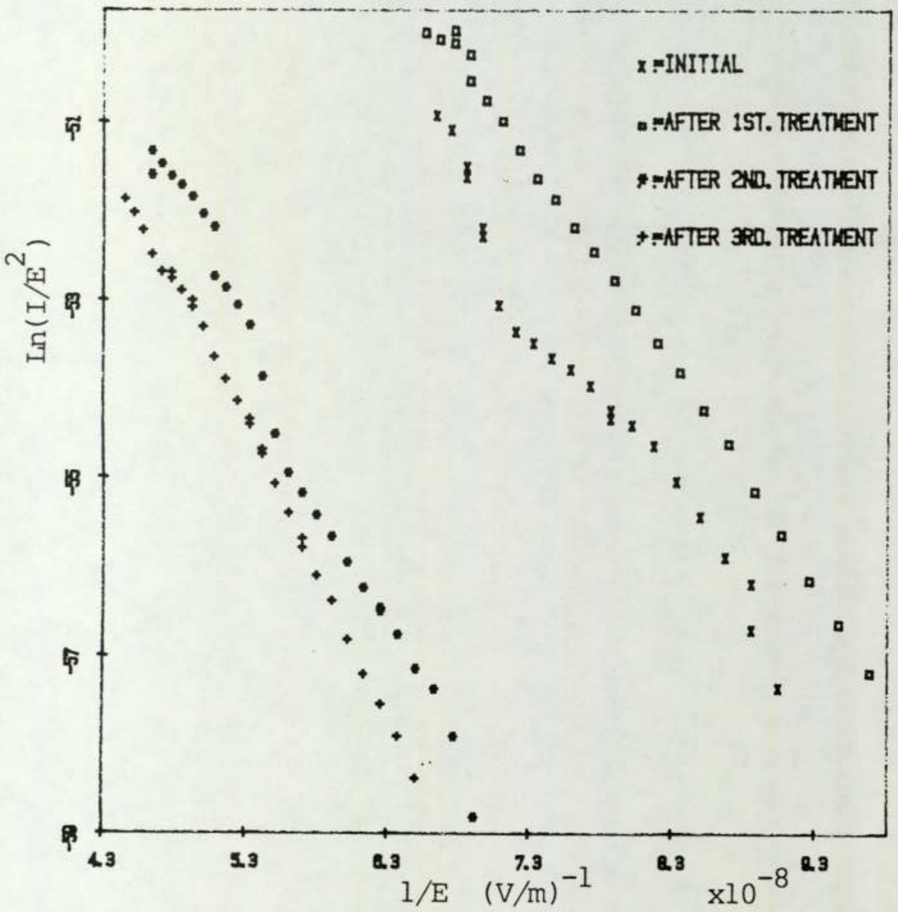

Fig.4.12(iii)

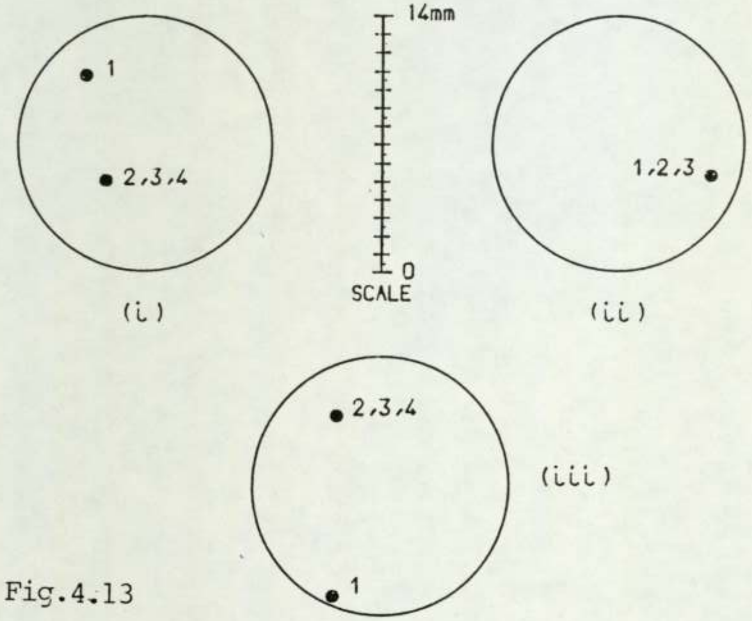

Fig.4.13

DIAGRAM SHOWING THE CHANGING LOCATION OF THE DOMINANT EMISSION SITE DURING CONDITIONING (GAS SPUTTERING)

4.3 Generalised Glow Discharge Conditioning

This conditioning technique produces a generalised surface treatment over the whole specimen, rather than just treating an individual emission sites. Of the three specimens studied, two (specimens 1 and 2) were processed using the argon/oxygen mixture described in Section 3.7.5, while the third specimen (specimen 3) was treated as a "control", and processed using pure argon in order to investigate whether any of the observed effects were due the presence of oxygen.

An important characteristic of this conditioning technique was that when a field was initially applied to the specimen after a glow discharge session, a very large improvement in voltage hold-off was typically found. However, if the applied field was increased until an emission current of $>5\times10^{-11}$A was obtained, a complex switch-on process occured which, after becoming fully stabilised, gave an F-N characteristic that was frequently only marginally better than that obtained before treatment. A schematic illustration of this switch-on process is presented in Fig.4.14. In order to describe this phenomenon, it is necessary to introduce two additional parameters: E_s and E_c. As described previously, E_s represents the field required to obtain an emission current of 5×10^{-11}A after switching was completed, whilst E_c represents the field required to achieve the same current when the field is first applied to the specimen after each phase of conditioning. Tables T4.4 shows the results obtained from the two argon/oxygen specimens, and includes the E_c and E_s values, details of the F-N characteristics for the individual dominant emission sites, and the ion dosage for each stage of the conditioning process, this figure relates to the amount of surface material removed and was calculated using the discharge current and discharge time; Table T4.5 contains the results for the control argon experiment. The figures in the ´Site No.´ column identifies the site, and refer to whether, after each stage of the conditioning process, the location of the major emission site was unchanged. If the original site no. was 1.1 then, if the location remained unchanged, the new site would be 1.2 etc.; however, if the position did change, it would be labelled 2.1 etc.

The variation in F-N characteristics for the three specimens are presented in Fig.4.15(i)-(iii), with the locations of the respective emission sites being shown in Fig.4.16(i)-(iii). These graphs show that even after the emission current had been stabilised as much as possible, numerous switching processes still occur. Table T4.6 shows the standard factors associated with the evaluation of the conditioning techniques, F_i and F_f, the improvement factors ,and the total ion-dosage for the specimens examined. Consideration of this table shows that a very reasonable improvement in voltage hold-off was achieved with this technique, particularly with oxygen present. No long term relaxation processes were observed with this technique, and its merits and effectiveness, relative to the local techniques, will be discussed in Chapter 6.

An S.E.M. photograph of the surface of a glow discharged specimen is shown in Fig.4.17(a), and may be compared with the photographs in Fig.4.17(b), which was obtained, using a similar technique, by workers at C.E.R.N., the significance of the surface ´snow´ effect will be discussed later.

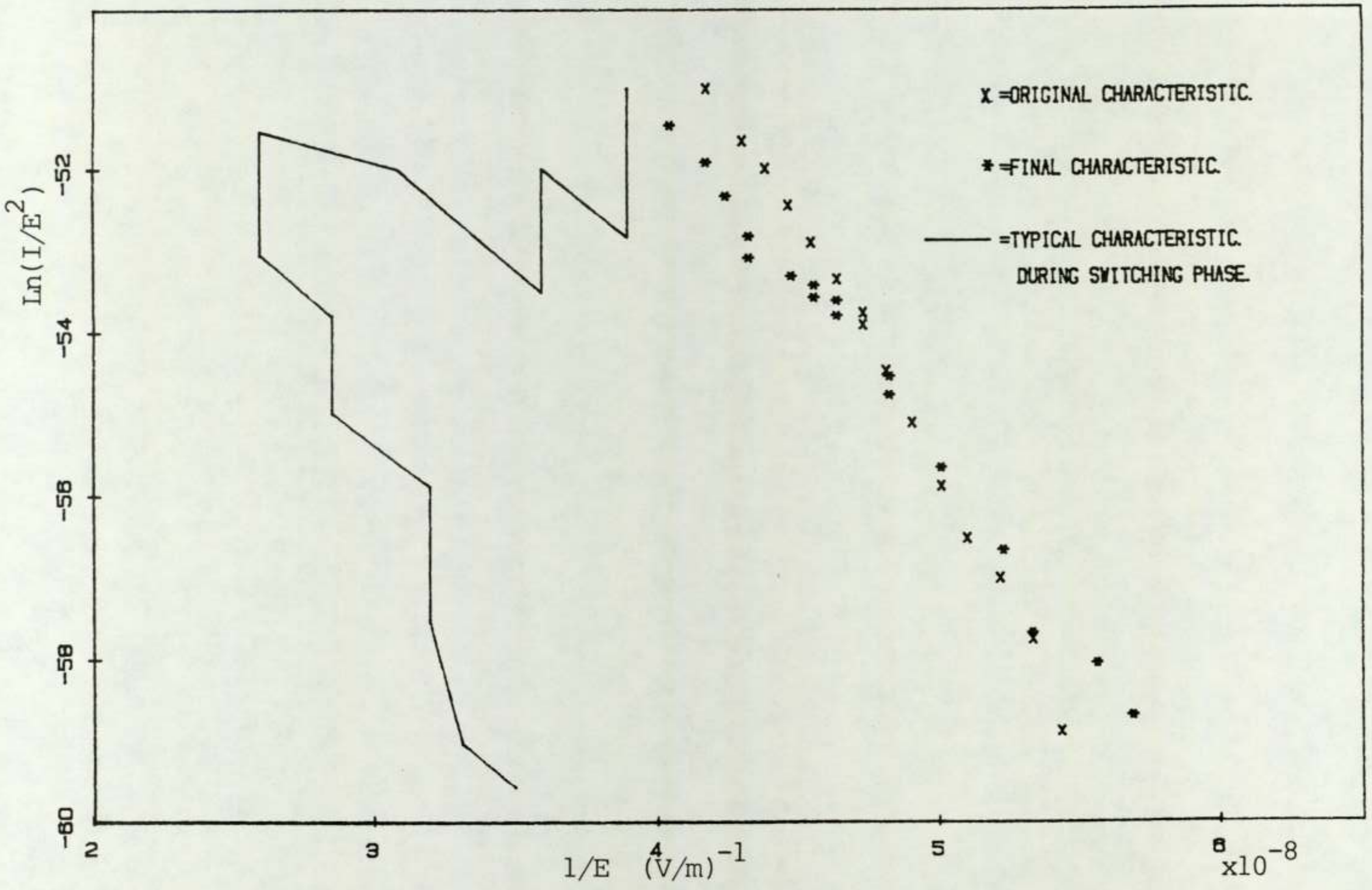

Fig.4.14 Schematic Illustration Of Complex Switching Processes Associated With Glow-Discharge Conditioning

Spec. No.	Site No.	E_s (MV.m^{-1})	E_c (MV.m^{-1})	β	Emission Area (m^2)	Ion-Dosage (ions/cm^2)
1	1.1	17.6	37.0	149	1.63E-15	4.6E16 (+)
1	1.2	17.2	42.0	147	6.30E-15	1.2E17 (+)
1	1.3	25.0	40.5	69	1.14E-09	9.0E16 (+)
1	1.4	38.0	44.0	65	1.06E-14	1.8E17 (+)
1	1.5	30.6	38.1	155	1.00E-19	1.0E17 (+)
1	2.1	26.6	-	90	2.27E-14	-
2	1.1	12.9	30.8	177	1.78E-13	1.5E17 (-)
2	2.1	15.0	30.0	176	1.91E-15	1.1E17 (+)
2	3.1	20.3	32.0	133	1.03E-15	6.7E16 (-)
2	3.2	19.2	31.9	120	8.33E-14	1.3E17 (-)
2	3.3	18.8	29.1	100	3.81E-11	9.1E16 (-)
2	4.1	19.2	29.2	161	1.03E-16	1.7E17 (+)
2	4.2	18.4	35.0	142	2.18E-15	3.0E17 (-)
2	5.1	34.6	-	58	1.98E-12	-
2	6.1	37.0	-	53	7.1E-12	-

Table T4.4 Table Showing Results From Ar/O_2 Glow-Discharge Experiments (specimens 1 & 2)

Spec. No.	Site No.	E_s (MV.m^{-1})	E_c (MV.m^{-1})	β	Emission Area (m^2)	Ion-Dosage (ions/cm^2)
3	1.1	16.5	26.2	122	1.5E-12	1.03E17
3	1.2	16.2	30.1	179	7.9E-17	8.20E16
3	1.3	20.7	30.2	114	1.5E-14	6.09E16
3	2.1	22.3	44.9	138	2.0E-17	6.70E16
3	2.2	20.9	-	151	1.4E-17	-

Table T4.5 Results From Ar Glow-Discharge Control Experiments

(specimen 3)

Spec. No.	F_i (MV.m^{-1})	F_f (MV.m^{-1})	γ	F_2/F_i; F_3/F_2; ...etc.
1	23.3	41.3	1.8	0.85; 1.5; 1.58; 0.89
2	16.0	44.0	1.5	1.25; 1.38; 0.91; 0.92
3	21.4	30.6	1.4	1.1; 1.18; 1.17; 0.93

Table T4.6 Effectiveness Of Glow-Discharge Conditioning

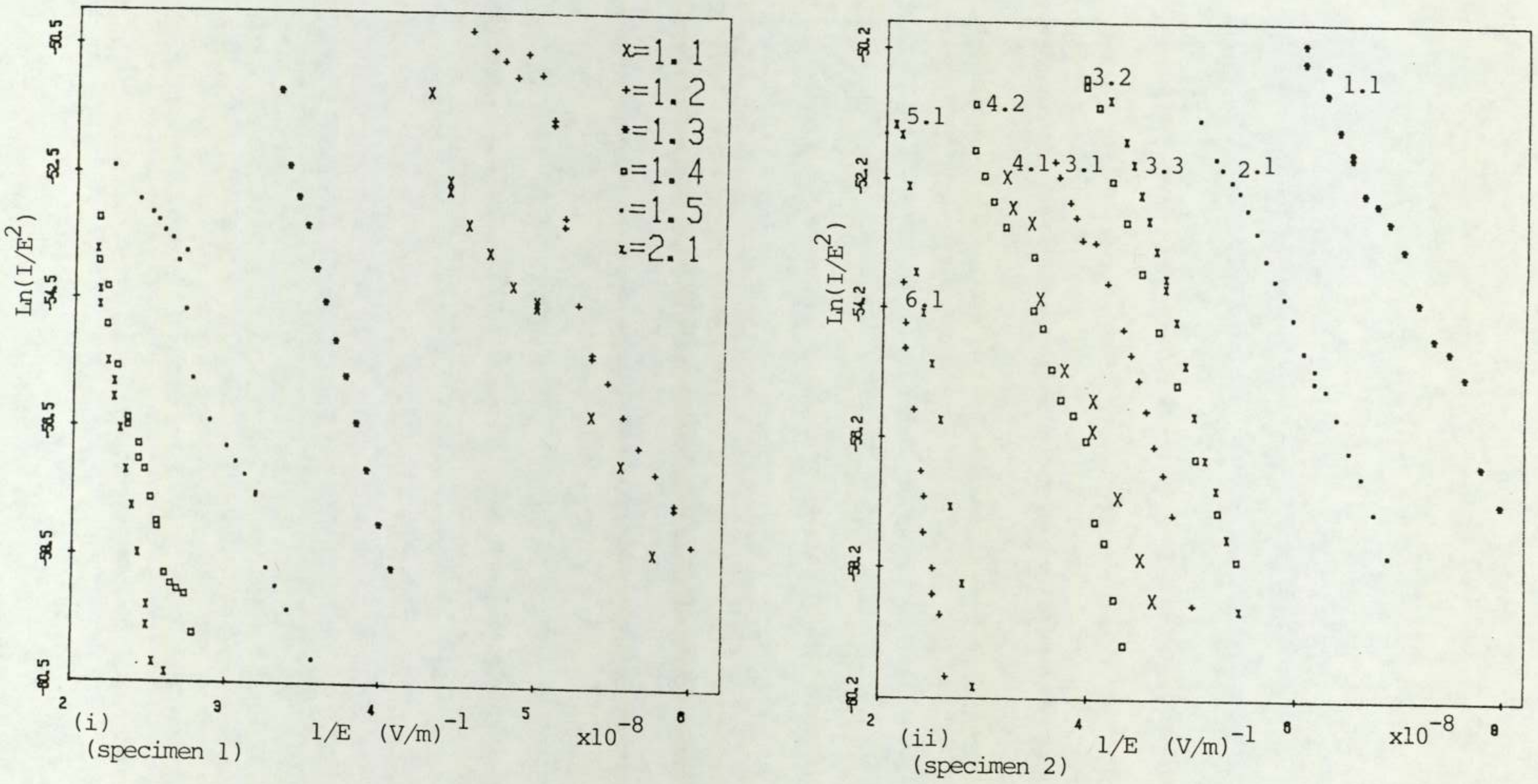

(i)
(specimen 1)

(ii)
(specimen 2)

Fig.4.15 (i)-(iii) F-N Plots Showing Changes In Emission Characteristics Produced By Glow-Discharge Conditioning (Ar/O_2)

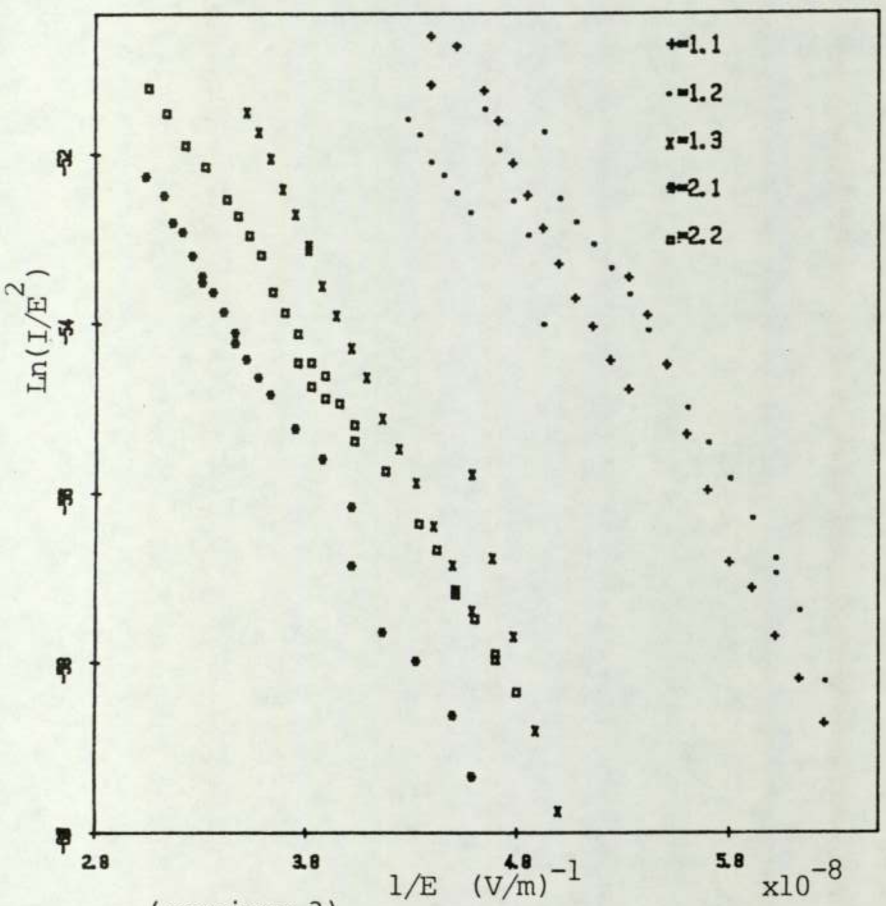

(specimen 3)

Fig.4.15(iii) (Ar Control)

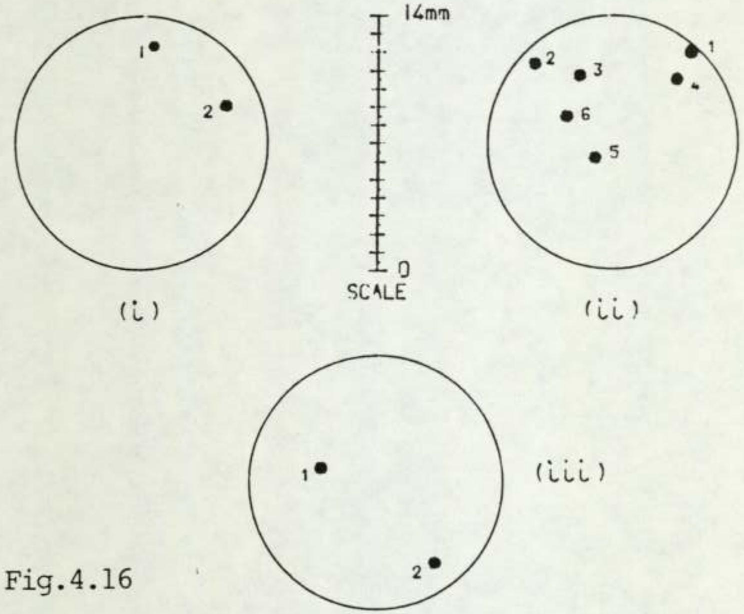

Fig.4.16

DIAGRAM SHOWING THE LOCATIONS OF THE EMISSION SITES OCCURING DURING GLOW-DISCHARGE CONDITIONING

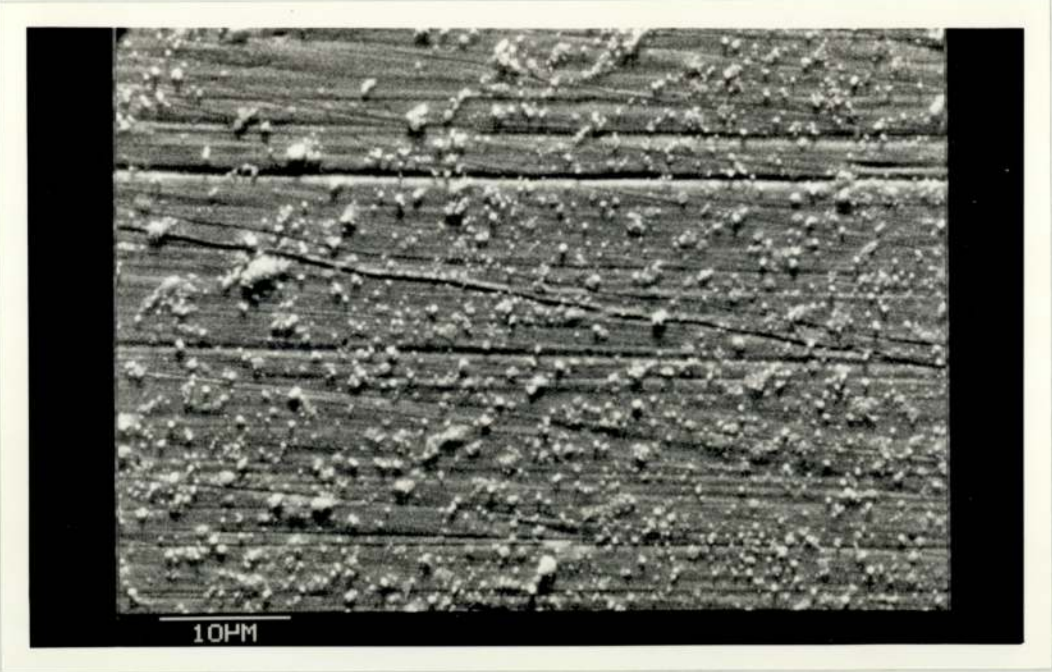

(a) Surface "Snow " Effect Found On Conditioned Electrode

Fig.4.17 S.E.M. Micrographs Of Glow-Discharged Surface

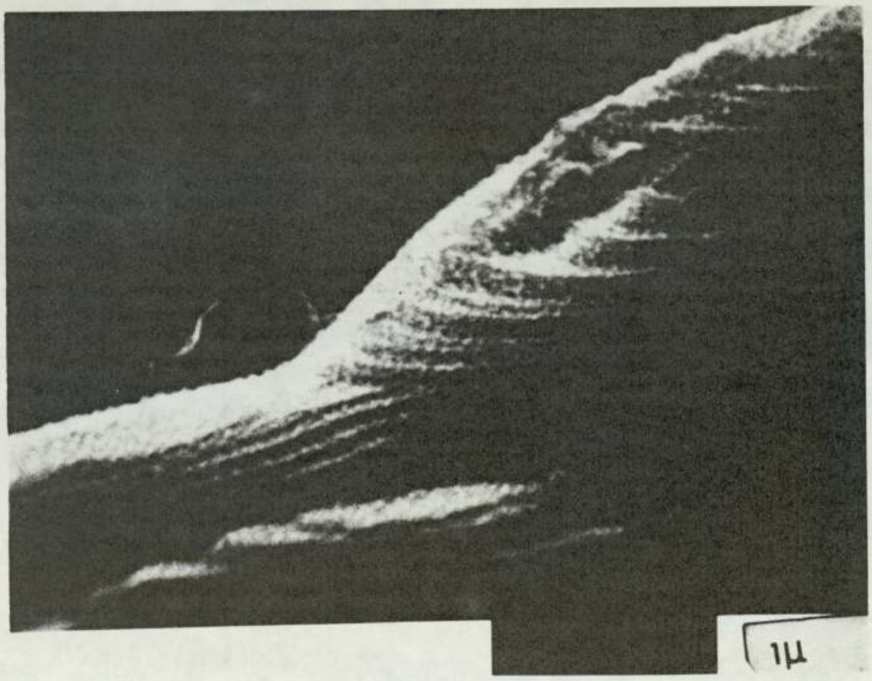

(b) Surface "Snow" From C.E.R.N. Specimen

CHAPTER 5

Fundamental Studies of Electron Emission Processes

5.1 Introduction

The major thrust of the investigation was into the effectiveness of various conditioning techniques. However, more fundamental studies were also pursued into various phenomena associated with the electron emission process itself. The aim of this chapter is to present an account of these experimental studies and discuss their physical significance.

One of the initial objectives of this work was to reproduce the electroluminescence observations of Hurley et al.(42,45,46,) described in Chapter 2, and to refine the measurements of the spectral distribution of the visible radiation. However, it will emerge that, even after extensive experimental investigations, no radiation was observed that could be catagorically attributed to cathode electroluminescence. The experimental requirements and techniques for this investigation into optical emission are descibed in detail in the following section, together with the experimental observations and discussion of the physical implications of these observations.

Further experimental work made use of the ion-beam module of Fig.3.8(a) to investigate various characteristics of electron emission sites. One factor investigated, was the variation in emission characteristics observed as the surface of the specimen was progressively etched away in the vicinity of the emission site. Also, in a further series of experiments, the ion-beam was used to lightly mark the location of the emission site for subsequent examination by S.E.M. and surface analysis using Auger/X.P.S. A final series of experiments were performed in conjunction with the U.H.V. electron spectrometer system used by Latham et al.(75-77,94-96)

5.2 Investigation Into Electroluminescent Emission

5.2.1 Background

As mentioned in Chapter 2, Hurley et al(42,45,46) performed extensive investigations into the phenomenon of cathode-generated electroluminescence. Their experimental arrangement is shown in Fig.5.1, and allows direct observation of the cathode surface. With broad-area electrodes and mean macroscopic gap fields of the order of 5 - 10MVm^{-1}, they noted points of light appearing on the cathode surface. Frequently, these were located on the high-field regions of the specimen (e.g. the radiussed edges etc.), but were also seen on the flat surface. They made optical measurements on this emitted light, using the image-intensifier/photomultiplier combination and a series of sharp-cut-off high-pass filters, and found the light typically had a spectrum with a sharp peak in the region 630-660nm, such as that shown in Fig.5.2(a); with the peak position remaining constant with changes in applied field. This observed spectrum seemed to correspond to neither black-body emission nor to any obvious discharge spectra, but suggested to the authors that the luminosity might be caused by electroluminescence produced by the action of the applied field on semiconducting inclusions on the cathode surface. This reasoning was suggested by the well-defined peaks which are typical of

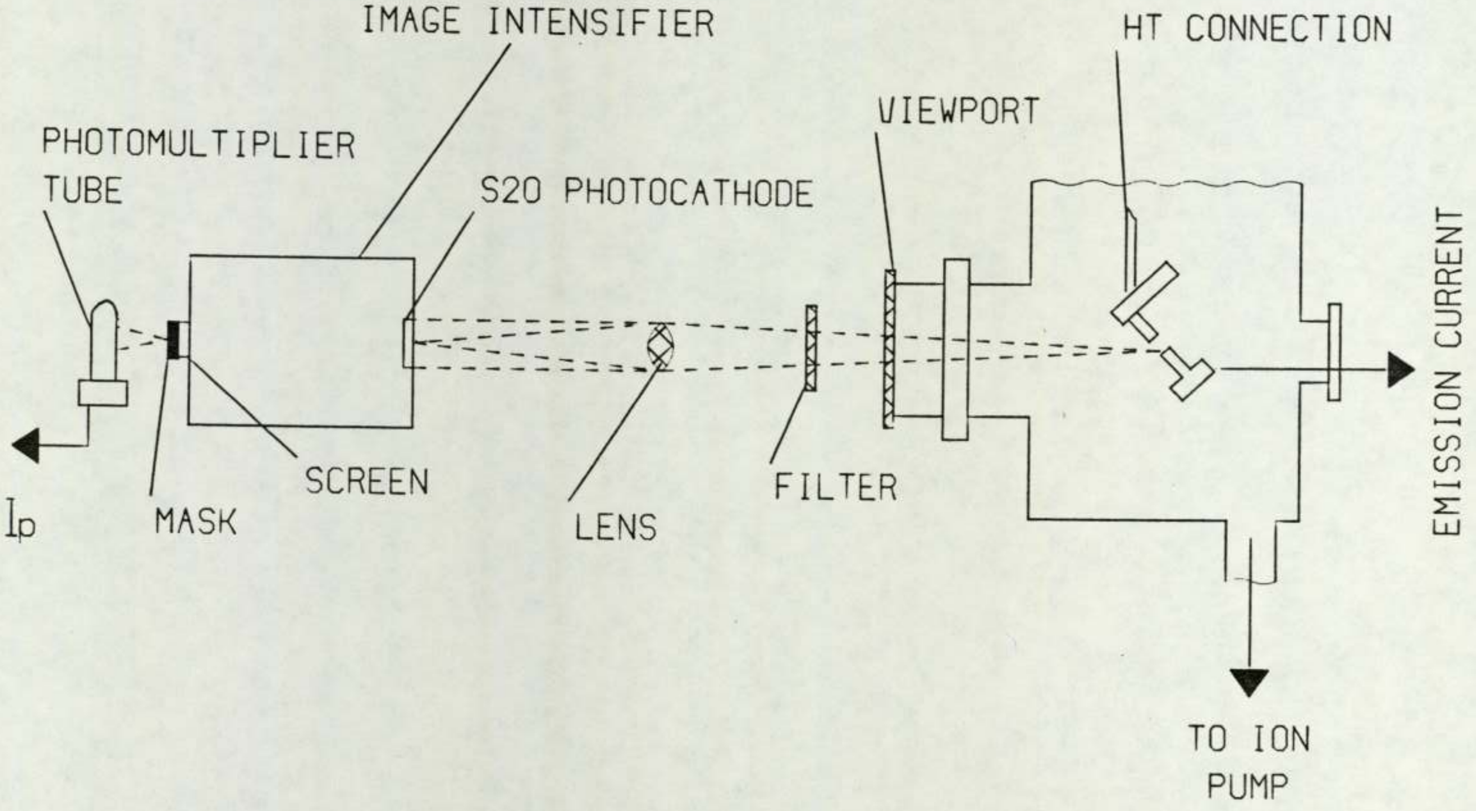

Fig.5.1 EXPERIMENTAL ARRANGEMENT USED BY HURLEY et al(42)

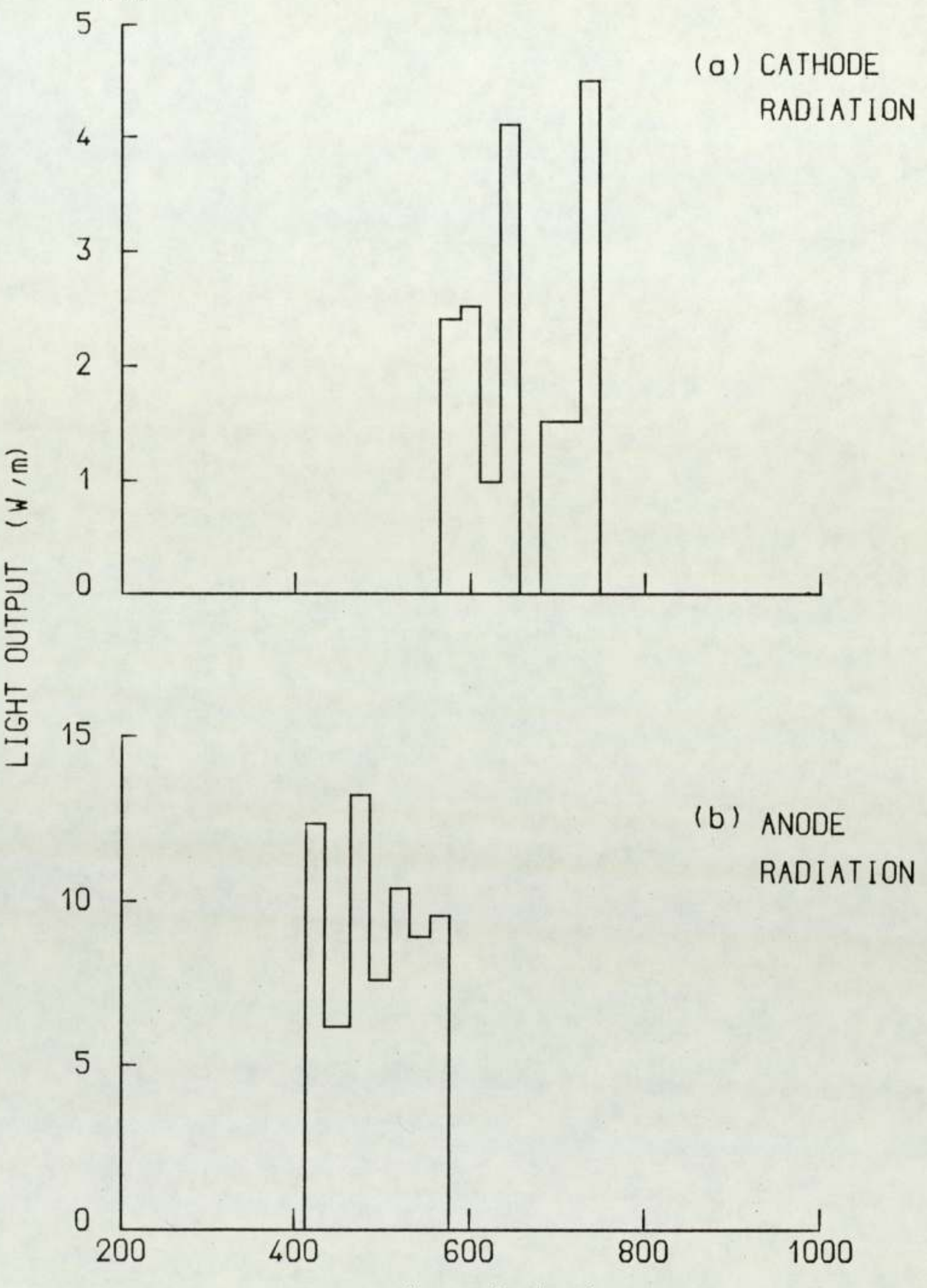

Fig.5.2 SPECTRA OF CATHODE AND ANODE OPTICAL EMISSION

(from Hurley)(45)

electroluminescence; where relatively sharp transitions are made between well defined energy levels, with phonon interaction producing low energy broadening. Alfrey & Taylor(44) studied electroluminescence from ZnS-Cu crystals and found that there was a linear relationship between the logarithm of brightness and the inverse square-root of applied voltage:

$$H = H_0 \exp(-C/ V^{0.5}) \;\ldots\; \text{Eq.5.1}$$

where H is the light output from an electroluminescent cell.

To confirm that the observed light was electroluminescent in nature, Hurley et al.(41) produced graphs of $\log(I_P-I_D)$ against $V^{-0.5}$ for each stable cathode spot, and showed they produced excellent agreement with an expression of the form:

$$I_P-I_D = A\exp(-B/V^{0.5}) \;\ldots\; \text{Eq.5.2}$$

where I_P was the photomultiplier current recorded for a given applied voltage V, and I_D was the photomultiplier dark-current. This equation is equivalent to the expression Eq.5.1 derived by Alfrey & Taylor, assuming the spectral distribution remains unchanged with varying light intensity; this form of graphical representation was adopted during this present work.

One difficulty experienced by Hurley et al(42,45,46) was to discriminate between the anode-based optical emission, or anode-spots, caused by transition radiation being emitted from points where electrons struck the anode surface, and the less bright optical emission from cathode processes. To eliminate the possibility that the cathode light was not merely a reflection of these much brighter anode-spots, Hurley et al(45,46) measured their spectra in the same way as for the electroluminescence spectra; a typical example of an anode-spot spectrum is shown in

Fig.5.2(b). They found that this type of spectra was typical of those obtained when metal surfaces are bombarded by energetic electrons, where the spectral characteristics are determined by the frequency-dependence of the bombarded materials dielectric constant, but are generally centered around a lower wavelength than cathode-generated light. Much work was done by Young(128) on this transition radiation, as he used these anode spots to investigate the distribution and properties of emission sites on broad-area electrodes. From a relationship established by Boersch, Radeloff & Sauerbrey(129), Young equated the intensity of the transition radiation to a complex function of the power of the electron beam giving rise to each anode spot. He then found that by plotting the function $\log((I_P-I_D).V^{-3})$ against 1/ V, a straight line resulted; with the gradient and intercept related to the emission areas and field-intensification factors obtained from a straightforward F-N plot.

As described earlier, the initial objectives for this phase of the work were to reproduce and then refine the observations of Hurley et al. However, due to the elusiveness of any electroluminescent radiation, the aims became merely to establish the anode or cathode origin of any optical emission recorded.

5.2.2 Experimental Technique

Fig.5.3 is a schematic representation of the experimental facility required to achieve the experimental objectives outlined above. Fig.5.4 shows the detailed structure of the optical observation module. It can be seen to consist of an electrically isolated and angled stainless steel mirror, such that, when the

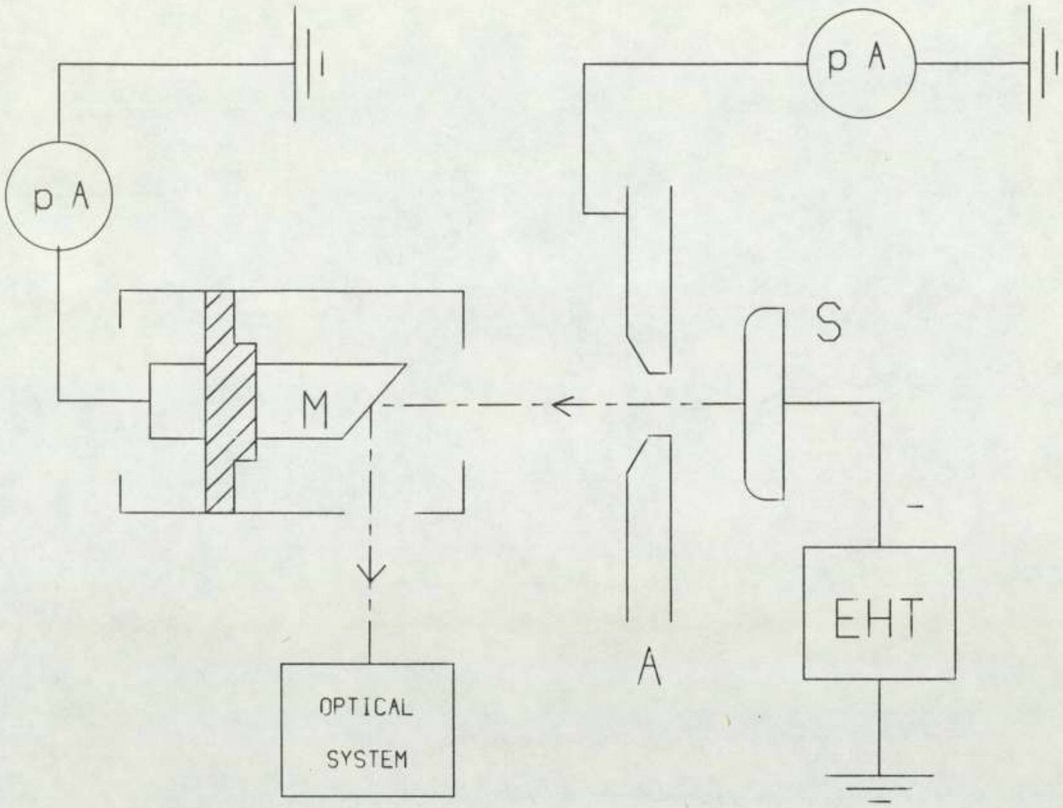

Fig.5.3 DIAGRAM SHOWING EXPERIMENTAL SYSTEM FOR THE STUDY OF ELECTROLUMINESCENCE

Fig.5.4 Photograph Of Module Used For Optical Investigations

module was inserted into the anode assembly, observations could be made of the specimen area immediately opposite the anode aperture. In addition, the stainless steel mirror M could be used both as an electron collector, to locate an emission site, and as a means of observing any optical activity in the region of the site. The optical system consisted of an image intensifier combined with a photo-multiplier or, when photgraphs were required, with a camera; this combination gave a very limited depth of field which caused some experimental difficulties when deciding which area of the mirror-image to focus upon.

As with the conditioning techniques, an increasing voltage was applied to the specimen until a steady emission current was obtained. The specimen was then scanned, in order to locate the dominant emission site, and the F-N characteristic recorded. The image-intensifier was focussed onto the part of the mirror showing the image of the aperture, with the portion of the copper specimen containing the emission site visible through it. Once this had been achieved, various optical measurements were taken. Initially, the distribution of any light was recorded using a time-exposure photograph. A single light spot was then selected using a masking technique, and the photo-multiplier attached to the end of the intensifier enabling measurements to be be obtained from this single spot, again a similar technique to that used by Hurley(45). The variation of light-intensity with applied field was then measured in order to establish whether the optical emission followed the Alfrey-Taylor relationship for electroluminescence. In addition, the spectral distribution of the light emitted by such a spot was measured by interposing a series of filters in front of the image intensifier.

In practice, the observation of possible electroluminescent activity at the emission site location was hampered by the production of anode-spot illumination on the edges of the aperture, and possibly also on the mirror surface; with the situation being further complicated by spurious reflections from both surfaces. In an attempt to minimise this production of anode spots, a probe-anode was used in place of the mirror and apertured anode. This is illustrated in Fig.5.5(i), which shows the probe, with a radius of 50 μm, in position opposite the specimen; Fig.5.5(ii) is a line drawing explaining the various features visible in the photograph. To produce the initial emission current the specimen electrode was located opposite an ancillary copper electrode, similar to that used for the glow-discharge experiments described in Section 3.7.5 and shown in Fig.3.24, and a steady current obtained. The approximate position of the dominant emission site was then found using anode spots produced on the electrode surface, and the specimen electrode then rotated into position opposite the probe and scanned slowly around the approximate location of the site; this pre-location of an emission area by means of anode-spot illumination was necessary because of the high spatial selectivity of the probe technique. Once the emission site was located, the optical systems were focussed at the point on the specimen surface opposite the end of the probe, and any optical phenomena recorded in an attempt to identify any electro-luminescent activity. To minimise the effects of reflections from the cathode surface, a pyrolytic graphite specimen was used on several occasions. The results obtained using

Fig.5.5 (i) Photograph Of Probe Opposite Specimen

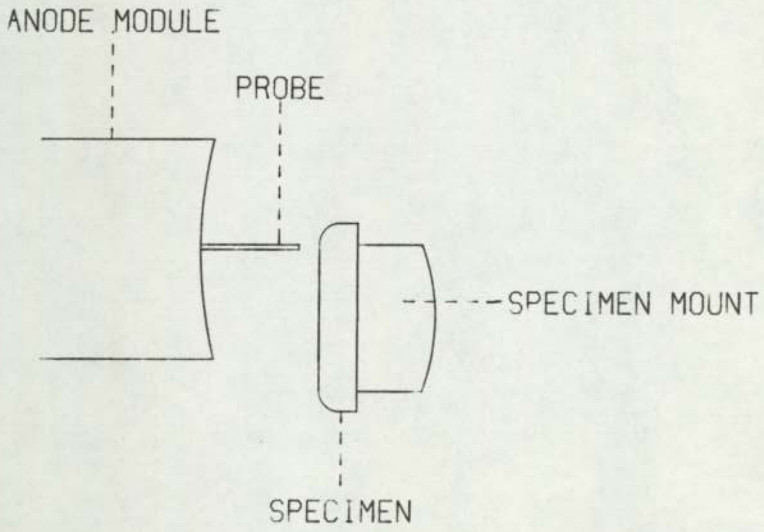

(ii) LINE DIAGRAM OF ANODE PROBE OPPOSITE SPECIMEN CATHODE this probe technique, and those using the mirror, are detailed below.

5.2.3 Experimental Observations of Optical Phenomena

Fig 5.6(i) is a photograph showing the area of the experimental system visible through the image-intensifier. As can be seen from Fig.5.6(ii), which is a line diagram explaining the features present in the photograph, primarily the image of the tapered anode aperture may be seen, together with spots of anode-generated light on the inner edge.

With an emission site centrally located, and with its current being collected on the mirror, it was normal to observe extensive optical activity around the edge of the anode aperture. This phenomena is not particularly suprising when the computer-generated, electron trajectory plots of Fig.4.1 are considered, since they show that a significant fraction of emitted electrons are likely to strike the edges of the aperture, even if the emission site was located centrally. It is the impact of these electrons emitted from a site located in the central dark area of the photograph shown in Fig.5.7, that generates the transition radiation, or anode spots, referred to earlier, and it is this light, along with assorted reflections, that account for the profusion of light spots shown in Fig.5.7. The above photograph also demonstrates the problem of the limited depth-of-field associated with this optical system: the system was focussed to record any light emitted from the centrally located emitted site and, as a consequence, the anode edges are out of focus. The transition radiation observed in this manner was typically a vivid

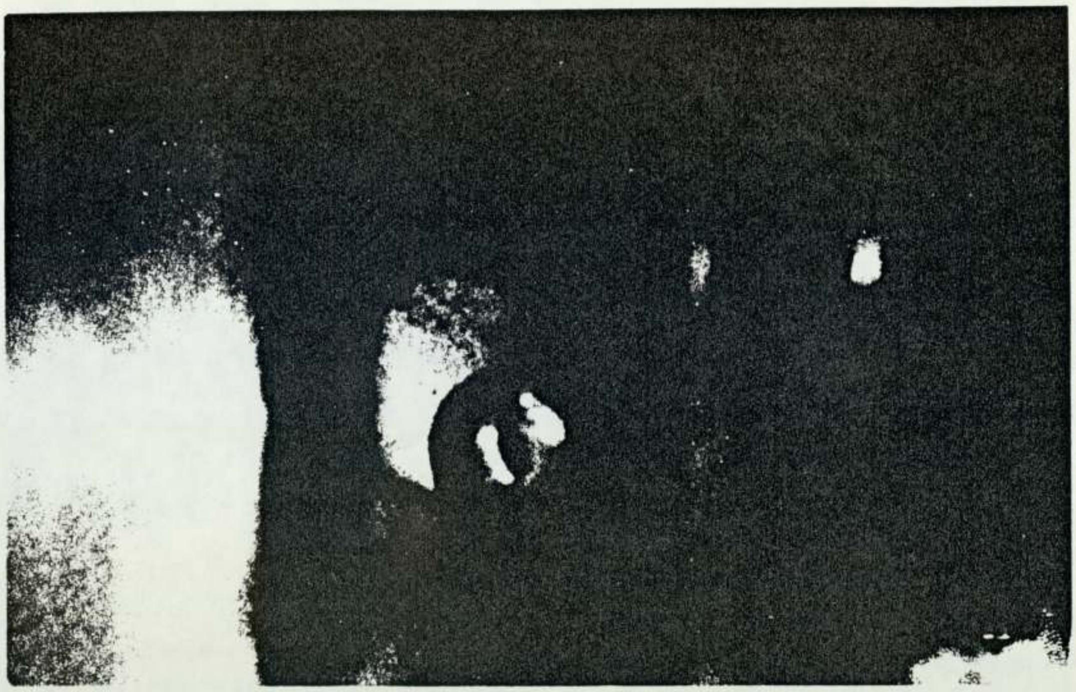

(i) Image Of Anode Aperture Area

(reflected from mirror)

Fig.5.6

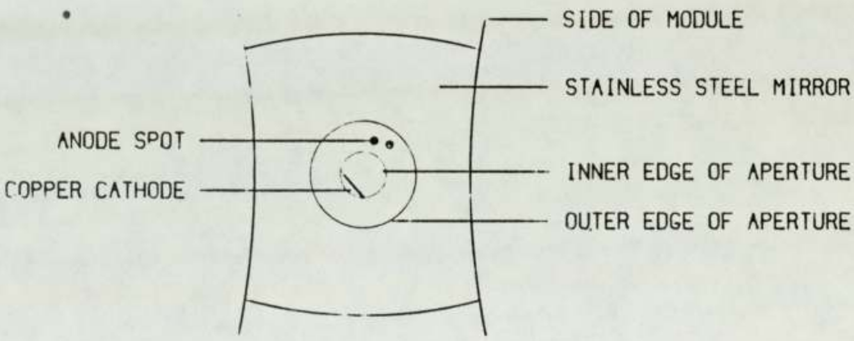

(ii) LINE DIAGRAM OF IMAGE AREA ILLUSTRATING THE VARIOUS FEATURES SHOWN IN THE PHOTOGRAPH

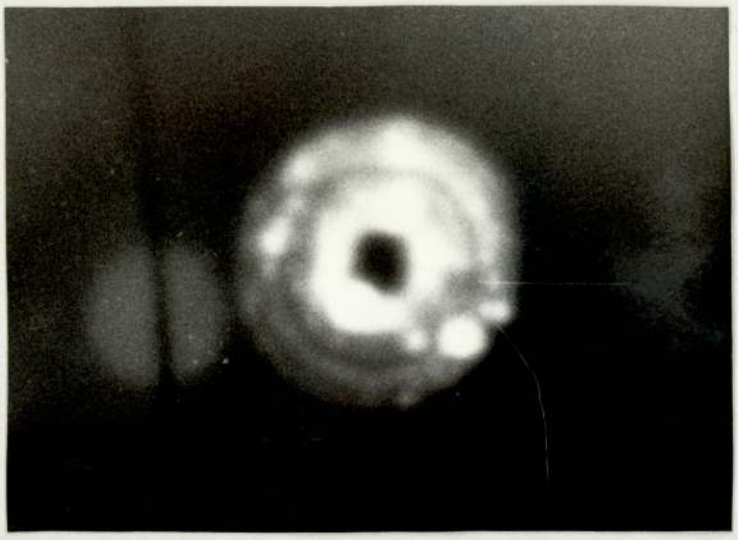

Fig.5.7

Profusion Of Light

Spots Around Aperture

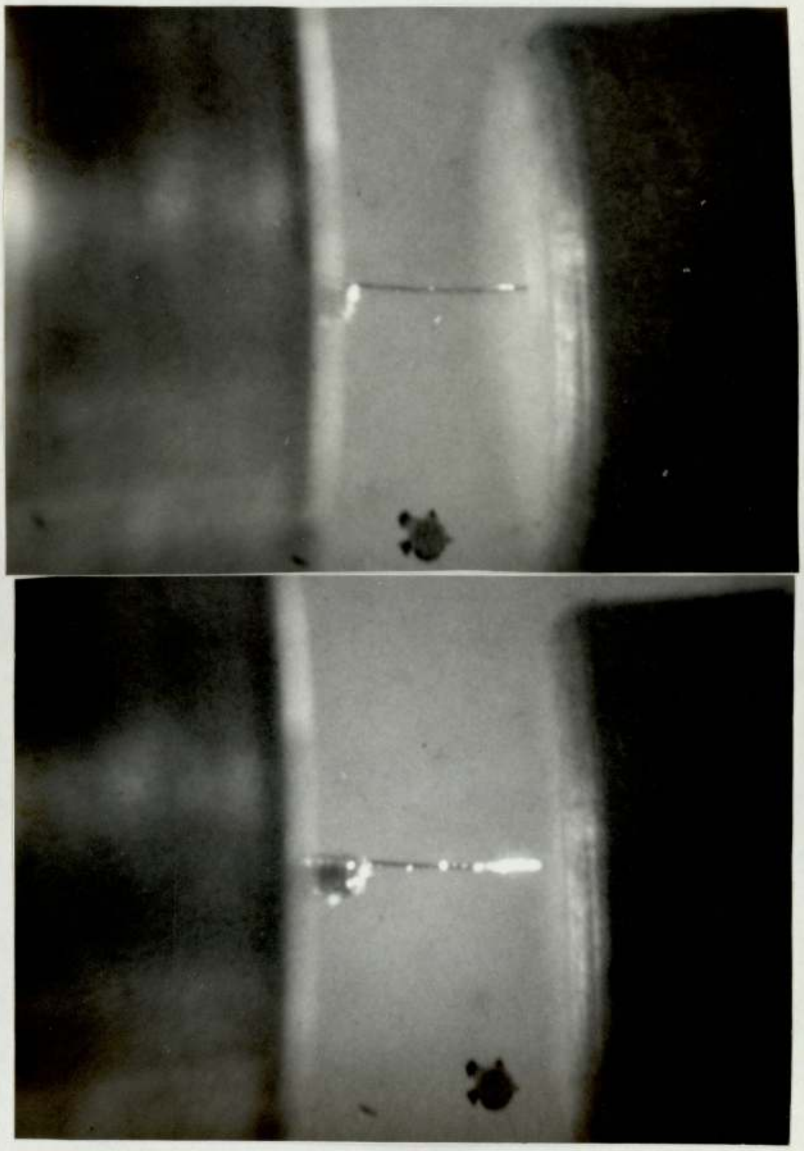

(i) Low Current

(ii) High Current

Fig.5.8 (i)-(ii) Probe With Anode Spots

blue in colour and, as described by Hurley$^{(45)}$, was considerbly more intense than any electroluminescent radiation emitted from the cathode surface. Hence, following his work, it was necessary to employ a masking procedure to eliminate anode spot light being superimposed on the cathode electroluminescence observations.

A consideration of the electron trajectory plots of Fig.4.1 shows that a centrally located ´small´ site should result in very little of the emission current being picked up by the edges of the anode aperture, and hence should produce no visible anode spots. However, time exposure photographs, taken through the image-intensifier, of such centrally located, spatially compact emission sites failed to show any light spots in the central region of the aperture image that could have been attributed to cathode electroluminescence; although very faint anode spots could sometimes be found on the aperture edges. It should be mentioned that a small negative voltage was applied to the mirror during the exposure time to avoid any light being generated by the impact of electrons on the mirror surface.

Although the probe technique was designed to discriminate between anode and cathode generated light, a multiplicity of anode spots were still generated along the length of the tungsten probe, especially at higher emission currents. Thus, Fig.5.8(i) shows the situation for an emission current of $1\text{x}10^{-7}$A, anode spots are visible up the length of the probe; while Fig.5.8(ii) is the same view as Fig.5.8(i), but with a greater emission current being collected ($5\text{x}10^{-6}$A). It can be seen that the higher applied field results in a changed pattern of brighter anode spots; with the anode-generated light at the probe tip being so intense that it would drown out any cathode electroluminescence, even if it were present.

As previously explained, Hurley et al.(42,45,46) used an Alfrey-Taylor plot to demonstrate that the observed light was electroluminescent in nature. This consisted of showing that a plot of the variation in light intensity (recorded as the change in photo-multiplier output I_P) against $V^{-1/2}$ (where V was the applied voltage), was linear. Whereas, for transition radiation, a plot of variation in light intensity against V would be expected to produce a linear result(128). Accordingly, these plots should be able to discriminate between anode and cathode radiation; thus, a similar approach was adopted for the analysis of the present data.

Fig.5.9 shows a definitely identified anode spot, visible on the anode edge; while Fig.5.10 shows an example of a possible cathode spot opposite the end of the probe. The graphs of Figs.5.11(i)-(ii) show the variation in photo-multiplier output (photo-multiplier current I_P minus the 'dark' current I_D) plotted against various functions of applied voltage V for the definite anode spot; consideration of these graphs show that, as expected, the plot of $\mathrm{Log}(I_P-I_D)$ against V produced the most linear result (as measured by the correlation coefficient); although both plots gave good straight-line fits. A similar process was followed for the light spot shown in Fig.5.10, to give the graphs shown in Fig.5.12(i)-(ii). Again, the plot of $\mathrm{Log}(I_P-I_D)$ produced the most linear result, suggesting that the light was just reflected transition radiation. To further confirm this finding, the spectrum of the emitted light, shown in Fig.5.13, was recorded

Fig.5.9 Definite Anode Spot On Edge Of Aperture

Fig.5.10 Possible Cathode Spot Opposite Probe

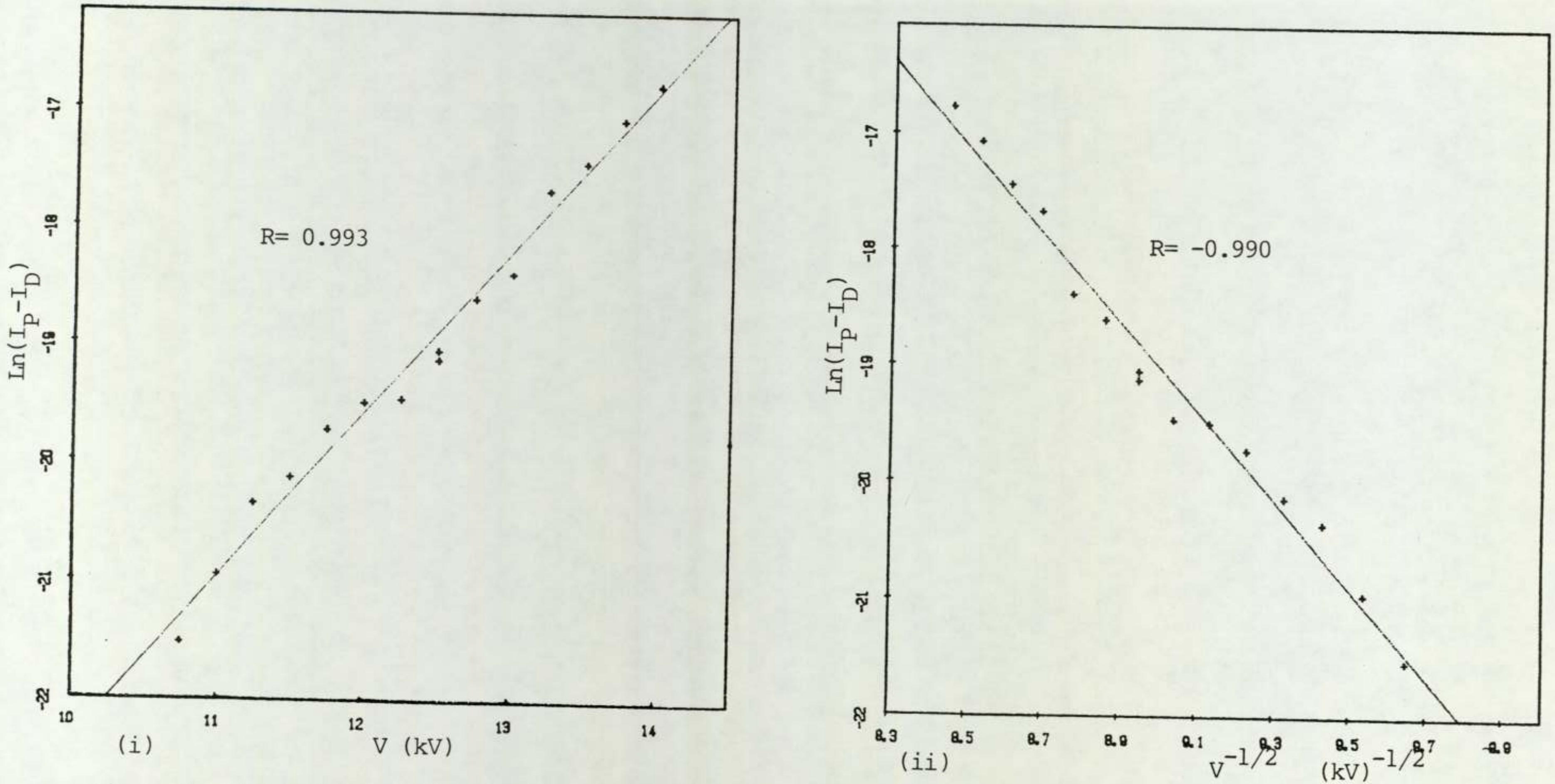

Fig.5.11 Plots Of Variation In Light Intensity With Various Functions Of Applied Field

(for the light spot shown in Fig.5.9)

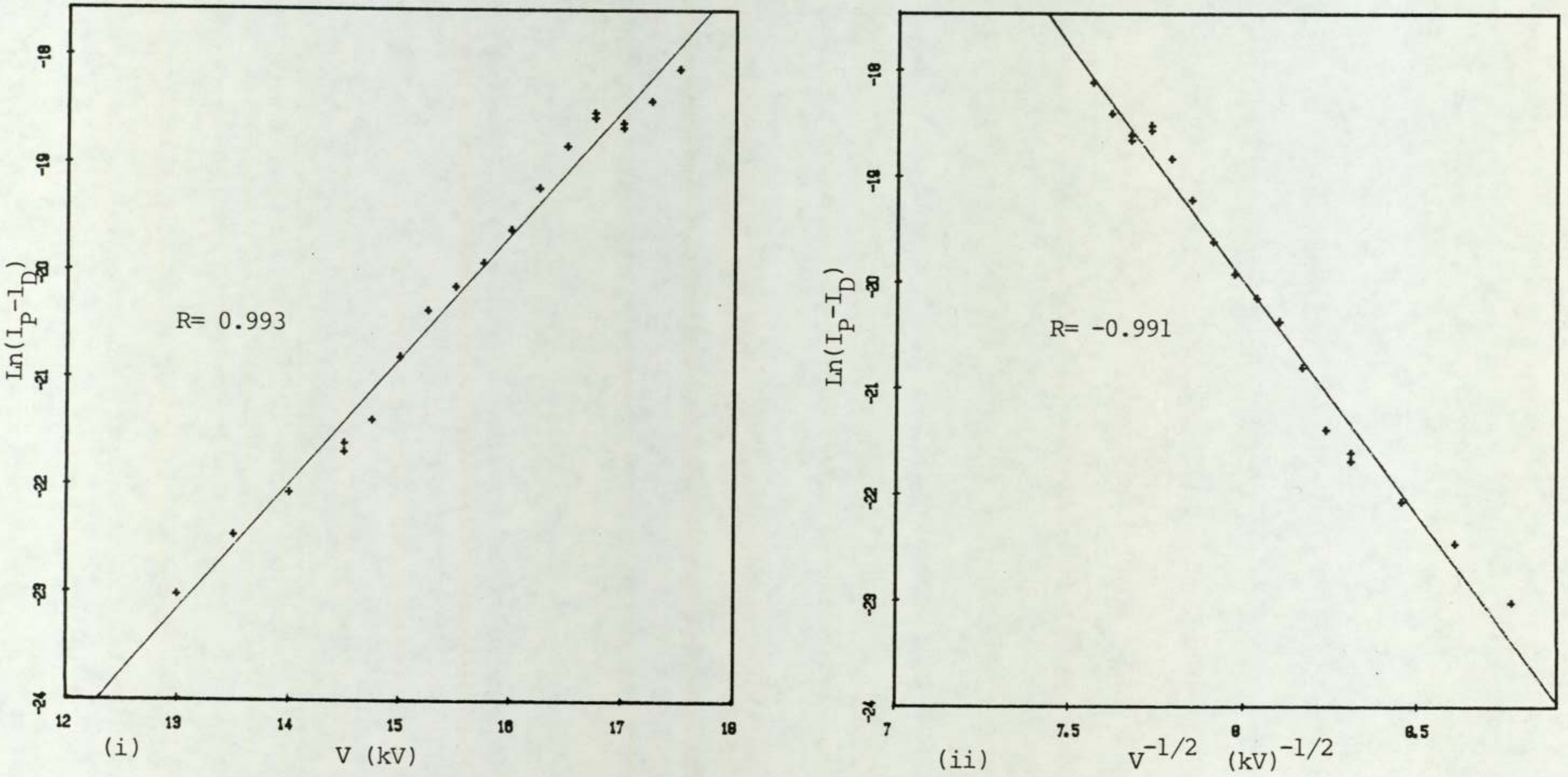

Fig.5.12 Plots Of Variation In Light Intensity With Various Functions Of Applied Field

(for the light spot shown In Fig.5.10)

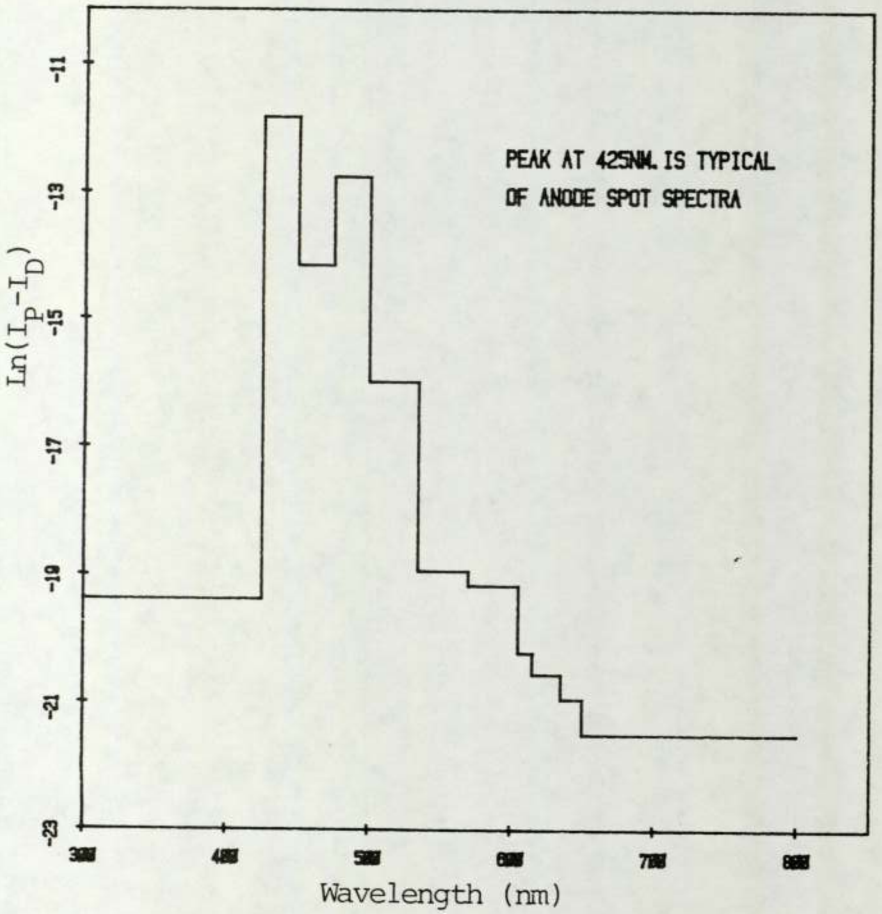

Fig.5.13 Spectrum Of Light Spot Shown In Fig.5.10

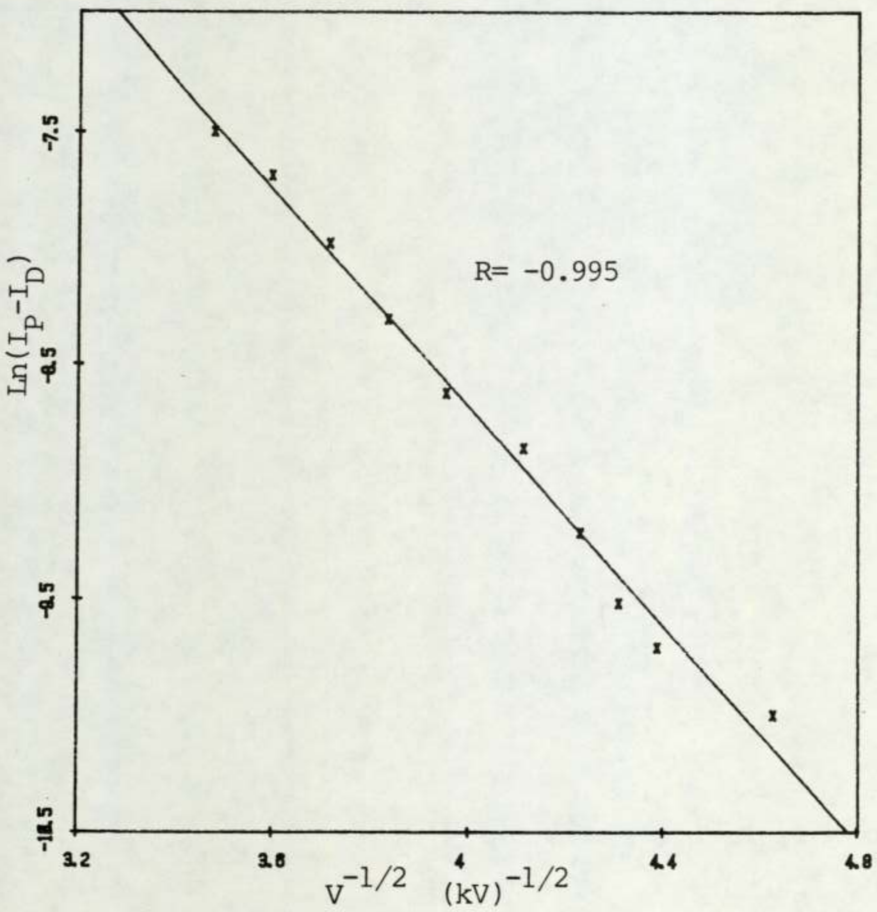

Fig.5.14(i) Plot Of Light Intensity Against $V^{-1/2}$ (data from Hurley)$^{(27)}$

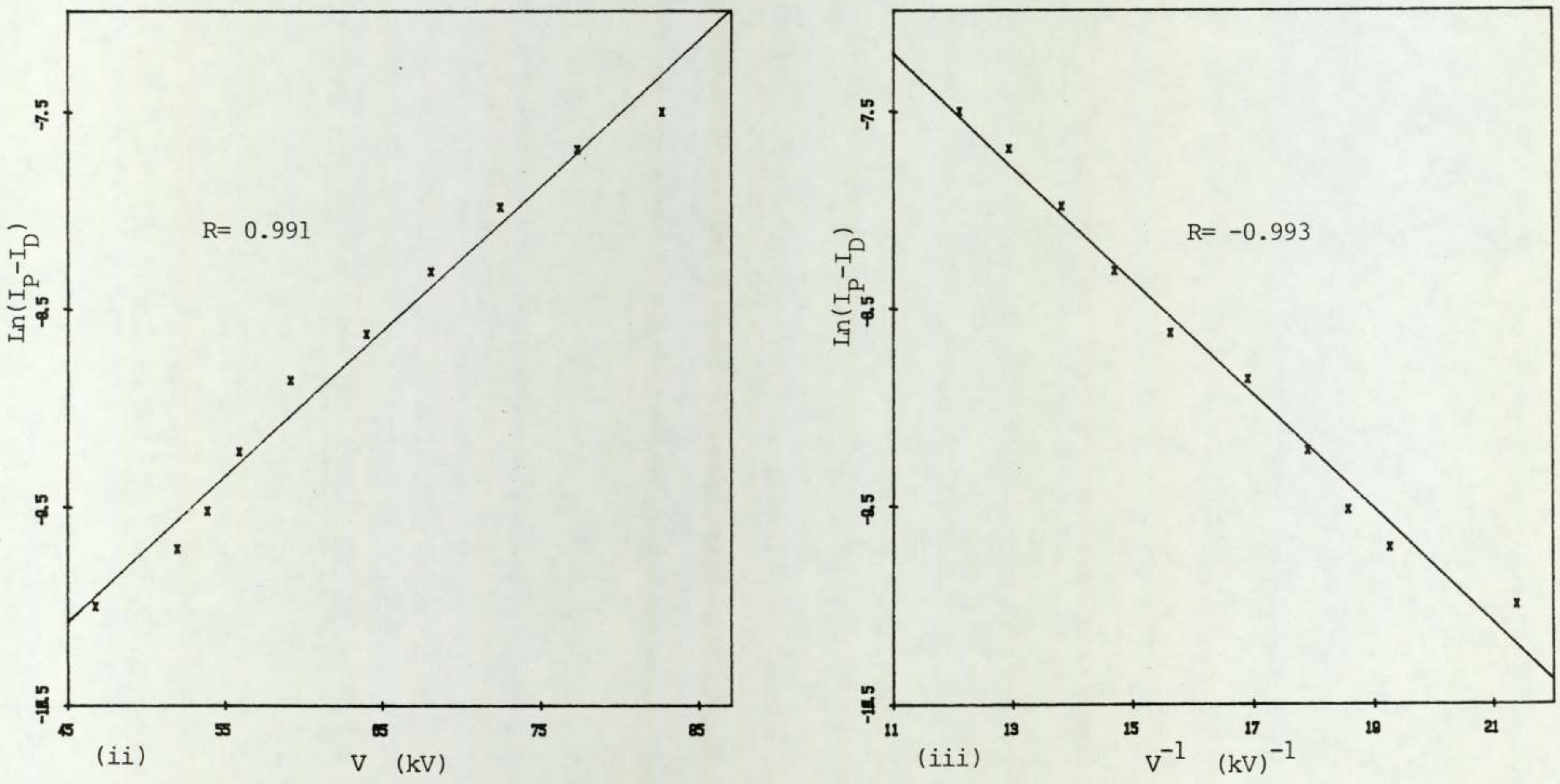

Fig.5.14(ii)-(iii) Plots Of Variation In Light Intensity With Various Functions Of Applied Field

(data from Hurley)$^{(27)}$

using the filter technique described earlier. The characteristics of this spectrum show that it was typical of an anode-spot; being composed mostly of higher frequency radiation peaking at 450nm.

In addition to the graphs shown in Fig.5.11 and Fig.5.12, a plot of $\log(I_P-I_D)$ against V^{-1} was also investigated, and little difference found between any of their associated correlation coefficients R. It appears that a plot of the log of the intensity of the emitted radiation against almost any function of applied votage gives a good straight line, at least over the range of voltages represented here. It should also be noted that the values of the constants obtained from the Alfrey-Taylor plots (Fig.5.11(ii) and Fig.5.12(ii)) for anode-spots, are similar to the values obtained by Hurley et al(42) for cathode electroluminescence processes.

One of the difficulties inherent in analysing electroluminescent data may be shown by the re-interpretation of Hurley´s data(42), presented in Fig.5.14(i)-(iii). These show that, even for radiation definitely identified as electroluminescence, almost any function of applied voltage may be plotted to give a good linear result.

5.2.4 Physical Significance of Optical Emission Phenomena

This series of experiments showed that no optical emission was observed that could be categorically attributed to cathode generated electroluminescence and, further, that for many centrally located emision sites, there was definitely no optical emission originating from the cathode. Several other sources, for example Bayliss(95), also mention this difficulty in observing electroluminescence generated by the emission process. All of these findings suggest that mechanisms enabling the production of electroluminescent centres, for example through impact excitation or recombination processes, should not be an integral part of an emission model. It should be noted that the present ′state-of-the-art′ emission model, proposed by Bayliss & Latham(77) and described in detail in Section 2.7, does not take any account of the production of electroluminescent centres; although such centres are not forbidden.

Considering the difficulty that has been encountered in observing electroluminescence, one alternative explanation for the optical emission observed by Hurley et al.(42,45,46) may possibly be that it is produced by some form of X-Ray fluorescent emission mechanism from the anode; this would explain why light was observable when using a planar anode system, and not with an apertured system. Although it is difficult to interpret the probe results on this basis.

5.3 Differential Ion Etching of Emission Sites

5.3.1 Calibration of Etching Rate of Ion Source

Before it was possible to quantify the effect of partial etching on the characteristics of an emission site, it was necessary to calibrate the etch rate of the ion beam incident on the specimen. This was achieved in two stages: firstly, a series of experiments were performed on 0.5 and 1micron copper films deposited on a glass substrate; secondly, to test whether these results were valid for bulk specimens, different regions of a standard copper specimen were subjected to a range of etching doses, i.e. various combinations of bombardment times and beam currents.

For the initial investigation, a variety of ion-beam currents and etch times were investigated, and evaluated by subsequent optical examination of the targets; thus showing the ion-currents and etch times required to etch through the film of copper. These experiments showed that the etch rate for any particular beam current (i.e. ion dosage rate) was the same for both of the film thicknesses, and that the films were penetrated by a 1×10^{-6}A beam current, with bomardment times of longer than 1 minute.

To test whether these results were valid for a bulk specimen, and to get a more accurate assessment of the etching rate, different ion currents and etch-times were used to etch different regions on the specimen surface. After removal from the experimental system, the depths of these etched spots were measured using a ´Tallysurf´ machine. This device profiles the surface of a specimen by means of a pin tracking across the surface; producing a printed output with the depth of any surface irregularities being calculated by the deflection from the surface base line. Several traces from the ´Tallysurf´ machine are shown in Fig.5.15(i)-(iii): where the sharp deflection in the line denotes the point where the probe passed over the etched spot; from the magniture of this deflection, the depth of the etched area may be calculated. These measurements are summarised in Table T5.1, from which it can be seen that the etch rate is doubled if the ion-beam current is doubled, and that for a beam current of 3×10^{-6}A, the etch rate is $0.25\,\mu$m.min^{-1}.

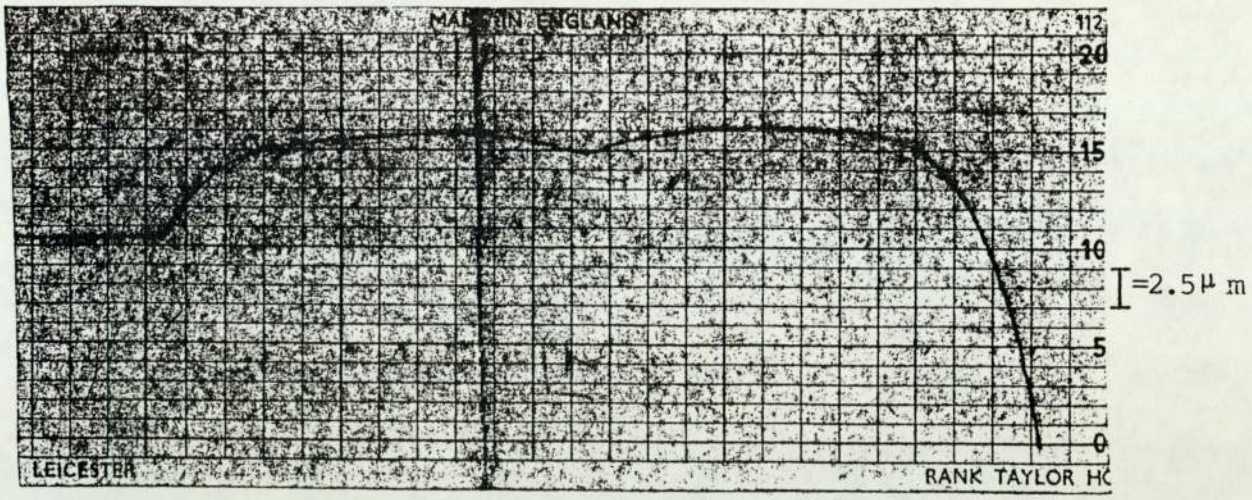

(i) 1.5µA for 10 mins.

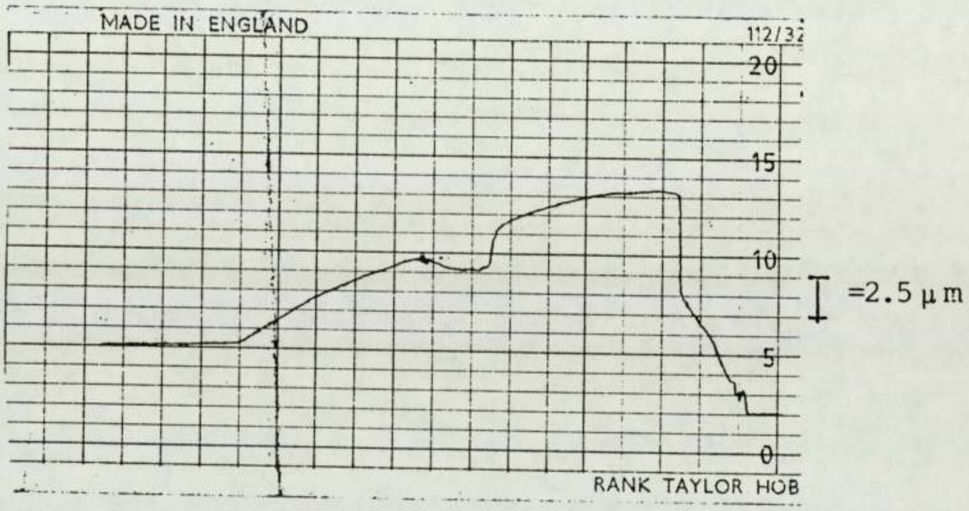

(ii) 1.5µ A for 20 mins.

Fig.5.15 (i)-(iii) ´Tallysurf´ Traces Showing Depth Of Surface Etching

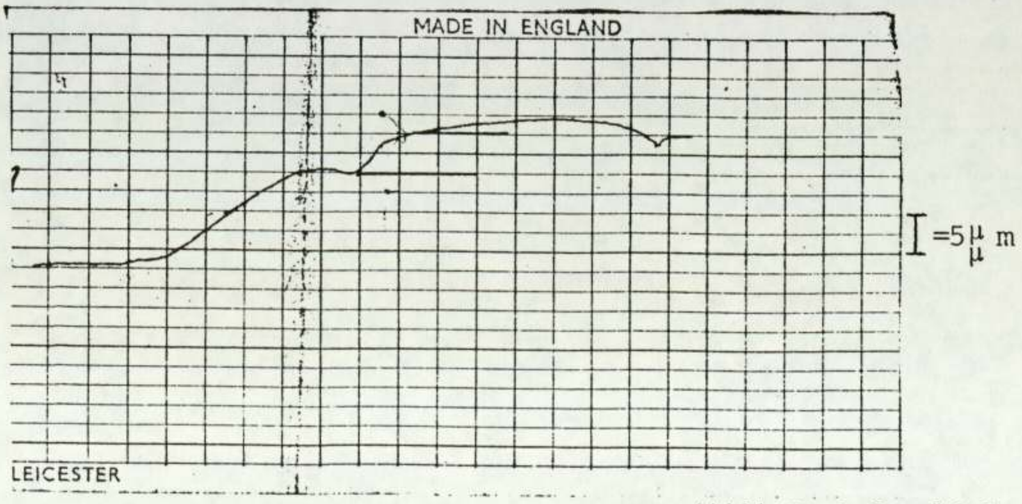

(iii) 3µ A for 16.5 mins.

Ion-Current μA	Etch Time (mins)	Spot Depth μm	Etch Rate μm/min
1.5	10	1.25	0.125
1.5	20	2.5	0.125
1.5	40	6	0.15
3	16.5	4	0.24
1.5	10+5+5+13	3.5	0.105
3	4+4.5	1.95	0.235

Table T5.1 Calibration Of Ion-Beam Etching Rate

5.3.2 Etching of Emission Sites

The purpose of this section is to give a brief description of the surface characteristics that result from etching away an emission site. Typically, it required a bombardment time of 10-15 minutes at a beam current of $3\text{x}10^{-6}$A to totally destroy an emission site. From the etching rate experiments, this corresponded to the removal of approximately 3 - 4 μm of copper from the surface of the specimen. Sometimes, however, the site would disappear after only 1 - 2 μm had been etched from the surface (about 5 minutes bombardment time). It should be mentioned that the etching rates were calculated on random portions of the surface of a copper specimen; while, for an actual emission site, it might be expected that the etching rate would be slower because of the presence of insulating or semiconducting material.

As shown by Fig.5.16(a)-(b), which are S.E.M. micro-graphs, recorded at the same magnification, of the unetched and etched surface respectively, the process of ion-beam bombardment produced significent enhancement of the grain boundaries within the copper.

5.3.3 Effects of Partial Etching on Emission Characteristics

For this investigation the specimen was scanned, and the dominant emission site located and characterised, in the usual manner. The emission site was then bombarded with an ion-beam current of $1.5\text{x}10^{-6}$A, i.e. about half the current used for the conditioning process, and for very short etch times. This procedure therefore gave a slower and more controllable etch rate, which allowed the investigation into possible changes in emission characteristics caused by this gradual removal of surface

⊢⊣ 10 µm

Fig.5.16 (i) S.E.M. Micrograph Showing Etched Area

(ii) S.E.M. Micrograph At Same Magnification Showing Unetched Area material. After each session of etching, the chamber was re-evacuated to U.H.V. conditions and the new emission characteristic of the same site measured. The graphs presented in Figs.5.17(i)-(ii) show the changes in emission characteristics produced by the removal of surface material for two typical sites. For the specimen in Fig.5.17(i), the experiment was terminated when the emission site was totally destroyed; while for the specimen in Fig.5.17(ii), etching was only continued until its emission current became so small that it was masked by the current produced by other emission sites. For each site, and each stage of etching, Table T5.2 presents the depth etched away, the β-factor and the emission area, together with the applied field required to produce an emission current of 1×10^{-8}A. As can be seen, there was a significant overall change in the emission characteristics as the site is etched away. However, the majority of the change occurred when 0.25 - 0.5 μm of material had been removed; after this, changes were comparatively minor until the emission site was completely destroyed.

5.3.4 Observations of Surface Features in the Emission Site Area

Two further powerful surface analytical techniques were used for obtaining additional information about the material composition of sites: these were an X-ray analysis facility, with its associated high-resolution S.E.M., and an Auger/X.P.S. machine. However, for these techniques to be of value, it was necessary to accurately mark the emission sites to allow their re-location in the two instruments. This was achieved by scanning a specimen and locating an emission site in the usual way, and

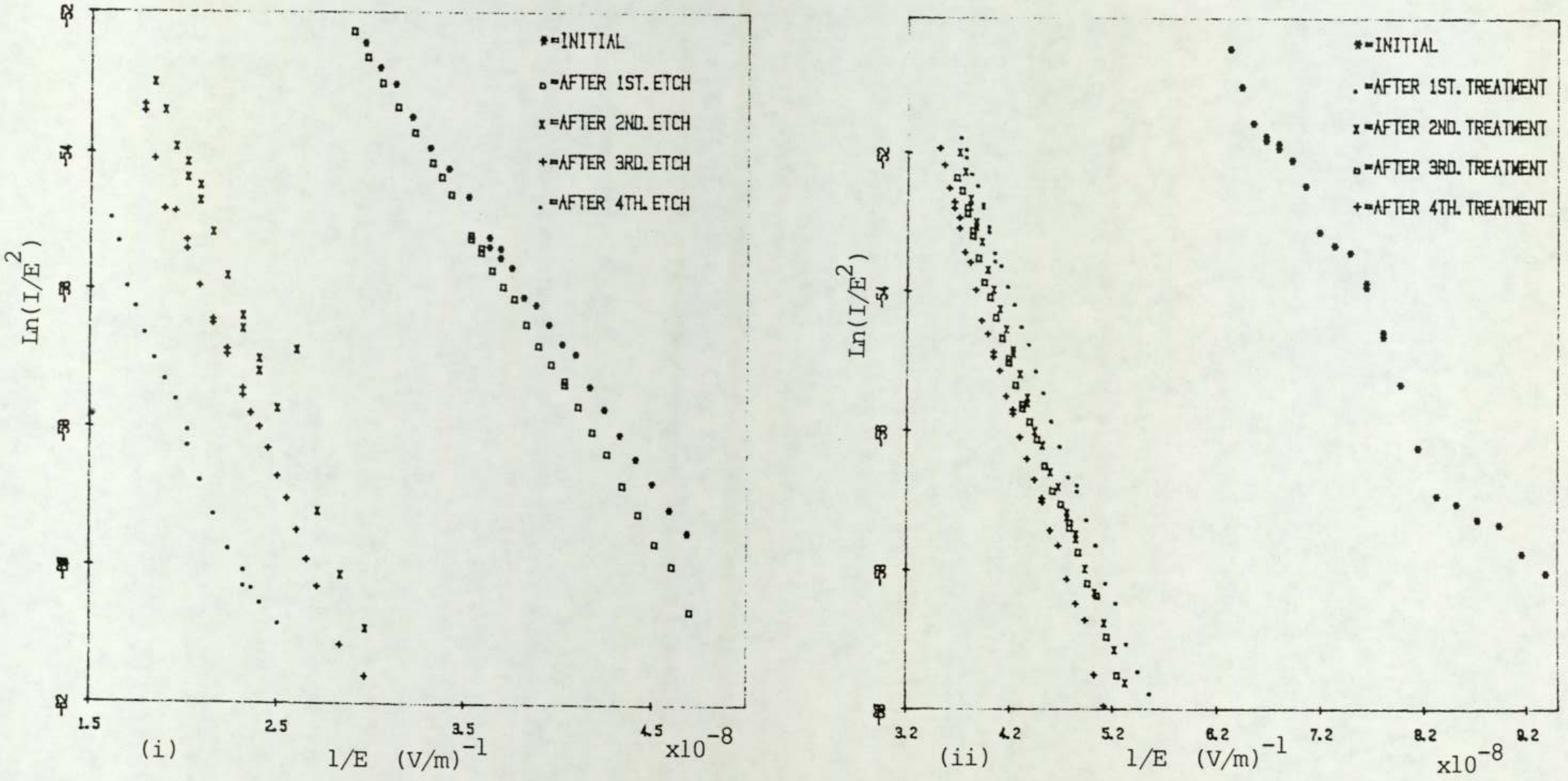

Fig.5.17(i)-(ii) F-N Plots Showing Changes Produced By The Partial Etching Of Emission Sites

	Etch Depth μm	β-Factor	Emission Area (m^2)	E′ ($MV.m^{-1}$)
INITIAL	-	151	3.17×10^{-16}	32
1st	0.125	135	1.56×10^{-17}	32.9
2nd	0.5	91	6.66×10^{-18}	52.5
3rd	0.25	89	3.08×10^{-18}	54.4
4th	0.875	92	1.12×10^{-19}	59.5

(i)

TOTAL DEPTH 1.75μm

Tables T5.2 (i)-(ii) Changes In Emission Characteristics Produced By Partial Etching Of Sites

	Etch Depth μm	β-Factor	Emission Area (m^2)	E′ ($MV.m^{-1}$)
INITIAL	-	239	4.35×10^{-16}	15.4
1st	0.5	142	3.39×10^{-16}	25.9
2nd	0.313	135	5.08×10^{-16}	26.5
3rd	0.313	141	1.49×10^{-16}	27.1
4th	0.375	129	5.73×10^{-16}	27.7

(ii)

TOTAL DEPTH 1.5μm

then using the ion-beam to lightly etch the site, i.e. just enough to provide visual evidence of its location, without eliminating the emission current. The specimen was then removed from the experimental system and mounted in an S.E.M. for initial examination. Subsequently, the specimens were suitably prepared and examined using one of the techniques mentioned above. For example, with the Auger/X.P.S. machine, the specimen had to be cut into a small 5 x 5mm section, as this was the maximum specimen size that could be introduced into the experimental chamber.

Within the ′marked′ area surrounding an emission site, it was typical to find certain anomalous surface features, or at least features that were present in a greater concentration than on the rest of the electrode surface. Fig.5.18(a)-(b) shows S.E.M. micrographs of the typical area around an emission site, and a number of these surface irregularities are visible. Fig.5.19(i)-(ii) shows higher magnification micrographs of several of these structures, and reveal that such surface features stand higher than the rest of the etched surface; suggesting that they were more resistant to the ion-beam etching. These surface anomalies occurred in a variety of shapes and sizes; the ones within the etched area seeming to protrude more from the specimen surface than those in unetched areas; this factor presumably being due to the preferential etching of the surrounding matrix of copper.

Fig.5.20 is a further interesting example of a ′marked′ emission site, in that it shows, close-by, some heavy surface damage, involving some sharp, field-enhancing, metallic edge structures. However, as noted by Athwal(76) in a similar example,

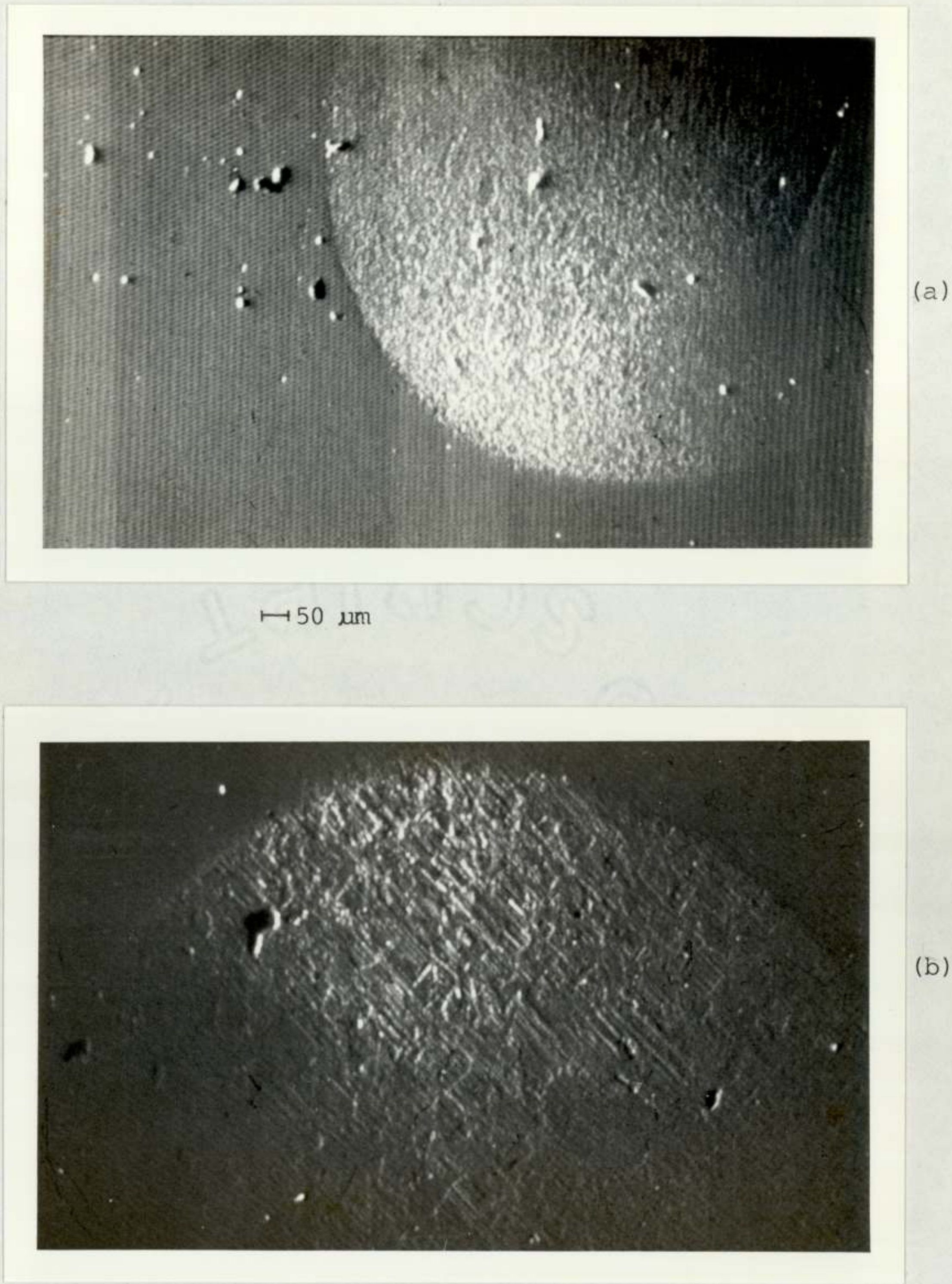

Fig.5.18 (a)-(b) S.E.M. Micrographs Of Marked Emission Site Areas

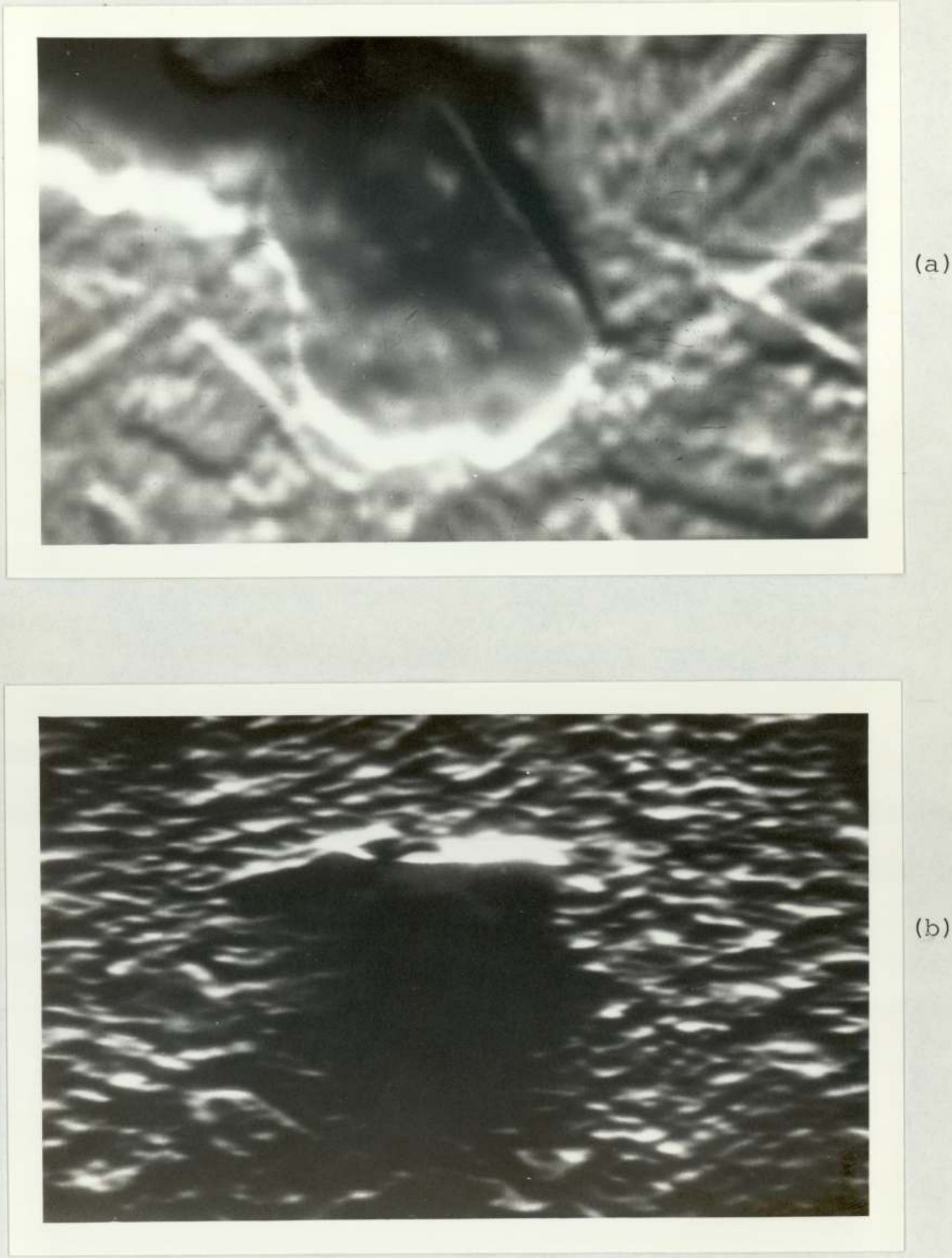

Fig.5.19 (a)-(b) S.E.M. Micrographs Of Anomalous Surface Microstructures

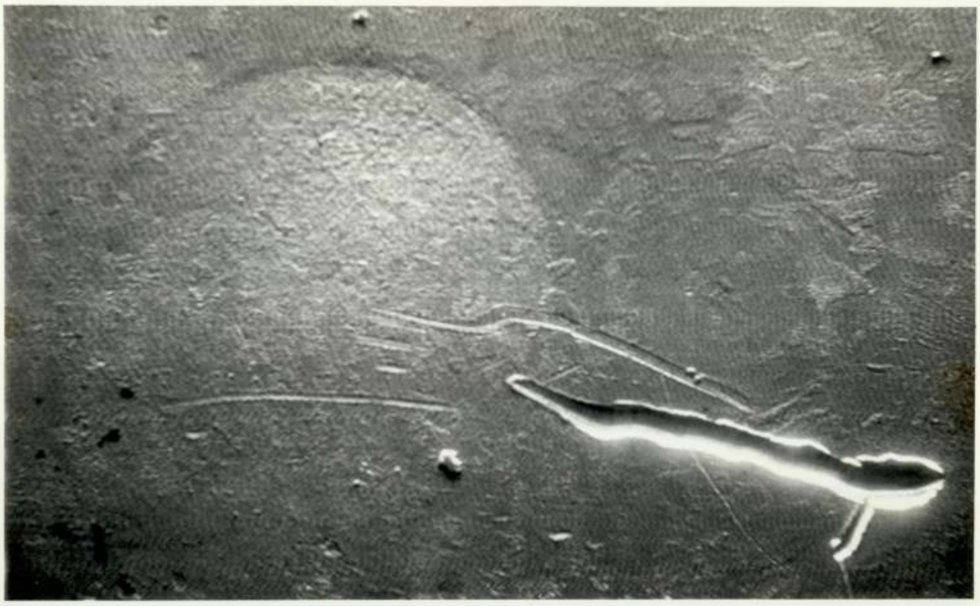

Fig.5.20 Marked Emission Site With Heavy Surface Damage Nearby

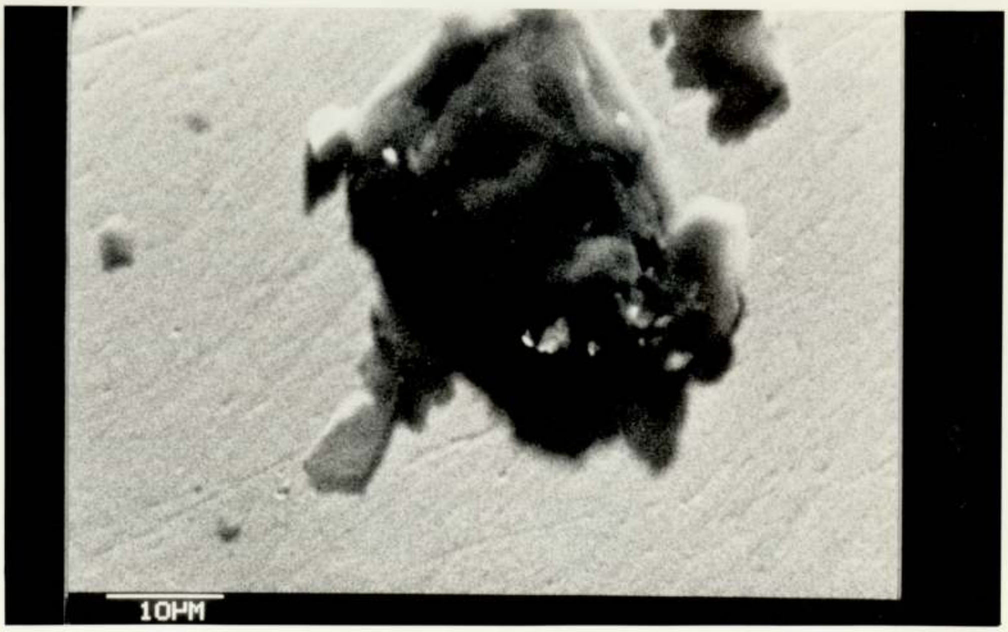

Fig.5.21 Microstructure Used For ´Kevex´ Analysis

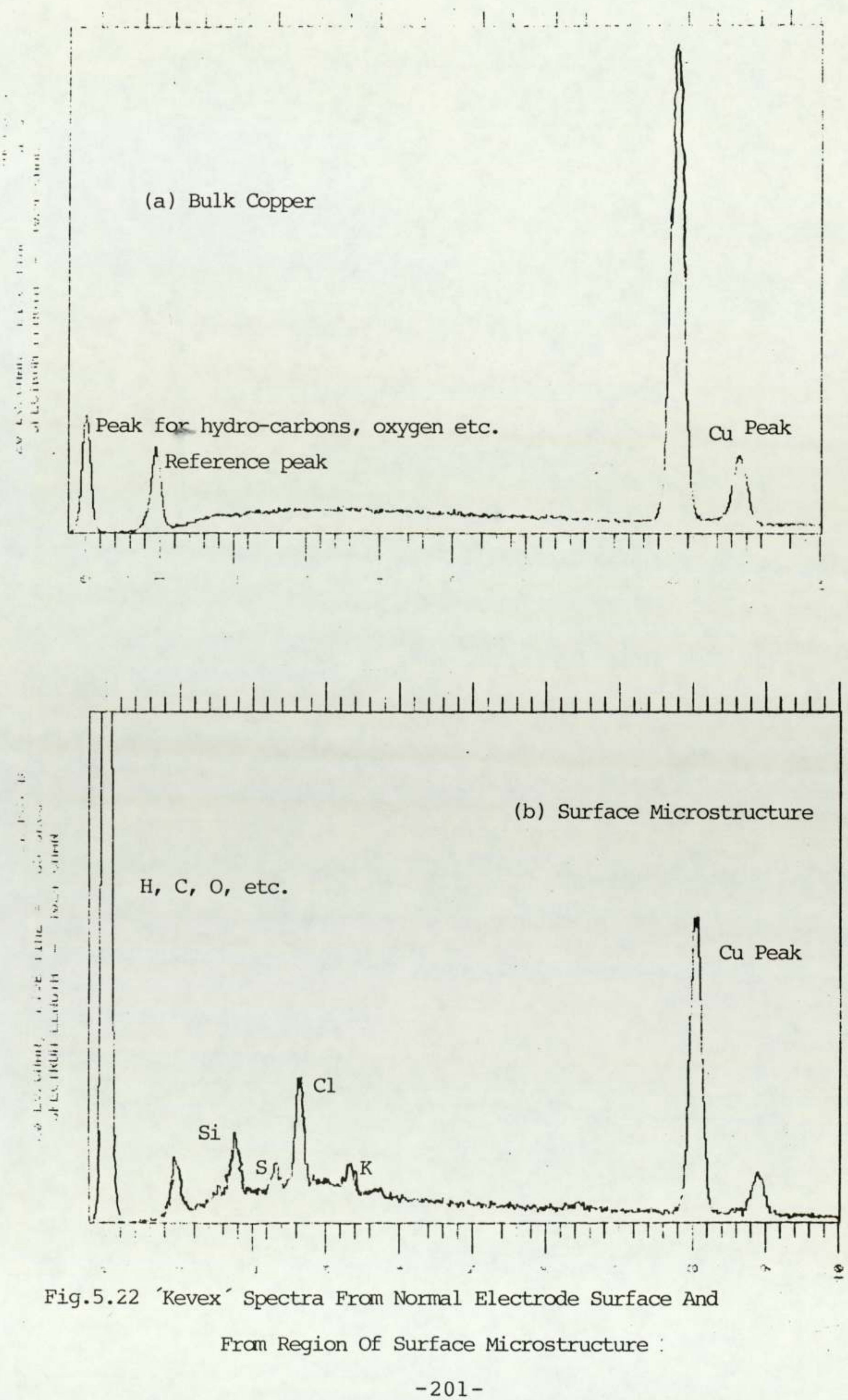

Fig.5.22 'Kevex' Spectra From Normal Electrode Surface And From Region Of Surface Microstructure

such structures do not seem to give rise to emission sites.

To provide further information about the micro-structure shown in Fig.5.21, ´Kevex´ (X-Ray) analyses for the bulk copper and for the centre of a micro-structure were obtained; shown in Fig.5.22(a)-(b). From a comparison of these X-ray spectra, it can be clearly seen that the micro-structure contains a, relatively, much lower proportion of copper, and that additional peaks are present that may be ascribed to the presence of silicon, sulphur, chloride and potassium. However, this technique is incapable of distinguishing the low atomic weight elements, but does produce a combined peak for carbon, oxygen, hydrogen etc. One of the major differences between the spectra lies in this combined peak, the anomalous surface structure seems to contain a much higher proportion of these low atomic weight elements, which may be tentatively identified as carbon or hydro-carbons.

Further emission sites were similarly located and lightly ´marked´ (<1micron of surface material removed), and subsequently examined using Auger Electron Spectroscopy, A.E.S. This A.E.S. instrument had a spatial resolution of about 20 μm and, as well as the standard ´elemental-trace´ facility, allowed an S.E.M. micrograph of an area to be obtained; thus showing the distribution of a particular element within that area. Thus, Figs.5.23(a)-(b) show, respectively, an S.E.M. micrograph of an emission site and an ´elemental map´, set for copper, of the same region, and reveals a low copper reading in the centre of the site area. The Auger traces, presented in Fig.5.24(i)-(ii), shows the relative proportions of copper and carbon on (i) the face of the specimen, and (ii) in the centre of the ´marked´ low-copper

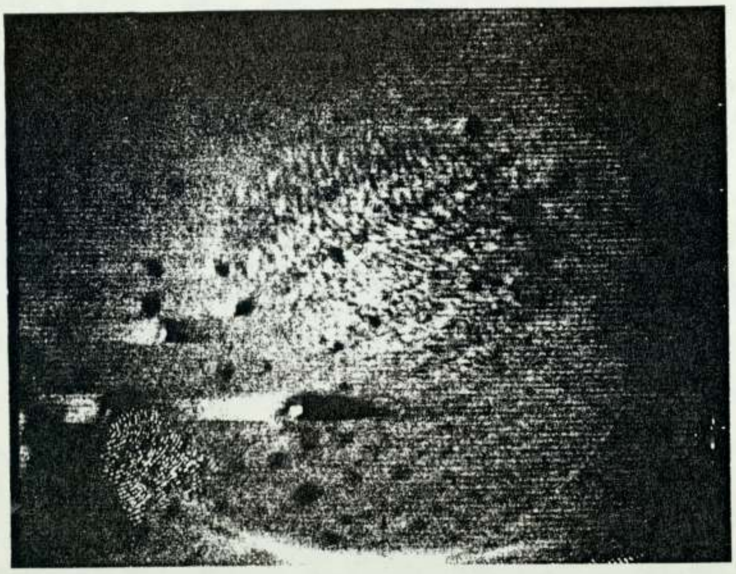

(a) ´Marked´ Emission Site

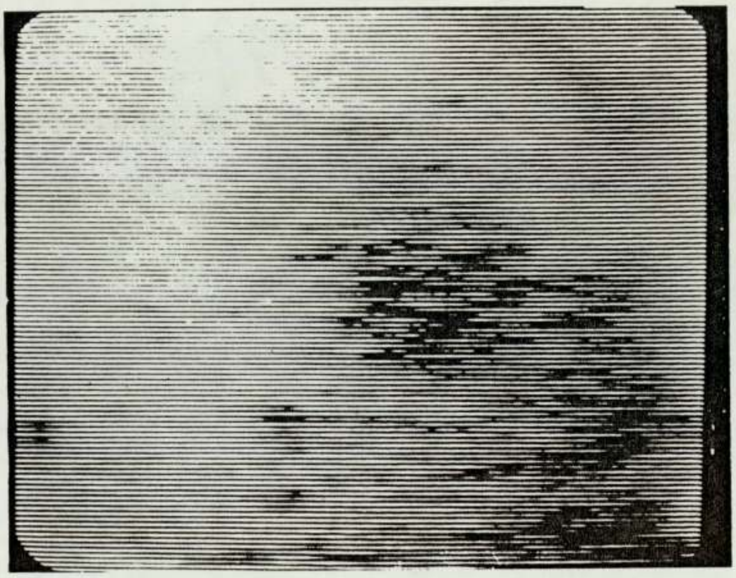

(b) ´Elemental Map´

Fig.5.23 S.E.M. Micrographs Of ´Marked´ Emission Site And Distribution Of Copper In The Same Region (dark regions are low concentrations)

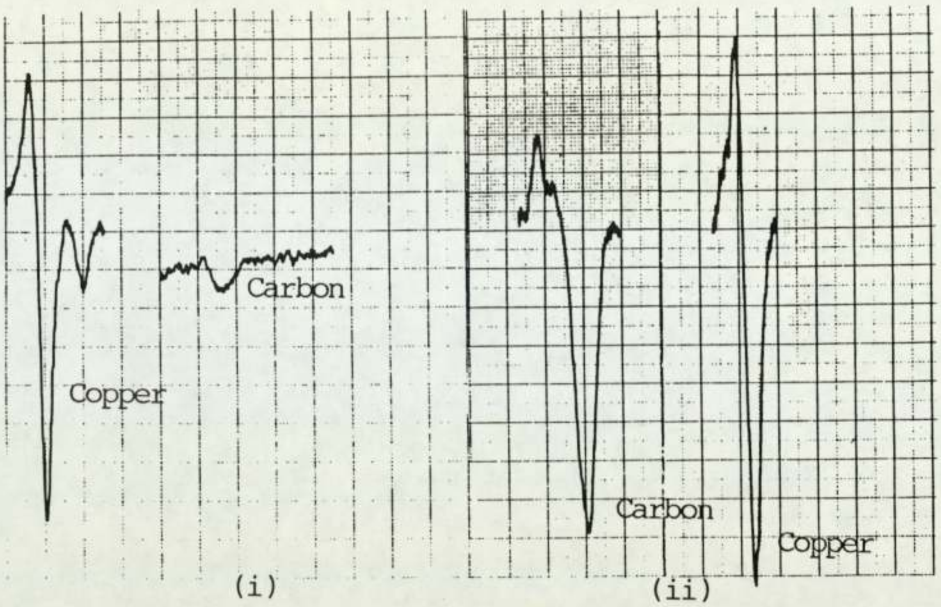

Fig.5.24 Auger Traces Showing: (i) Cu/C Concentrations In Bulk
(ii) C/Cu Conc. In Site Region

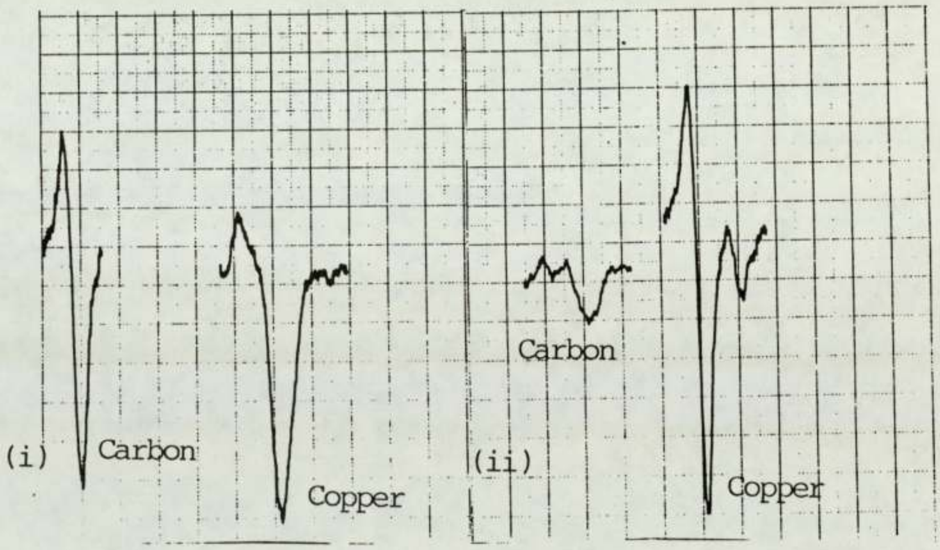

Fig.5.25 Further Traces Showing: (i) C/Cu In Site (ii) C/Cu In Bulk

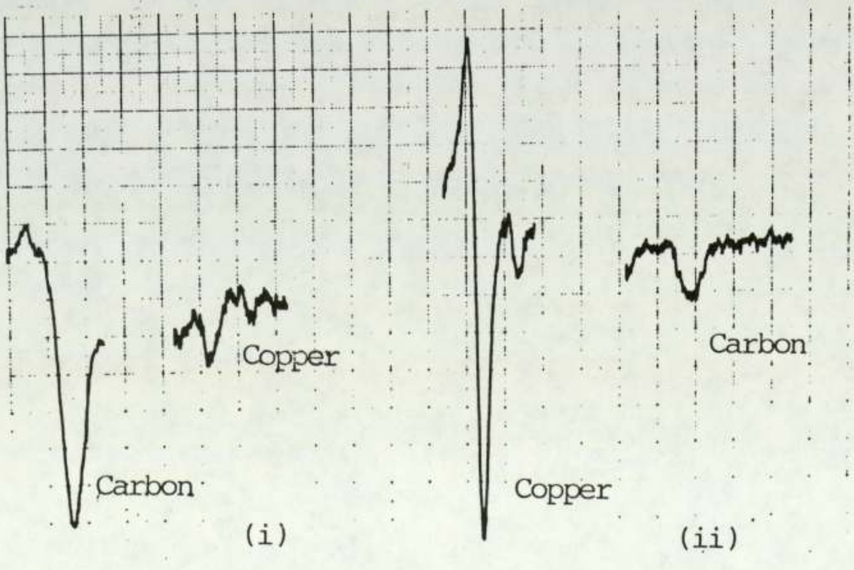

Fig.5.26 Auger Traces From (i) Surface Microstructure (ii) Bulk

region; thus suggesting that this emission site area corresponds with a region of higher carbon concentration, and lower copper. For a second ´marked´ emission site area, Fig.5.25(i)-(ii) shows the associated C/ Cu Auger traces for (i) the centre of the site region and (ii) an area away from the ´marked´ position; again, a relatively much higher carbon reading was obtained from the site region. Finally, Fig.5.26(i)-(ii) show the relative copper/carbon concentrations for (i) the normal specimen surface and for (ii) the centre of the surface microstructure visible in Fig.5.23(a). As was expected, following the results of the ´Kevex´ analysis, a relatively high carbon reading was, once again, obtained from the microstructure.

5.4 Electron Spectrometry Studies of the Emission Process

The experimental findings described above, which will be discussed in more detail in Section 5.5, all tended to confirm that emission arises from a non-metallic process. Further evidence was obtained by recording the energy distributions of the emitted electrons, using the same U.H.V. electron spectrometer system that Latham et al.(45,48,75-79,94-97) used to produce their sucessive models of electron emission, described in Chapter 2. Another reason for pursuing this series of experiments, was to ensure that the process of localised conditioning, using the ion-beam technique, did not create further emission sites by the destruction of the initially dominant site. This necessitated an initial examination in the electron-spectrometer system, followed by transfer to, and subsequent conditioning in, the usual experimental system. Fig.5.27 shows a simple schematic diagram of the electron spectrometer system; while Fig.5.28 shows F-N plots of the emission characteristics before and after transport between experimental systems, together with the changes produced in emission characteristics by ion-beam conditioning.

Following the normal surface preparations, a standard copper specimen was mounted in the spectrometer system. After the initial switch-on of emission sites, a high-resolution spiral scan was made of the specimen to record the spatial distribution of all the emission sites; an example is presented in Fig.5.29, and is seen to represent a ′site map′. This technique used a very sensitive electron multiplier detector system, and was able to record even the sites that make very small contributions to the whole gap current; thus providing the possibility of showing the spatial location of both major and minor emission sites. These locations were displayed on a storage oscilloscope and subsequently photographed. For the dominant emission site, the variation in energy distribution of the emitted electrons with applied field could also be displayed and photographed, an example is shown in Fig.5.30. It is from this sort of data that the sophisticated interpretations of the emission characteristics of Latham(97), Bayliss(95) and Bayliss & Latham(77), described in the Chapter 2, were developed. Following the measurement of the standard I-V characteristic, the specimen was removed from the electron spectrometer facility and installed in the usual experimental chamber.

After scanning the specimen and locating the dominant emission site (the others could not be detected), the characteristic of the site was first measured and it was then treated using the ion

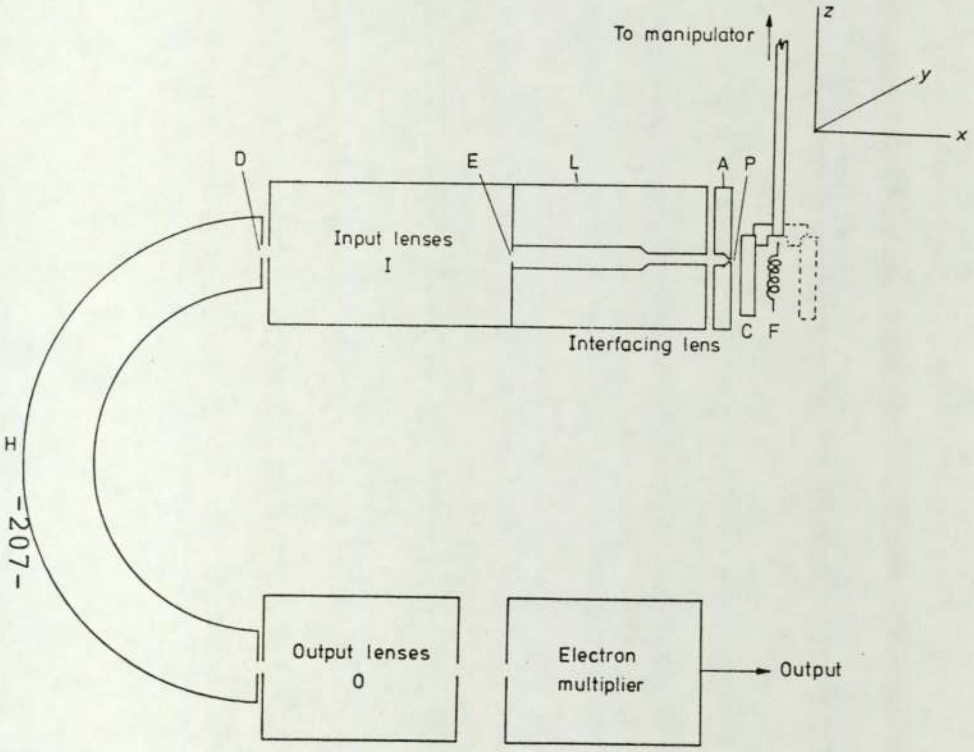

A schematic diagram showing the lay-out of the spectrometer, ancillary electron lens systems and the 'test' high-voltage gap.

Fig.5.27 (from Allen & Latham)$^{(79)}$

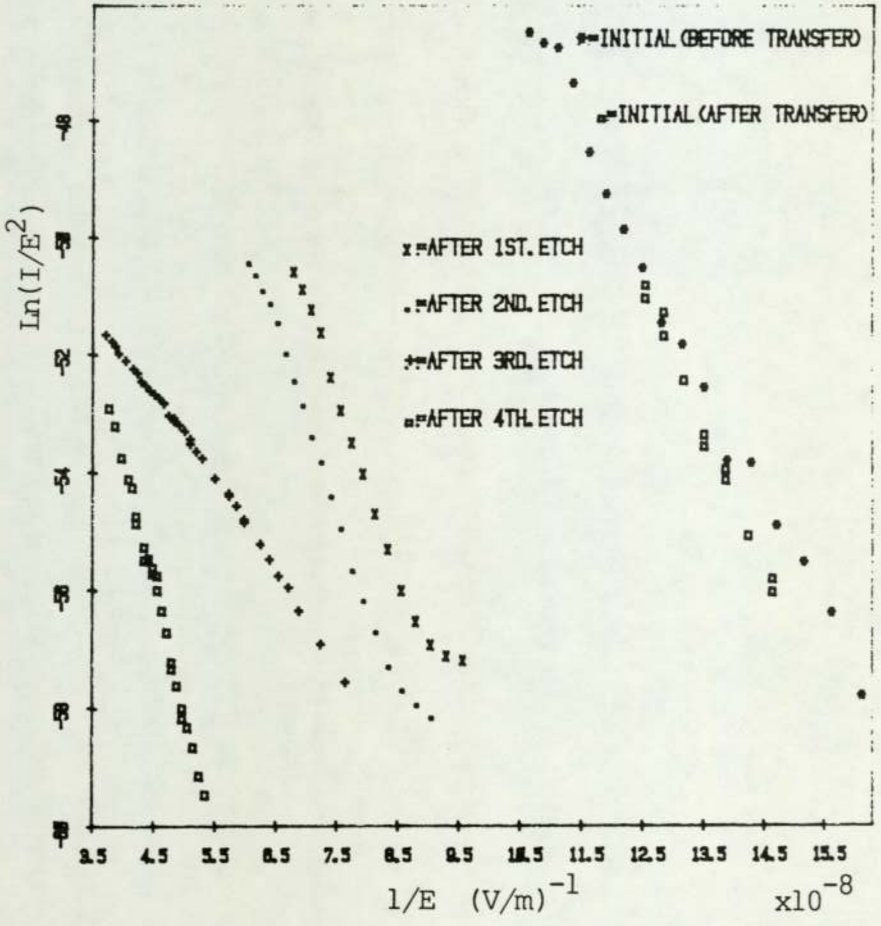

Fig.5.28 F-N Plots Showing Changing Emission Characteristics During Transfer And Conditioning

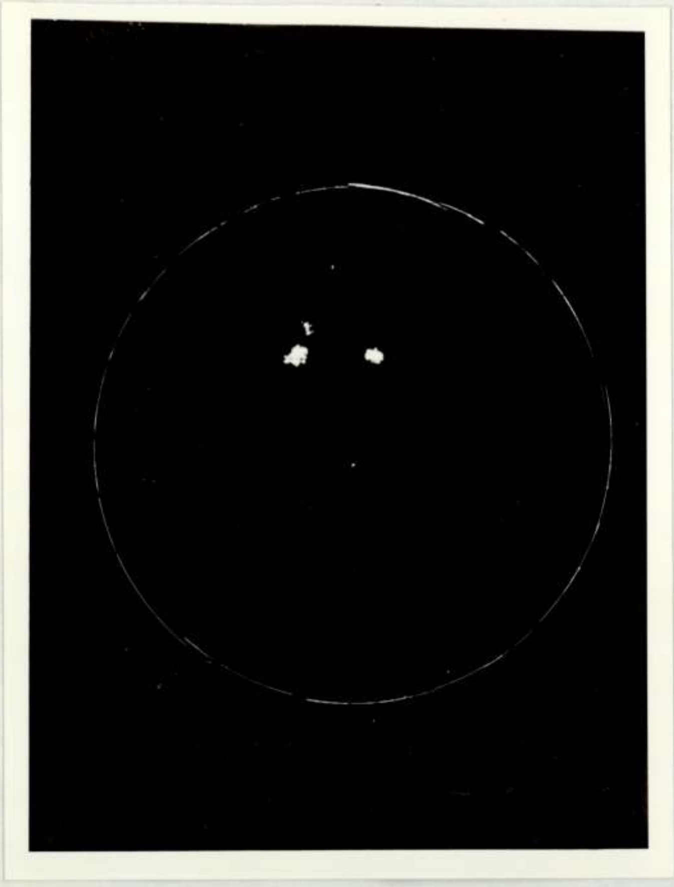

Fig.5.29 'Site Map' Produced By Spectrometer System

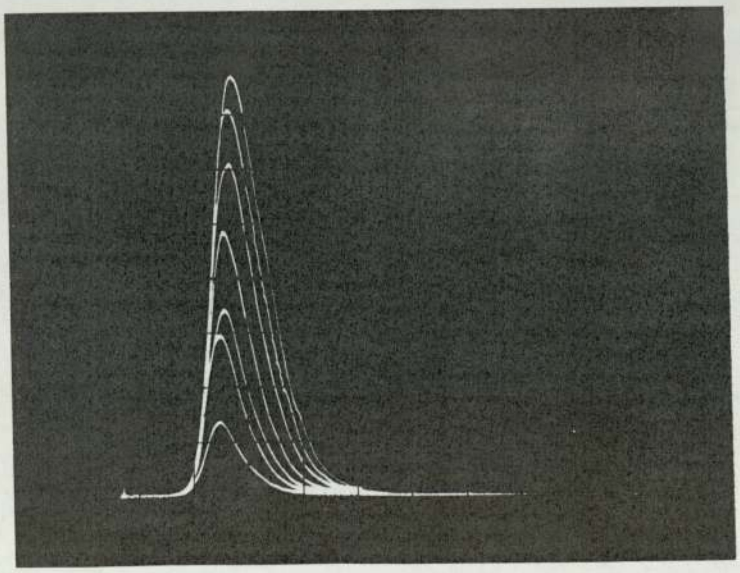

Fig.5.30 Changes In F.E.E.D. With Applied Field For Dominant Site In Spectrometer System

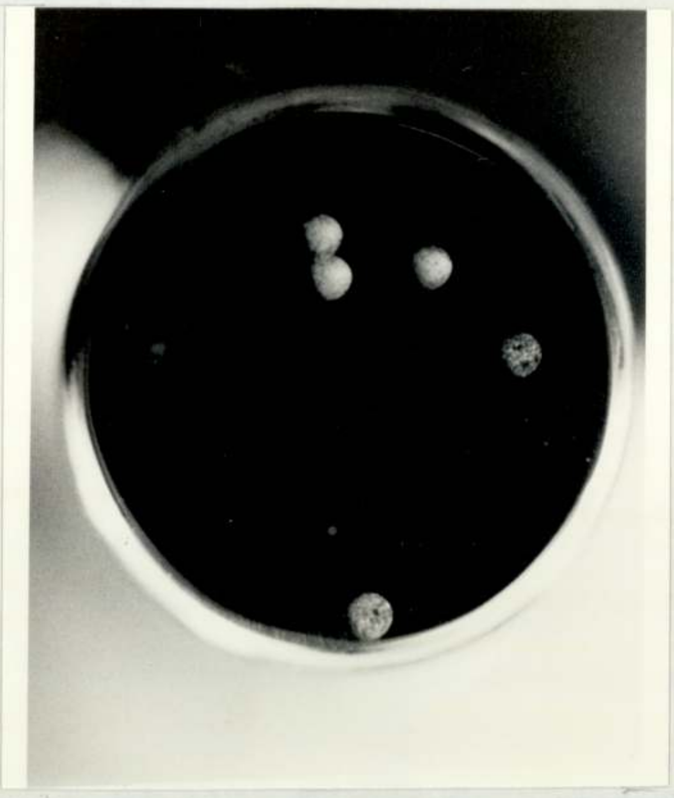

(i) Distribution Of Etch Scars Produced By Conditioning

Fig.5.31

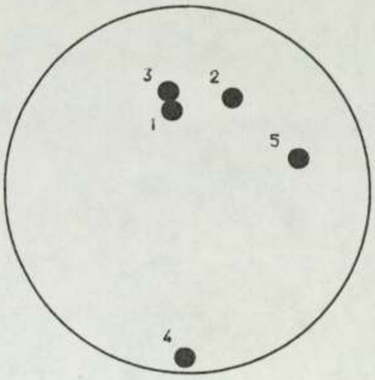

(ii) DIAGRAM LABELLING THE EMISSION SITES
SHOWN IN THE ABOVE PHOTOGRAPH

beam; this procedure was repeated until the dominant site could no longer be located. This ion-etching produced typical etch scars on the face of the specimen, shown in Fig.5.31(i); with the line diagram of Fig.5.31(ii) labelling the etched sites. Thus, the distribution of etched spots on the face of the specimen reflected the position of sites as they came to dominate the emission characteristics. If a comparison of this spatial distribution is made with that obtained from the high-resolution ´site-mapping´ technique, the question, of whether or not the secondary emission sites were created by the conditioning process, can be answered. A comparison of Fig.5.31 and Fig.5.29, shows that localised conditioning does not effect the subsequent distribution of emission sites.

A non-metallic emission mechanism is confirmed by the shift from the Fermi-level and the spectral shape observed in the energy distributions of Fig.5.30. The increasing shift from the metal Fermi level, and increasing F.W.H.M., with applied field are expected on the basis of the hot-electron model.

5.5 Physical Implications of Subsidiary Experimental Investigations

Most of the experimental investigations described in the previous sections of this chapter provide some information as to the physical nature and composition of the emitting micro-regime; this is particularly true of those described in Section 5.3.

Results from the partial etching of emission sites showed that, although around 3 - 4 μm of surface material had to be removed to ensure the complete destruction of an emitting site, the removal of the initial 0.25 - 0.5 μm provided the most significant reduction in emission. This finding suggests that the surface oxide layer is an important factor in determining the magnitude of the emission current. The ´marking´ experiments showed that certain types of surface micro-structures are frequently associated with the occurrence of emission sites, and that the analysis of such micro-structures show them to consist of relatively high proportions of carbon, silicon, sulphur etc. Further analysis of the general area of an emission site, using the Auger technique, shows that it is generally high in carbon compared with the bulk of the specimen surface. This finding is not suprising when the work of Athwal, Latham et al.(94) on artificial ´carbon´ sites is considered

These findings confirm that an emission site is composed of an insulating region embedded in the metal surface(48,46,77), and that the oxide layer in the vicinity of this insulating inclusion plays an important role in the emission process. The differential etching produced by the ion-beam, illustrated in Fig.5.32, removes the oxide layer surrounding the inclusion, and it is this region that influences the metal-insulator junction effects which determines the likelihood of a particular site switching-on. The dense distribution of insulating particles on the surface of a specimen, evidenced by the surface ´snow´ effect produced by the generalised glow-discharge conditioning technique, implies that there are many potential emission sites; however, this investigation has shown that at fields <25MV.m^{-1}, only a few actually switch-on at any one time. In contrast, the large-scale

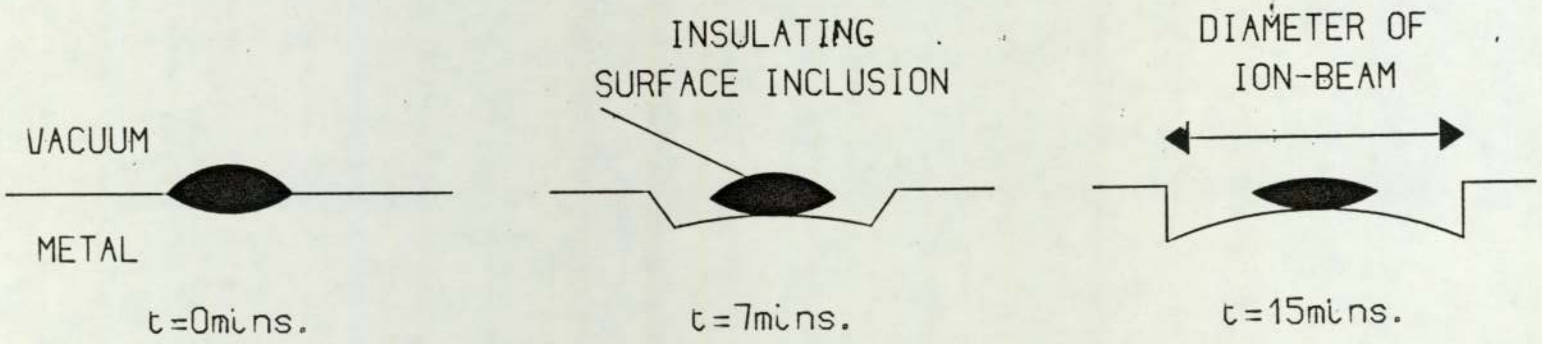

DIAGRAM ILLUSTRATING DIFFERENTIAL SURFACE ETCHING USING THE ION-BEAM

Fig.5.32

multiple switch-on of sites observed in the ion-beam conditioning experiments, usually in the field range 35 - 45MV.m^{-1}, suggests that many of these potential sites can be activated under the right conditions. A finding which seems to be confirmed by subsequent optical studies within the laboratory.

CHAPTER 6

Technological Implications of Localised Electrode Conditioning

6.1 Evaluation of Conditioning Techniques

As discussed previously, the concept of localised conditioning seems to possess several advantages over the ´general´ approach adopted in previous studies(104-117). Firstly, localised conditioning provides a means of controlling the emission characteristics of an electrode, by only destroying the dominant emission site. Secondly, there is a benefit, from the conditioning point-of-view, of only treating a localised surface area: for example, several previous studies, using general ion-etching as a means of in-situ specimen cleaning(76,95), have shown that as many, or sometimes more, emission sites are uncovered as the specimen surface is etched away, as are destroyed. It should be noted that no significant conditioning effect was produced by this method; in fact, Bayliss(96) reported a de-conditioning effect.

One factor to bear in mind, when considering the following observations on the various conditioning methods, is the reproducibility of the results. Thus, from an inspection of the findings presented in the previous chapter, it will be seen that there is a very large variation in, not only the switch-on fields, and the final operating fields achieved, but also in the reasons for terminating a conditioning treatment. Tables T6.1 - T6.3 summarise some of the more important factors resulting from the use of the conditioning techniques described in previous chapters.

F_i ($MV.m^{-1}$)	F_f ($MV.m^{-1}$)	γ
7.8	28.1	3.5
13.2	35.0	2.7
18.8	41.8	2.2
12.9	31.3	2.4
16.1	32.6	2.1

Table T6.1 $\bar{\gamma} = 2.6$

Ion-Beam Conditioning

F_i ($MV.m^{-1}$)	F_f ($MV.m^{-1}$)	γ
21.0	41.1	1.9
10.2	14.2	1.4
15.2	21.2	1.4
16.9	32.1	1.9
17.3	29.7	1.7

Table T6.2 $\bar{\gamma} = 1.7$

Gas Sputtering

	F_i ($MV.m^{-1}$)	F_f ($MV.m^{-1}$)	γ
1	23.1	41.0	1.8
2	16.0	23.2	1.5
3	21.3	30.2	1.4

Glow Discharge

Table T6.3 $\bar{\gamma} = 1.6$

Tables Summarising Results From The Successful Conditioning Experiments

For the ion-beam and gas-sputtering methods, only a representative sample of the experimental data has been included; accordingly, those results obtained from the occasional specimen with abnormally low switch-on fields etc., have been omitted. Consideration of the γ-values show that the ion-beam technique produced the highest and most consistent improvement in voltage hold-off, with an average γ-value of 2.6. Moreover, this technique always resulted in the destruction of the treated emission site (assuming it could be accurately located).

Although the gas sputtering technique was localised in concept, it was, in practice, a generalised technique; with the localisation of the emitting area around the syringe aperture producing no noticeable difference in the effectiveness of te conditioning. Both this technique and the general glow-discharge method produced similar average γ-values (1.65 and 1.57 respectively). Another characteristic shared by these methods was the general tendency to introduce a progressive instability in the emission current after each phase of the conditioning process; a factor which, particularly for the gas discharge technique, often prevented further conditioning. A second shared feature was the re-location of previously treated emission areas. Although the emission characteristics of the two sites were usually considerably different, often more so than for a spatially different site, the location was the same; a phenomenon which was particularly marked with the glow-discharge method. It should be noted that the re-emergence of a previously treated area as the ´dominant emission site´ sometimes only occured after several other sites had been treated. The implication of this finding is that the initial treatment did not always completely destroy the emission regime, merely modifying it so that the emission current was reduced by several orders of magnitude. The physical significance of this conclusion is that the combination of the factors determining the emission characteristics must vary considerably between emission sites, with some being more ´resistant´ to surface disruptions than others.

The two other techniques investigated, viz. electron-beam bombardment and ´spot-knocking´, both showed promise, although more refinement is needed in their application. The electron-beam method in fact produced a considerable improvement in HV hold-off (′γ=1.38) for the titanium electrode, before the intense localised heating (>2000 deg.K) led to a significant deposit of polymerised pump-oil molecules on the electrode surface; resulting in a final $\underline{\gamma}$ value of only 0.95. If the performance of the electron gun could be improved, such that it could produce a beam of suficient intensity to cause localised surface melting of a copper electrode, this technique could be of great interest. It would provide a conditioning action that would be extremely localised, and would provide a means of destroying an emission site without bombardment of "foreign" particles (argon ions in the case of the ion-beam technique), which may contaminate the emitting area. A further advantage is that the conditioning process occurs under almost UHV conditions, rather than the relatively high pressures needed for the other techniques, 10^{-4}mbar for ion-beam conditioning and 10^{-2}mbar for the glow-discharge technique.

The spot-knocking technique suffered from the disadvantage of inducing many micro-discharges, and hence surface contamination.

These events occurring all over the specimen electrode due to the nature of the method used. However, the technique could be profitably employed for electrode conditioning if a suitable experimental system could be designed; such as that shown, for example, in Fig.6.1. Thus, after location and characterisation of an emission site, the test electrode would be rotated into opposition with a probe/arc electrode, which would be used to produce a localised micro-discharge. This system would avoid excessive contamination of the specimen cathode by anode material, especially if the probe electrode was also made of OFHC copper. This method of conditioning produces a rather uncontrolled treatment of the emission site; often resulting in quite substantial surface damage, including the possible production of sharp, metallic micro-protrusions. However, under laboratory conditions, the capacitative energy of the experimental system, and hence the energy delivered during the arc, can be more easily regulated; so minimising surface damage. Despite these drawbacks, this method is commonly used in the HV engineering industry, particularly, for example, in the production of vacuum capacitors, where the energy disipated in the discharge can be very high, due to the inherent capacitance of the device, and the consequent substantial surface damage. More will be said on the applicability of this technique to industrial requirements later in this chapter.

A consideration of these factors suggests that the localised ion-beam technique represents the most useful conditioning method. Thus, from a technological point-of-view, it leads to the highest average γ-value, and from an investigative viewpoint, it allows

(a) DETECTION AND CHARACTERISATION

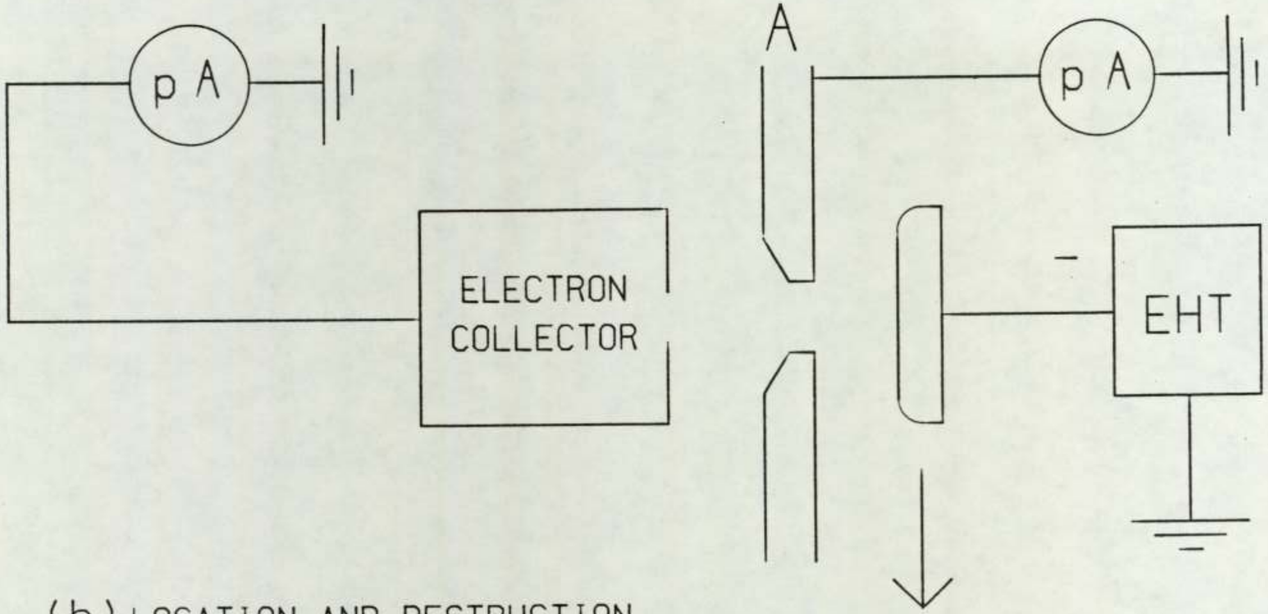

(b) LOCATION AND DESTRUCTION

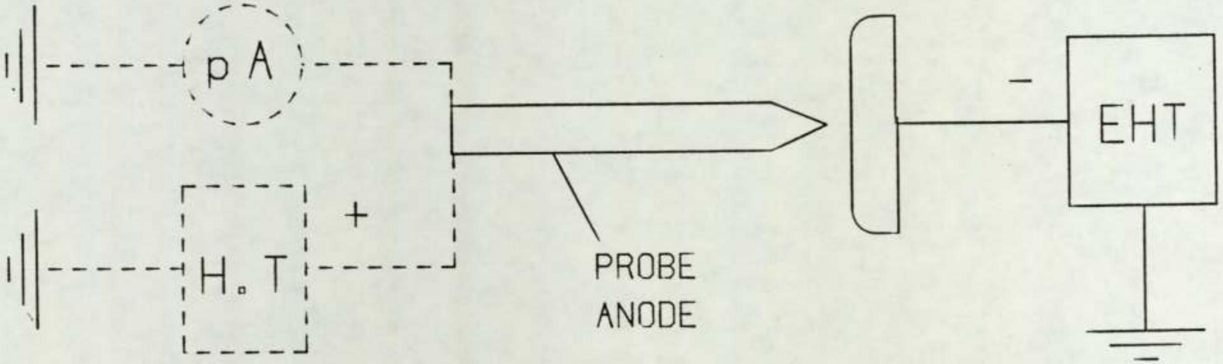

Fig.6.1 POSSIBLE SPOT-KNOCKING MODULE

the controlled study of individual emission sites, with little affect on the characteristics of subsequent dominant sites. The more generalised surface treatments of gas sputtering and glow-discharge, although producing a significant conditioning performance, were found to have a detrimental effect on the stability of later emission characteristics. This instability, particularly for the gas sputtering, led to an enhanced probability of the conditioning process being terminated by an inter-electrode discharge event.

6.2 Problems of Localised Conditioning

Despite the many advantages of the localised treatment of emission sites which were outlined above, it does result in two major areas of difficulty: namely, residual and untreatable edge sites, and the switch-on of multiple sites at higher fields (35 - 45MV.m^{-1}). The occurrence of edge sites has been a perennial problem in the study of the electron emission process, occurring with various degrees of frequency in all the areas of study within this laboratory. An edge site in this discussion normally refers to a site located on the radiussed section of the specimen, rather than on the actual edge, but still subject to significant distortions from the ideal linear applied field. The primary problem associated with edge sites is field-intensification at these radiussed edges; with the probability of such sites being aggravated by a number of additional factors: firstly, there is a greater likelihood of contamination in this region ofthe electrode, due to difficulties involved in specimen handling and insertion, and, secondly, greater surface roughness caused by the difficulties inherent in mechanically polishing this rounded area.

The work on conditioning was particularly prone to the occurrence of edge sites, as the process of conditioning led to a number of dominant emission sites, distributed over the surface of the specimen, being studied on any one specimen; so an edge site was obviously statistically more likely to occur than if only one or two dominant sites were studied. As a result of field distortion, an edge site is, by definition, difficult to locate accurately over the apertured anode; this, in turn, leads to problems for a "localised" treatment. This limitation was particularly acute for the ion-beam technique; although, with experience, some edge sites could be treated by estimating their location and moving the specimen around somewhat during etching. A further means of treatment that was sometimes used involved positioning the specimen such that the majority of the emission current passed through the aperture; even though the site was not located opposite it. The ion-beam was then "fired", with a negative HV applied to the specimen, such that the ion-beam was deflected towards the edge of the specimen; producing a ′clean′ area and the "treatment" of a site. These two methods of treatment sometimes enabled results to be obtained from specimens that, otherwise, would have had to be abandoned after the appearence of an edge site. Similar problems with edge sites were also encountered with the more generalised conditioning techniques, although it is difficult to see why these, particularly the gas sputtering method, should have found edge sites any more difficult to treat than sites on the face of the specimen. One possible explanation is that emission from this edge region might be stimulated by the presence of a gross surface feature, such as heavy contamination, lathe marks etc., which would be very difficult to remove with the slow sputtering action of this technique.

As discussed in a previous chapter, at applied fields in the region of 35 - 45MV.m^{-1} there is a switch-on of multiple sites, typically around 10-100, distributed over the surface of the electrode. This phenomenon has considerable implications from a technological point-of-view, since it seems to provide a practical limit to the potential of localised conditioning techniques.

6.3 Conditioning of Commercial Devices

6.3.1 Electrode Preparation

Various factors have to be weighed when considering the suitability of applying the various conditioning techniques to commercial HV equipment. For example, the physical design of the device would decide just how readily applicable any particular technique would be; an additional consideration would be the cost of successfully applying the technique to the device. The industrial co-sponsor of this project, EEV Ltd., considered that an improvement in voltage hold-off of their vacuum capacitors should be of initial concern, so the discussion of commercial conditioning shall be restricted to this particular device.

In laboratory experiments, one of the most important factors in determining the eventual voltage hold-off of the test electrode was its preliminary surface treatment. This is also true for commercial devices, and every care should be taken to ensure that the surfaces exposed to HV are as free of contamination, loosely adhering micro-particles and field-enhancing surface features, as possible. EEV Ltd. require strict specifications for their OFHC copper and, after machining, the parts are cleaned chemically, using an acid ´bright´ bath, before assembly; also, at several stages during assembly, the device is subjected to ultra-sonic cleaning in distilled water. However, although some precautions are taken during this assembly procedure, it is carried out in far from ´clean-room´ conditions, and there is considerable scope for air-borne contamination. The electrode surface preparation is particularly important, since the performance of any conditioning system incorporated into the manufacture of commercial devices would ultimately be limited by the surface density of the micron-sized contaminant particles, that are either superficially attached to the surface or partially embedded in it, since each of these represent a potential emission site. Hence, a significant practical advantage in terms of the increased effectiveness and simplification of the conditioning process would be gained by reducing the level of particulate contamination present on the electrode surfaces. The technological advantage that may be gained by pursuing such an approach may be illustrated by considering the assembly of RF super-conducting cavities at CERN, where chemical polishing, de-ionised rinsing and 'clean-room' assembly', followed by helium conditioning, led to a considerably improved voltage hold-off(2). It should be noted that for certain devices, for example klystrons, transmitting valves etc., EEV Ltd. carry-out some of the final stages of assembly under ´semi-clean-room´ conditions.

6.3.2 Feasibility of Conditioning

At present, the most common method of industrial conditioning involves subjecting a fully-assembled device to repeated spot-knocking, or localised arcing, until it can hold-off an applied field approximately 50% higher than required in normal service. This process often causes significant surface damage, and frequently produces a reduction in voltage hold-off; a vacuum capacitor may sometimes require many thousands of "sparks" in order to hold-off the required field, and its subsequent performance may still fall short of that required. Fig.6.2 shows the surface damage typically found on a capacitor surface; although some of the damage resulted when the device failed in service, the small circular marks are spot-knock scars.

The results of the conditioning experiments carried-out in the course of this investigation show that the systematic application of localised electrode conditioning, particularly when using the ion-beam technique, provides both a more reliable and more effective method of conditioning than conventional ´total electrode´ techniques. However, there are several practical difficulties in applying the "local" approach to a commercial device. In order to employ, for example, the ion-beam technique for in-situ processing of a fully assembles device, the active surfaces of individual electrode elements would need to be treated externally in a special processing chamber, and then remotely assembled in an ultra-clean environment. The difficulties in designing the required processing chamber would be considerable, with the need to employ a combined anode probe/ion gun module, in conjunction with robotic technology, in order to scan an electrode

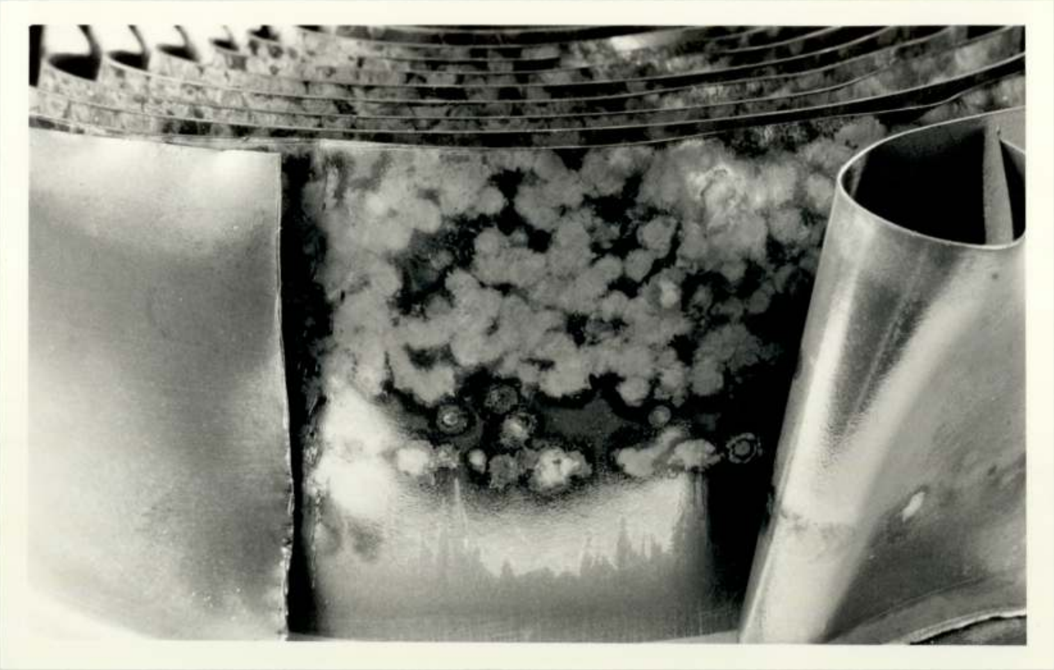

Fig.6.2 Surface Damage Produced By Commercial ´Spot-Knocking´ Of HV Capacitor (failed in service)

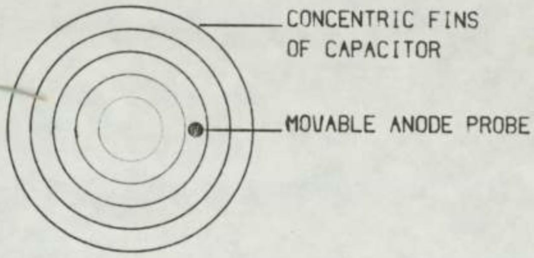

Fig.6.3 POSSIBLE PROBE METHOD FOR SPOT-KNOCKING COMMERCIAL HV CAPACITORS

surface for the detection and elimination of emission sites. The same type of problems would be faced if the localised electron beam technique were to be used for conditioning. When treatment of this order of sophistication is required, cost may become a vitally important factor; the importance of the cost being dependent on the purpose intended for the device. Certainly, for commercial production-line devices, a very high "treatment" cost could mean that the device becomes financially non-viable, compared with less effective but cheaper treatments; whereas, for special purpose devices, such as the RF cavities for the CERN accelerators, where performance is more important than commercial competitiveness, this type of treatment could be of vital importance.

The concept of "local" conditioning could be profitably employed with respect to spot-knocking a vacuum capacitor. Instead of applying the technique to a fully assembled device, with the problems of causing excessive surface damage due to the large inherent capacitance of the device and its uncontrolled application, it could be applied to a partially assembled device. For example, a movable anode probe could be automatically scanned in circles around each fin of the capacitor before the two halves are assembled; i.e. as illustrated in Fig.6.3. However, this would require some investment in new equipment, especially as the spot-knocking process would need to be carried-out under vacuum.

In contrast, the "total" electrode treatments could more readily be applied to an assembled device. For example, the gas sputtering method could be profitably and easily employed in the production of commercial devices; requiring no expensive processing, merely the introduction of argon or helium into, for example, the capacitor whilst maintaining an emission current of 10^{-7}- 10^{-5}A between the electrodes (the level of emission required for optimum conditioning effect being determined by investigation). This process would only require minimum modification of existing machinery; e.g. a standard spot-knocking machine could be adapted for gas handling, introducing very litle additional cost into the production process. The glow-discharge technique could be introduced equally as easily, just as an additional step in the production process requiring minimal extra cost. In fact, EEV Ltd. already use a ´Townsend discharge´ using oxygen during their production of vacuum capacitors, with an apparently beneficial result on subsequent performance.

It should, however, again be emphasised that although either of these general conditioning methods could be profitably introduced into the production of commercial devices, a significant benefit from such procedures would only be derived if it was combined with increased care and cleanliness in assembly.

CHAPTER 7

Conclusion

7.1 General Considerations

This chapter seeks to summarise the findings obtained from both the conditioning experiments and the subsidiary experiments designed to provide fundamental information as to the distribution and composition of emission sites.

As described in Chapter 3, the initial task of the project was to design and construct an experimental system that was capable of locating and characterising an emission site, prior to its localised treatment by one of several conditioning techniques. An additional feature of the chosen experimental system was the modular concept adopted in the design of the various conditioning units.

One of the major innovations arising out of this investigation is the concept of the "localised" treatment of emission sites. This procedure, firstly, provided a means of studying the emission characteristics of individual sites, and investigating how a dominant site contributed to the total gap I-V characteristic. Secondly, it avoided the need for causing extensive surface damage to passive regions of the electrode surface in order to eliminate a single micron-sized site. An additional benefit of this "local" treatment of sites was that it provided a means of "marking" an emission site, thereby allowing the subsequent examination of the site region using a range of surface analytical facilities, e.g.

S.E.M., Auger etc.

7.2 Experimental Findings

7.2.1 Conditioning Experiments

The findings of this investigation were extensively discussed in the previous chapter. The essential conclusion drawn was that the localised ion-beam technique provided the most consistent and effective electrode conditioning procedure. The conventional gas sputtering and glow-discharge "total-electrode" methods gave a significant improvement in voltage hold-off for the test electrodes, but possessed some undesirable characteristics: the deleterious effects on the stability of subsequent dominant emission sites, and the ´resistance´ of certain sites to erosion by these methods. However, although the new localised technique proved the most effective for conditioning the simple planar electrode geometry investigated in this project, difficulties would be encountered in applying the technique to a commercial HV device.

Apart from evaluating the conditioning performance of the various techniques, these experiments provided confirmatory evidence as to the distribution and nature of potential emission sites. For example, the "snow" effect, noticed in the glow-discharge technique, probably resulted from the differential etching rates of the metal matrix and the insulating impurities embedded on the electrode surface. In addition, it identified the multiple switch-on effect noticed in the higher applied field ranges (>40MV.m^{-1}) for the ion-beam experiments.

7.2.2 Analytical Investigations

The series of experiments, described in Chapter 5.2, designed to investigate more thoroughly the reported optical emission processes associated with electron emission sites, provided no evidence that could be categorically attributed to a cathode-generated electroluminescence phenomenon. This was an important finding, since it called into question the need to provide a means of possible "light" production when developing a model to explain field-emission phenomena. A possible explanation of the optical phenomena observed by Hurley et al has been proposed, whereby it was attributed to an X-ray fluorescent emission mechanism.

The experiments in which the ion-beam was used as a site "marker", gave considerable information as to the fundamental nature of emission sites. Thus, it was established that the localised removal of approximately 3 - 4 microns of surface material produced the complete destruction of an emitting site, with the disruption of the surface oxide layer providing the biggest reduction in emission. An Auger analysis of the localised region of an emission site, demonstrated that the surface in this area frequently possesses high levels of carbon contamination relative to the general surface levels. Furthermore , X-ray analyses of micro-structures found to be commonly associated with emission sites, showed them to consist of relatively high proportions of carbon, silicon, sulphur etc. These findings confirmed the emission regime proposed by Latham et al.(75,77,94-97)

7.3 Future Work

7.3.1 Conditioning

Whilst the localised ion-etching technique has been demonstrated to have considerable promise, there remain two major limitations to the technological application of the technique. Firstly, the occurrence of residual edge sites and, secondly, the multiple switch-on of high-field ($>40MV.m^{-1}$) emission sites. Future work on this technique should therefore attempt to design instrumental systems or processes specifically aimed at combating these edge sites. For example, by incorporating a deflection capaability to act with the localised ion-beam etching to destroy sites on the surface of the specimen. Also, this approach could be combined with a "total-electrode" technique, such as gas sputtering, to treat edge sites. Another area of interest that could benefit from further study is the phenomenon of high-field multiple switch-on of sites, At present, results in this range were obtained near the maximum limit of applied field; so the electrode gap was small (<0.35mm), and any departure from linearity in the scanning mechanism produced large instabilities in the emission current. This instability, together with the possibility of the multiple switch-on occuring during the scanning, often led to localised micro-discharges. Therefore, a higher applied field capability would mean that this phenomenon could be studied in more depth. It would also be advantageous to evaluate the ion-beam technique using a greater range of gases; one obvious alternative would be an ´active´ gas such as oxygen, which is to produce some conditioning benefits just by its presence on the electrode surface(109,114).

There is obviously considerable scope for further work on the electron beam and spot-knocking techniques; in particular, a more detailed comparison should be made between the effectivenesses of these conditioning methods and that of the ion-beam technique. However, the primary problem associated with this proposal would be the development of suitable experimental systems to allow this investigation, such as that already outlined in the previous chapter and shown in Fig.6.1.

Further work could also profitably be done on the "total-electrode" techniques of gas sputtering and glow-discharge; where more consideration should be given to the appropriate ion dosages required for maximum conditioning effect; in particular there is scope for investigating the composition of the gas used in the latter technique.

7.3.2 Nature of Emission Sites

There is also considerable scope for further work aimed at obtaining a more detailed knowledge of the emission process. Thus, a continuing programme of ion-beam experiments aimed at marking emission sites more precisely for subsequent analysis should be duplicated a number of times, in order to allow an in-depth study to be made of the elemental constitution of emission sites. An obvious extension of the marking technique would be to use it in the study of the high-field sites, i.e. those produced during a multiple high-field switch-on, to see if the physical and chemical composition of these sites are different to those that switch-on singly at lower fields.

The study of the variation in emission characteristics produced by the partial etching of an emission site could also benefit by further work. A higher applied field capability would be of use here, but the primary need is for a more localised current collector, possibly using a probe technique, in order to eliminate the ´interference´ caused by the emission current from neighbouring sites.

REFERENCES

1. R.J. NOER, J. Appl. Phys. A (Germany) A28 No. 1, 1-24 (1982)
2. R.V. LATHAM, High Voltage Insulation (Academic Press, London (1981)
3. R.A. MILLIKAN & R.A. SAWYER, Phys. Rev. 12, 167-170 (1918)
4. R.A. MILLIKAN & C.F. EYRING, Phys. Rev. 27, 51-67 (1926)
5. W. SCHOTTKY, Z. Physik. 14, 63-106 (1923)
6. R.H. FOWLER & L. NORDHEIM, Proc. Roy Soc. Ser. A118 (1928)
7. R.H. GOOD & E.W. MULLER, Encycl. Phys. 21, p176 (1956)
8. A.G. VAN OOSTROM, Phillips Res. Reports Supplemats, No. 1 (1966)
9. H.C. MILLER, J. Franklin Inst. 289, 347-351 (1969)
10. R. HAEFER, Z. Physik 116, 604-622 (1940)
11. W.P. DYKE, J.K. TROLAN, E.E. MARTIN, Phys. Rev. 91, 1043-1054 (1953)
12. W.P. DYKE, J.K. TROLAN, W.W. DOLAN, J.Appl. Phys. 84, 570-576 (1953)
13. H.E. TOMASCHKE & D. ALPERT, J. Vac. Sci. Tech. 4, 192-198 (1967)
14. W.S. BOYLE, P. KISLIUK & L.H. GERMER, J. Appl. Phys. 26, 720-725 (1955)
15. D. ALPERT, D.A. LEE, E.M. LYMAN, H.C. TOMASCHKE, J. Vac. Sci. Tech. 1, 35-50 (1964)
16. R.P. LITTLE & S.T. SMITH, J. Appl. Phys. 36, 1502-1504 (1965)
17. H.E. TOMASCHKE & D. ALPERT, J. Appl. Phys. 38, 881-883 (1967)
18. R.P. LITTLE & W.T. WHITNEY, J. Appl. Phys. 34, 2430-2432 (1963)
19. I. BRODIE, J. Appl. Phys. 35, 2324-2332 (1964)

20. I. BRODIE, J. Vac. Sci. Tech. 2, 249-456 (1965)

21. R. GOMER, J. Chem. Phys. 21, 293-303 (1953)

22. D.K. DAVIES & M.A. BIONDI, J. Appl. Phys. 37, 2967-2977 (1966)

23. D.K. DAVIES & M.A. BIONDI, J. Appl. Phys. 37, 2979-2990 (1968)

24. H.P. POWELL & P.A. CHATTERTON, Vacuum, 20, 419-429 (1971)

25. R. HACKMAN & S.K. SALMAN, Proc. IEE, 119, 377-384 (1972)

26. B.M. COX, CEGB Laboratory Note, RIMIN1021 (1979)

27. R.E. HURLEY, J. Phys. D. Appl. Phys. 13, 1121-1128 (1980)

28. R. HAWLEY & A.A. ZAKY, Progress in Dielectrics, 7, 115-215 (1967)

29. L.I. PIVOVAR & V.I. GORDIENKO, Sov. Phys. Tech. Phys. 3, 2101-2105 (1955)

30. L.I. PIVOVAR & V.I. GORDIENKO, Sov. Phys. Tech. Phys. 7, 908-912 (1963)

31. R.H. GOOD & E.W. MULLER, Handbuch dev. Phys. ch. (Springenerlay Berlin) 21, 176-231 (1956)

32. R.V. LATHAM & E. BRAUN, J. Phys. D: Appl. Phys. 1, 1731-1735 (1968)

33. B.M. COX & D.E. WORT, Vacuum, 22, 453-455 (1972)

34. B.M. COX, J. Phys. D: Appl. Phys. 8, 2065-2073 (1975)

35. B.M. COX & W.T. WILLIAMS, J. Phys. D: Appl. Phys. 10, L5-L9 (1977)

36. E.E. DONALDSON & M. RABINOWITZ, J. Appl. Phys. 34, 319-322 (1963)

37. A.S. POKROUSKAYA-SOBOLEVA, V.V. KRAFT & L.K. MAZUROVA, Proc. 5th Int. Symp. Discharges and Elect. Ins. in Vac. Poznan Poland, 105-109 (1972)

38. J.T. MASKREY & R.A. DUGDALE, J. Sci. Instrum. 42, 284-286 (1966)

39. G.A. FARRALL & M. OWENS, J. Appl. Phys. 43, 938-943 (1977)

40. G.A. FARRALL, M. OWENS & F.G. HUDDA, J. Appl. Phys. 46, 610-617 (1975)

41. G.A. FARRALL, F.G. HUDDA & R.H. JOHNSON, J. Appl. Phys. 40, 3608-3614 (1979)

42. R.E. HURLEY & P.J. DOOLEY, J. Phys. D: Appl. Phys. 10, L195-L201 (1977)

43. B.N. KLYARFEL'D & A.S. POKROVSKAYA-SOBOLEVA, Sov. Phys. Tech. Phys. 15, 149-152 (1970)

44. G.F. ALFREY & J.R. TAYLOR, Brit. J. Appl. Phys. 6, Suppl. 4, 544-549 (1955)

45. R.E. HURLEY, J. Phys. Appl. Phys. 12, 2247-2252 (1979)

46. R.E. HURLEY & P.J. DOOLEY, Vacuum, 28, 147-149 (1978)

47. C.S. ATHWAL & R.V. LATHAM, J. Phys. D: Appl. Phys. 17, 1029-1043 (1984)

48. N.K. ALLEN & R.V. LATHAM, J. Phys. D: Appl. Phys. 11, L55-L57 (1978)

49. J.E. HENDERSON & R.E. BADGLEY, Phys. Rev. 38, S90 (1931)

50. J.E. HENDERSON & R.K. DAHLSTRON, Phys. Rev. 55, 473-481 (1939)

51. E.W. MULLER, Z. Physik, 102, 734-761 (1936)

52. E.W. MULLER, Z. Physik, 120, 261-269 (1943)

53. R.D. YOUNG & G.W. MULLER, Phys. Rev. 113, 115-120 (1959)

54. R.D. YOUNG, Phys. Rev. 113, 110-114 (1959)

55. L.W. SWANSON & L.C. CROUSER, Phys. Rev. 163, 622-641 (1967)

56. N. NICOLAOU & A. MONINOS, Phys. Rev. B11, 3687-3697 (1976)

57. N.J. DIONNE & T.N. RHODIN, Phys. Rev. B14, 322-340 (1976)

58. J.W. GADZUK & E.W. PLUMMER, Rev. Mod. Phys. 45, 487-548 (1973)

59. R. STRATTON, Proc. Roy. Soc. B68, 746-757 (1955)

60. R. STRATTON, Phys. Rev. 125, 67-82 (1962)

61. R. STRATTON, Phys. Rev. 135, A794-A805 (1964)

62. C.M. BASKIN, LVOV & N. FURSEY, Phys. Stat. Sol. B47, 49-62 (1971)

63. J.R. ARTHUR Jr. J. Appl. Phys. 36, 3221-3227 (1955)

64. O.H. HUGHS & P.M. WHITE, Phys. Stat. Sol. 33, 309-316 (1969)

65. L.T. SALMON & E. BRAUN, Phys. Stat. Sol. A16, 527-532 (1973)

66. B.F. LEWIS & T.E. FISCHER, Surf. Sci. 42, 371-376 (1974)

67. A. MODINOS, Surf. Sci. 42, 205-227 (1973)

68. P. HANDLER, J. Phys. Chem. Solids, 44, 1-8 (1960)

69. W.B. SHEPHERD & W.T. DERIA, Surf. sci. 38, 461-498 (1973)

70. D.E. SYKES & E. BRAUN, Phys. Stat. Sol. B69, K137-K140 (1975)

71. N.RIHON, Surf. Sci. 70, 92-100 (1978)

72. C.R. DUKE & H.G. ALFERIEFF, J. Chem. Phys. 46, 923-937 (1967)

73. E. MERZEBACHER, Quantum Mechanics (Wiley, New York) 121-130 (1961)

74. C.W. SWANSON & L.C. CROUSER, Surf. Sci. 23, 1-29 (1970)

75. N.K. ALLEN, R.M. COX & R.V. LATHAM, J. Phys. D: Appl. Phys. 12, 969-977 (1979)

76. C.S. ATHWAL, Ph.D. Thesis, University of Aston, England (1981)

77. K.N. BAYLISS & R.V. LATHAM, Proc. Roy. Soc. London, Ser A, 403 No. 1825, p285-311 (1986)

78. N.K. ALLEN & R.V. LATHAM, Proc. 8th Int. Sym. Disch & Elec. Ins. in Vac. Alburquerque, B3, 1-13 (1978)

79. N.K. ALLEN, Ph.D. Thesis, University of Aston, England (1979)

80. G. DEARNLEY, A.M. STOWEHAM & D.V. MORGAN, Rep. Prog. Phys. 33, 1129-1191 (1970)

81. E.L. COOK, J. Appl. Phys. 41, 551-554 (1970)

82. T.W. HICKMOTT, J. Appl. Phys. 37, 4380-4388 (1986)

83. B. JUTTNER, W. ROHRBECH & H. WOLFF, Proc. 5th Inst. Symp. Disch. & Elec. Ins. in Vac. 65-69 (1972)

84. B. JUTTNER, H. WOLFF, R. ALTRICHTER, Phys. Stat. Sol. 27, 403-412 (1975)

85. G. DEARNLEY, Thin Solid Films, 3, 161-174 (1969)

86. G.R. OVSHINSKY, Phys. Rev. Lett. 21, 1450-1453 (1968)

87. K. HOMMA, H.K. HENISCH & S.R. OVSHINSKY, J. Non-Cryst Solids, 35, 36, 1105-1110 (1980)

88. R. COELHO & J. DEBEAU, J. Phys. D: Appl. Phys. 4, 1266-1280 (1971)

89. D. ADLER, Amorphous Semiconductors, (Butterworth's London) (1972)

90. D. ADLER, H.K. HENISCH & N.F. MOTT, Rev. Mod. Phys. 50, 209-220 (1978)

91. N.F. MOTT, Philos. Mag. 32, 159-171 (1975)

92. Solid Luminescent Materials, (J. Wiley & Sons Inc. New York) 1948.

93. K.E. PETERSON & D. ADLER, J. Appl. Phys. 47, 256-263 (1976)

94. C.S. ATHWAL, K.H. BAYLISS, R. CALDER & R.V. LATHAM, J. Phys. D: (GB) 17, No. 5. p1029-1043 (1984)

95. K.H. BAYLISS, Ph.D. Thesis, University of Aston, England (1984)

96. K.H. BAYLISS & R.V. LATHAM, Vacuum (GB), 35, No. 6, p211-216 (1985)

97. R.V. LATHAM, Vacuum, 32, 137-140 (1982)

98. J.G. SIMMONS, Brit. J. Appl. Phys. 18, 269-273 (1967)

99. J.G. SIMMONS, J. Phys. D: Appl. Phys. 4, 613-657 (1971)

100. A. MAITLAND, Brit. J. Appl. Phys. 13, 122-125 (1962)

101. W. ROGOWSKI, Archiv. für Electrotechnch, 12, 1-15 (1923)

102. F.M. BRUCE, J.I.E.E.E. 94, 138-149 (1947)

103. J.A. HARRISON, Brit. J. Appl. Phys. 18, 1617-1622 (1967)

104. G.P. BEUKEMA, J. Phys. D: Appl. Phys. 7, 1740-1755 (1974)

105. J.C. CORNISH, R.V. LATHAM & E. BRAUN, Proc. 1V-DEIV, 28-32 (1970)

106. J.A. PANITZ, J. Appl. Phys. 44, 372-375 (1973)

107. H.C. MILLER & G.A. FARRALL, J. Appl. Phys. 36, 1338-1344 (1965)

108. B.M. COX, J. Phys. D: Appl. Phys. 7, 143-151 (1974)

109. R. HACKAM, J. Appl. Phys. 46, 3769-3799 (1975)

110. B. JUTTNER, Beitr. Plasmaphys, 19, 259-265 (1979)

111. E.M. LYMAN, D.A. LEE, H.E. TOMASCHKE & D. ALPERT, proc. 2nd DEIV, 33-39 (1966) .

112. D. ALPERT, D.A. LEE, E.M. LYMAN & H.E. TOMASCHKE, J. Appl. Phys. 38, 880-881 (1967)

113. S.Y. ETTINGER & E.M. LYMAN, Proc. 3rd DEIV, 128-133, (1968)

114. R. HACKAM & L. ALTCHEH, J. Appl. Phys. 46, 627-636 (1975)

115. L. DANLOY & P. SIMON, Proc. 5th DEIV, 367-372 (1972)

116. G.F. STEIB & E. MOLL, J. Phys. D: Appl. Phys. 6, 243-255 (1973)

117. R. HACKAM & G. RAJU, J. Appl. Phys. 45, 4784-4794 (1974)

118. A.H. McILRAITH, Nature, 212 No. 5069, 1422-1424 (1966)

119. R.K. FITCH, T. MULVEY & A.H. McILRAITH, J. Phys. D: Appl. Phys. 13, 1339-1402 (1970)

120. J. VINE & P.A. EINSTEIN, Proc. IEEE, 111, 921-930 (1964)

121. Electron Beam Welding (Welding Inst. Cambridge)

122. W.J. THATCHER, Ph.D. Thesis, University of Aston, England (1970)

123. A.H. McILRAITH, J. Vac. Sci. Tech. 9, No. 1, p209-212 (1971)

124. M. KHORASSANY & R.K. FITCH, Vacuum, 27, No. 3, p159-162 (1975)

125. R.K. FITCH, E.A. MAHMOUD & S.M. GHAFOURI, Proc. 4th Int. Conf. on Solid Surf. 1084 (1980)

126. R.K. FITCH, S.N. GHAFOUR & E.A. MAHMOUD, Vacuum, 31, p18-21 (1981)

127. K.S. ALI & R.K. FITCH, 9th Int. Vac. Cong. (Madrid) (1983)

128. R.W. YOUNG, Vacuum, 24, 167-172 (1973)

129. H. BOERSCH, C. RADELOFF & L. SUERBERG, Z, Phys. 65, 464-469 (1961)

ACKNOWLEDGEMENTS

This work was carried out with the support of an S.E.R.C. CASE Award; accordingly, I would like to thank both them and the industrial sponsor EEV Ltd. In particular, I should like to thank my Supervisor, Dr R.V Latham, both for his encouragement and for his many useful discussions and suggestions throughout the course of this work. I would also like to thank my industrial Supervisor, Mr. A.P.O. Collis, for his suggestions and help. In addition, I would like to extend my thanks to the many technical staff in this department who have assisted in this work. Finally, I would like to express my deepest thanks to my parents, for their help and support.

```
 10 PHI=4.5
 100 PRINT"⊐":PRINT"  DO YOU WANT FIELD VALUES CALCULATED▩▶▶▶▶-IF SO PRESS F.";
 110 PRINT" OTHERWISE,PRESS ANY KEY"
 120 GETF$:IFF$=""THENGOTO120
 130 IFF$="F"THENFI=1:GOTO150
 140 FI=0
 150 PRINT"▩▩"
 160 PRINT"▶ THIS PROGRAM CALCULATES THE▶ FOWLER-▶▶NORDHEIM COORDINATES";
 170 IFFITHENPRINT"▶(LN(I/E*E)AND1/E)▶▶FROM BASIC I,V DATA":GOTO190
 180 PRINT"(LN(I/V*V)&1/V)FROM BASIC I,V DATA"
 190 PRINT
 195 PRINT"▩▩▶▶▶▶▶▶PRESS ▣RETURN▤ TO CONTINUE"
 196 GETZ$:IFZ$=""THEN196
 197 IFASC(Z$)<>13 THEN196
 200 PRINT"⊐AFTER THE COORDS.HAVE BEEN CALCULATED   ";
 210 PRINT"THEY CAN BE FED INTO A ▣LINEFIT▤ PROGRAM"
 220 PRINT"THIS CALCULATES THE GRADIENT & INTERCEPT(WITH ERRORS)."
 230 PRINT"▩▩▶IF A WORK-FUNCTION OTHER THAN 4.5EV IS ▩REQUIRED, THIS MAY BE ENTE
RED"
 240 PRINT
 290 PRINT
 300 PRINT"▩▩DO YOU WANT TO: 1.FEED YOUR RESULTS STRAIGHT INTO THE ▣LINEFIT"
 310 PRINT:PRINT"        2.HAVE THE F.N COORDS. CALCULATED."
 315 PRINT"▩▶▶▶▶3. ENTER NEW VALUE FOR WORK-FN.":PRINT
 320 PRINT"INPUT REQUIRED OPTION";
 322 GETOP$:IFOP$=""THEN322
 324 R=(ASC(OP$)-48):IFR>3THENPRINT"⊐":GOTO300
 325 IFR<>3THEN330
 326 INPUT"⊐▩▩▶▶ENTER THE WORK-FUNCTION (IN EV)";PHI:GOTO300
 330 DIM X(100),Y(100)
 340 PRINT "⊐":INPUT "HOW MANY PAIRS OF RESULTS";N:PRINT
 350 IFFI THEN INPUT"WHAT IS THE GAP(IN METRES)";GAP:PRINT
 360 IFR=2THENPRINT"TYPE THE";N;"PAIRS OF RESULTS IN THE FORM V(IN KV),I":PRINT:
GOTO380
 370 PRINT"TYPE IN THE";N;"PAIRS OF RESULTS":PRINT"IN THE FORM X,Y":PRINT
 380 FOR  I=1TO N:PRINT I;:INPUT X(I),Y(I)
 390 IFR=2THENX(I)=X(I)*1000
 400 IFFI THEN X(I)=INT(X(I)/GAP+1)
 410 NEXT
 420 N2=1
 430 N3=N2+8:IF N3<=N THEN 450
 440 N3=N
 450 PRINT"⊐  N","  X","  Y","  D"
 460 IF FI THEN PRINTTAB(10)"(MV/M)"
 470 FOR I=N2 TO N3
 480 IFFI=0 THENPRINTI,X(I),Y(I),
 490 IF FI THEN PRINTI,X(I)/1E6,Y(I)
 00 IF X$="" THEN 520
 10 PRINT INT((Y(I)-(M*X(I)+C))*10000+.5)/10000;
 20 PRINT:NEXT
 30 PRINT "ARE THE RESULTS SHOWN CORRECT? Y OR N"
 40 GET A$:IF A$="" THEN 540
 50 IF A$="N" THEN 590
 60 IF A$<>"Y"THEN 530
 0 IF N3=N THEN 690
 0 N2=N3+1:PRINT"⊐":GOTO 430
 0 PRINT:INPUT "WHICH PAIR OF RESULTS IS INCORRECT";I:PRINT:X$=""
 0 IF I> N THEN 630
 0 IF I-INT(I)<>0 THEN 630
 0 IFABS(I-INT(I+.00001))<.0001THEN650
 PRINT"⊐TYPE THE INTEGER IN COLUMN 1 OPPOSITE  "
 PRINT"THE INCORRECT RESULTS";:INPUT I:GOTO 620
 PRINT"TYPE THE CORRECT RESULTS FOR X(";I;") AND Y(";I;")";
 INPUT X(I),Y(I)
 PRINT"⊐":GOTO 450
 PRINT"HAVE YOU A PRINTER?(Y/N)"
 GETQ$:IFQ$="Y" THEN OPEN 1,4:CMD1
```

```
570 IF N3=N THEN 690
580 N2=N3+1:PRINT"]":GOTO 430
590 PRINT:INPUT "WHICH PAIR OF RESULTS IS INCORRECT";I:PRINT:X$=""
600 IF I> N THEN 630
610 IF I-INT(I)<>0 THEN 630
620 IFABS(I-INT(I+.00001))<.0001THEN650
630 PRINT"TI]TYPE THE INTEGER IN COLUMN 1 OPPOSITE  "
640 PRINT"THE INCORRECT RESULTS";:INPUT I:GOTO 620
650 PRINT"TYPE THE CORRECT RESULTS FOR X(";I;") AND Y(";I;")";
660 INPUT X(I),Y(I)
670 PRINT"]":GOTO 450
690 PRINT"HAVE YOU A PRINTER?(Y/N)"
700 GETQ$:IFQ$="Y" THEN OPEN 1,4:CMD1
710 IFQ$="" THEN700
715 IFR=1THENPRINT"POINT","X ","Y ":GOTO795
720 IF FI=0 THEN GOTO750
730 PRINT:PRINT"GAP=";GAP*1000" MILLI-METRES":PRINT
740 PRINT"  N"TAB(8)"LN(I/E*E)"TAB(25)"1/E":GOTO760
750 PRINT"  N"TAB(8)"LN(I/V*V)"TAB(25)"1/V"
760 FOR I=1 TO N
770 Y(I)=LOG(Y(I)/X(I)/X(I))
780 X(I)=1/X(I)
790 PRINTITAB(8)INT(Y(I)*1000)/1000TAB(20)X(I):NEXT:IFQ$="Y"THENPRINT#1:CLOSE1
795 IFR=1THEN FORI=1TON:PRINTI,X(I),Y(I):NEXT:IFQ$="Y"THENPRINT#1:CLOSE1
800 PRINT"DO YOU WANT TO SAVE DATA ON DISC(Y/N)":INPUTD$:IFD$<>"Y"THENGOTO830
810 PRINT"INPUT FILENAME":INPUTF$:C$="@1:"+F$+",S,W":OPEN6,8,2,C$
820 FORI=1TON:PRINT#6,X(I),CHR$(13);:PRINT#6,Y(I),CHR$(13);:NEXT:CLOSE6
830 PRINT"DO YOU WANT THE ▒LINEFIT▀? Y OR N":
840 GET B$: IF B$="" THEN 840
850 IF B$="N" THEN 1110
860 IF B$<>"Y" THEN 63999
870 S1=0:S2=0:X1=0:X2=0:Y1=0:PRINT"COMPUTING"
880 FOR I=1 TO N
890 X1=X1+X(I):Y1=Y1+Y(I):X2=X2+X(I)*X(I):Y2=Y2+Y(I)↑2:S1=S1+X(I)*Y(I):NEXT
900 D=N*X2-(X1)↑2:M=(N*S1-X1*Y1)/D:C=(X2*Y1-S1*X1)/D:DY=(Y2/N)-(Y1/N)↑2
905 DX=(X2/N)-(X1/N)↑2
910 IFQ$="Y" THEN OPEN1,4:CMD1
920 IF C<0 THEN 940
930 PRINT"]":PRINT" Y = (";M;"* X)+";C:GOTO 950
940 PRINT"]":PRINT" Y = (";M;"* X)";C
950 FOR I=1 TO N
960 D2=(M*X(I)+C-Y(I))↑2:S2=S2+D2
970 NEXT
980 M2=SQR(S2/(N-2))*SQR(N/D):C2=SQR(S2/(N-2))*SQR(X2/D)
990 PRINT:PRINT"STANDARD DEVIATION OF M";M2
1000 PRINT"STANDARD DEVIATION OF C";C2
1010 S1=S1/N:X1=X1/N:Y1=Y1/N
1020 CO=(S1-X1*Y1)/(SQR(DX*DY))
1030 PRINT:PRINT" CORRELATION COEFFICIENT=";CO
1031 IFFI=0THEN1050
1039 BET=INT(-6.53E9*(PHI)↑1.5/M)
1040 PRINT:PRINT"BETA= ";BET
1041 ICO=(EXP((4.52*(PHI)↑-.5)*LOG(10))*1.54E-6*(BET)↑2)/PHI
1045 PRINT:PRINT"EMISSION AREA="EXP(C)/ICO;" SQ.METRES"
1050 IFQ$="Y" THEN PRINT#1:CLOSE1
1060 PRINT"PRESS RETURN TO CONTINUE!":IFR=2THEN1110
1070 PRINT:PRINT"TO CHECK THE RESULTS AGAIN TOUCH":PRINT"          ´RETURN´"
1080 GET X$:IF X$="" THEN 1080
1090 IF ASC(X$)<>13 THEN 1110
1100 GOTO 420
1110 GETX1$:IFX1$=""THEN1110
1120 IFASC(X1$)<>13 THEN1140
1130 CLR:GOTO10
1140 STOP
READY.
```